DISSERTATION

INFECTIOUS DISEASE, AGE, AND ENVIRONMENTAL CONTAMINANTS AS NEUROTOXICANTS THAT MODULATE GLIA AND CONTRIBUTE TO NEURODEGENERATIVE PATHOLOGY

Submitted by

Amanda Shellee Latham

Department of Environmental and Radiological Health Sciences

In partial fulfillment of the requirements

For the Degree of Doctor of Philosophy

Colorado State University

Fort Collins, Colorado

Spring 2024

Doctoral Committee:

Advisor: Julie A. Moreno
Co-Advisor: Randall J. Basaraba

Ronald B. Tjalkens
Kelly S. Santangelo
Jessica Elf

ABSTRACT

INFECTIOUS DISEASE, AGE , AND ENVIRONMENTAL CONTAMINANTS AS NEUROTOXICANTS THAT MODULATE GLIA AND CONTRIBUTE TO NEURODEGENERATIVE PATHOLOGY

Neurodegenerative disease cases are expected to double over the next twenty years. These diseases, which include Alzheimer's Disease (AD) and Parkinson's Disease (PD), are incurable with a largely unknown etiology. It is acknowledged within the field that age is the greatest risk factor for neurodegenerative disease, and that genetics and environmental factors, such as neurotoxicants and infectious agents, likely play a role. Despite this knowledge, it is not entirely understood why select individuals are pushed into a state of disease, while others progress into a state of normal brain aging. This is further complicated by the shared neuropathology between brain aging and neurodegenerative disease, which includes blood-brain barrier (BBB) modulation, gliosis, misfolded protein accumulation, and loss of function or degradation of neurons. To address these gaps in our understanding, the studies herein provide valuable insight as to how infectious disease, specifically through infection with *Mycobacterium tuberculosis*, contributes to the progression of neuropathology, evaluates an alternative model of brain aging that better recapitulates human disease, and provides mechanistic understanding of the neuroprotective and neurotoxic roles of glia in disease. Altogether, these data elucidate the etiology and mechanisms that drive neurodegenerative disease, as well as possible therapeutic avenues that may bring us one step closer to a cure.

ACKNOWLEDGEMENTS

The works herein and the completion of this doctoral degree would not have been possible without the support from my mentors, friends, and family. I would like to first thank my advisors, Dr. Julie Moreno, Dr. Randall Basaraba, and Dr. Ronald Tjalkens. I am incredibly grateful that Dr. Moreno took a chance in allowing me to complete my training in her lab, and I have the pleasure of being one of her first Ph.D. students. From her guidance, I better understand what it means to be a good scientist. I would next like to thank Dr. Basaraba, who is the reason I fell in love with research. Seven years ago he allowed me to train in his laboratory while completing my undergraduate studies. I can whole-heartedly say that opportunity, in addition to his consistent encouragement, is the reason I am the scientist I am today. I would also like to thank Dr. Ronald Tjalkens. While he is not officially my adviser (on paper), Dr. Tjalkens has provided me with years of mentorship and support, that of which this dissertation would not exist without. Students are lucky if they get one great advisor during their Ph.D., but I am one of the fortunate few to have three amazing mentors, all of whom have shaped me in different ways.

I would also like to that the past and present members of the Basaraba lab, Moreno lab, and Tjalkens lab. A special thank you to Forrest Ackart in the Basaraba lab; none of these studies could have happened without his help. Whether it be study design, a helpful hand in the lab, or guidance writing manuscripts, Forrest has been an amazing resource. I am very thankful that he has indulged my spontaneous bombardment of questions, and has had seemingly never-ending patience with me. In the Tjalkens lab, I would like to especially thank Dr. Savannah Rocha, who has spent a considerable amount of time teaching and training me. She is one of the kindest and most intelligent people I know, and I am fortunate to have had such an amazing friend to guide me through my studies. To Casey McDermott, who has been my office and BSL-3 buddy, and who I am not sure I could have survived graduate school without. From the Moreno lab I would like to personally thank Charlize Geer, Isla Anderson, and Kristin Weninger, all of whom I have had the pleasure of mentoring. Charli was my first ever mentee, and I have

never met someone so thorough and concise in everything they do. I am extremely appreciative of her efforts, those of which have substantially contributed to these works. To Isla and Kristin, both of whom I have had the pleasure of working with, and who have also contributed considerably to the data presented in this dissertation. You all have greatly impacted me and mentoring you has been one of the highlights of my graduate studies, I only hope I was a helpful mentor to you. While not specifically listed, I would like to thank the other members of these three laboratory groups, all of which have made graduate school a memorable experience.

I would also like to thank the other members of my graduate committee, Dr. Kelly Santangelo and Dr. Jessica Elf, for providing me with guidance and suggestions throughout my studies. Dr. Santangelo has been instrumental in teaching me about guinea pig pathology and, my least favorite subject, statistics. Dr. Elf has given me a valuable perspective, helping me to view my research beyond the lab bench and to consider the populations of people who are most affected.

Finally, I would like to thank both my family and friends for their love and support. To my dad, who might be my biggest fan and supporter, and has never stopped telling me how proud he is. And to my mom, Grammy, and Tiffani who have always had my back and supplied endless encouragement, especially when life gets stressful. I would like to give a particularly huge thank you to my amazing fiancé Shelby and his family. Shelby taught me what love really is, and has both helped me through failure and celebrated my successes. I could not have done any of this without him.

DEDICATION

The research herein is dedicated to those who have been affected by the neurological effects of age or disease. I perform this research in respect to those who have suffered, and hope this research allows us to better understand the intricacies of disease, which may allow us to better recognize their lasting effects and treat, if not one day cure, them.

TABLE OF CONTENTS

CHAPTER 1

LITERATURE REVIEW

1.1 Tuberculosis

1.1.1 History and Epidemiology of Tuberculosis

Tuberculosis (TB), an infectious disease caused by infection with *Mycobacterium tuberculosis* (Mtb), was first described thousands of years ago. Egyptian mummies dating back to 2400 B.C. have skeletal deformities and abscesses typical of TB, as well as evidence of tubercle bacilli [1, 2]. TB, called Phthisis, was also described in ancient Greece by Hippocrates, Isocrates, and Aristotle, who first referenced its contagious nature [3]. Known as the “king's evil", TB wreaked havoc throughout the Middle Ages in England and France, and Girolamo Fracastoro clearly defined TB as a contagious agent in the sixteenth century [3, 4]. TB became epidemic in the 17th and 18th centuries, giving rise to names such as consumption, white plague, and the "robber of youth", until it was officially given the name Tuberculosis by Johann Lukas Schönlein in the mid-19th century [3]. Early research by Philipp Friedrich, Hermann Klencke, and Jean-Antoine Villemin established the infectious nature of TB, by reproducing generalized TB through the inoculation of rabbits with material from human lung tubercles, but the causative agent was still unknown. It wasn’t until 1882 when microbiologist Robert Koch used methylene blue staining to identify, isolate, and then culture the bacteria that is now known as Mtb. This discovery led to increased knowledge of the pathogenesis of TB disease, development of therapeutic interventions, strategies for disease prevention, and, ultimately, an overall reduction in global TB cases.

In an 1882 lecture, Robert Koch once said "if the importance of a disease for mankind is measured by the number of fatalities it causes, then tuberculosis must be considered much more important than those most feared infectious diseases, plague, cholera and the like" [5]. Worldwide, an estimated 23% of the population is infected with Mtb. To address the TB global health crisis, the World Health Organization (WHO) created the “End TB Strategy”, which aims to decrease the incidence of TB-associated deaths by 95% and reduce cases of TB by 90% between 2015 and 2035, including a 4 – 5%

reduction in incidence by 2020 and a 10% decline by 2025. To do so, the WHO proposed the implementation of three primary principles: patient-centered TB care and prevention, bold policies and supportive systems, and intensified research and innovation. The first involves early diagnosis of disease, screening of contacts or high-risk groups, treatment of disease, vaccinations and preventative treatments, and management of co-morbidities. Bold policies include engagement of communities and providers, poverty alleviation, universal health coverage policies, and infection control. Finally, increased funding and encouragement of research for intervention was also proposed [6].

Despite research advances and the formation of intensive strategies, current reports do not meet target numbers. Between 2015 and 2018, global TB incidence was reduced only by 6.3% and TB deaths decreased by 11%, which fails to meet the desired decreases of 20% and 35% (compared to data from 2015) by 2020, respectively. In 2021, the World Health Organization (WHO) described a grim outlook in their annual report, with an estimated 10.6 million people diagnosed with the disease (half a million more than 2020) and 1.6 million deaths from TB (100,000 more than 2020). Compared to 2020, the incidence rate of TB increased by 3.6%, opposing the 2% decrease per year that occurred the previous two decades. The burden of drug-resistant TB also increased by 3% between 2020 and 2021, with 450,000 incident cases of rifampicin-resistant TB reported in 2021. If current trends continue, few countries will meet the End TB Strategy targets for 2030 [7]. Ultimately, an estimated 1.7 billion people are infected with Mtb, and TB is the second leading cause of death by an infectious disease, second only to COVID-19 [8, 9].

1.1.2 Transmission of Mycobacterium tuberculosis

Mtb infection occurs via human-to-human transmission through airborne respiratory droplets ranging from 0.65μm (small) to > 7.0μm (medium–large) in size. Droplets are produced through coughing, sneezing, talking, shouting, or other gestures that result in respiratory excretion [10]. TB is one of the few communicable diseases with obligatory airborne transmission [11]. Riley et al. first demonstrated this unique mode of transmission by placing guinea pigs in an experimental TB ward, exposing them to the patients there without direct contact, and counting the number of pulmonary

granulomatous lesions [12]. Notably, a single bacillus within the lung can induce the development of a lesion, which heightens the transmissibility of the disease [13]. That being said, while approximately 1.7 billion people are infected with Mtb, only those with active disease are infectious. It has been increasingly difficult to predict the intricacies of transmission and the required quantity of Mtb that must be aerosolized from a host to establish infection, especially considering the variable lengths of time between a contact event and the formation of disease. The most straightforward explanation directly correlates the number of bacilli in an infected person's sputum to the likelihood of developing active TB, and that individuals with more severe disease likely produce higher numbers of infectious droplet nuclei at an elevated rate [5]. The most infectious individuals are sputum (smear) and culture positive for bacteria, where approximately 43% of people produce respiratory droplets with culturable bacilli, and only a quarter of droplets contain more than 10 bacilli [14, 15]. Smear negative and culture negative people have an extremely low risk of transmitting infection [14]. Still, only approximately 28% of individuals with active disease produce culturable bacteria in their aerosols [16]. Modeling data demonstrates that the likelihood of Mtb transmission is proportional to the duration of exposure to an infectious person and inversely proportional to the volume of space in which the exposures occur [17].

Unfortunately, Mtb transmission is likely not as straight forward as a correlation of bacterial quantity in respiratory secretions. Multiple factors must be considered, including: 1. infectious individuals, 2. susceptible individuals, 3. environment, and 4. the inherent biological features of the pathogen itself. The prevalence of people with active disease, the quantity of those who may come in close contact, and the frequency and proximity of interactions between infectious and susceptible individuals all play a role in disease transmission. Other host factors include co-infection (especially of human immunodeficiency virus (HIV)), comorbidities (diabetes), smoking, excessive alcohol use, and malnutrition, which can increase susceptibility to TB [18]. Additionally, environmental factors can increase transmissibility, including closed, indoor spaces with limited air circulation and humidity, which affects the settling and evaporation of droplet nuclei [12]. The bacteria itself also plays a role, as some strains are more easily transmitted and potentially better adapted for airborne survival [18, 19].

1.1.3 Diagnosing Tuberculosis

Accurate and rapid diagnosis is the key to controlling TB, yet there are no simple, reliable, and widely available tests to definitively diagnose the disease [20]. Clinical guidelines have been developed by the WHO for the identification of latent and active TB, however, adoption of these methods varies by region, and TB diagnosis is often delayed due to limited access to diagnostic and treatment services in high burden countries. This hinders the potential for treatment initiation and increases the risk of transmission in communities [21]. Therefore, diagnostics have been revised, and TB testing is generally grouped into two categories: triage tests and confirmatory tests. Triage testing is designed for at-risk individuals who may have the disease and require further investigation [22]. Implementation of triaging may improve case finding and reduce overload of health systems, which makes addressing TB more cost effective, as expensive confirmatory testing is only offered to patients with high probability of disease [23].

Most triage testing screens simply for TB symptoms, which may miss asymptomatic or minimally symptomatic cases. More recent approaches involve chest x-rays, to determine if pulmonary lesions are present, and sputum smear examination for Mtb [22, 24]. Although these methods have helped identify millions of TB cases, there are also limitations. Sputum smears lack sensitivity, and chest x-rays alone can be not only be inconclusive but the availability of high-quality radiography is limited, especially in resource poor countries and communities. Sputum culturing, while more specific to Mtb, is time consuming (identification can take up to 42 days) and requires specialized laboratory facilities. Another triage diagnostic, which is not yet widely implemented, includes testing for elevated C-reactive protein in blood, which is indicative of inflammation or infection (but not necessarily Mtb). Overall, triaging has led to the identification of millions of cases worldwide, and is considered a more effective option, allowing clinicians to identify the patients who need expensive, and sometimes difficult to obtain, confirmatory testing [22].

Confirmatory testing, which is used to confirm disease and justify starting treatment regimens, can identify Mtb, or components of bacteria, in sputum, blood, and urine. The RIF Ultra test, which is recommended by the WHO as the first line test for diagnosing TB, can be performed on sputum. This test detects Mtb-specific amino acid sequences. It is quick (takes on average 2 hours) and highly sensitive, although it can be quite costly. This method can even identify the presence of specific rifampin resistance genes, which are responsible for 95% of rifampin resistant strains of Mtb [22]. Similarly, the Xpert MTB test also detects nucleic acids and can quickly provide test results, usually within 30 minutes of blood collection, but is also very expensive. This method, when compared to standard smear microscopy methods, is estimated to increase TB detection by 23% [22, 25]. Other tests can be performed on urine samples for the presence of biomarkers, like lipoarabinomannan (LAM), a glycolipid component of the mycobacterial cell wall that is shed during bacterial replication, or short extracellular Mtb DNA fragments. These tests may be especially beneficial for HIV^+ individuals or those with extrapulmonary Mtb infection [22]. Although diagnostics have advanced substantially, fast and reliable methods that can differentiate between active and latent Mtb infection are also lacking. The current routine diagnostics for latent TB, although they cannot distinguish between latent and active disease, are the tuberculin skin test (TST) or interferon-gamma release assays.

1.1.4 Clinical Tuberculosis Disease

Historically, TB disease has been described simply as latent or active disease. Based on this classification system, the majority of TB cases are defined as latent infection, where bacilli exist in a dormant state; on average, only 5 – 10% of infections develop into active or clinical TB, and it usually occurs within 5 years of infection [26]. Although useful, this binary classification does not account for variability in symptomology, immune responses, and bacterial activity; it is now clear that the disease exists within a continuous spectrum of bacterial activity and immune responses. New stages of TB disease have recently been proposed: latent, incipient, subclinical, and active/clinical. These additional stages aid

in preparing diagnostic and therapeutic interventions, allowing clinicians to better prevent infection from progressing into clinical disease [27].

Once Mtb infection has been established in a host and evaded the immune response, the bacteria will colonize, and infection will remain as a latent infection or undergo rapid/slow progression through incipient and subclinical stages into active disease. Latency is the most common course. There is no way of predicting who will progress into active TB, however, underlying risk factors like comorbidities, poor immunological responses, or larger Mtb inoculum are strongly correlated to advanced disease.

Latent TB (LTB), according to the WHO, is evidence of Mtb infection without clinical, radiological, or microbiological evidence of active TB disease (**Figure 1**). Currently, there is no direct way of confirming LTB or microbiological load at this stage [27]. Incipient Mtb infection is the most difficult to diagnose and has the least amount of laboratory and clinical evidence of infection. This stage is marked by the presence of viable Mtb that likely alternates between periods of dormancy and reduced metabolic activity. Incipient TB will probably progress into active disease, but patients do not yet have clinical symptoms, radiographic abnormalities, or microbiologic evidence consistent with active TB disease, and are likely not infectious (**Figure 1**) [27, 28]. Subclinical TB disease, again, does not show clinical symptoms but TB-related abnormalities can be detected using radiologic or microbiologic assays (**Figure 1**) [27]. It is possible that bacteria are replicating and metabolically active at this stage, which also means patients may be infectious [27, 28]. This stage was created primarily due to patients that are culture positive with radiological chest abnormalities, but symptom-free; an estimated 34% to 68% of sputum smear positive patients have no symptoms [29]. Finally, active TB disease has viable, replicating Mtb that results in characteristic clinical symptoms, which typically includes chronic cough (>2 or 3 weeks duration) but may also involve chest pain, dyspnea, and bronchiectasis (**Figure 1**) [30]. Patients will also have radiographic abnormalities and microbiologic evidence of infection [27, 28].

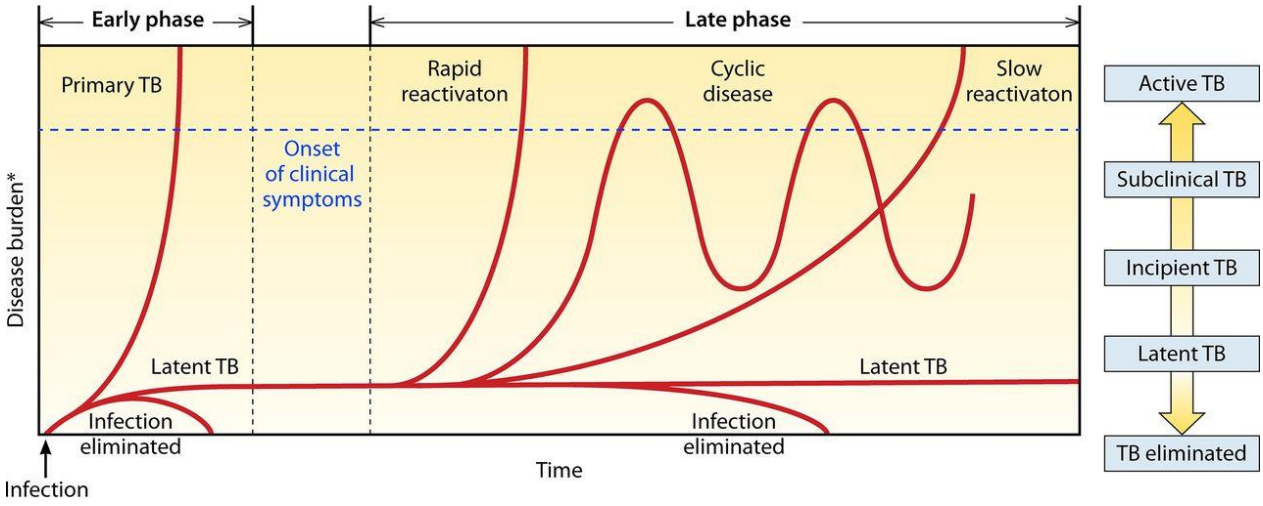

Figure 1: Stages of Clinical TB Disease. Adapted from Drain et al [27].

1.1.5 Immunopathogenesis of Tuberculosis

TB is primarily considered a pulmonary disease, but bacteria can disseminate to extrapulmonary tissues in approximately 15 – 20% of cases. Aerosolized Mtb is inhaled through the nose and mouth, passes through the trachea, bronchus, and bronchioles before reaching the alveoli in the lung. Along this route, the bacteria encounter numerous obstacles, including the respiratory mucosa, which consists of epithelial cells, a layer of connective tissue and resident immune cells called the lamina propria, and a coat of airway surface liquid. Once Mtb has entered the body, it will either be eliminated by innate immune responses, adhere and replicate into active clinical disease, or persist in quiescent forms.

Mtb is an obligate intracellular pathogen, which may be its most valuable defense mechanism, as that allows the bacteria to protect itself from host defenses. Bacteria largely inhabit phagocytic cells in the lung, allowing Mtb to hide from the immune response. The bacteria's survival within these host cells is dependent upon its ability to manipulate host immunity. Professional phagocytic cells, especially macrophages, encounter and endocytose the bacteria. Normally, the pathogens are eliminated via the phagolysosome, but Mtb is unique in that it can evade degradation by both modulating cellular trafficking of phagosomes and preventing maturation of phagolysosomes, which allows the bacteria to reside within the cell intact [31]. Additionally, Mtb contains numerous virulence factors that promote cellular necrosis,

and in doing so bacterial dissemination, instead of traditional apoptotic processes that facilitate bacterial eradication and adaptive immune responses. For example, Mtb interferes with the formation of apoptotic cell envelopes, and creates disruptions in the plasma membrane that promote necrosis [32, 33].

Infection and disease occur in multiple stages. In the first, bacilli are phagocytosed by alveolar macrophages, and either destroyed or become chronic inhabitants. In the next stage, the bacteria undergo replication but do not cause damage to host tissues. This is followed by a period of cellular necrosis, then clinical disease and cell-mediated immune responses. The final stage, where bacilli evade host defenses, results in caseous granulomas and robust bacterial replication [34]. These events, and their cellular constituents, are described more in-depth below.

1.1.5.1 Innate Immune Responses

The innate branch of the immune system is considered the body's first line of defense, as it recognizes pathogens and initiates adaptive immune responses. Cellular components of the innate immune response include macrophages, neutrophils, and dendritic cells. Of note are the airway epithelial cells (AECs), which are the first host cell to encounter Mtb as it traverses the lung. AECs constitutively express toll-like receptors (TLRs) which recognize bacterial antigens and initiate inflammatory signaling. Studies suggest that TLR signaling, which is dependent on the TLR mediator molecule myeloid differentiation factor 88 (MyD88), is crucial for innate immune responses against Mtb. Upon recognition of pathogens, AECs attempt to clear the pathogen by phagocytosis, as well as secrete antimicrobial peptides, like bactericidal secretory leukocyte proteinase inhibitor (SLPI), enzymes, reactive oxygen species (ROS), nitric oxide (NO), and pro-inflammatory mediators. Although Mtb clearance by AECs is unsubstantial, they play a considerable role in recruiting immune cells to the site of infection.

Alveolar resident macrophages may be considered the most important innate immune cell involved in Mtb infection, as they are the predominant host cell implicated in entry, growth, and restriction of Mtb. Although functionally similar, tissue-resident macrophages are phenotypically distinct

from circulating ones [35]. Macrophages recognize pathogens through their TLRs and phagocytose them; their ability, or inability, to successfully kill the bacteria dictates if infection persists. Successful phagocytosis involves endocytosis of the bacilli into an intracellular phagosome, which fuses with a lysosome to form a phagolysosome. This structure undergoes acidification of the vacuole, activating digestive enzymes and reactive molecular species that, together, degrades the pathogen. In many cases, the bacteria can manipulate host machinery, evading degradation and existing within the cell.

Dendritic cells (DCs), which bridge innate and adaptive immunity by presenting antigens, are robust in the respiratory tract and play a part in the immune response to Mtb [36]. Their role is not straight forward, as contradicting reports state that DCs are ineffective at mediating T cell responses during infection, while other state that they are instrumental. DCs identify, phagocytose, and degrade pathogens, which allows them to process and present antigen. Activation of DCs results in upregulation of major histocompatibility complex (MHC) I and MHC II, as well as other markers of an activated or pro-inflammatory phenotype, including the co-stimulatory markers CD40, CD54, CD58, CD80, and chemokine receptor 7 (CCR7). They also increase production of pro-inflammatory cytokines such as interleukin-12 (IL-12), tumor necrosis factor (TNF), interleukin-1 (IL-1), and interleukin-6 (IL-6). Altogether, these changes allow DCs to migrate to draining lymph nodes where they prime naïve T lymphocytes, initiating adaptive immune responses.

Neutrophils, the most abundant leukocyte in the blood, are a major component of the innate immune response to Mtb, although their exact role is unclear. Neutrophils have shown protective roles in non-human primate models of TB, and an inverse correlation is observed between neutrophil counts and risk of infection in humans, highlighting their importance in the early immune response to infection [37, 38]. Alternatively, other studies show that depleting neutrophils did not change the pathology caused by Mtb. Neutrophils are experts at chemotaxis, using C-X-C motif chemokine receptor (CXCR) 1 and 2 (CXCR1 and CXCR2) to quickly follow an interleukin-8 (IL-8) gradient towards sites of infection [39]. As such, they appear in large numbers immediately following infection. Similar to the function of macrophages, neutrophils can phagocytose pathogens, but are primarily associated with the release of

secretory vesicles containing enzymes and ROS into the extracellular space that degrade bacteria [40]. They can also secrete mycobactericidal peptides, which are identified in high concentrations at sites of Mtb pulmonary infection. Not only do these peptides kill bacteria, but they can enhance macrophage-mediated killing [40]. While effective at eliminating pathogens, degranulation results in massive cellular death and tissue destruction, and must be tightly managed. These cells can also produce neutrophil extracellular traps (NETs), structures composed of proteins like chromatin and cellular DNA which can catch pathogens, limiting bacterial dissemination to other organs and increasing recognition by passing immune cells. While this may be beneficial early in infection, NETs themselves do not degrade Mtb and may actually promote pro-inflammatory responses and tissue damage [41]. Though neutrophils play an important role in early disease, accumulation of neutrophils is observed in patients with active disease. Therefore, their continued presence within the granuloma exacerbates inflammation, bacterial dissemination, and, subsequently, disease severity [42, 43].

Other innate lymphoid cells, such as natural killer (NK) cells or γδT cells, a unique lymphocyte that is present in both innate and adaptive immunity, are involved in the cellular response to Mtb. NK cells can directly degrade Mtb by secreting bactericidal molecules. They also indirectly contribute to bacterial elimination by inducing apoptosis of infected cells and activating immune cells through production of interferon-γ (IFN-γ) and TNF [43, 44]. γδT cells respond rapidly to mycobacterial antigens and express a variety of effector functions [45].

In other infectious diseases, recruiting phagocytic innate immune cells can eliminate pathogens, but this response is ambiguous in TB. Overall, the dynamic innate immune response during TB has little antibacterial impact but is instrumental in generating adaptive immune responses. Maturation of Mtb-specific lymphocytes, in response to antigen presentation by innate cells, enhances cell-mediated bacterial killing.

1.1.5.2 Adaptive Immune Responses

The importance of adaptive immunity has been demonstrated both in humans, by studying disease

progression in HIV$^+$ individuals, and in animal models, where the T cell response has been manipulated. HIV infection is the biggest risk factor for reactivation of latent TB, and CD4$^+$ T cell deficiency implicated in acquired immunodeficiency syndrome (AIDS) exacerbates TB-associated pathology [46]. Similarly, mouse models deficient in CD4$^+$ T cells demonstrate increased susceptibility to Mtb infection and a reduction in early interferon responses [47].

In both humans and mice, generation of adaptive immunity in response to Mtb is delayed compared to that of other pathogens; adaptive immune responses occur, on average, 42 days following exposure in humans or 11 – 14 days in mice [48, 49]. Delayed lymphocyte recruitment allows for sufficient infection of alveolar macrophages, which permits the bacteria to multiply and disseminate. This delay is likely because live bacteria must be transported by DCs to the lung-draining lymph node (LDLN), which occurs 9 – 11 days after infection. In the LDLN, DCs initiate priming and activation of Mtb-specific T cells through MHC-mediated antigen presentation, specialized co-stimulatory signals, and cytokine production. This has been shown in numerous studies, where transfer of naive CD4$^+$ T cells specific for Mtb antigens also show delayed lymphocyte activation following aerosol infection [48]. Initiation of lymphocyte responses is increasingly complex in TB, as only lymph node residing DCs are known to facilitate proliferation of Mtb-specific CD4$^+$ T cells; Mtb-infected DCs infiltrating the lymph node likely release soluble, intact bacterial antigens that are taken up by uninfected, resident DCs that more efficiently facilitate CD4$^+$ T cell expansion [50, 51].

Following stimulation, T cells leave the lymph nodes and migrate to sites of infection, following a cytokine gradient produced by innate immune cells. The primary mediators of protection by adaptive immunity are IFN-γ-expressing helper type 1 T cells (TH1 cells). It is well established that deficits in TH1 cytokine production, particularly of IFN-γ, increase the risk of TB disease progression in humans [51]. Secretion of IFN-γ by T cells induces nitric oxide-mediated apoptosis and killing of Mtb by macrophages that is independent of autophagy; mice deficient in IFN-γ exhibit increased tissue necrosis and mortality in response to Mtb infection [52, 53]. These CD4$^+$ T cell responses are critical in determining whether disease is controlled or progresses into more severe pathology; certain T cell

specificities are more important for mycobacterial control than others [54]. While IFN-γ is protective, latent disease (as opposed to active disease states) is correlated to high quantities of polyfunctional IFN-γ^+TNF$^+$IL-2$^+$ CD4$^+$ T cells [51]. That is likely because TNF production mediates lymphocyte recruitment to sites of infection, organization of the granuloma, and expression of anti-inflammatory molecules. Similarly, IL-2 promotes T cell proliferation and differentiation into effector cells [55]. Therefore, the combined production of these cytokines enhances protection. In addition to the previously mentioned cytokines, interleukin-17 (IL-17)-expressing T cells (TH17) demonstrate a role in protection against Mtb. IL-17 signaling allows T cells to localize within lymphoid follicles in the lung and activate macrophages, as well as recruit early (and therefore protective) neutrophil responses [51].

While CD4$^+$ T cell responses have been highly implicated in disease severity, CD8$^+$ T cells also play a role. Latently infected individuals demonstrate increased cytotoxic activity compared to those with active disease. High Mtb burden may be a determinant of CD8$^+$ T cell responses, as high bacterial antigen levels are correlated with CD8$^+$ T cell dysfunction [51]. Additionally, CD8$^+$ T cells can also produce IFN-γ, although not to the same extent as CD4$^+$ T cells. Overall, the production of multiple cytokines by infiltrating T cells stimulates immune cell function and mediates the balance between pro- and anti-inflammatory signaling, which is critical for controlling bacteria and preventing excess tissue damage.

1.1.5.3 Peripheral Pathology and the Formation of the Granuloma

The defining pathology of TB is the formation of the granuloma, which are organized aggregates of macrophages, neutrophils, DCs, B cells, T cells, NK cells, and fibroblasts that most often arise in response to a single bacterium [56]. It was once considered that granuloma formation was protective, to prevent bacterial dissemination, especially considering only a small proportion of Mtb infected individuals develop active disease. Unfortunately, granulomas not only provide an ideal microenvironment for Mtb survival but can actually promote bacterial dissemination [57]. Although the structure of a granuloma has been well described, its composition can be highly variable; between individuals, and even within the same respiratory tract, unique granulomas form that progress

independently over time, with different inflammatory profiles, sizes, and bacterial ecology [58].

The primary cellular component of the granuloma is the macrophage. Infected alveolar macrophages release factors, including IL-8, chemokine ligand 2 (CCL2), chemokine ligand 3 (CCL3), chemokine ligand 4 (CCL4), chemokine ligand 5 (CCL5), and TNF, that recruit immune cells to the lung [59]. Newly arriving liver-resident and blood-derived macrophages phagocytose Mtb and aggregate together, resulting in the development of the early granuloma (**Figure 2**). While macrophage populations are highly motile under normal physiological conditions, during granuloma formation they undergo various morphological changes and become static [60]. They can also differentiate into foam cells, which are characterized by triglyceride accumulation, and transform into epithelioid cells (or epithelioid histiocytes) that upregulate adhesion molecules to increase contact with adjacent cells [61, 62].

DCs also phagocytose Mtb, presenting microbial antigens that stimulate lymphocytes. As the granuloma matures, and the adaptive immune response is generated, macrophages are surrounded by a cuff of $CD4^+$ and $CD8^+$ T lymphocytes, NK T cells, and B lymphocytes (**Figure 2**). T cells within the granuloma are mobile and produce a moderate amount of cytokines; on average, < 10% of the T cells within granulomas are cytokine-producing [63]. There are numerous hypotheses regarding the low level of T cell responsiveness, including decreased stimulation by other immune cells and the spatial organization of cells within granulomas, where T cells are limited to the outer layer [63]. Regardless, they play a substantial role in controlling infection and balancing anti-inflammatory versus pro-inflammatory signaling. Initial pro-inflammation leads to remodeling within the granuloma and necrosis, whereas anti-inflammatory mediators resolve inflammation and limit tissue damage [63, 64].

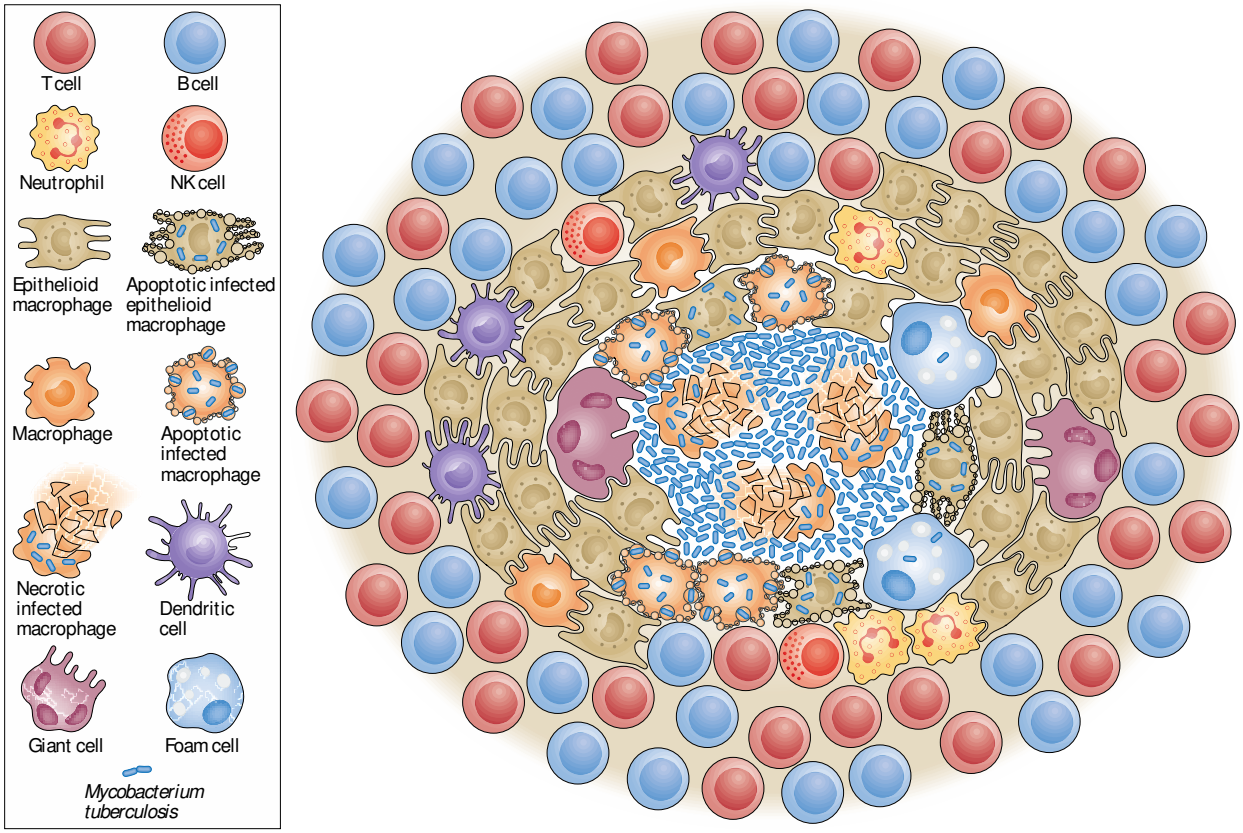

Figure 2: Cellular Composition and Organization of the Tubercular Granuloma. Adapted from Ramakrishnan [57].

Multiple types of granulomas can form, but TB is typically associated with caseous necrotic granulomas. Within the core of the granuloma, cellular debris, caused by necrotic cell death, accumulates; this leads to the formation of a soft, cheese-like consistency called caseum. Granulomas can also be characterized as non-necrotizing, neutrophil-rich (where the necrotic core is infiltrated by neutrophils), calcified (where the necrotic core is mineralized), fibrotic (encapsulated by a layer of fibrotic tissue as a result of fibroblast infiltration), or cavitary (when necrosis invades through the wall of an airway, distorting the structure, and causing discharge of necrotic debris into the bronchial tree) [65, 66].

Unfortunately, while the granuloma does sequester bacteria, Mtb exploits the structure in order to proliferate and disseminate throughout the host lung and extrapulmonary tissues. Macrophages are continuously recruited to sites of infection, through bacterial induction of epithelial matrix metalloproteinase-9 (MMP9) [67]. Mtb itself actually drives granuloma formation, through microbial

production of Early Secreted Antigenic Target 6 (ESAT-6), which mediates not only macrophage aggregation but reduces their motility, increasing the likelihood they will phagocytose bacteria or pathogen-riddled necrotic cells and become infected themselves [68, 69]. The constant recruitment of macrophages to the granuloma allows for continuous turnover of viable host cells, permitting Mtb to persist within granulomas for as long as decades [59]. This process also facilitates intercellular bacterial spread, as it increases the likelihood that newly infected macrophages will egress from the primary granuloma, initiating secondary granulomas and potentially disseminating to extrapulmonary tissues, which is known as miliary TB [57]. Typically, Mtb disseminates first to vascular organs like the liver and spleen, although bacteria can disseminate to any organ [70, 71].

1.1.4 Tuberculosis of the Central Nervous System

As mentioned above, TB is primarily considered a pulmonary disease, but it can affect every organ, including the brain. In 1.3% of TB cases, or 6.3% of extrapulmonary TB cases, Mtb disseminates to the central nervous system (CNS). The most common form of CNS infection is TB meningitis (TBM), but tubercular encephalitis, intracranial tuberculoma, or tuberculous brain abscesses can also occur [72]. TBM is considered the most severe form of extrapulmonary disease, with a 30 – 60% mortality rate for adults and 4 – 20% for children [73]. Children and people co-infected with HIV are more at risk for bacterial dissemination to the CNS. Other risk factors include malnutrition, alcoholism, malignancies, and use of immunosuppressive drugs. Adults with TBM often present with fever, headache, stiff neck, and neurological deficits like behavioral changes and alterations in consciousness. Children with TBM show similar signs, but will often also present with seizures, abdominal symptoms like nausea, and neurological symptoms ranging from lethargy to coma [72].

Dissemination to the brain occurs when bacteria are trafficked by macrophages and DCs to distant sites in the body; bacteria typically disseminate to highly oxygenated tissues, which includes the brain. Disease begins with the development of small TB foci in the brain, spinal cord, or meninges. The

location of the foci and the immune response to infection determines the extent of disease [72]. The blood-brain barrier (BBB) is specifically designed to keep pathogens out, which makes dissemination to the CNS perplexing. It is likely that local production of TNF increases BBB permeability, allowing infected immune cells or bacteria to infiltrate the brain [74]. Once Mtb has penetrated the CNS, it can infect microglial cells, in a similar fashion to alveolar macrophages, and replicate. Microscopically, TBM and intracranial tuberculomas consist of accumulated granulomas (both necrotic and non-necrotic) at the meninges and in the brain parenchyma. TBM is also characterized by the formation of a dense exudate composed of erythrocytes, neutrophils, macrophages, and lymphocytes; the exudate envelops arteries and nerves, reducing flow of cerebral spinal fluid (CSF) that causes hydrocephalus. Vasculitis also develops in the vessels of the circle of Willis, the vertebrobasilar system, and the perforating branches of the middle cerebral artery [72]. TB abscesses do not present with granulomas; instead, viable bacilli are found within accumulations of neutrophils and pus, surrounded by a capsule [73].

Many models of TBM and CNS TB have been used, which typically involve intracranial injections of Mtb or *Mycobacterium bovis* into guinea pigs, mice, and rabbits. These models demonstrate that bacterial infection of the brain results in rapid onset of TBM with clinical symptoms. These methods also initiate acute inflammatory responses, infiltration of lymphocytes, microglial activation, elevated chemokine levels in the CSF, and bacterial growth in both brain and CSF [72].

1.1.6 Treating Tuberculosis

Treatment for TB is designed with the following aims: eliminate bacterial infection, restore quality of life, prevent relapse, reduce transmission, and to reduce the development and transmission of drug resistance [75]. The treatment regimen prescribed is dependent upon disease state, risk factors and other comorbidities, and Mtb drug susceptibility. In standard cases, patients undergo a 2-month period of intensive antibiotics with isoniazid, rifampicin, pyrazinamide, and ethambutol (intensive phase), followed by 4 months of rifampicin or isoniazid (continuation phase). In areas where isoniazid resistance is common or in repeat cases, 6 months of treatment with rifampicin, ethambutol, pyrazinamide, and

levofloxacin is recommended. Patients with multidrug- or rifampicin-resistant TB are typically treated with a 9 – 11-month regimen of anti-TB agents. If this fails, longer, upwards of 20 months, regimens of anti-TB drugs can be prescribed. Advised drug regimens are lengthy, involving multiple months of daily treatment, and the antibiotics are often associated with adverse side effects including hepatotoxicity and gastrointestinal issues. As a result, poor treatment compliance is common, which has only exacerbated disease transmission and drug resistance [75].

1.2 Alzheimer's Disease and Alzheimer's Disease Related Dementias

1.2.1 History and Epidemiology of Alzheimer's Disease

In November 1901, a 50-year-old woman named Auguste D was admitted into the Frankfurt Psychiatric Hospital. Complaining of sleep disruption, disturbances of memory, aggressiveness, crying, and progressive confusion, Dr. Alois Alzheimer documented her symptomology and, following her death in 1906, distinctive neuropathology. From Auguste's unique clinical presentation rose the first known case of Alzheimer's Disease (AD) [76, 77]. Later, in 1911, Alzheimer made the first official diagnosis of AD in a male patient named Josef F [78].

Today, AD is the primary cause of dementia in elderly populations and affects approximately 32 million people globally. The prevalence of prodromal AD increases exponentially with age; approximately 2.7% between 60 and 64 years of age, to as high as 25.8% by ages 85 – 90. AD dementia is also more common among women than men [25]. Devastatingly, cases of AD are expected to reach as many as 150 million worldwide by 2050 [79].

1.2.2 Clinical Symptomology and Neuropathological Progression of Alzheimer's Disease

Impaired memory is the hallmark clinical presentation of AD. Initially, it is characterized by subtle memory deficits, for example, misplacing objects, forgetting conversations, problems remembering names, and missing appointments, that progress in severity over time. AD does not always present as a neuropsychologically homogeneous disease with an initial memory deficit followed by cognitive

impairment; some patients can have deficits in multiple areas of cognition, like executive functioning, especially in early stages of the disease [80]. A study conducted on AD patients showed that 79% of the patients had both verbal and visual memory deficits, 6% had only visual memory deficits, and 7% had only verbal memory affected. Interestingly, memory loss is not initially identified in all cases of AD [81]

Stages of AD, including a preclinical phase, prodromal phase, and clinical phase, have been proposed. Using this scheme, the preclinical stage is where amyloid and tau begin to accumulate; misfolded proteins are likely present in CSF and positron emission tomography (PET) imaging. At this stage, there are no signs of neurodegeneration, and cognition/memory are considered normal, although evidence of a delayed learning curve and recall may be present. There could be signs of behavior changes like apathy and irritability. In the prodromal stage, more misfolded proteins are accumulating, and there is evidence of mild cognitive impairment. This includes obvious episodic memory loss, repeated questions, misplacing items, disorientation, and reduced executive abilities like problem solving and decision making. A person's ability to function daily might be impaired at this stage. The clinical stage is characterized by dementia, substantial misfolded protein deposition, and neuronal loss or dysfunction [82, 83].

AD neuropathology is defined by both macroscopic and microscopic features. Macroscopically, moderate brain atrophy is typically seen, especially of the frontal and temporal cortices, amygdala, and hippocampus that likely results in decreased brain weight. While these changes are usually seen in those diagnosed with AD, they are not specific to AD and people without the disease may also show cortical atrophy. Another common feature of AD is the loss of neuromelanin pigmentation in the locus coeruleus which, again, is not necessarily specific to AD [84].

Microscopic changes are much more definitive for AD diagnoses, specifically, the presence of extracellular amyloid plaques and neurofibrillary tangles. Tau aggregates are initially found in the medial temporal lobe structures, especially the hippocampus and entorhinal cortex, and then spread to temporal, parietal, and frontal lobe association areas. Aβ deposits in parietal, temporal, and frontal association areas [85]. Other misfolded protein pathologies can be identified, as well as glial inflammation. Ultimately,

synaptic loss and neurodegeneration results in clinical symptoms. One widely accepted hypothesis is that the clinical symptomology of AD results from degeneration of cholinergic neurons, which decreases acetylcholine (ACh) signaling in neuronal regions [86].

1.2.3 Diagnosis and Clinical Progression of Alzheimer's Disease and Alzheimer's Disease Related Dementias

Dementia is defined as the decline of memory and other cognitive functions. The classification of dementia subtypes has been routinely revised. The diagnosis of AD is largely a clinical one, as there is no definitive premortem test able to confirm the diagnosis during life, but the primary clinical criteria for the diagnosis of AD was created by the National Institute of Neurological and Communicative Disorders and Stroke and Alzheimer's Disease and Related Disorders Association in 1984. The criteria are broken into probable, possible, and definite disease. The criteria for diagnosis of probable AD include the following: 1. Gradual onset of dementia or memory loss established by clinical examination (Mini-Mental Test, Blessed Dementia Scale) and confirmed by neuropsychological tests, 2. Aphasia, apraxia, agnosia, or deficits in executive functioning, 3. Progressive worsening of memory and cognitive function, 4. No disturbance of consciousness, 5. Onset between ages 40 and 90, and 6. Absence of systemic disorders or other brain diseases [87, 88]. A diagnosis of probable AD dementia is supported by symptoms of depression, insomnia, hallucinations, and emotional outbursts. Possible AD dementia is typically made on a case-by-case basis, usually for research purposes, and encompasses the symptoms of probable disease with a gradually severe cognition deficit. This occurs in persons who meet the core clinical criteria for probable AD dementia, documented cognitive decline increases the certainty that the condition represents an active, evolving pathologic process, but it does not specifically increase the certainty that the process is that of AD pathophysiology [87, 88]. Cumulative evidence has defined a definite diagnosis of AD based on the presence of these three elements: clinical dementia (cognitive impairment with a memory component that impacts daily living skills), substantial numbers of neocortical neurofibrillary tangles (NFTs) at autopsy as quantified using Braak staging, and substantial numbers of amyloid plaques.

Medical diagnosis of AD can be difficult because many early symptoms are disregarded as normal consequences of aging [89]. Additionally, AD symptomology is shared with many other diseases, including manic-depressive disorder, Parkinson's Disease, multi-infarct dementia, and, in more rare cases, thyroid disease, pernicious anemia, luetic brain disease, infection of the CNS, subdural hematoma, occult hydrocephalus, Huntington's disease, Creutzfeldt-Jakob disease, and cancer [87]. These shared symptoms between a variety of disorders make it increasingly challenging to differentiate AD.

Cumulative evidence from patients clinically diagnosed with the disease suggests that the pathophysiological process of AD begins years, sometimes even decades, before clinical diagnosis. For this reason, and the progressive nature of the disease, staging schemes have been implemented. Typically, AD is defined by mild, moderate, and severe dementia. Recently, more thorough dementia staging schemes (1 – 6) have been implemented based on cognition, function, behavior, and disease-specific biomarkers. Stage 1 shows no abnormalities of cognition. Stages 2 and 3 are preclinical stages, where memory and cognition are compromised compared to a person's baseline, but in stage 3 a person's ability to perform daily tasks is affected. Behavior changes characteristic of preclinical stages include irritability and apathy. Stage 4 is considered mild dementia; patients show episodic memory loss, such as decreased learning, but can function normally and show no overt clinical symptoms. Stage 5 is considered moderate dementia, where there is extensive impact to an individual's ability to function daily, and they often require assistance to perform daily tasks. Stage 6 is severe dementia; people likely cannot even perform self-care at this stage. Grouping individuals into these refined clinical stages may be beneficial in creating treatment regimens and selecting participants for trial or research participation.

1.2.4 Etiology of Alzheimer's Disease

The complete etiology of AD is not well understood, but current evidence from human patients and experimental models describe multiple possible etiologies, including genetic mutations, exposure to environmental neurotoxicants, and infectious agents.

1.2.4.1 Genetics

The heritability is AD is high, estimated to be the cause of between 60% and 80% of cases [90]. The first three genes discovered that can cause early-onset AD are *APP*, which encodes the amyloid precursor protein, as well as *PSEN1* and *PSEN2*, both of which encode presenilins 1 (PS1) and 2 (PS2), respectively. Mutations in the *APP* gene result in altered cleaving of the amyloid precursor protein (APP), which causes accumulation of the neurotoxic 42 amino acid peptide ($A\beta_{1\text{-}42}$) [91]. PS1 is the catalytic subunit of γ-secretase, the protease that cleaves APP. Mutations in the *PSEN1* gene result in an increased ratio of neurotoxic $A\beta_{1\text{-}42}$ proteins and loss of presenilin functions in the brain, which contribute to neurodegeneration [92]. In *PSEN1* alone, over 150 mutations in 400 pedigrees have been reported. Alternatively, mutations in *PSEN2* are rare, causing partial loss of function of γ-secretase [91]. Another gene, which is typically associated with late-onset AD, is *APOE*, which encodes apolipoprotein E (ApoE), a serum cholesterol carrier synthesized by astrocytes that supports lipid transport and injury repair in the brain. There are three major known isoforms, 2 (ApoE2), 3 (ApoE3), and 4 (ApoE4); others exist but are extremely rare. ApoE4 is strongly associated with risk for AD, as it binds $A\beta_{1\text{-}42}$ and encourages deposition of senile plaques [93].

1.2.4.2 Infectious Agents

Infectious agents, including viruses and bacteria, have been routinely implicated in AD neuropathogenesis. The basis of these hypotheses are centered on the presence of microbes in not only the brain of most elderly individuals but also in association with AD pathology, localized damage to the brain caused by infections, and that genetic polymorphisms common in disease also modulate immune function [94]. It is likely that multiple infectious agents, or infection combined with an environmental or genetic component, contribute to the manifestation of disease [95].

First established in the 1980s, the viral etiology hypothesis of AD posits that viruses in the brain contribute to the pathological progression of disease. Strong connections between herpesviruses and AD have been made, especially Herpes Simplex Virus-1 (HSV-1) and Herpes Simplex Virus-2 (HSV-2), as

well as Cytomegalovirus (CMV; HHV-5), Epstein-Barr Virus (EBV; HHV-4), Varicella-Zoster Virus (VZV; HHV-3), and Hepatitis C Virus (HCV), as detailed below.

Herpesviruses are large, double-stranded DNA viruses that establish lifelong latency; following initial primary infection, herpesviruses remain latent in cells specific to each virus, rarely causing death of the host [96]. HSV-1, which typically causes oral and sometimes genital herpes, is a widespread neurotropic virus that likely reaches the brain via retrograde transport through olfactory or trigeminal nerves, but could possibly enter by hematogenous dissemination. Infection of the CNS causes a rare form of encephalitis, as a result of primary infection and from reactivation of latent virus by stress or inflammation [97]. Viral DNA has been identified in post-mortem brain specimens from numerous AD patients, particularly in those who carry the type 4 allele of the gene that encodes apolipoprotein E (APOE4), another potential risk factor for AD [14, 56]. HSV-1 DNA has also been localized to amyloid plaques from the temporal and frontal cortices of those diagnosed with AD [58]. Prospective, population-based studies show people with positive titers of anti-HSV-1 IgM antibodies, which indicates primary or reactivated HSV-1 infection, increases the risk of AD [59]. Murine models of herpes simplex encephalitis (HSE), via inoculation with attenuated virus, resulted in persistent microglial activation followed by neuronal loss and behavior deficits; these neuropathologies increase susceptibility to neurodegenerative diseases [98]. This is just one example of how microbes play a role in AD pathogenesis.

1.2.5 Current Treatments for Alzheimer's Disease

There is no cure for AD, and current treatment options are merely symptomatic. The only drugs that have been approved by the Federal Drug Administration (FDA) are brexpiprazole, donepezil, galantamine, and memantine. Of these drugs, donepezil (Aricept), rivastigmine (Exelon), and galantamine (Razadyne), are acetylcholinesterase enzyme (AChE) inhibitors. It is hypothesized that many AD symptoms are caused by degeneration of cholinergic neurons. By inhibiting AChE, which hydrolyzes acetylcholine into acetic acid and choline, cholinergic neurotransmission is enhanced. While these drugs have shown some level of efficacy, it is only in mild to moderate disease, and they typically cannot be

used as the disease progresses. They are usually well-tolerated, aside from some side effects, including nausea, vomiting, diarrhea, loss of appetite, weight loss, bradycardia, dizziness, insomnia, fatigue, drowsiness, headache, and muscle cramps. A fourth drug, tacrine, is no longer in clinical use due to hepatotoxicity. Cholinergic enhancers have also been used to modulate cortical function but have not been remarkably successful in clinical trials.

The other approved drug, memantine (Namenda), is a non-competitive N-methyl-D-aspartate (NMDA) antagonist that works by regulating glutamate activation, thereby blocking the toxic effects associated with excess glutamate. This drug has been used to treat the symptoms of moderate to severe AD. Similar to the other approved drugs, side effects include dizziness, headache, diarrhea, constipation, and confusion [99].

1.3 Parkinson's Disease and Lewy Body Dementia

1.3.1 History and Epidemiology of Parkinson's Disease

It is understood that Parkinson's Disease (PD) was first described as long ago as 1000 BC in ancient Indian texts, which detailed tremor of the head, loss of movement, stiffness, stammering, dementia, and confusion [100]. Chinese texts from 425-221 BC describe a similar syndrome with limitation of movement, postural disturbances, stiffness, and tremor, which closely mimics modern-day PD [101]. James Parkinson was the first to medically describe PD in 1817, defining a disorder with "involuntary tremulous motion, with lessened muscular power, in parts not in action and even when supported; with a propensity to bend the trunk forward, and to pass from a walking to a running pace: the senses and intellects being uninjured" [102]. Later, scientists expanded upon James Parkinson's initial description, detailing the histological hallmarks of the disease. Édouard Brissaud was the first to distinguish the substantia nigra (SN) as the pathological origin of disease in 1899 [103]. Soon after, in 1912, Frederick Lewy identified aggregated inclusions in the SN, which are now known as the Lewy body [103]. Interestingly, it was not until 1960 that Oleh Hornykiewicz identified dopamine (DA), or to be more specific, the loss of DA, as the major contributor to PD symptomology [103].

Today, PD is the second most common neurodegenerative disease after AD, and the most prevalent movement disorder in aging populations [104, 105]. Assessments of PD burden worldwide vary between studies, but the Global Burden of Disease (GBD) study reported that the global estimates of PD prevalence and incidence were approximately 8 million and 1 million, respectively, in 2017 [106, 107]. Studies also predict that the burden of PD will grow substantially over the coming years [108]. This disease is strongly associated with aging; 1% of diagnosis are made in individuals at or above the age of 60, and 4 – 5% in individuals over the age of 80, with 60 years being the average age of onset [109, 110]. Not only is age a risk factor, but prevalence of PD in men is 1.5 – 2.0 times higher than in women; this disparity persists across age groups [110]. Despite these staggering statistics, it is possible that PD may actually be underrepresented within the context of neurodegenerative disease cases, as its overlap in clinical symptomology makes accurate diagnostics challenging [111].

1.3.2 Clinical Symptomology and Neuropathological Progression of Parkinson's Disease

Due to the heterogeneous nature of PD, classifying the disease into specific stages, which determines how advanced the disease is and allows clinicians to formulate treatment plans, has been challenging. The most prominent staging system, defined by neuropathology and clinical symptoms, describes several phases of PD: the risk phase, preclinical phase, prodromal phase, and clinical phase [112]. The risk phase, which occurs prior to neurodegeneration, is when genetic and environmental factors contribute to dysfunction in the SN. Following this period is the preclinical phase, where neurodegeneration is initiated. This is an asymptomatic stage without reliable biomarkers. Symptoms first become evident during the prodromal phase of PD, which can occur upwards of two decades before clinical diagnosis. Markers of the prodromal phase include rapid eye movement (REM) sleep behavior disorder (RBD), insomnia, hyposmia, autonomic dysfunction, behavioral changes, depression, anxiety, gastrointestinal dysfunction, and mild motor signs [112, 113]. Unfortunately, the majority of these symptoms lack specificity and therefore may be poor predictors of PD, though studies have shown that patients with tremor, balance problems, depression, constipation, fatigue, and urinary dysfunction are at

higher risk for developing PD than those without these symptoms [114]. Even if these early symptoms do not reliably predict PD, they often correlate to more severe motor symptoms in those diagnosed with the disease [115].

Motor symptoms fully manifest during the clinical phase of PD. These include bradykinesia (general slowness and paucity of spontaneous movement), axial rigidity, hypomimia (masked facial expressions), speech deficits, impaired handwriting and grip force, and tremor of fully resting limbs which is suppressed during the initiation of movement [116]. A resting, pill-rolling tremor of the hands, where the thumb and the index finger form circular movements, is a unique symptom of PD [117]. Notably, these presentations, especially bradykinesia and tremor, are asymmetric at onset and unlikely to become symmetrical as the disease progresses [118].

Pathologically, PD is characterized by a loss of dopaminergic neurons (DAn) in the substantia nigra pars compacta (SNpc) and striatum (ST). Motor symptoms manifest after degeneration has occurred in the nigrostriatal pathway; current data estimates that 40 – 60% of DAn have degenerated in the SNpc and 60 – 70 % of dopamine has been depleted in the ST by the clinical phase of the disease [112, 119-121]. Intraneuronal accumulation of proteinaceous aggregates of α-synuclein (α-syn) into Lewy bodies, a characteristic neuropathology of PD, contributes to neuronal loss. These aggregates spread throughout the brain as disease progresses, in Braak stages that can correspond to disease severity [122]. Initially, Lewy bodies are identified in the dorsal motor nucleus and, sometimes, in the anterior olfactory nucleus (stages 1 and 2). Synucleinopathy then spreads to the brain stem (stage 3), anteromedial temporal mesocortex (stage 4), neocortex (stage 5), and finally to the sensory and motor cortices (stage 6) [122].

1.3.4 Diagnosis and Clinical Progression of Parkinson's Disease and Lewy Body Dementia

Similar to AD, the diagnosis of PD is based on clinical symptomology, as there are no definitive, premortem tests available that can confirm the diagnosis. Biomarkers can be tested, such as detecting α-syn or neuroinflammatory markers in blood or cerebral spinal fluid (CSF), but these methods are not

always reliable [123]. This has led to three clinical diagnoses for PD: clinically possible PD, probable PD, and definite PD [124]. First, a history of premotor symptoms, including sleep-related REM sleep behavior, loss of smell, and constipation, are evaluated, followed by clinical examination for characteristic symptoms [125]. Possible PD is based on the presence of any two of the following motor features: recent onset resting tremor, rigidity, bradykinesia, and asymmetric symptomology, where at least one symptom is tremor or bradykinesia [124, 126]. Male PD patients typically present with akinesia, cognitive impairment, daytime sleepiness, and RBD more frequently than female PD patients, who usually present with anxiety, depression, and dyskinesia more frequently [110]. The patients must also not present with a feature characteristic of other another diagnosis and, if performed, a substantial response to a dopaminergic treatment such as Levodopa [126]. Clinically probable PD meets all the criteria for possible PD but encompasses the combination of three of the aforementioned motor features [124, 126]. Clinically definite PD meets the criteria for possible PD but includes a neuropathological component [124, 126]. Pathological features required for this diagnosis include neuronal loss, gliosis, and at least one Lewy body in the SN [126]. It has been suggested that adding other requirements, such as a five-year duration of symptoms, or emphasizing the response to dopaminergic drugs may improve diagnostic accuracy [127].

Neurodegenerative diseases share similar symptomology, which makes it increasingly difficult to accurately diagnose them. In fact, studies have shown that inaccurate diagnoses of PD are made in as many as 32% of clinical cases, and that current diagnostic capabilities have not advanced over the past few decades [127, 128]. Dementia with Lewy bodies (LBD) may be the best example of the difficulty in diagnosing this neurodegenerative disease. While PD and LBD clinically overlap, as they share neuropathologies including aggregation of α-syn into Lewy bodies as well as loss of DAn in the SN, they are, in fact, different disorders [129, 130]. The only true indication that PD-like disease presentation may be LBD is the time dementia presents relative to motor symptoms, as dementia arises after at least 1 year of motor symptoms in PD but may come earlier in LBD [129]. Other indications that PD-like disease may be LBD, or another disorder, are the absence of symptom asymmetry, extremely fast disease progression,

changes in eye movement, and indications of cerebellar dysfunction. PD is a progressive disease, so it is also unexpected to see severe cognitive deterioration or psychosis, drastic lower limb involvement, frequent falls, or marked autonomic dysfunction in early disease stages [125].

1.3.3 Etiology of Parkinson's Disease

The complete etiology of PD is incompletely understood, but current evidence from human patients and experimental models describes multiple possible risk factors. Most clinical cases of PD are idiopathic with unknown etiology; only 15% of PD patients have a family history of the disease, and 5–10% of PD patients have Mendelian inheritance. To date, the greatest risk factor is age, but studies have implicated exposure to environmental neurotoxicants and infectious agents in disease pathogenesis. It is likely that PD is a multifactorial disease involving many etiological factors that contribute to the progression of disease, as the vast majority of people with PD-related genetic mutations or who have been exposed to environmental risk factors rarely develop clinical disease.

1.3.3.1 Genetics

Five definitive causal PD genes have been identified: *SNCA* (*PARK1*), *Parkin* (*PARK2*), *PTEN-induced putative kinase* 1 (*Pink1; PARK6*), *Dj-1* (*PARK7*), and *Leucine-rich repeat kinase 2* (*Lrrk2; PARK8*). Of these genes, mutations in *SNCA* and *Lrrk2* are responsible for autosomal-dominant forms of PD, where one copy of an altered gene in each cell is sufficient to cause disease [131]. Rare mutations in *SNCA*, which encodes the α-synuclein protein, results in the formation of stable β sheets that exacerbate misfolding into neurotoxic oligomers and fibrils [132]. Mutations in *Lrrk2* are more frequent, of which over 50 have been described. This gene encodes the cytoplasmic protein leucine-rich repeat kinase 2 (LRRK2), which likely modulates kinase activity, although the exact mechanism is unknown [131]. Mutations in *Parkin*, *Pink1*, *DJ-1*, and *ATP13A2* are accountable for autosomal recessive modes of PD inheritance. *Parkin* mutations result in decreased catalytic activity of the ubiquitin E3 protein-ligase, aberrant ubiquitination, and impairment of proteasomal degradation [133]. The others, *Pink1*, *DJ-1*, and

ATP13A2, cause disturbances in mitochondrial function and oxidative stress [134-136]. Other genes have also been implicated in PD, including a total 15 causal genes and over 25 genetic risk factors [137].

1.3.3.2 Environmental Exposures

The number of PD cases without a genetic origin makes it clear that there is an environmental component to PD, although it is unknown if disease is caused by independent exposure or if it is the result of accumulative exposures across a person's lifetime. Several causative agents have been identified that induce neuropathologies similar to those recognized in idiopathic PD patients. These include neuroleptic drugs (risperidone, olanzapine, aripiprazole), trace metals (manganese (Mn), iron, selenium, copper), organophosphates, pesticides (paraquat and rotenone), and infectious agents [138].

1.3.3.2.1 Pesticides: Rotenone

While pesticides are used globally to control disease vectors and protect crops, they have also been heavily associated with neurological disease. Pesticides were first implicated in PD pathology when it was recognized that the structure of a commonly used herbicide, paraquat, closely resembled a neurotoxic metabolite of 1-methyl-4-phenyl-1,2,3,6-tetrahydropyridine (MPTP), MPP+ (1-methyl-4-phenylpyridinium). MPP+ is a mitochondrial complex-I inhibitor that selectively damages DAn in the SN [139]. Following this finding, the relationship between pesticide exposure, including paraquat, permethrin, dieldrin, and rotenone, and the risk of developing PD was more thoroughly evaluated [140].

Rotenone is a naturally occurring insecticide, pesticide, and piscicide derived from specific plants. Its reported use dates back hundreds of years, as native tribes used it to harvest fish. In the 1800's, rotenone's insecticidal effects were reported, and French botanist Emmanuel Geoffroy extracted it from the *Lonchocarpus nicou* plant. Since then, rotenone became one of the most widely used pesticides, insecticides, and piscicides, until its toxic effects became known in the 1990's [141].

It is now understood that rotenone is an inhibitor of mitochondrial complex I (by interrupting the activity of nicotinamide adenine dinucleotide-dehydrogenase (NADH-dehydrogenase)), which results in

the toxic production of superoxides and reactive oxygen species [142]. Its hydrophobic nature allows it to not only readily pass the BBB into the brain, but easily cross cellular membranes, causing systemic inhibition of complex I [143]. Interestingly, rotenone toxicity results in selective degeneration of DAn in the nigrostriatal pathway, formation of α-syn aggregates, glial inflammation, and behavior deficits that mimic PD [144].

1.3.3.2.2 Infectious Agents

The possibility that infectious agents contribute to neurodegenerative pathology, including PD, has been documented for over a century. This idea has been supported by individuals presenting with PD-like symptoms following infectious outbreaks of both viruses and bacteria. In fact, meta-analytic results suggest that infection with a biologic agent can increase a person's risk of developing PD by as much as 20% compared to controls [145].

Viral infections have been most highly implicated in PD, and the most well understood connection is through postencephalitic Parkinsonism, as demonstrated by the 1918 influenza pandemic ("Spanish Flu") caused by the H1N1 influenza virus [146]. Calculations estimate that approximately 500 million people were infected during this pandemic. A unique presentation, termed "encephalitic lethargica", was described among influenza patients, with some developing somnolence, ptosis, delirium, and parkinsonism.

It is expected that there are two pathophysiological mechanisms: immediate damage resulting in para-infectious (within 15 days from the initial infectious episode) PD and delayed mechanisms resulting in post-infectious forms of parkinsonism. It is thought that post-infectious Parkinsonism is caused by latent viral infection, resulting in persistent inflammatory processes, or pathogen-induced autoimmunity, where molecular mimicry between viral and host antigens produces damaging T and B cell responses [147]. Epitopes of herpes simplex virus 1 (HSV-1), identified in PD patient brains, are cross reactive with α-syn, which could stimulate T and B cell responses against neurons in the SN. In fact, antibodies specific to these HSV-1 epitopes have been identified in PD patients [148]. Similar cross reactivity was seen with

Epstein-Barr virus (EBV) [149].

Numerous other viruses have been associated with PD, including varicella zoster virus (VZV), West Nile Virus, Japanese Encephalitis Virus, HIV, and Western Equine Encephalitis Virus (WEEV) [150-153]. Most encephalitic viruses (West Nile Virus, Japanese Encephalitis Virus, and WEEV) cause immediate onset PD-like symptomology. These viruses enter the brain through peripheral nerves, cross the blood–brain barrier (BBB) or blood-cerebrospinal fluid barrier. They cause CNS damage or indirectly wreak havoc by inducing inflammation in the nigrostriatal pathway. Others, including influenza and HIV, are associated with delayed Parkinsonism, occurring months to years following initial infection [150-153]. Causal roles of neurotrophic bacterial infections have been implicated in PD, including Gram negative *Borrelia budgdoferi*, which is the causal agent of Lyme disease in North America. *Borrelia budgdoferi* infection damages the SN and causes a syndrome that resembles PD, although no epidemiological correlations have been made between areas high in incidence of Lyme disease and increased prevalence of PD [154, 155].

Constipation is one of the most common features of the prodromal phase of PD, which suggests that the gut microbiome may play a role is disease pathogenesis, and that the gut may even be the origin of PD pathology that subsequently spreads to the brain. The gastrointestinal tract typically contains over 1,000 bacterial species, and the composition of these strains is altered in PD patients [156]. Bacterial infections, and strains colonizing the gut microbiome, can stimulate pro-inflammatory immune responses and produce neurotoxic factors, such as endotoxins like lipopolysaccharide (LPS). It has been well described that LPS mediates aggregation of α-syn, which can travel from the gut to the brain via the vagus nerve [157, 158]. One pathogen commonly found in the gut microbiome is *Helicobacter pylori* (*H. pylori*), a Gram negative bacterium that can cause gastric and duodenal ulcers, those of which have been described in PD patients. As such, *H. pylori* infection results in a 1.5-3 fold increased risk of developing PD, depending on the study. Similarly, *Clostridium difficile* (*C. difficile*), which colonizes the intestines but can cause diarrhea and pseudomembranous colitis, is correlated to higher risk of PD [159]. While not as thoroughly explored as neurotrophic infections, bacterial infections in peripheral tissues have also been

implicated in PD. *Porphyromonas gingivalis* (*P. gingivalis*), which contributes to periodontitis and periodontal inflammatory disease (PID), infection may increase the likelihood of developing PD [160]. Patients with TB, caused by Mtb, independently have a 1.38-fold risk of PD [161].

1.3.5 Current Treatments for Parkinson's Disease

1.3.5.1 Clinical Treatments

Currently, there are no treatments in clinical use that modify or prohibit the pathological progression of PD; the most commonly prescribed treatments address PD symptoms or replace dopamine. The gold standard drug used today, despite its discovery sixty years ago, is levodopa, a precursor of dopamine that compensates for neurotransmitter loss in the nigrostriatal pathway [162, 163]. Levodopa is primarily absorbed in the small intestine and metabolized by the liver and kidneys; only 1% of the drug enters the brain [164]. Combined treatment with a dopa-decarboxylase inhibitor can increase levels up to 10% in the brain. While successful at rapidly ameliorating motor symptoms, including gait and speech disruptions, levodopa has five major pitfalls: inability to treat non-motor symptoms, severe side effects, short periods of effectiveness, clinical complications, and limited bioavailability in the brain.

While motor signs are alleviated with levodopa use, most of the non-motor symptoms, including cognitive dysfunction, dementia, confusion, and insomnia, do not respond to the treatment [165]. There is some evidence that anxiety, depression, and anhedonia may be addressed by levodopa [165]. Side effects of levodopa treatment, which can be both acute and chronic, include nausea, vomiting, anorexia, hypotension, chorea, dystonia, myoclonus, akathisia, and hallucinations [164]. Generally, women have greater responses to levodopa, due to increased bioavailability of the drug, but experience more levodopa-induced dyskinesias, mobility limitations, and sensory symptoms than men [166]. Many of these side effects can be addressed by reducing the dosage or combining drug therapies. Dopa-decarboxylase inhibitors (carbidopa/Lodosyn), anti-nausea drugs (diphenidol, cyclizine, ondasetron, hydroxyzine, granisetron/Kytril), or peripheral dopamine receptor blockers (domperidone) can be used to reduce the adverse effects associated with levodopa use [164]. Off-target effects in both the brain and the periphery

contribute to these side-effects; delivery to areas of the brain other than the ST, which is thought to be the basis for the occurrence of neuropsychiatric adverse effects, causes hallucinations and impulse control disorder.

Unfortunately, levodopa is only effective for a limited period of time, creating what is often referred to as the "honeymoon period", and therefore cannot be used long-term. Following the "honeymoon period" comes motor fluctuations and dyskinesia. Studies have shown that more than 50% of PD patients develop motor complications and/or dyskinesia after only 4 years of levodopa treatment (400 mg/day), and almost all patients experience dyskinesia following long-term treatment [167, 168]. Although men may exhibit more severe motor dysfunction, women are known to develop more dyskinesias [32,54,55]. This short window of effectiveness has led to controversy over both the appropriate time to initiate levodopa treatment and the proper dosage. It has been suggested that levodopa treatment should not be introduced until more severe stages of disease, as it does not slow disease progression. Use of other dopamine agonists, like pramipexole, can be used in clinical settings to lower the likelihood of dyskinesia presentation, but are only appropriate in mild cases, as they are unable to control severe motor disturbances [169].

An alternative to pharmaceutical treatment is deep brain stimulation (DBS), or the direct electrostimulation of the subthalamic nucleus (STN) or the globus pallidus internus (GPi). This treatment decreases the hyperactivity in these regions caused by loss of DA in the midbrain, and can therefore reduce the motor symptoms associated with PD. This therapy has its own challenges; it is highly invasive in nature, is not a viable option for many PD patients, does not address all motor symptoms, can induce adverse side effects such as aggravating gait freezing and worsening of verbal fluency, and speech is often not improved [170-174]. Optimal candidates for DBS are idiopathic PD patients, with motor fluctuations and levodopa induced dyskinesias; a patient's response to levodopa is the best outcome predictor [175].

1.4 Aging

Aging is defined as the inevitable process of gradual physiological deterioration experienced by all organisms with time, which increases the risk for disease and death [176, 177]. The rate of deterioration is incredibly complex, as it is dependent upon the species, cell or tissue, and physiological context of the particular organism. Biologically, aging is characterized by molecular changes and damage which leads to structural and functional deviances in cells and tissues, including loss of mitochondrial homeostasis, impaired intercellular communication, senescence, inflammation, and decreased regenerative capacity. Considering this, it is not surprising that age is the greatest risk factor for neurodegenerative disease.

Between 2020 and 2050, the population of people aged 60 years and over is expected to double, from approximately 1 billion to 2.1 billion; by 2030, it is expected that 1 in every 6 people worldwide will be aged 60 years or over. Similarly, the number of persons aged 80 years or older is expected to triple between 2020 and 2050, reaching an estimated 426 million [178].

By the third decade of life, core cognitive abilities, including processing speed, reasoning, episodic memory, and spatial visualization, begin to decline and consistently drop over a lifetime, at different rates between individuals. Certain skills, called "fluid skills", tend to decline first. These include processing speed, memory, and reasoning, all of which involve integrating new information and problem solving. Alternatively, skills that are overlearned, practiced, and enhanced by experience, called "crystallized skills", tend to remain intact, including vocabulary and fund of knowledge [179]. These changes are likely mediated by gradual decline in cerebral gray matter volume, especially in the frontal and parietal lobes [179].

1.5 Neuropathologies Common to Age and Neurodegenerative Disease

1.5.1 Glia

1.5.1.1 Microglia

Microglia are the resident immune cells of the brain, which encompass 5 – 12% of cells, depending upon the brain region [180]. $CD45^{-}c\text{-}kit^{+}$ erythromyeloid precursors derived from the embryonic yolk sac travel via the circulation and colonize the brain [181, 182]. Formation of microglia from erythromyeloid progenitors is dependent on the transcription factors Irf8- and Pu.1 (but not Myb, Id2, Batf3, and Klf4), as well as the presence of cell survival factor (CSF) 1-receptor (CSF1-R) signaling and its ligand, interleukin-34 (IL-34) [183-185]. Microglial colonization can be influenced by fibronectin, macrophage migration inhibitory factor (MIF), and CXCL12 [184]. Following colonization, microglia proliferate during the first 2 postnatal weeks, then decline by approximately 50% to adult levels between the third and sixth postnatal weeks [186].

Although microglia share similar functions to macrophages, single-cell RNA-sequencing has revealed that microglia are molecularly distinct from perivascular, meningeal, and choroid plexus macrophages [187]. The ability of microglia to self-renew establishes them as a unique population within the brain [188]. These cells have the longest lifespan of any documented immune cell, renewing at a median rate of 28% per year, with populations surviving on average 4.2 years in humans [189].

Microglial colonization, function, and morphology differ in a sex- and brain region-dependent manner throughout the lifespan of the organism. Early in postnatal development, murine males have more microglia in the parietal cortex and amygdala, as well as the CA1, CA3, and dentate gyrus of the hippocampus [190]. During adolescence and adulthood, females have more microglia in these brain regions [190]. In the rat hippocampus, female microglia have a more activated or amoeboid morphology and greater phagocytic capacity, with higher expression of several phagocytic pathway genes, than males [191]. Microglia also demonstrate different secretory and molecular phenotypes upon stimulation in male versus female cells; *ex vivo* microglia from male mice upregulate pro-inflammatory IL-1β upon stimulation with LPS compared to females [192].

In addition to quantitative differences based on sex, microglia are not uniformly distributed throughout the brain. More microglia are found in the gray matter compared to white matter, especially in the hippocampus, olfactory telencephalon, basal ganglia, and SN [180]. It is possible that the increased

quantity of microglia in these regions contribute to their susceptibility to neurodegeneration. Fiber tracts, cerebellum, and brainstem have the fewest microglia, whereas the cerebral cortex, thalamus and hypothalamus have average cell densities [180]. Resting morphology is also brain region-dependent. Microglia in the cerebellum and brain stem are less complex than microglia in the hippocampus, frontal cortex, and ST, which is sustained even following stimulation [193, 194]. Altogether, these sex- and brain region-differences may shape microglial responses to neurotoxicants and infectious agents.

1.5.1.1.1 Homeostatic Functions of Microglia

As their status as resident macrophage establishes, microglia execute key immune functions in the CNS. They perform immunological surveillance by using their ramified processes to detect and eliminate pathogens, debris, and other neurotoxic proteins. The primary receptors involved in this function are toll-like receptors (TLRs), which recognize pathogen associated molecular patterns (PAMPs), and major histocompatibility complex II (MHCII) receptors, like other professional antigen-presenting immune cells [195]. Through these receptors, microglia can recognize microbial and viral antigens.

Other homeostatic roles include maintaining and forming neurons. Microglia can induce differentiation of oligodendrocyte progenitor cells to promote myelinogenesis [196, 197]. Increasing evidence indicates that microglia also stimulate neurogenesis; microglial contact promotes the formation and elongation of neuronal spines. As such, depleting microglia during key developmental timepoints decreases spine formation in the motor cortex [198]. This glial cell is also involved in synapse remodeling and maturation by secreting brain-derived neurotrophic factor (BDNF), glycine, and L-serine. It was reported that microglia can reduce high levels of neuronal activity be selective synaptic pruning, which prevents excitotoxicity [199, 200]. Under pathologic conditions, microglia activate into neuroprotective and neurotoxic phenotypes, depending on the stimulus.

1.5.1.1.2 Microglial Responses to Disease, Infection, and Age

Neuroprotective or anti-inflammatory microglia are produced in response to stress and damage, promoting neurogenesis, phagocytosing debris, and reducing inflammatory signaling in the brain [201]. However, during cellular stress, infection, or injury, microglia can polarize into a neurotoxic phenotype that is commonly associated with chronic disease states. These activated microglia are often called disease-associated microglia (DAM), and typically form ameboid-like cells with retracted processes [202, 203]. Reactive microglia activate neuroinflammatory signaling pathways, notably the nuclear factor kappa B (NF-kB) and mitogen-activated protein kinase (MAPK) signaling cascades, as well as increase their capacity for migration and phagocytosis [204, 205]. Prolonged microglial activation, which promotes neuroinflammation, can cause damage to neurons [206].

In both the aged and diseased brain, microglia have dystrophic morphology, reduced normal functioning, and increased susceptibility to producing pro-inflammatory mediators. Aged microglia typically have cell body hypertrophy and fewer branched dendritic arbors, yet reduced capacity for migration and immunological surveillance [207, 208]. To compensate for this decrease in function, microglial populations are often increased in the aged brain, but this typically does not confer greater protection. As microglial populations increase with age, so do the proportion of dysmorphic cells [207, 209]. In addition to their inability to detect and react to ligands, their capacity to physically degrade them is also affected by age. Aged microglial lysosomes often become overburdened by debris and neurotoxic proteins, which leads to cellular disfunction [210]. Other aspects of homeostatic functioning are altered with age, including the ability of microglia to produce molecules that aid in oligodendrocyte progenitor cell (OPC) differentiation [211]. Most notably, aged microglia continuously secrete pro-inflammatory cytokines, including tumor necrosis factor (TNF), interleukin-1β (IL-1β), and interleukin-6 (IL-6), even in their resting or inactive state, resulting in excessive neuronal damage [208, 212 2011]. This may be due to chronic upregulation of NF-κB signaling or leakage of lysosomal proteases that stimulate neuroinflammation [213].

Importantly, microglia can become more sensitive towards forming pro-inflammatory states in

response to stimuli, called priming, which results in exacerbated neuroinflammatory damage. Priming occurs when the cells are repeatedly introduced to stress, such as infectious agents and neurotoxicants; it is often intensified by co-morbidities, disease, and age. Age, especially, is considered a contributing factor, as the shift towards a more inflammatory brain may sensitize glia to form exaggerated responses in the presence of stimuli. This alteration to microglia is likely a result of repeated stress, which may be encountered throughout the lifespan, which weakens immunoregulatory mechanisms, thus lowering the threshold required for cellular activation [209]. For example, *ex vivo* data demonstrates that following LPS exposure, aged microglia are primed toward exacerbated secretion of pro-inflammatory cytokines and upregulate MHCII [214]. While these priming events may seem miniscule, they can actually lead to profound deficits to neuronal function in the already delicate aged brain, which may permanently alter cognition and memory.

1.5.1.2 Astrocytes

Astrocytes are the most abundant cell type in the CNS. They are generated from neural stem cells, or radial glia (RG), in the ventricular–subventricular zone (V-SVZ). RG, derived from the neuroepithelium, are the primary cell type implicated in glial production, beginning at embryonic day 18 [215]. After birth, RG cells are reduced, and astrocytes generated between postnatal day 0 – 14 come from SVZ progenitors in the ventricular and subventricular zones that migrate to the white matter and cerebral cortex. $Gli1^+$ progenitors in the SVZ generate half of the total cortical astrocyte population. Once established in the cortex, mature astrocytes proliferate, substantially increasing during the first postnatal weeks; in the outer cortical layers, proliferating astrocytes contribute to nearly half of astrocyte populations. Astrocytes are incredibly complex in morphology, and their intricacy and volume increases from postnatal day 7 to 21 [216]. Protoplasmic astrocytes have a soma, 4–10 major branches emanating from the soma, and thousands of branchlets and leaflets, which are higher order structures that lie close to synapses; Approximately 90 – 95% of an astrocyte's area is composed of the branches, branchlets, and leaflets.

Similar to microglia, astrocytes display brain region-dependent differences. The cerebral cortex is composed of 6 layers, and astrocytes in cortical layers 2 and 3 have greater process arborization and come in contact with more synapses than the cells in layer 6. Astrocytes in the cerebellum actually ensheath almost all of the synapses present, whereas the cells in cortex and hippocampus approximately 50% [217]. Astrocytes in males produce more pro-inflammatory molecules, including IL6, TNF, and IL1β, following exposure to LPS compared to those in females. Androgenized females also show an exacerbated response, indicating that testosterone may contribute to these responses [218].

1.5.1.2.1 Homeostatic Functions of Astrocytes

The primary role of astrocytes is to stimulate neurons, remove neurotransmitters from the synaptic cleft, and modulate ion and metabolite concentrations, altogether contributing to proper CNS function [209]. These cells are also critical for synapse formation and maintenance due to the presence of astrocyte-derived molecules [219-221]. Astrocytes contribute to a glutamate-glutamine cycle, where they remove glutamate from the synaptic cleft through GLT-1 and GLAST transporters, converting it to glutamine via glutamine synthetase. The glutamine produced by astrocytes is essential for active neurotransmission by excitatory neurons [222]. Perhaps one of the most significant functions of the astrocyte is that of blood-brain barrier (BBB) formation and maintenance, which regulates cellular and biomolecular traffic into and out of the brain. At the end of astrocyte processes are what is referred to as "endfeet", which physically contact the vasculature and contain transporters that aid in molecular diffusion. Importantly, astrocytes secrete factors that stimulate endothelial cell junctions and BBB impermeability [223, 224].

1.5.1.2.2 Astrocyte Responses to Disease, Infection, and Age

Following stress, astrocytes activate into neurotoxic or neuroprotective phenotypes, similar to microglia. Although restricted compared to their glial counterpart, astrocytes constitutively express some TLRs and PRRs, in addition to cytokine and chemokine receptors that upon stimulation, polarize the cells

[225, 226]. While often regarded as damaging, reactive astrocytes can display protective functions by increasing phagocytic activity; reactive astrocytes upregulate expression of MHC and aid microglia in the clearing of pathogens, debris, and protein aggregates [209, 227, 228]. Despite this role, activated astrocytes also secrete pro-inflammatory mediators that can be damaging to neurons over time.

Astrocytes in the aged and diseased brain retain activated morphologies, with cell body hypertrophy and increased complexity of their processes, and upregulate glial fibrillary acidic protein (GFAP) [229, 230]. These changes typically occur in the hypothalamus and hippocampus with age, which may explain why certain anatomical regions are more susceptible to damage and neurodegenerative disease [231]. Aged astrocytes upregulate pro-inflammatory cytokines and complement proteins that facilitate protective misfolded protein removal, but also synapse engulfment and neuronal disfunction [231-233].

Microglia and astrocytes interact with one another through secretion of cytokines and chemokines, initiating either cellular recruitment or reducing glial activation; through activation of interleukin-10 receptors (IL-10R), astrocytes can attenuate microglial activation. With age, astrocytes decrease IL-10R expression and become desensitized to IL-10, promoting microglial activation and, subsequently, a pro-inflammatory brain phenotype [234, 235]. In addition to altered communication with microglia, aged astrocyte processes do not properly come in contact with vessels and reduce expression of proteins in their endfeet, like aquaporin-4 (AQP4), which affects ion concentrations in the brain [236, 237]. Therefore, astrocytes have been implicated in mediating BBB dysfunction, which is commonly associated with age-related neurological diseases and neurodegeneration. This could allow infectious agents and toxic biomolecules to enter the brain [238].

1.5.2 Protein Misfolding and Aggregation

Proteins are formed through a process of transcription and translation; DNA sequences are transcribed into coding mRNA sequences, which are translated by ribosomes into the protein's primary structure, the amino acid chain. Amino acids within the chain carry inherent charges, neutral, positive, or

negative, which help predict the 3-dimensional (3D) structure of the protein. Anfinsen's thermodynamic principle has been used to explain how proteins fold; proteins maintain the structure that minimizes the total free energy of the system. It is hypothesized that proteins rapidly change conformation from their high-energy, unfolded structure towards its lowest-energy, folded structure (**Figure 3**). Based on this hypothesis, there are many high-energy conformations that, at random, form intramolecular contacts that alter their structure incrementally downhill in energy until reaching the most favorable conformation, in which there are few low-energy, native-like conformations [239]. Despite sequencing their amino acid compositions, it has been increasingly difficult to predict protein structure; one possible explanation is that there may not be one ideal protein conformation, but instead multiple allosteric variations that are equally thermodynamically optimal. We see this in substrate-induced enzyme changes and hormone ligand-induced modifications of steroid and peptide hormone receptors [240].

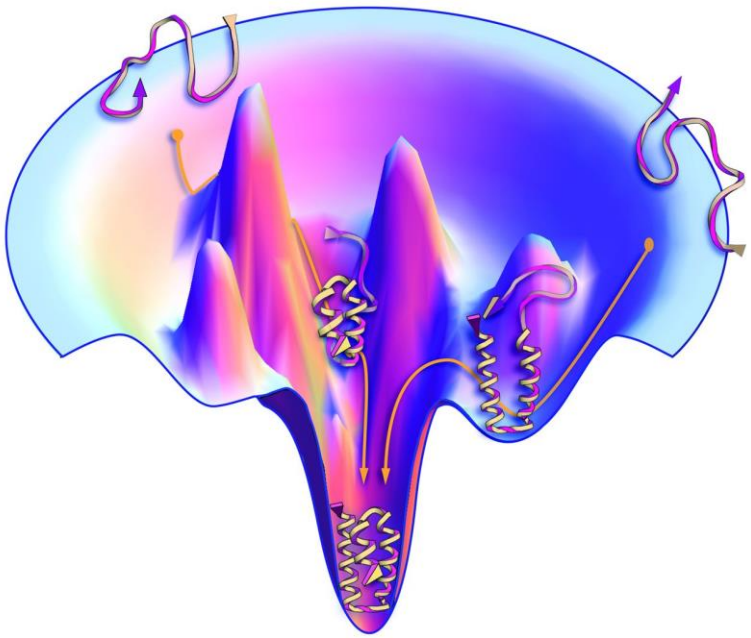

Figure 3: Thermodynamics of Protein Folding. Adapted from Dill and MacCallum [239].

Many forces contribute to protein folding and stability, including van der Waals interactions, backbone angle preferences, electrostatic interactions, hydrophobic interactions, and hydrogen bonding [239]. Hydrogen bonds formed between amino acids within the chain create the secondary structure of the

protein, or its composition of α-helices and β-sheets [241]. The protein then folds into its tertiary structure based on hydrophobic interactions, where nonpolar amino acids are at the interior core of the protein and polar amino acids are exposed. Other interactions, such as close-range van der Waals interactions, preferred angling of neighboring backbone bond orientations, electrostatic interactions based on amino acid charges, and chain entropy maintain the stability of the native conformation. It is the final 3D structure that is the primary determinant of a protein's biological function [242].

Due to the complexity of the cellular environment, and the efficiency necessary for cellular function, many proteins require molecular chaperones to effectively fold. A chaperone is any protein that interacts with, stabilizes, or aids a protein into its native conformation, without being present in its final structure [243]. These helpers perform many functions within the cell, including promoting protein folding by pushing kinetically trapped conformations past free-energy barriers and binding to hydrophobic regions to prevent multi-protein aggregation [243]. In addition to the aforementioned interactions, post-translational modifications (PTM) aid in forming a protein's 3D structure. There are more than 400 possible PTMs, which can be categorized into three groups: adding a chemical, complex group, or polypeptide to a target residue. The most common PTMs are phosphorylation, methylation, acetylation, and ubiquitylation [244].

While the cell utilizes multiple systems to ensure accuracy during the incredibly complex process of folding proteins, it is highly unlikely that misfolding, where a protein with a conformation different than its native form is created, never occurs. Misfolding can happen due to somatic mutations in the gene sequence, errors with either transcription or translation, malfunction of folding and chaperone machinery, mistakes in PTM, errant trafficking of proteins, environmental changes or toxicity, and seeding mechanisms by existing misfolded proteins [245]. To address the creation of misfolded conformations, cells contain degradation systems that effectively identify and remove non-functional proteins. There are two primary pathways, the ubiquitin-proteosome pathway and the autophagy-lysosomal pathway, that are constitutively involved in proteostasis. Typically, smaller proteins are degraded by proteasomes, whereas lysosomes are responsible for the degradation of larger, long-lived proteins.

Removal of damaged or non-functional proteins via the proteosome occurs by first covalently attaching multiple ubiquitin molecules to the protein, which is then recognized and degraded by the cytoplasmic, 26S proteasome complex [246]. Proteins must be unfolded during this process, via the regulatory cap of the complex and chaperone proteins, which makes degradation of large aggregates difficult, if not impossible [247]. Alternatively, larger misfolded proteins are primarily degraded via autophagy; cytoplasmic proteins are trafficked by macroautophagy, chaperone-mediated autophagy, and microautophagy. Macroautophagy, which is a constitutive pathway regulated by mammalian target of rapamycin (mTOR), encapsulates proteins into autophagosomes that fuse with a lysosome for degradation [247]. Chaperone-mediated autophagy uses cytosolic Hsc70, a chaperone, to identify and bind to KFERQ (Lys-Phe-Glu-Arg-Gln) sequences, which are present in approximately one-third of soluble cytosolic proteins but only become exposed in misfolded conformations. The protein is then unfolded and translocated from the cytosol into the lysosome for degradation [247, 248]. Microautophagy is not well-characterized in mammals, but likely involves cytosolic sequestration by the lysosomal membrane [248]. Misfolded proteins localized to the plasma membrane catalyze ubiquitination by CHIP (C- terminus of Hsp70 interacting protein) ubiquitin ligase, resulting in endocytosis and lysosomal trafficking of the protein for degradation [247, 249]. At the termination of these processes, lysosomes, which have the capacity to degrade misfolded and even aggregated proteins, degrade the proteins through a process of acidification and protease activation [250].

When these systems can no longer recognize and degrade misfolded proteins, due to disrupted proteostatic mechanisms or protein overload, aggregates form that are not cleared effectively. It was previously assumed that misfolding of specific proteins result in unique pathologies that are directly implicated in one neurodegenerative disease. It is now understood that neurodegenerative diseases share misfolded protein pathologies, but they are regionally distinct and facilitate disease in different ways, as detailed below.

1.5.2.1 Amyloid beta

First identified in 1984, β-amyloid (Aβ) is a protein found in the extracellular space or associated with the plasma membrane of neurons. This protein is derived from the amyloid precursor protein (APP). Mature APP, located at the plasma membrane, is created through a process of sequential proteolytic cleavages. First, APP is cleaved at residue Lys688 by α-secretase, then at the N-terminal of the Aβ domain (residue Asp672 or Glu682) by β-secretase to create soluble APPβ (sAPPβ) and membrane-bound APP-CTF (C99). The C99 protein is further cleaved by γ-secretase to generate Aβ peptides of various sizes, between 37 and 43 amino acids long [251]. In the normal brain, it is estimated that 80 – 90% of Aβ is 40 amino acids long ($A\beta_{1-40}$); the 42 amino acid peptide ($A\beta_{1-42}$) is considered the pathogenic or neurotoxic form, as it is more hydrophobic and, therefore, more prone to aggregation [252]. $A\beta_{1-42}$ is the major pathologic component of amyloid plaques, although $A\beta_{1-43}$ has also been identified. The complete physiological function of Aβ has not yet been elucidated, but cumulative evidence demonstrates its role in neurogenesis, synaptic function, angiogenesis, antimicrobial responses, memory formation and cognition, metal sequestration, and antioxidant activity [253].

Aβ progressively aggregates, beginning as amyloid monomers which form oligomers, then into insoluble fibrils, and finally into insoluble plaques. All types of cerebral, nonvascular Aβ deposits are typically referred to as "senile plaques" regardless of their morphology. Cumulative evidence demonstrates that oligomers may be more neurotoxic than fibrils or plaques, as they elicit abnormalities in neuronal function. Oligomers have been associated with synaptic dysfunction, reduced dendritic spine density, impaired cognition, and memory deficits [254-257]. More specifically, Aβ is toxic to neurons by causing pore formation that results in ion leakage, disrupting the balance of calcium within the cell, causing oxidative stress and loss of membrane potential. This promotes apoptosis and inflammation. Aβ is also indirectly toxic by altering kinase activity, hyperphosphorylating tau proteins and contributing to tangle formation [252]. The propagation of Aβ, based on current evidence, occurs when the pathogenic protein induces misfolding of native Aβ. It is less understood, however, how Aβ is spread to nearby

neurons and brain regions. Multiple hypotheses have been generated, including extracellular spread to nearby cells or transsynaptic intracellular spread in connected cells.

The 'amyloid hypothesis' argues that Aβ deposition initiates AD pathogenesis based on the following observations: 1. Aβ is a major component of the amyloid plaques 2. Aβ aggregation can precede neurodegeneration by decades, and 3. Aβ peptides, particularly $A\beta_{1\text{-}42/43}$, induce neuronal death *in vitro* [84, 252]. Unfortunately, Aβ deposits are not necessarily indicative of disease, and have been identified in a number of cognitively normal individuals. The anatomical distribution of deposits do differ, where people diagnosed with AD demonstrate Aβ deposits in the midbrain, brain stem, and cerebellum, but cognitively normal individuals typically show deposits in the cerebral cortex, basal ganglia, thalamus, and hypothalamus [258].

1.5.2.2 Tau

Tau, the major proteinaceous component of tauopathies, has been identified most notably in AD and PD, but also in progressive supranuclear palsy and corticobasal degeneration. This protein, which is encoded by the microtubule-associated protein tau (*MAPT*) gene, is primarily located in neurons, but is also present at low levels in glia. There are six isoforms of tau, which differ depending on the number of 29-residue near-amino-terminal inserts and range from 352 to 441 amino acid residues total [259]. These isoforms are generated by alternative splicing of exon 2 (E2), exon 3 (E3), and exon 10 (E10) [260]. Structurally, tau is a natively unfolded protein with a "paperclip-like" conformation, which makes it highly flexible [259].

Neurons are morphologically complex, forming processes called axons and dendrites that are critical for proper transmission. In fact, 99% of the cytoplasmic volume of the entire neuron is localized to the axon [261]. The structure and function of these processes rely on the cytoskeleton, which is composed of microtubules, microfilaments, and intermediate filaments. Microtubules are highly dynamic and must become stabilized during the formation of axons and dendrites [262]. Microtubule-associated proteins (MAPs), one of which being tau, stabilize microtubule bundles by regulating their assembly and

organization, although the exact mechanism is unclear [259]. Some evidence actually contradicts this role, instead postulating that tau is localized to the labile domain of microtubules, not the stable domain, and promotes instability. This hypothesis states that tau supports microtubule assembly/lengthening by limiting the binding of stabilizers, like microtubule associated protein 6 (MAP6) [263]. Regardless, tau is known to be localized to axons and plays a substantial role in microtubule assembly [264]. In addition to this role as a cytoskeletal stabilizer (or disruptor, depending on the source), tau has also been implicated in stabilizing DNA by binding to various chromosomal regions, regulating axonal transport by preventing binding of kinesin and dynein to microtubules, and mediating synaptic function [265].

Tau can become phosphorylated, the most common PTM, at 85 known putative sites: 45 serine (Ser) residues, 35 threonine (Thr) residues, and 5 tyrosine (Tyr) residues. This modification allows the tau protein to perform different functions depending on the which epitope is phosphorylated. For example, *in vitro* experiments demonstrate that phosphorylation of tau at Ser262/356 is required for the development of cell processes, while phosphorylation of Ser/Thr-Proline motifs inhibit the production of cell extensions [266]. In fact, some residues are phosphorylated in order to decrease tau's affinity for microtubules, therefore allowing for plasticity of microtubules for neurite growth [267]. While phosphorylation has necessary physiological function, it also comes with pathological implications. Under disease conditions, tau is hyperphosphorylated, likely caused by imbalanced kinase and phosphatase activity. In adults, tau contains on average two phosphates per molecule, but phosphorylation is increased in pathological states to approximately eight phosphates per protein [268]. This modification decreases tau's affinity for microtubules, detaching it and destabilizing neuronal cytoskeletons. This reduces the physiological function of the protein, which can be damaging to neurons.

Pathogenic tau is altered both post-translationally and conformationally, allowing it to not only lose function, but become prone to aggregation. Tau monomers interact via disulfide bonding or hexapeptide motifs, conformationally changing into β-sheet-rich, sphere-shaped oligomers ranging in size from 6 to 20 nm [265]. It is likely that detachment of tau from microtubules creates a pool of free tau that enhances its assembly into oligomers [269]. The presence of tau oligomers in human brain samples are 4–

fold higher in those diagnosed with AD compared to control tissue [270]. Clinical data also shows that the onset of AD symptoms correlates to elevated amounts of oligomeric tau [271]. Following oligomerization, tau further aggregates into protofibrils, fibrils, and, finally, into neurofibrillary tangles (NFTs). Phosphorylation at Thr231, Ser396, and Ser422 especially promotes self-aggregation of tau into filaments [272].

It is likely that the direct pathogenesis caused by misfolded tau is caused by both the consequences of loss of normal function and toxic gains of function. Whether the reduction in functional tau alone is sufficient to cause microtubule destabilization is under some debate; tau deficiency does not prevent the formation of neurites *in vitro*, nor produce major cytoskeletal abnormalities *in vivo*, likely due to compensatory functions by microtubule-associated proteins. This does not mean loss of functional tau is not detrimental to the cell, as overt breakdown of the microtubule system may not be required to cause neuronal injury; transport and function can still be altered without changes in microtubule morphology [269]. Certain phosphorylation sites are more strongly correlated with microtubule destabilization, including phosphorylation at Ser262, Ser293, Ser324 and Ser356, located at the four microtubule binding repeats. Phosphorylation at Thr214, Thr231 and Ser235 may also contribute to the dissociation of tau from microtubules.

Historically, NFTs were considered the primary driver of neuropathology, but deficits preceding the formation of advanced aggregates suggest that soluble tau in the form of monomers or oligomers may be the most neurotoxic form of the protein [270]. This is demonstrated by numerous studies identifying neuronal loss, synaptic changes, mitochondrial dysfunction, and behavior deficits *in vivo* caused by tau oligomers, but not fibrils [270]. It is even possible that forming NFTs is actually a neuroprotective mechanism, as it allows the cell to sequester neurotoxic forms of tau [273]. Regardless, there is some data showing that the presence of an NFT is detrimental to the cell, and that the number of NFTs in the neocortex of AD patients positively correlates with the severity of cognitive decline [274]. NFTs can act as physical barriers in the cytoplasm, compromising cellular functions by displacing cytoplasmic organelles from their usual location and decreasing the number of normal organelles [275]. It must also be

considered, however, that tau does not readily aggregate, especially in experimental models, even in transgenic mice overexpressing wild-type human tau. Perhaps the lack of evidence on the neurodegenerative effects of NFTs are due, in part, to the difficulty in reproducing them in a laboratory setting. In addition to direct mechanisms, misfolded tau can also stimulate glial responses and neuroinflammatory signaling which can be chronically damaging. Neurons with tau inclusions abnormally expose phosphatidylserine on their plasma membranes, which can be recognized by microglia. In response, microglia initiate phagocytic responses, degrading neurons [276].

As detailed above, tau (and other misfolded proteins) is normally a substrate of chaperone mediated autophagy, but monomers can also act as proteasomal substrates because they are relatively small, cytosolic proteins [277]. There are interruptions with both processes of protein elimination. During autophagy, hyperphosphorylated tau, with altered conformation, is cleaved by cathepsin D, which generates a fragment that is unable to cross the lysosomal membrane [248]. Not only does this perpetuate the presence of misfolded proteins, but it also globally reduces autophagy within the cell. In addition, proteases that normally degrade tau, like thrombin, calpain, and caspase, which are increased with age and disease, generate potentially neurotoxic byproducts. Proteolytically generated fragments of tau have greater propensity to aggregate compared to full-length proteins, and often can due to inefficient clearance mechanisms [277].

In contradiction to data indicating that Aβ spreads by extracellular, proximity-based diffusion, current evidence postulates that pathologic spread of tau occurs in neuroanatomically connected brain areas. Seeds of misfolded tau oligomers, but not fibrils, from a "donor cell" are released and taken up by endocytosis by a "recipient cell" where endogenous tau is recruited into pathologic forms [271]. Release of tau into the extracellular space can occur following cell death, neuronal stimulation, secretory lysosomes, or microvesicle shedding from the plasma membrane [278]. Following this concept, tau may be able to translocate between synaptically connected neurons, likely from the entorhinal cortex to the hippocampus, then to the limbic and association cortex. Where pathogenic tau is located in the brain helps account for variability of clinical symptoms and cognition between patients.

1.5.2.3 Alpha Synuclein

Alpha synuclein (α-Syn) is a small, 140-amino-acid protein that is mainly associated with the CNS, but has also been identified throughout the body in non-neuronal tissues. It is highly abundant in the brain and accounts for as much as 1% of the total protein in soluble cytosolic brain fractions. The protein, which is encoded by the *SNCA* gene, has several isoforms resulting from alternative splicing, including shorter peptides, but the 140-amino-acid protein is the major variant [279]. Its physiological function is not completely understood, but α-Syn is associated with presynaptic signaling and membrane trafficking via vesicular transport, as it is localized to the pre-synaptic terminal. It is also found throughout the cell, in the nucleus, mitochondria, and endolysosome, which suggests additional roles of the protein [280-283].

The protein is intrinsically disordered with three primary components: an amphipathic N-terminal region (amino acids 1 – 60) that anchors the protein to cell membranes where it adopts partial α-helix conformation, a hydrophobic non-amyloid component (NAC) region (AA 61 – 95), and an unorganized C-terminal domain (96 – 140). The polar C-terminal domain contains most of the post-translational modifications of α-Syn, mediating the proteins interaction with other proteins, ligands, and metals; it has been suggested that increased negative amino acid residue content reduces protein aggregation [279]. The NAC has been most closely associated with misfolding and aggregation [284]. This hydrophobic region is prone to intermolecular interactions, which allows it to adopt numerous conformations, promoting aggregation of soluble α-synuclein monomers into insoluble oligomers and, following the formation of highly ordered β-sheets, fibrils. Neurotoxicants, genetic mutations, and protein modifications (including phosphorylation, ubiquitination, nitration, and truncation) contribute to the misfolding of α-Syn into oligomers and fibrils [279]. The protein is usually a substrate of chaperone mediated autophagy, but misfolded α-Syn is unable to cross the lysosomal membrane. This results in not only persistence of the pathogenic α-Syn protein, but also decreased identification and removal of other proteins by this system, as the α-synuclein remains tightly bound to Hsc70 and prevents translocation into lysosomes. Not only can pathogenic α-Syn cause this, but overexpression of α-Syn in general can hinder protein degradation

through this pathway.

It is widely accepted in the field that α-Syn fibrils are the primary component of Lewy bodies, which are inclusions found within the cytoplasm of DAn; there can be multiple inclusions within one neuron [285, 286]. There is debate, however, what form of misfolded α-Syn is the most toxic, and its exact mechanism of toxicity. Murine models of α-Syn knockout demonstrate normal neuronal architecture compared to wildtype controls, but there were alterations in dopaminergic signaling in the nigrostriatal pathway, which suggests that pathogenesis of misfolded protein is due to both a gain of toxic function and loss of its normal function [287]. Aggregated protein can cause mechanical distortion of cellular compartments. Fibrils can also induce misfolding of other α-Syn proteins within the cell, propagating the formation of neurotoxic proteins that can spread in a prion-like manner between cells and anatomical regions. Misfolded α-Syn is primarily correlated with PD, but cytoplasmic accumulation has also been identified in AD.

1.5.3 The Blood-Brain Barrier

1.5.3.1 Normal Blood-Brain Barrier Function

Neuronal function and communication, using a combination of chemical and electrical signals, within the CNS is a delicate process; neurons are extremely sensitive to disrupted ion levels and neurotoxicants. Additionally, the adult CNS has little regenerative capacity in response to damage; fully differentiated neurons are not able to divide and replicate normally. To address these requirements, the brain forms the blood-brain barrier (BBB), which utilizes a combination of physical, enzymatic, and transport barriers. The BBB has numerous functions, the most well-known is preventing infiltration of proteins, immune cells, and neurotoxicants from the blood into the brain parenchyma. While oxygen can rapidly diffuse into the brain, and carbon dioxide out, the BBB prevents many macromolecules, like albumin, pro-thrombin and plasminogen, from infiltrating; this is important because plasma has much higher protein content than CSF. If these proteins infiltrate the parenchyma, it can result in cellular activation and glial inflammation which, eventually, results in cell death [288, 289]. Large proteins that

need to cross the BBB, like glucose, amino acids, insulin, leptin, and iron transferrin, enter through carrier-mediated transporters or receptor-mediated endocytosis [290, 291]. In addition to macromolecules, the BBB functions to protect the brain from neurotoxic substances that may be circulating in the blood, such as endogenous metabolites, xenobiotics, or environmental contaminants. Other functions of the BBB include ion regulation and reducing contamination of neurotransmitters [289]. Solute concentrations differ in the plasma and CSF. Therefore, the BBB contains specific ion channels and transporters which allows for maintenance of optimal ion concentrations in the brain, especially that of potassium, Ca^{2+}, Mg^{2+}, and pH. The BBB minimizes 'cross-talk' of neurotransmitters in the peripheral and central nervous systems. This is important because excitatory NTs, like glutamate which is found in high concentrations in the blood, could enter the brain and induce excitotoxicity of neurons.

Transport across the BBB occurs through passive diffusion, active efflux, carrier mediated transport, receptor-mediated transport, and adsorptive mediated transport. Passive diffusion allows small (< 400 Da), lipophilic molecules forming < 8 hydrogen bonds to readily cross through the BBB and enter the brain; the more lipid soluble, the more rapidly a solute can enter into the CNS. It is likely this process occurs through small, transitory pores within the phospholipid bilayer [290]. Active efflux occurs via ATP-binding cassette proteins located on the luminal, endothelial plasma membrane of the BBB. These highly expressed, ATP-driven proteins pump xenobiotics and endogenous metabolites [290]. Polar molecules, like glucose and amino acids, do not readily enter the brain; therefore, carriers are used. Carrier mediated transport (CMT) involves membrane-bound proteins that facilitate the transport of amino acids, carbohydrates, monocarboxylic acids, fatty acids, hormones, nucleotides, organic anions, amines, choline, and vitamins [290]. Similarly, molecules that cannot be transported via CMT, likely due to the presence of peptide bonds, use receptor mediated transport. Molecules include neuroactive peptides, regulatory proteins, hormones, and growth factors [290].

The neurovascular unit (NVU), or the components involved in regulating BBB function, are composed of three primary cellular elements: endothelial cells (ECs), astrocyte endfeet, and pericytes (PCs) (**Figure 4**). In addition to these cells are multiple layers, the luminal membrane, endothelial layer,

abluminal membrane, and basement membrane (**Figure 4**). The ECs in the brain, which are connected to the basement membrane by integrins, are phenotypically different from those in the periphery; they have a flattened appearance, few caveolae at their surface, and are mitochondria rich [290]. ECs in the brain have reduced endocytosis/transcytosis activity than cells in the periphery, contributing to a 'transport-barrier' property. Most notable is the formation of tight junctions (TJs) and adherens junctions (AJs) between cerebral endothelial cells, which forms a 'physical-barrier' that blocks substances in the blood from entering the brain. AJs are composed primarily of cadherin proteins, as well as alpha-actinin and vinculin, that span the intercellular cleft and are connected intracellularly by alpha, beta, and gamma catenin. AJs hold endothelial cells together, providing structural support that is essential for the formation of TJs.

Unlike cellular junctions located throughout the periphery, TJs in the brain are more restrictive [292]. During development, vessels gradually became impermeable in a brain region-dependent manner [293]. TJs are complex cell-cell adhesion complexes involving proteins that span the intercellular cleft. These proteins primarily consist of claudins, occludin, and junctional adhesion molecules (JAMs); claudins are the most abundant proteins found in TJs and have the greatest cell-adhesion activity [294, 295]. There are approximately 20 known isoforms of claudin (claudin 1–20), which are actually considered the "gatekeepers of neurological function" [296]. Overexpression of claudins in fibroblast cultures, which typically lack TJs, induces tight junction-like networks [297, 298]. Additionally, overexpression, knockdown/knockout, and mutations of claudin alters paracellular permeability [299]. Murine models lacking claudin V have a compromised BBB, allowing small molecular weight molecules to enter the brain [300].

Similar to claudins, occludin connects intracellularly to the scaffolding proteins ZO-1, ZO-2, ZO-3, and cingulin. This 65 kDa protein is important for BBB function but not necessarily structure and assembly, as occludin deficiency does not prevent TJ formation [301]. Select junctional adhesion molecules (JAM), which are 40 kDa proteins, are expressed in the brain; JAM-1 and JAM-3 are expressed, but not JAM-2 [302]. Studies also show their role in cell-to-cell adhesion and cellular migration across the BBB, but its function is not entirely understood [290]. In addition to TJs, the

production of intracellular and extracellular enzymes at the BBB creates an ‘enzymatic-’ or 'metabolic-barrier' that breaks down peptides and inactivates certain compounds [303].

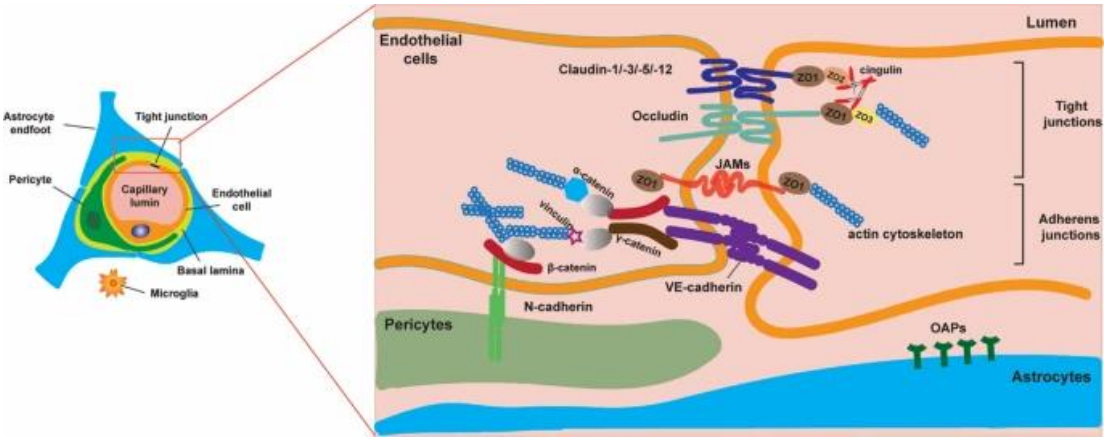

Figure 4: Cellular and Proteinaceous Components of the Blood-Brain Barrier. Adapted from Kadry et al [290].

Although they do not directly function within the BBB, astrocyte processes ensheath vessels to maintain ion concentrations and induce barrier tightness. It is believed that even though these cells differ morphologically in a brain region-dependent manner, approximately 99% of astrocytes in the gray matter (except in the hippocampus) come in contact with at least one vessel, but usually three, as defined by vessel density [304]. Endfeet cover 70–100% of arterioles, capillaries, and venules in the brain; the size of these endfeet positively correlate with the size of the vessel it comes into contact with [305, 306]. Perhaps the most important function of astrocytes in the neurovascular unit is their ability to induce BBB properties in endothelial cells [307, 308].

Similar to astrocytes, pericytes are a cell that project elongated processes that ensheath vessels, as much as 37% of the endothelial layer [309]. While an essential constituent of the brain, pericytes do not directly form barriers. Instead, they maintain BBB integrity and permeability, regulate cerebral blood flow, aid in angiogenesis, clear toxic cellular byproducts, improve microvascular stability, and mediate attachment of astrocytic endfeet [310, 311]. Their contractile nature allows them to help control capillary diameter, as capillaries lack smooth muscle to do so themselves, which regulates cerebral blood flow

[312, 313]. Pericytes are attached to the basement membrane by integrins, as are ECs. The close proximity of ECs and pericytes allows intercellular transfer of nutrients, metabolites, secondary messengers, and ions [310]. Although not as significant as the role of the astrocyte, pericytes also contribute to endothelial BBB-specific gene and protein expression profiles, specifically by upregulating CD71 expression [311].

1.5.3.2 Blood-Brain Barrier Dysfunction and Contribution to Disease

Loss of BBB function has been identified in numerous neurological events, including stroke, multiple sclerosis, epilepsy, AD, and PD. Barrier dysfunction can range from mild leakage to massive breakdown, which can be transient or chronic changes. During BBB breakdown, disruption of TJs typically occurs, but degradation of the basement membrane, glial activation, and enzymatic loss can also cause physical breakdown of the BBB [314]. In addition to being degraded with disease, the BBB is altered with age, with reduced expression of proteins comprising TJs [209]. These alterations allow infiltration of proteins, immune cells, and neurotoxicants into the brain, contributing to neuroinflammatory signaling and neurodegeneration.

Post-mortem studies of patients diagnosed with AD show accumulation of immunoglobulins, albumin, fibrinogen, and prothrombin in the hippocampus and cortex, as well as microhemorrhages [315-317]. Similarly, microbleeding can be observed by magnetic resonance imaging (MRI), indicating BBB leakage [318]. Such evidence is strengthened by data demonstrating thinning of the microvascular basement membrane, altered endothelial morphology in blood vessels, and reduced pericyte coverage in key areas involved in AD [319, 320]. Although it is unclear if BBB dysfunction causes AD pathology, or if it is simply a consequence of pathology, it is obvious that the two are intertwined.

In particular, pericytes have been implicated in disease and loss of BBB function. Pericyte degeneration is documented with age and in AD, dementia, amyotrophic lateral sclerosis (ALS), and stroke [290, 321]. Pericyte deficiency increases BBB permeability to low and high molecular weight molecules, leading to accumulation of serum proteins and neurotoxic macromolecules [311, 322].

Pericyte-deficient mice demonstrate neuronal loss in the cortex and hippocampus, learning and memory impairment, and neuroinflammation, highlighting their important role [322]. Expanding upon this, pericyte deficiency in AD models (APP overexpressing transgenic mice) exacerbates brain Aβ levels, tau pathology, neuronal loss, and cognition decline [323].

Similarly, astrocytes have been heavily implicated in BBB dysfunction. Ablating astrocyte endfeet usually leads to rapid re-covering, but if this does not occur BBB damage often occurs; the ability of astrocytes to replace their endfeet is often reduced with age [223, 237]. These findings highlight the importance of astrocyte endfeet for brain function. In models of experimental allergic encephalomyelitis (EAE), loss of tight junctions, which is associated with glia mediated neuroinflammation, reduces the functional capacity of the BBB [324].

1.6 Impact and Summary

It is vital that resources be appropriately allocated to the most fragile populations, including the elderly and those at increased risk of disease. TB is a considered a disease of poverty; 87% of cases reside in 30 high-burden countries, which are predominantly low- and middle-income countries. The incidence of TB, progression of disease, and high mortality rates are heavily associated with socio-economic factors. These include social factors, including living and working conditions, overcrowding, malnutrition, co-morbidities and co-infection, and social habits like high alcohol consumption. For example, when comparing TB burden, childhood TB rates are substantially higher in low socio-economic cities, like Cape Town, compared to high socio-economic cities, like New York and London [325]. Additionally, the primary known cause of the rising incidence of drug resistance is due to inadequate treatment regimens and high rates of non-compliance by patients. The main barriers to TB treatment adherence are related to a lack of social support, food security, income security, knowledge, and proximity to treatment centers and diagnostic resources [326, 327]. Hence, every aspect of eradication of

TB, which is entirely dependent upon reduced transmission and proper treatment, is increasingly difficult considering how entangled the disease is to prevailing socio-economic deficits [328].

Elderly patients are another vulnerable population, which is increasing due, in part, to availability of healthcare and disease-preventing services that have improved life expectancy. With these impending population changes, it is critical that we obtain a better understanding of age-related pathologies. Age is the greatest risk factor for the formation and progression of neurological disease. The elderly are also prone to being immunocompromised and malnourished, which increases their vulnerability to infectious agents and causes them to progress into more severe disease states, such as sepsis.

Millions of dollars and countless hours have been spent trying to understand the mechanistic intricacies of neurodegenerative disease, and the possible ways we can treat them. Yet, we are no closer to a complete understanding of disease processes, nor a cure. This is likely because neurodegenerative diseases are highly complex, and the aged brain, which is already more fragile due to low-level, sustained neuroinflammation mediated by glia, is prone to excessive damage if exposed to known (or perhaps unknown) stressors. The combined effects of multiple etiological factors, including environmental contaminants and infectious agents, may push the brain into a state of neurodegenerative disease. It is estimated, based on detectible antibodies in sera, that the average person has been exposed to 10 different viral species in their lifetime [329]. This estimation does not account for additional infections by bacteria, or the effects of potential compounding factors that may place a person at increased risk of infection. Therefore, investigative focus on the perhaps unknown contributors to neurological disease, better models that allow for more accurate laboratory study, and investigation into improved therapeutics should be implemented, as highlighted below.

CHAPTER 2

GLIOSIS, MISFOLDED PROTEIN AGGREGATION, AND NEURONAL LOSS IN A GUINEA PIG MODEL OF PULMONARY TUBERCULOSIS

Latham A, et al. Gliosis, misfolded protein aggregation, and neuronal loss in a guinea pig model of pulmonary tuberculosis. Front Neurosci. 2023 May 19;17:1157652. doi: 10.3389/fnins.2023.1157652. PMID: 37274195; PMCID: PMC10235533.

2.1 INTRODUCTION

Tuberculosis (TB), resulting from aerosol infection by *Mycobacterium tuberculosis* (Mtb), is the thirteenth leading cause of death across the globe and the second leading cause of death due to an infectious agent [8]. TB is an ongoing global crisis; there are an estimated 10 million active cases of disease and 1.5 million deaths each year worldwide [330, 331]. The COVID-19 pandemic has exacerbated the problem, with increased incidence of TB cases that have gone undiagnosed and untreated [332-335]. Eradication of the disease is difficult; the bacteria are transmitted primarily through respiratory droplets from patients with active disease, and treatment requires a lengthy, intensive antibiotic regimen. Mtb primarily infects the pulmonary system, although it can also disseminate to other tissues, including the central nervous system (CNS) in rare cases. The immune response to Mtb is characterized by a massive influx of immune cells in an attempt to control infection, primarily macrophages and $CD4^+$ T cells, followed by an overwhelming production of cytokines and chemokines, namely tumor necrosis factor (TNF) and interferon-gamma (IFNγ) [336-338].

Mtb infection has been widely researched, and the pulmonary immune response is well-documented, however, there is a gap in knowledge on how TB affects the CNS. Current research on the neurological impact of TB disease utilizes either *in vitro* experimentation or *in vivo* methods involving

direct intracerebral injection of Mtb, excessive bacterial aerosol exposures, or models of tuberculosis meningitis (TBM) [339-355]. TBM is a progressive form of the disease where bacteria cross the blood–brain barrier (BBB) and cause inflammation of the meninges. Although these methods elucidate important findings related to mechanisms of neuronal infection and neuroinflammatory signaling in direct response to the bacteria, these studies do not translate to clinical settings. Diagnoses of TBM are rare, encompassing less than 2% of TB cases [356]. Physical brain infection or high bacterial inoculum models are ineffective representations of most disease cases, where infection occurs due to inhalation of a few aerosolized bacilli. Therefore, knowledge of the neurological changes that occur in response to solely peripheral infection is needed.

Epidemiologic studies show that patients with TB, without a diagnosis of TBM, are at an increased risk for Parkinson's Disease (PD) and dementia [161, 357, 358]. Additionally, TB patients demonstrate decreased performance on evaluations of memory, cognition, and neuropsychological functioning [46]. It is also shown that patients who are co-infected with Human Immunodeficiency Virus (HIV) and pulmonary TB have decreased neuropsychological functioning and are three times more likely to experience cognitive impairment compared to uninfected patients, and nearly twice as likely as those who have HIV alone [359]. Such data demonstrate substantial risk for CNS-related symptoms associated with TB, despite Mtb rarely penetrating the brain. Accordingly, the permanent neurological implications of peripheral TB, independent of CNS infection, must not be overlooked.

Studies of other peripheral infections and diseases show evidence of a connection between CNS health and systemic inflammation. Patients with rheumatoid arthritis, a chronic inflammatory disease of the joints, have increased depression and anxiety, cognition decline, and markers of neuroinflammation compared to healthy individuals [360-362]. In another study, repeated systemic bacterial infection activated native microglia and increased synthesis of pro-inflammatory cytokines, including interleukin-1β (IL-1β), TNF, and interleukin-12 (IL-12). This occurred even after the infection was resolved [363]. Additional evidence in murine models of colitis demonstrates an altered expression of inflammatory

modulators, including cyclo-oxygenase 2 (COX-2) and glial fibrillary acidic protein (GFAP), in the brain [364]. Moreover, peripheral inflammation is known to exacerbate symptoms of PD in both human patients and animal models, cause glial reactivity, and increases the synthesis of IL-1β in the prion-diseased brain [365-369]. Similar findings are found in models of Alzheimer's Disease (AD), where infection worsens cognitive decline and induces reactive glia [370-372]. Research has also revealed a correlation between neurological state and peripheral inflammation; patients diagnosed with major depressive disorder have markedly increased peripheral blood levels of pro-inflammatory cytokines, including TNF, and interleukin-6 (IL-6) [373, 374]. These findings prove a relationship between systemic disease and health status of the CNS, further establishing the need for research on the neurological changes attributed to TB.

With 1.7 billion people infected worldwide, it is pertinent that we better understand the effects of TB on the brain to limit CNS damage and permanent neurological deficits in patients [9]. Although there are studies showing the long-term cognitive effects associated with Mtb infection, they are limited to cross-sectional designs and do not fully characterize neuropathology or evaluate the mechanism behind their findings. Here, we will assess TB-associated cognitive impairments and behavioral changes in an established low-dose aerosol guinea pig model of TB disease. We correlate these deficits to signs of neurotoxicity throughout the progression of disease; these include biomarkers of glial inflammation and neurodegeneration.

Glial reactivity is a universal characteristic of neuroinflammation and neurodegeneration, irrespective of the particular disease state [375]. Inflammation of the brain, or gliosis, is caused by phenotypically pro-inflammatory glial cells, including astrocytes and microglia. Although glia perform critical homeostatic functions in the brain, such as forming the BBB, maintaining synaptic neurotransmitters, regulating synaptogenesis, neuronal pruning, and immunological surveillance, they can also contribute to neuropathogenesis [376, 377]. Activation and proliferation of glial cells by inflammatory signals and microbial components results in neurotoxic phenotypes. Neurotoxic microglia

are more amoeboid, allowing for increased migration through dense parenchyma and produce pro-inflammatory molecules [378-380]. Liddelow et al. established that microglia release interleukin-1α (Il-1α), TNF, and complement component 1q (C1q) upon activation, all of which play a crucial role in inducing neurotoxic astrocytes [381]. Alternatively, activated astrocytes are more ramified, increasing contact with blood vessels and nearby cells, and upregulate expression of proteins such as GFAP [382, 383]. Although the critical role microglia play in astrocytic polarization has been confirmed, additional research shows that low-level, early activation of astrocytes mediates microglial reactivity, which propagates the cycle of gliosis. Astrocytes promote microglial activation through the production of C-X-C motif chemokine ligand 10 (CXCL10), lipocalin-2 (Lcn2), and complement 3 (C3), as seen in models of stroke and epilepsy [384, 385]. This early astrocytic role may be understated, despite these cells comprising 60–70% of the total cells in the brain and that their contact with the microvasculature allows them to function as a first responder during altered brain states.

Glial inflammation and reactivity are determined not only by transcriptional expression and morphology, but also through quantity, proliferative state, and location within brain regions [386]. Upregulation of S100 calcium-binding protein β (S100β) and GFAP indicate astrocyte activation. Together, this glial polarization results in the release of reactive oxygen species (ROS) and nitric oxide (NO), contributing to oxidative stress in neurons, and pro-inflammatory mediators [387, 388]. Chronic neuroinflammation disrupts synaptic function and causes irreversible damage to neurons, ultimately leading to the degeneration and death of these essential cells [389].

Gliosis contributes to the misfolding of proteins, resulting in oligomers that form stable, insoluble aggregations. These aggregates are characteristic biomarkers of neurodegenerative diseases, including AD, PD, and dementia. One such protein is microtubule associated protein tau (Tau), which becomes phosphorylated in its misfolded form (pTau). Tau is normally involved in microtubule stabilization during axonal transport, and plays a role in DNA stabilization and synaptic functioning [259]. Phosphorylated residues have been identified and correlated to early and late stages of disease, and can aggregate into

toxic neurofibrillary tangles. Similarly, amyloid β is another physiologically relevant protein that is thought to play a role in neuroprotection from viral and bacterial pathogens. Due to improper cleavage events of the amyloid precursor protein (APP) by the gamma-lyase protease, the amyloid β_{1-42} protein can accumulate into extraneuronal plaques [390]. Another misfolded protein of interest in PD pathology is alpha-synuclein, which is found in phosphorylated and aggregated forms. The formation and accumulation of these proteins propagate increased misfolding [391, 392]. This occurs, in part, due to the amplified production of enzymes and the native proteins themselves, to overcompensate for the loss of function. Misfolded proteins spread in a "prion-like" manner throughout various regions of the brain. This spread occurs through a cycle of intracellular formation and secretion followed by transcellular uptake by nearby cells [392, 393]. Ultimately, the formation of these misfolded oligomers and aggregates results in reduced activity and survival of neurons, due to impaired physiological functioning by the proteins [394]. Aggregates also exacerbate neuroinflammatory signaling events, which leads to endoplasmic reticulum stress and translational inhibition, which further contributes to neuropathogenesis [394, 395].

In our study, animals are infected by low-dose aerosol of Mtb, similar to the natural route of infection in humans. Here, we demonstrate that this guinea pig model of Mtb exposure shows cognition and behavior changes that cannot be attributed to bacterial dissemination to the brain. Further, we characterize the induction and proliferation of pro-inflammatory glia throughout the progression of disease in multiple brain regions vital to physiological function, sensation, and cognition. Finally, we show neurodegenerative biomarkers and neuronal loss in animals. Although further investigation is necessary to fully elucidate the mechanism of neuropathogenesis, our data illuminate fundamental neurological changes in a rodent model that supports published epidemiological data.

2.2 METHODS

2.2.1 Animals and Sample Collection

Experiments consisted of 2- to 4-week-old, female, outbred Dunkin–Hartley guinea pigs (Elm Hill, USA). They were housed in a biosafety level 3 laboratory at the Colorado State University Laboratory Animal Resources facility accredited by the American Association for Accreditation of Laboratory Animal Care (AAALAC). All experimental animals were pair housed under constant temperature and humidity conditions (21° ± 2°C temperature and 30 ± 5% humidity). A 12-h light/12-h dark cycle was used, and animals had *ad libitum* access to food and water. Animals were monitored using a clinical scoring system for signs of morbidity and weighed weekly by laboratory staff for the duration of the experimental period. All animal experiments were performed in accordance with the National Research Council's Guide for the Care and Use of Laboratory Animals and were approved by the Institutional Animal Care and Usage Committee (IACUC) at Colorado State University.

At the time of euthanasia, guinea pigs were administered 50 mg/kg of ketamine and 5 mg/kg of xylazine via intramuscular injection for anesthetic induction. Under terminal anesthesia, blood was collected, and then guinea pigs were euthanized by intraperitoneal overdose of pentobarbital. Tissues were collected for histopathology by fixing in 4% paraformaldehyde or 10% buffered formalin, or stored at −80°C for subsequent homogenization and quantification of Mtb.

2.2.2 Mtb Aerosol Exposure

Culture stocks of *Mycobacterium tuberculosis* (Mtb) strain H37Rv (TMC #102, Trudeau Institute) were collected at an OD600 nm between 0.8 and 1.0, and frozen at −80°C in Proskauer-Beck liquid medium containing 0.05% Tween-80. Titer was determined and bacteria were diluted in sterile water to 1×10^6 colony-forming units (CFU)/mL. Animals were exposed to a low- dose of Mtb by aerosol, calibrated to deliver 20–50 bacilli per animal. Approximately 20 CFU of Mtb were delivered by aerosol to each animal with the Glas-Col Airborne whole-body exposure apparatus. Guinea pigs were exposed over the course of 2 days. Each run contained a single guinea pig for euthanasia and necropsy

24 hours after exposure to confirm Mtb low-dose delivery to the lungs. Uninfected animals were exposed to sterile water using the same procedure in the Glas-Col device.

2.2.3 Behavioral Testing

In order to minimize stress caused by the tests and discourage freeze behavior, all animals were handled daily 2 week prior to testing and throughout the duration of the experiments. Two total tests were performed: the Novel Object Recognition (NOR) Test and open field test. Tests were performed on randomized days, between 10 am and 7 pm, once every 2 weeks throughout the experimental period. Testing occurred under dim light in the same room as the animals were housed, separated by plastic drapes, to eliminate unnecessary stress caused by transfer to an alternate testing room. The researcher remained outside the testing room while trials occurred, and a white noise machine was used to alleviate the effects of background noise. Each test was recorded using a mounted GoPro HERO 5 and analyzed; behavior was scored blind to the treatment groups. All objects and chambers were thoroughly cleaned using Quatricide (diluted 1:64 in H_2O; Pharmacal, Cat #: 65020F) followed by 70% EtOH between animals and decontaminated using Accel TB Disinfectant between groups.

2.2.3.1 Novel object recognition test

The Novel Object Recognition (NOR) Test is used to assess non-spatial, hippocampal, long- and short-term memory in animal models. Prior to testing, the guinea pigs were habituated to the chamber for 5 min per animal. The test consists of two periods: an acquisition phase and a testing phase. During the acquisition phase, the animals were placed in a chamber (24 inches × 24 inches × 18 inches) made of black acrylic with two of the exact same objects (A,A') for ten min to familiarize themselves with them. Six hours later, the guinea pigs were placed in the same chamber with one of the same objects (A) from the acquisition period and one completely new object (B) for 5 min; animals were recorded for the entirety of the testing phase. The objects, approximately two inches wide by three inches tall, were constructed with Legos of various colors and shapes. They were placed approximately six inches apart in

the apparatus. Data analysis was manually performed blind to the treatment groups by laboratory personnel. Time exploring the novel (b) and familiar (a) objects during the testing phase was determined, which only included direct contact the animal had with the object. This included, but was not limited to, biting, sniffing, or climbing on the object; any time the animal was not directly engaging with the object, such as standing near it, was excluded from the exploration time for that object. Total exploration time (e) was calculated by finding the sum of the exploration time for the familiar object (a) and novel object (b) (a + b). The absolute discrimination measure was calculated by subtracting the familiar object exploration time (a) from the novel object exploration time (b) (b – a). The discrimination index is evaluated as the novel object exploration time (b) minus the familiar object exploration time (a) divided by total exploration time (e) [(b – a)/e]. A positive discrimination index value means the animal spent more time exploring the unfamiliar object, which indicates that it remembers seeing the familiar object and has no memory loss or an intact long-term memory. Alternatively, a negative discrimination index means the animal spent more time exploring the familiar object and is indicative of non-spatial memory loss.

2.2.3.2 Open Field Test

Overall movement, locomotor activity, and anxiety-like behavior were determined using the open field test. The open field apparatus consisted of a square open field (24 inches × 24 inches × 18 inches) constructed of black acrylic. Twenty-four hours prior to testing, the guinea pigs were habituated to the chamber for 5 minutes per animal. Each guinea pig was taken from its home cage, placed into the center of the apparatus, and allowed to explore freely for a period of 5 minutes; animals were recorded for the entirety of the testing period. Video data were analyzed with Toxtrac [396]. Time spent in the interior portion of the apparatus is a standard way of identifying anxiety in animal models.

2.2.4 Bacterial Burden/CFU Counts

For confirmation of bacterial enumeration at 24 hours and quantification of bacterial dissemination at each timepoint, lung, spleen, and brain were collected, weighed, and homogenized in

PBS. Total liquid homogenate was diluted 1:10 and serial dilutions of tissue homogenate were performed in PBS and plated on nutrient 7H11 agar. Plates were incubated for 3–6 weeks at 37°C, CFU were counted, and CFU's per gram of tissue were calculated.

2.2.5 Tissue Processing for Histopathology

Brains and visceral organs were extirpated *en bloc* and fixed whole in 10% buffered formalin or 4% paraformaldehyde at room temperature for at least 48 h. Tissues were processed using a Leica TP1020 Automatic Benchtop Tissue Processor and embedded in paraffin wax (Cancer Diagnostics, Cat #: EEPAR56). They were then sectioned on a Thermo Scientific HM 325–2 Manual Microtome at 5 μm thickness and mounted on positively charged glass slides (Superfrost Plus, Cancer Diagnostics, Cat #: 4951) for staining and analysis. One whole-tissue section per animal was stained with hematoxylin and eosin (H&E) for determination of morphological and histopathological changes.

2.2.6 Immunohistochemistry

Whole brain sections were stained for markers of gliosis and neurodegeneration. Tissue sections were deparaffinized in xylene and rehydrated through graded ethanol, followed by chemical and heat induced antigen retrieval using 0.01 M sodium citrate (pH 6.0) or EDTA buffer (1 mM EDTA disodium salt dihydrate, 0.05% Tween; pH 8.0) for 20 min at 100°C. This was followed by removal of endoperoxides by 0.3% hydrogen peroxide for 30 min at room temperature. Tissue was permeabilized [0.1% Triton-X in 1 M Tris Buffered Saline (TBS)] and blocking was performed in 10% goat, donkey, or horse serum diluted in 1 M TBS. Primary antibodies were diluted to their optimized concentrations in 1 M TBS and incubated on the tissue at 4°C overnight. A goat anti-ionized calcium binding adaptor molecule 1 (Iba1) antibody (1:400; Abcam, Cat #: ab5076) was used to identify microglia. A rabbit anti-S100 calcium-binding protein β (S100β) antibody (1:750; Abcam, Cat #: ab41548) was used for astrocyte identification. Amyloid β was identified using an anti-beta Amyloid$_{1–42}$ antibody (1:250; Invitrogen, Cat #: 44–344). Identification of phosphorylated tau was performed using the following antibodies: anti-

phospho-Tau (Ser404) (1:400; Cell Signaling, Cat #: 35834), anti-phospho-Tau-T217 (1:200; ABclonal, Cat #: AP1233), and anti-phospho-Tau (Thr181) (1:800; Invitrogen, Cat #: MN1050). Neurons were identified using an anti-neuronal nuclei (NeuN) antibody (1:500; Cell Signaling, Cat #: 24307). Wash steps were performed using 2% bovine serum albumin and 2% Triton-X in 1 M TBS. An ABC HRP peroxidase detection kit (Vector Laboratories, Cat #: pk-4,000) and ImmPACT DAB Substrate, Peroxidase (HRP) Kit (Vector Laboratories, Cat #: sk-4,105) was used as chromogen and slides were counterstained with hematoxylin (Thermo Fisher Scientific, Cat #: 7231) and bluing solution (Cancer Diagnostics, Cat #: FX2107). All slides for each antigen of interest received the same immunoreaction period, which were visualized by a single pathologist in a blinded fashion. Slides were secured with a coverslip in mounting medium and stored at room temperature until imaging. Whole tissue images were taken using an Olympus BX53 microscope with an Olympus DP70 camera using an Olympus UPlanSApo 20x objective (N.A. = 0.75). Representative images were taken using an Olympus BX53 microscope with an Olympus DP70 camera using an Olympus UPlanFL N 40x objective (N.A. = 0.75).

2.2.7 Immunofluorescence

Paraffin embedded brain sections were deparaffinized in xylene and rehydrated through graded ethanol, followed by chemical and heat induced antigen retrieval using EDTA buffer (1 mM EDTA disodium salt dihydrate, 0.05% Tween; pH 8.0) for 20 min at 100°C. This was followed by permeabilization using 0.01% Triton X diluted in 1 M TBS. Blocking was performed with 2% donkey and goat serum diluted in 1 M TBS. Sections were stained for microglia using a goat anti-ionized calcium binding adaptor molecule 1 (Iba-1) antibody (1:50; Abcam, Cat #: ab5076) and a donkey anti-goat Alexa Fluor 555 secondary antibody (1:500; Invitrogen, Cat #: A21432). Astrocyte stains used a mouse anti-S100 calcium-binding protein β (S100β) (1:750; Abcam, Cat #: ab212816) with a goat anti-mouse Alexa Fluor 555 secondary antibody (1:500; Invitrogen, Cat #: A21422) and a rabbit anti-glial fibrillary acidic protein (GFAP) (1:250; Dako, Cat #: Z0334) with a donkey anti-rabbit Alexa Fluor 647 secondary antibody (1:500; Invitrogen, Cat #: A31573). Following DAPI (Sigma), slides were mounted on glass

coverslips in ProLong Gold Antifade mounting medium (ThermoScientific), fixed for 24 h at room temperature, and then stored at 4°C until imaging. Representative images were captured using an Olympus BX63 fluorescence microscope equipped with a motorized stage and Hamamatsu ORCA-flash 4.0 LT CCD camera using a 40x Olympus X-Apochromat air objective air objective (N.A. = 0.80). All slides quantified were imaged on the same day with the same exposure per channel.

2.2.8 Cellular quantifications

Whole-slide images of brain tissue stained for Iba-1 and S100β by immunohistochemistry were analyzed. Regions of interest were manually drawn for each brain region and number of positive cells was quantified using manual thresholding on the Count and Measure function of Olympus CellSens software (v1.18). Whole-slide images of brain tissue stained for GFAP by immunofluorescence was also analyzed. Regions of interest were manually drawn for each brain region, and mean gray intensity of GFAP expression for each ROI was determined using manual thresholding on the Count and Measure function of Olympus CellSens software (v1.18). Percent total expression or cell number was calculated for each protein of interest by determining the minimum (min) and maximum (max) quantifications for the data set. Each raw quantification (raw) for that brain region received the following calculation: [(raw – min)/(max – min)*100]. Slides stained for NeuN were imaged at 40× magnification (3–4 images per hippocampal region), and manually counted by a blinded scientist.

2.2.9 Pathological scoring

Whole slides stained for Amyloid β_{1-42} and phosphorylated tau were independently scored, in a blinded fashion, by three researchers. Positive immunohistochemical staining in the hippocampus and brain stem was designated a score between 0 and 5 based on the following factors: number of positive cells, amount of extracellular protein accumulation, and intensity of expression. A higher score equates to worse pathology. The mean of the three scores for each animal was calculated and represented.

2.2.10 Statistical analysis

All data were presented as mean +/− SEM. A ROUT (Q = 1%) outlier test was performed on all data to identify potential outliers, which were removed from the data set. Differences between experimental groups were analyzed using either an unpaired t-test with Welch's *post hoc* correction or a one-way ANOVA with Tukey's *post hoc* test. Statistical analysis was performed using Prism. Fit spline analysis was performed on glial data (200 segment output, 4–5 knots). Significance is denoted as * = $p \leq 0.05$, ** = $p \leq 0.01$, *** = $p \leq 0.001$, and **** = $p \leq 0.0001$.

2.3 RESULTS

2.3.1 Low-dose aerosol with Mtb H37Rv failed to disseminate to the brain of guinea pigs.

Histopathology and colony-forming unit (CFU) assays were used to determine infection of peripheral organs and the brain in animals at 60 and 90 days post-infection (dpi). Lung, spleen, and brain tissue were collected from Dunkin-Hartley guinea pigs uninfected or infected with aerosolized Mtb H37Rv. Paraffin-embedded tissue sections were stained with hematoxylin and eosin (H&E) and examined. Representative hippocampal sections show no characteristic granulomatous inflammation, with an absence of cellular infiltration and microvascular abnormalities, in any of the animals infected for 60 and 90 days post-infection, similar to healthy tissue shown from uninfected animals (**Figure 5A–C**). Granulomatous lesions were not found in any brain region of all infected animals. H&E of lung from uninfected animals shows healthy vascular and pulmonary structure (**Figure 5D**). Lung tissue from Mtb-infected animals reveals granulomas characterized by areas of central necrosis, marked infiltration of peripheral immune cells, giant cells, and calcification (red arrow) across large areas of the pulmonary parenchyma (**Figure 5E** and **F**; between brackets). CFU assays show significant bacterial load in lung and spleen homogenates of animals infected for 60 and 90 days post-infection, but no colonies were detected from the brain homogenate of animals at either timepoint, which is indicative that detectable bacteria did not disseminate to the brain (**Figure 5G**). The limit of detection for this assay was 2 CFU.

2.3.2 Memory loss and hyperactivity evident in guinea pigs at 90 days post-infection.

Behavioral tests were performed to determine activity and loss of cognition in animals uninfected or infected with Mtb throughout the progression of the disease. The open field test was used to measure overall activity and mobility in animals. Although a decrease is seen at 30 dpi, Mtb-infected animals show a significant increase in mobility rate at 45 dpi and 60 dpi, and a trending increase at 75 dpi (**Figure 6A, E, I,** and **M**). A significant increase in distance moved and velocity is also seen at 30 dpi, 45 dpi, and 60 dpi (**Figure 6B, C, F, G, J,** and **K**). Animals spent more time in the interior portion of the apparatus at 45 and 60 dpi (**Figure 6H** and **L**). There was no difference in mobility rate, distance, velocity, or time spent in the interior in animals uninfected compared to those infected with Mtb for 75 dpi (**Figure 6M–P**). Together, these data suggest anxiety-like behavior associated with disease. The novel object recognition (NOR) test, which evaluates hippocampal memory, shows a significant decrease in discrimination index with progressive disease. This is indicative of non-spatial memory loss in infected animals (**Figure 6Q** and **R**).

2.3.3 Glial proliferation with progression of tuberculosis disease in multiple anatomical regions across the brain.

Brains from guinea pigs infected for 0, 15, 30, 60, and 90 days post-infection with aerosolized Mtb were analyzed for glial migration and proliferation. Iba-1$^+$ microglia as well as S100β$^+$ and GFAP$^+$ astrocytes were detected in brain regions critical for motor function, memory and cognition, and special senses. This included the following anatomical regions: cerebellum, brain stem, somatomotor cortex, hippocampus, somatosensory cortex, dorsal motor nucleus, visual cortex, and olfactory cortex. Microglial quantifications in the aforementioned regions, except for the dorsal motor nucleus, show a significant increase in Iba-1$^+$ cells at 30 dpi that decreases back to baseline by 90 dpi (**Figure 7F, P, V, FF, LL, VV; 4F, P, V, FF; 5V, FF, LL, VV**). The dorsal motor nucleus, where the vagus nerve innervates the brain, shows an increase in microglia at 60 dpi that decreases by 90 dpi (**Figure 9F** and **P**). Representative images in the cerebellum (**Figure 7A–E**), brain stem (**Figure 7Q–U**), somatomotor cortex

(**Figure 7GG–KK**), hippocampus (**Figure 8A–E**), somatosensory cortex (**Figure 8Q–U**), dorsal motor nucleus (**Figure 9A–E**), olfactory cortex (**Figure 9Q–U**), and visual cortex (**Figure 9GG–KK**) show these cellular fluctuations across progressive disease.

Astrocytes in those same brain regions were also quantified. S100β$^+$ astrocytes peak at 60 dpi in the dorsal motor nucleus (**Figure 9L** and **P**). A similar finding is seen in other brain regions, except an increase in cell number at 15 dpi precedes the 60 dpi peak, in the cerebellum (**Figure 7L** and **P**), brain stem (**Figure 7BB** and **FF**), hippocampus (**Figure 7L** and **P**), and visual cortex (**Figure 9RR** and **VV**). Little to no change is seen in the somatomotor cortex (**Figure 7RR** and **FF**), somatosensory cortex (**Figure 8BB** and **FF**), or olfactory cortex (**Figure 9BB** and **FF**). Representative images in the cerebellum (**Figure 7G–K**), brain stem (**Figure 7W–AA**), somatomotor cortex (**Figure 7MM–QQ**), hippocampus (**Figure 8G–K**), somatosensory cortex (**Figure 8W–AA**), dorsal motor nucleus (**Figure 9G–K**), olfactory cortex (**Figure 5W–AA**), and visual cortex (**Figure 9MM–QQ**) show these cellular fluctuations across progressive disease. To see if astrogliosis is present in regions without changes in S100β$^+$ cell number, or if glial reactivity progresses past 60 dpi, GFAP expression was quantified at 0, 60, and 90 days post-infection. Significant increases occur at 90 dpi in the somatomotor cortex (**Figure 7UU** and **VV**), hippocampus (**Figure 8O** and **P**), somatosensory cortex (**Figure 8EE** and **FF**), and olfactory cortex (**Figure 9EE** and **FF**) with trending increases in brain stem (**Figure 7EE** and **FF**) and DMN (**Figure 9O** and **P**). Graphical representations show the interaction between glia across the progression of the disease (**Figures 7P, FF, VV; 4P, FF; 5P, FF, VV**).

2.3.4 Glial reactivity is sustained as tuberculosis disease progresses.

Brains from animals infected with Mtb for 0, 60, and 90 days were evaluated by immunofluorescence scanning microscopy for Iba1$^+$ microglia and S100β$^+$/GFAP$^+$ astrocytes. Representative images of the eight brain regions stained above are shown, including the cerebellum, brain stem, somatomotor cortex, hippocampus, somatosensory cortex, dorsal motor nucleus, olfactory cortex, and visual cortex. Separated and merged channels from each brain region at 0 dpi show ramified

microglia, or a non-reactive, anti-inflammatory cellular phenotype (**Figure 10A, G, M, S, Y, EE, KK,** and **QQ**). Alternatively, pro-inflammatory microglia with an ameboid-like morphology are seen in all brain regions in animals 60 days post-infection (**Figure 10B, H, N, T, Z, FF, LL,** and **RR**) and 90 days post-infection (**Figure 10C, I, O, U, AA, GG, MM,** and **SS**). Similarly, separated and merged channels show non-reactive astrocytes, with fewer branches and shortened processes, at 0 dpi (**Figure 10D, J, P, V, BB, HH, NN,** and **TT**) but activated astrocytes, characterized by increased branch density, are found in all brain regions 60 dpi (**Figure 10E, K, Q, W, CC, II, OO,** and **UU**) and 90 dpi (**Figure 10F, L, R, X, DD, JJ, PP,** and **VV**). Some astrocytes identified in the brains of Mtb-infected animals also come in contact with nearby cell nuclei (**Figure 10E, F, K, L, Q, X, DD, II, JJ, OO, PP, UU,** and **VV**). The data establish that glial cells sustain neurotoxic phenotypes throughout the course of tuberculosis disease.

2.3.5 Amyloid beta aggregation presents in guinea pigs at 90 days post-infection with Mtb.

Amyloidosis was determined in guinea pigs infected with Mtb for 90 days. Representative images of intracellular amyloid β_{1-42} in the hippocampus (**Figure 11A** and **B**) and brain stem (**Figure 11D** and **E**) are shown. Additionally, representative images show extracellular aggregates identified in the brain stem of animals 90 dpi that are absent in uninfected animals (**Figure 11G–I**). Pathological scoring indicates amyloid β_{1-42}accumulation was significantly increased in both brain regions in animals 90 dpi compared to uninfected controls (**Figure 11C** and **F**).

2.3.6 Intracellular accumulation and extracellular tangles of hyperphosphorylated tau in guinea pigs at 90 days post-infection with Mtb.

The presence of the neurodegenerative biomarker phosphorylated and aggregated tau was evaluated in Mtb-infected guinea pigs. Three different phosphorylation sites of tau (pTau) were analyzed by immunohistochemistry, including tau phosphorylated at serine 404 (pTau S404), threonine 217 (pTau T217), and threonine 181 (pTau Th181). Representative images and pathological scoring show no difference in pTau S404 and pTau T217 in both the hippocampus (**Figure 12A–C, G–I**) and brain stem

(**Figure 12D–F, J**) of animals infected for 90 dpi compared to uninfected controls. There is a significant increase in the pathological score of pTau Th181 in both brain regions by 90 dpi (**Figure 12O** and **R**), including the formation of fibrils (**Figure 12N**) and hyperphosphorylated tau tangles (**Figure 12Q**) that are absent in uninfected animals (**Figure 12M** and **P**).

2.3.7 Neurodegeneration in multiple anatomical regions of the hippocampus in guinea pigs at 90 days post-infection with Mtb.

Staining was performed to determine neuronal loss and degradation in two relevant anatomical regions of the hippocampus, the Cornu Ammonis 1 (CA1) and Cornu Ammonis 3 (CA3). Paraffin-embedded tissue sections were stained with hematoxylin and eosin (H&E) and examined. Representative brain sections show an increase in the number of pyknotic neurons (identified as shrunken cells with condensed dark purple chromatin) in both hippocampal regions in guinea pigs infected with Mtb for 90 days (**Figure 13A, B, F,** and **G**). Immunohistochemical staining for the neuronal marker NeuN was also performed, and representative images are shown (**Figure 13C, D, H,** and **I**). Quantifications demonstrate a significant decrease in the number of $NeuN^+$ neurons in the CA1 (**Figure 13E**) and CA3 (**Figure 9J**) regions of the hippocampus in Mtb-infected animals compared to uninfected controls.

2.4 DISCUSSION

Pulmonary tuberculosis is associated with cognitive deficits and neurodegenerative disorders, establishing this infectious disease as an important risk factor for neurological impairment [161, 357-359, 397]. However, the pathology and cellular reactions in the brain associated with this disease are unknown. Our data are the first, to our knowledge, to fully characterize the cellular changes and etiology of neuropathology throughout the brain during this progressive inflammatory disease. Additionally, current experimentation relies on laboratory models and experimental methods that do not translate to clinical settings, such as the physical injection of bacteria into the brain or the use of Mtb-resistant murine models [351, 354]. Research that appropriately translates to clinical disease is necessary in order to fully

understand what is causing neurological detriments and, eventually, provide possible interventions to prevent them. Guinea pigs are not only susceptible to a variety of Mtb strains but exhibit pulmonary pathology and cellular immune responses similar to human disease [398-400]. In addition, their neurologically relevant proteins show a high degree of protein homology to that of humans (**Supplementary Figure S2**). Therefore, it is reasonable to infer that our guinea pig model of Mtb infection by low-dose aerosol closely mimics clinical disease in human patients.

Animals infected by aerosol with approximately 20 CFU of Mtb H37Rv bacteria established infection of peripheral organs, including the lung and spleen (**Figure 5**), without signs of morbidity or mortality or significant weight loss (**Supplementary Figure S1**). Despite evidence of bacterial dissemination, no characteristic granulomatous lesions were found in any brain region of the animals, and CFU assays did not detect bacteria in tissue homogenate (**Figure 5**). This indicates that the resulting neuropathogenesis is not a direct response to bacterial infection of the brain, but is instead a reaction to pulmonary and extrapulmonary disease, as is documented in patients with cognitive deficits that lack CNS infection [46, 161, 357-359]. While the CFU assay is the gold standard for quantifying bacterial load, it is recognized that unculturable or killed bacteria may not be detected by commonly used methods. Regardless, the absence of granulomatous lesions in the brains of all infected animals suggests that bacterial dissemination to the CNS did not occur, and it is within reason to consider these data as an effect of solely peripheral disease.

To determine whether cognition deficits similar to those documented in human patients are seen in our animal model, behavioral testing was performed on the Mtb-infected guinea pigs. This included the NOR test, which showed a decrease in hippocampal non-spatial memory, and the open field test, where animals exhibited anxious behavior, including increased mobility rate, distance moved, velocity, and time spent in the interior of the chamber (**Figure 6**). Combined, these data are consistent with clinical research and suggests damage to the brain that must be further investigated.

Neuroinflammation is an important pathological contributor to brain injury, disease, and homeostatic dysfunction [375]. Glial cells are critical mediators of this response; thus, the proliferation

and reactivity of these cells were explored. In the cerebellum, brain stem, hippocampus, and visual cortex, a trending, although insignificant, increase in astrocyte number is seen as early as 15 dpi but decreases by 30 dpi in those same brain regions. Subsequently, a significant increase in microglia at 30 days post-infection in those same brain regions is observed. Similar to other disorders, this indicates that early activation of astrocytes occurs in the brain which, in turn, plays a role in initiating microglial reactivity (**Figures 7–9**) [384, 385].

Following the significant microglial migration and proliferation seen at 30 dpi, there is an exacerbated astrocytic response at 60 dpi in the cerebellum, brain stem, hippocampus, dorsal motor nucleus, and visual cortex. This highlights the interplay between these two glial cells, which has been established, where microglia play a role in astrocytic activation [381]. Even though a change in S100β^{+}astrocytes is not found in all brain regions, including the somatomotor cortex, somatosensory cortex, and olfactory cortex, a significant increase in GFAP expression occurs in those regions at 90 dpi. Though changes in cellular quantifications indicate gliosis, astrocytes also upregulate GFAP when reactive and during neuroinflammation, supporting findings of astrogliosis in these brain regions [401]. This upregulation in GFAP expression is particularly relevant considering a change in astrocyte cell number is not seen in all models of neuroinflammation [402]. It must also be considered that glia have heterogenous roles and density depending on their brain region, making some areas more susceptible to glial reactivity than others. Cortical and hippocampal regions have high glial density and lower expression of immune activating genes, whereas the cerebellum and brain stem are less glia rich but proliferate at high rates [403]. Altogether, these indications of gliosis throughout multiple brain regions, especially those related to motor function, explain the hyperactivity demonstrated by Mtb-infected animals during the open field test at the same post-infection timepoints [404]. While common in neurological research, Iba-1 is not solely a marker of microglia but is also present in macrophages. Therefore, these data set may also quantify infiltrating macrophages from the peripheral system. Optimization of antibodies against microglia-specific markers, such as transmembrane protein 119 (TMEM119), in guinea pigs could pose a potential way to address this in future studies. Furthermore,

evidence reports that oligodendrocytes upregulate S100β protein in response to stress [405-408]. It must also be considered that cellular quantifications may include oligodendrocytes, but additional GFAP expression data supplement our discovery of astrogliosis.

To further investigate the glial response to peripheral Mtb infection, morphological changes of the microglia and astrocytes in numerous brain regions were investigated. Neurotoxic glial phenotypes correlate to the production of pro-inflammatory molecules and reactive species that can compromise the brain over time. Astrocytes in guinea pigs 60 and 90 days post-infection appear to have an increased number and length of cellular protuberances compared to uninfected animals, which distinguishes a pro-inflammatory phenotype [383]. This change in cell arbor allows for amplified communication with nearby glia and neurons, as is seen in infected animals, where astrocyte processes come in contact with neighboring cell nuclei. Additionally, the microglia in these brain regions no longer have a ramified neuroprotective phenotype. Instead, they demonstrate decreased process length and branching, or an ameboid-like morphology, with cell body hypertrophy (**Figure 10**) [379]. Although a decrease in the cell number of both astrocytes and microglia are seen in the later stages of disease, the cells in those regions sustain glial reactivity as indicated by their morphology.

Glial priming, especially of microglia, causes these cells to become more sensitive to stimuli and plays a damaging role during age and in neurodegenerative disease [409]. This is seen in cases of neuroinflammation, which leads to the priming of microglia that contributes to AD later in life [410]. The prolonged reactivity of the glia found in the Mtb-infected brain could result in cellular priming that makes these cells more sensitive to additional stimuli and exacerbates their neurodegenerative effects, increasing susceptibility to environmental toxicants and age-related neurodegenerative disease later in life.

Aside from neuroinflammation, other mediators of neurodegenerative disease are misfolded proteins. Found in disorders such as AD, PD, and dementia, these proteins induce inflammatory signaling and lose their normal, but critical, function in neurons. Two neurotoxic proteins of interest are phosphorylated tau and amyloid $\beta_{1\text{-}42}$. Intracellular accumulation, as well as extracellular aggregates, of amyloid $\beta_{1\text{–}42}$ is identified in Mtb-infected guinea pigs (**Figure 11**). While the toxic effects of amyloid β

oligomers and plaques are disputed, it is believed that they are present in the AD brain, establishing their relevancy to the study of neurodegenerative effects. In addition to amyloid β, tau phosphorylated at three amino acids is identified in animals at 90 dpi, which includes serine 404, threonine 217, and threonine 181. Both threonine phosphorylation sites are found in the proline-rich portion of the tau protein, whereas serine 404 is a component of the C-terminus [411]. Phosphorylation at these sites decreases tubulin polymerization and microtubule affinity by the tau protein [412, 413]. Expression of only one residue, pTau Th181, is significantly increased in Mtb-infected guinea pigs, including the formation of extracellular aggregates; the other two phosphorylation sites have no significant change with exposure (**Figure 12**). Studies have shown that aggregation of misfolded proteins results in cellular senescence [414]. Therefore, although there is no change in the phosphorylation of pTau S404 or pTau T217, the presence of extracellular tau tangles in infected animals reveals a worsened disease state. Research also postulates that even though pTau T217 may be a better diagnostic indicator, it is also found in intermediate to late stages of AD progression. In contrast, pTau Th181 is found in earlier, even pre-clinical, stages [415, 416]. Thus, increased accumulation of pTau T217 may occur in Mtb-infected guinea pigs as the disease progresses past 90 dpi. Additionally, misfolded alpha-synuclein, phosphorylated at serine 129, shows a trending increase in expression in the hippocampus and brain stem. Future experimentation of the substantia nigra, a critical region for PD neuropathology, is necessary to fully elucidate these effects (**Supplementary Figure S3**).

Finally, the effect of the reported neuroinflammation and misfolded protein accumulation on neurons was determined. Reactive species produced by pro-inflammatory glia reduce neuronal integrity and ultimately cause the death of these cells [417, 418]. Additionally, misfolded proteins, including amyloid β and tau, result in loss of function and exacerbate inflammation, which further contributes to neurodegeneration. Animals infected with Mtb for 90 days show pyknotic neurons, cells characterized by nuclear condensation caused by necrosis or apoptosis. This is in combination with significant neuronal loss in two anatomical regions of the hippocampus, the Cornu Ammonis 1 (CA1) and Cornu Ammonis 3 (CA3) (**Figure 13**). In both regions, the CA1 especially, neurons are involved in forming, consolidating,

and retrieving memories, which is decreased according to our behavior testing [419]. They are also implicated in neurodegenerative disease, especially in AD [420-422]. Together, these detrimental neuronal effects are likely caused by the sustained glial reactivity and presence of aggregated neurotoxic proteins identified in that brain region (**Figures 8, 11,** and **12**). This cellular clearance and loss of neuronal function may explain the behavior changes and memory deficits demonstrated by Mtb-infected animals at 90 dpi (**Figure 6**). Although $NeuN^+$ neurons decreased with infection, the function of NeuN is not entirely understood. This protein is found in the nucleus and perinuclear cytoplasm of neurons and plays an undetermined role in genetic regulation [423]. Due to the uncertain function of NeuN, there may be neuronal disruptions that cannot be identified by immunohistochemical staining for the protein alone. However, loss of expression combined with morphological identification of pyknotic neurons definitively identifies degenerating cells.

In conclusion, pathological changes within the brain in a pertinent model of pulmonary tuberculosis assist in uncovering the cause of the cognitive deficits and neurodegeneration that is evident in human patients. Although these data play a key role in explaining the neuropathology associated with the disease, further research is necessary to reveal the mechanistic link between peripheral disease and neurological deficits. Here, we demonstrate that there is no detectible, replicating bacteria or granulomatous lesion formation within the brains of these animals, which illuminates an alternative route of cellular activation and ensuing neurodegeneration that cannot be attributed to Mtb itself. The glial response in the dorsal motor nucleus of the vagus nerve proposes a possible point of origin (**Figure 9**), especially considering the vagus nerve innervates organs affected by TB and is known to trigger neuroinflammation in response to peripheral stimulation [424, 425]. Additionally, the effects of the peripheral immune system may also play a pivotal, mechanistic role. Increased evidence indicates that the blood–brain barrier (BBB) is more permeable to peripheral immune cells, such as T cells, macrophages, dendritic cells, and B cells, than previously proposed. Due to the intense cellular reaction in the lungs occurring in response to Mtb infection, it is logical to hypothesize that infiltrating cells may play a role on the activation of glia in the brain, especially considering increased lymphocytes are seen in other models

of systemic infection [426, 427]. Although continued research is necessary, these data unravel important pieces of pulmonary TB-associated neuropathology.

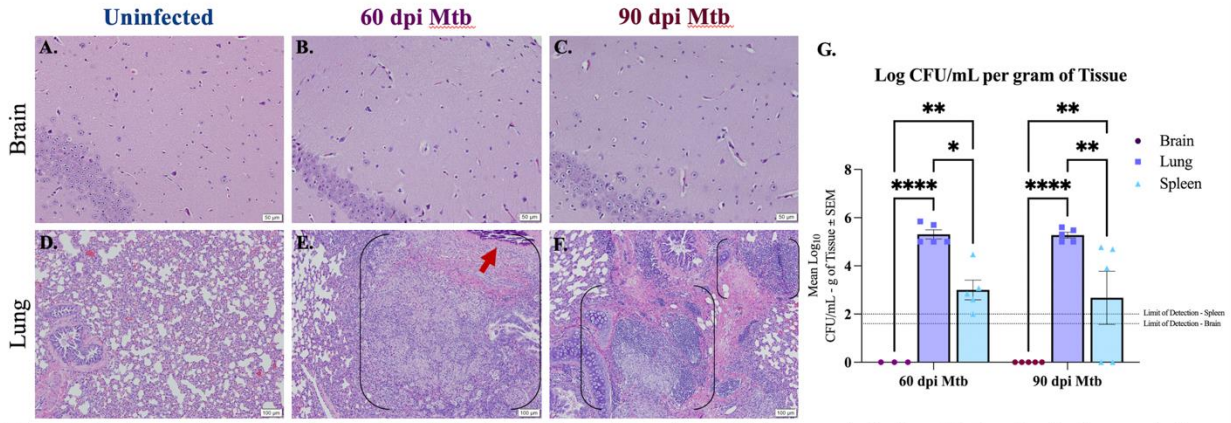

Figure 5. Lesions and bacterial colonies absent in brains of guinea pigs at 60 and 90 days post-infection. H&Es of brain show no lesions in animals uninfected (A) and infected with Mtb for 60 (B) and 90 days post-infection (dpi) (C). Scale Bar = 50 µm. Lung histology shows granulomas (black brackets), including necrotic tissue and calcification (red arrow), in animals 60 and 90 dpi with a low-dose of Mtb by aerosol (E,F) but no granuloma formation is seen in uninfected animals (D). Scale Bar = 100 µm. Colony-forming unit (CFU) assays indicate bacterial dissemination in lung and spleen homogenates, but no bacterial colonies were detected in brain at 60 or 90 dpi with Mtb (G). The limit of detection for this assay is 2 CFU. Each bar represents the mean ± SEM (N = 3–5/group). One-way ANOVA analysis performed; * $p \leq 0.05$, ** $p \leq 0.01$, **** $p \leq 0.0001$.

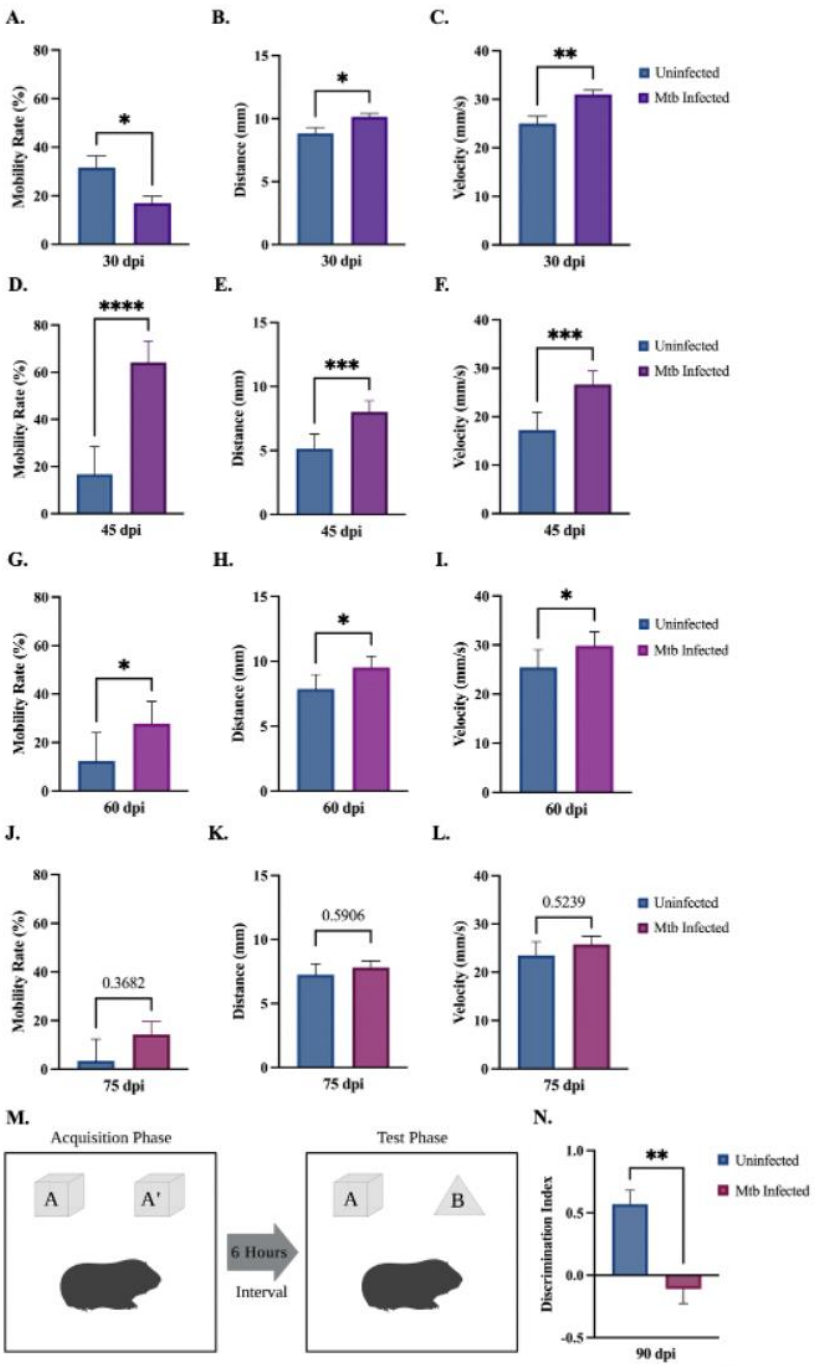

Figure 6. Behavioral deficits detected in guinea pigs at 90 days post-infection. Overall movement and cognition were evaluated in animals infected with Mtb compared to uninfected controls. The open field test assessed animal mobility rate, distance moved, velocity, and percent time spent in the interior of the apparatus over the progression of the disease. At 30 dpi a significant increase in distance and velocity was seen, although a decrease in mobility rate and time spent in the interior also occurred (A–D). All readouts increase at 45 dpi (E–H) and 60 dpi (I–L) until 75 dpi, where no statistical difference is seen between groups (M–P). Overall, these readouts show increased anxiety in infected animals at 45 and 60 dpi. Representation of the novel object recognition (NOR) test is provided (Q). A significant decrease in discrimination index (DI) is demonstrated in animals by 90 dpi compared to controls, which is indicative of non-spatial memory loss. DI = (novel object exploration time – familiar object exploration time)/(total exploration time) (R). Each bar represents the mean ± SEM (N = 3–5/group). Unpaired t-test analysis performed; *p ≤ 0.05, **p ≤ 0.01, ***p ≤ 0.001, and ****p ≤ 0.0001. Created with BioRender.com.

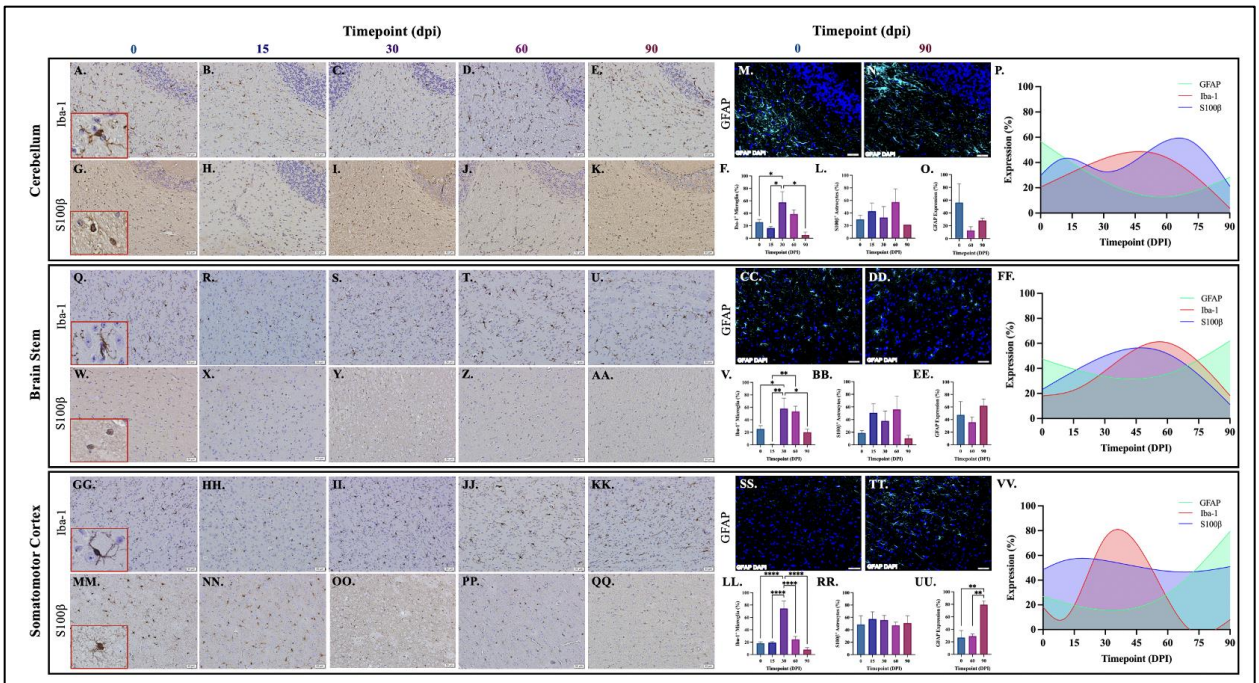

Figure 7. Mtb-associated gliosis in brain regions related to motor function. Immunohistochemical and immunofluorescent staining of guinea pig brain tissue for the microglial marker Iba-1 and astrocytic markers S100β and GFAP was performed. Glial cells in brain regions related to motor function were evaluated over the course of infection with aerosolized Mtb. Representative images of Iba-1$^+$ microglia and S100β$^+$ astrocytes at 0, 15, 30, 60, and 90 days post-infection (dpi) in the cerebellum (A–E,G–K), brain stem (Q–U,W–AA), and somatomotor cortex (GG–KK,MM–QQ) are shown. Iba-1$^+$ cells significantly peak at 30 days post-infection then decrease by 60 and 90 dpi in the cerebellum (F), brain stem (V), and somatomotor cortex (LL). S100β$^+$ cell numbers show a trending increase at 15 and 60 days post-infection in the cerebellum (L) and brain stem (BB). No change in S100β$^+$ cells is seen in the somatomotor cortex (RR). No change in GFAP expression is seen in the cerebellum (O), but a trending increase is found in the brain stem (EE) and significant increase in somatomotor cortex (UU) at 90 dpi. Graphs are shown to visualize the cellular changes of both microglia (Iba-1 in red) and astrocytes (S100β in blue and GFAP in green) in relation to one another across the progression of disease in the cerebellum (P), brain stem (FF), and somatomotor cortex (VV). Each bar represents the mean ± SEM (N = 3–12/group). One-way ANOVA analysis performed; *p ≤ 0.05, **p ≤ 0.01, ***p ≤ 0.001, and ****p ≤ 0.0001. Scale Bar = 50 µm.

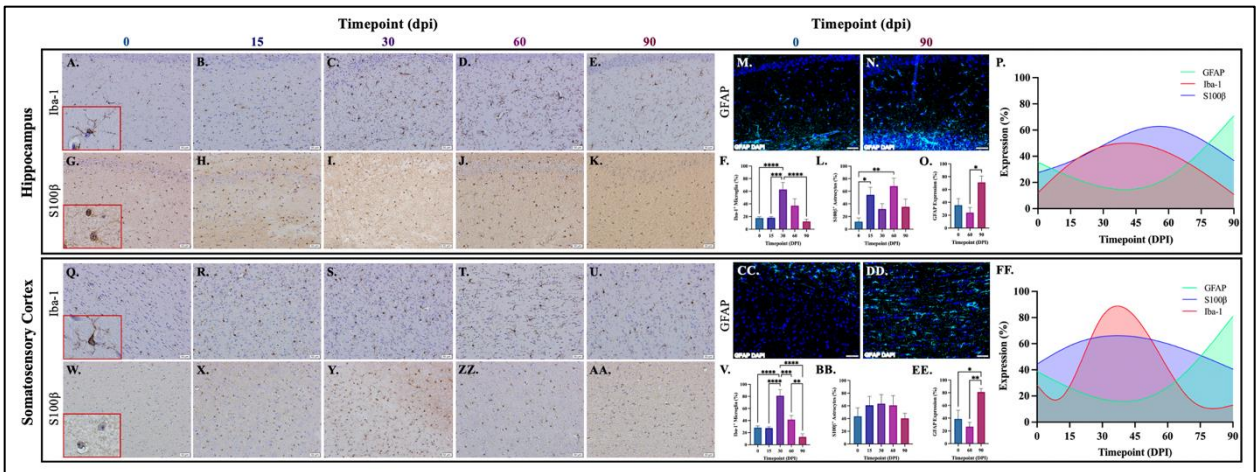

Figure 8. Mtb-associated gliosis in brain regions related to memory, cognition, and sensation. Immunohistochemical and immunofluorescent staining of guinea pig brain tissue for the microglial marker Iba-1 and astrocytic markers S100β and GFAP was performed. Glial cells in brain regions related to memory and cognition were evaluated over the course of infection with aerosolized Mtb. Representative images of Iba-1$^+$ microglia and S100β$^+$ astrocytes at 0, 15, 30, 60, and 90 days post-infection (dpi) in the hippocampus (A–E,G–K) and somatosensory cortex (Q–U,W–AA) are shown. Iba-1$^+$ cells significantly peak at 30 days post-infection then decrease by 60 and 90 dpi in the hippocampus (F) and somatosensory cortex (V). S100β$^+$ cell numbers significantly increase at 15- and 60 days post-infection in the hippocampus (L) but no change is seen in the somatosensory cortex (BB). GFAP expression significantly increases by 90 dpi in both brain regions (O,EE). Graphs are shown to visualize the cellular changes of both microglia (Iba-1 in red) and astrocytes (S100β in blue and GFAP in green) in relation to one another across the progression of disease in the hippocampus (P) and somatosensory cortex (FF). Each bar represents the mean ± SEM (N = 4–12/group). One-way ANOVA analysis performed; *p ≤ 0.05, **p ≤ 0.01, ***p ≤ 0.001, and ****p ≤ 0.0001. Scale Bar = 50 μm.

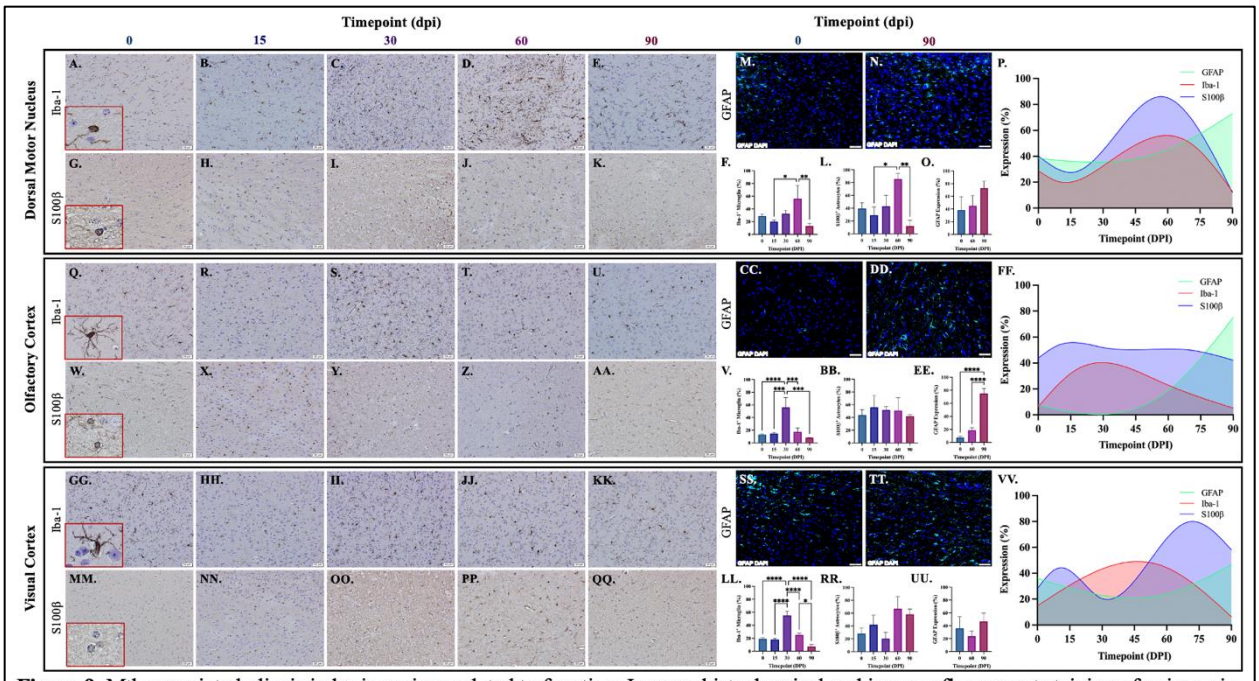

Figure 9. Mtb-associated gliosis in brain regions related to function. Immunohistochemical and immunofluorescent staining of guinea pig brain tissue for the microglial marker Iba-1 and astrocytic markers S100β and GFAP was performed. Glial cells in brain regions related to special senses and parasympathetic function were evaluated over the course of infection with aerosolized Mtb. Representative images of Iba-1$^+$ microglia and S100β$^+$ astrocytes at 0, 15, 30, 60, and 90 days post-infection (dpi) in the dorsal motor nucleus (DMN), where the vagus nerve innervates the brain (A–E,G–K), olfactory cortex (Q–U,W–AA), and visual cortex (GG–KK,MM–QQ) are shown. Iba-1$^+$ cells significantly peak at 30 days post-infection then decrease by 60 and 90 dpi in the olfactory cortex (V) and visual cortex (LL). Microglia in the dorsal motor nucleus peak later, at 60 dpi, before decreasing (F). S100β$^+$ cell numbers do not change in the olfactory cortex (BB) but a trending increase is seen at 60 dpi in the dorsal motor nucleus (L) and visual cortex (RR). A trending increase in GFAP expression is found in the DMN (O) and significant increase at 90 dpi in the olfactory cortex (EE). No change in GFAP expression is seen in the visual cortex (UU). Graphs are shown to visualize the cellular changes of microglia (Iba-1 in red) and astrocytes (S100β in blue and GFAP in green) in relation to one another across the progression of disease in the DMN (P), olfactory cortex (FF), and visual cortex (VV). Each bar represents the mean ± SEM (N = 3–12/group). One-way ANOVA analysis performed; *p ≤ 0.05, **p ≤ 0.01, ***p ≤ 0.001, and ****p ≤ 0.0001. Scale Bar = 50 μm.

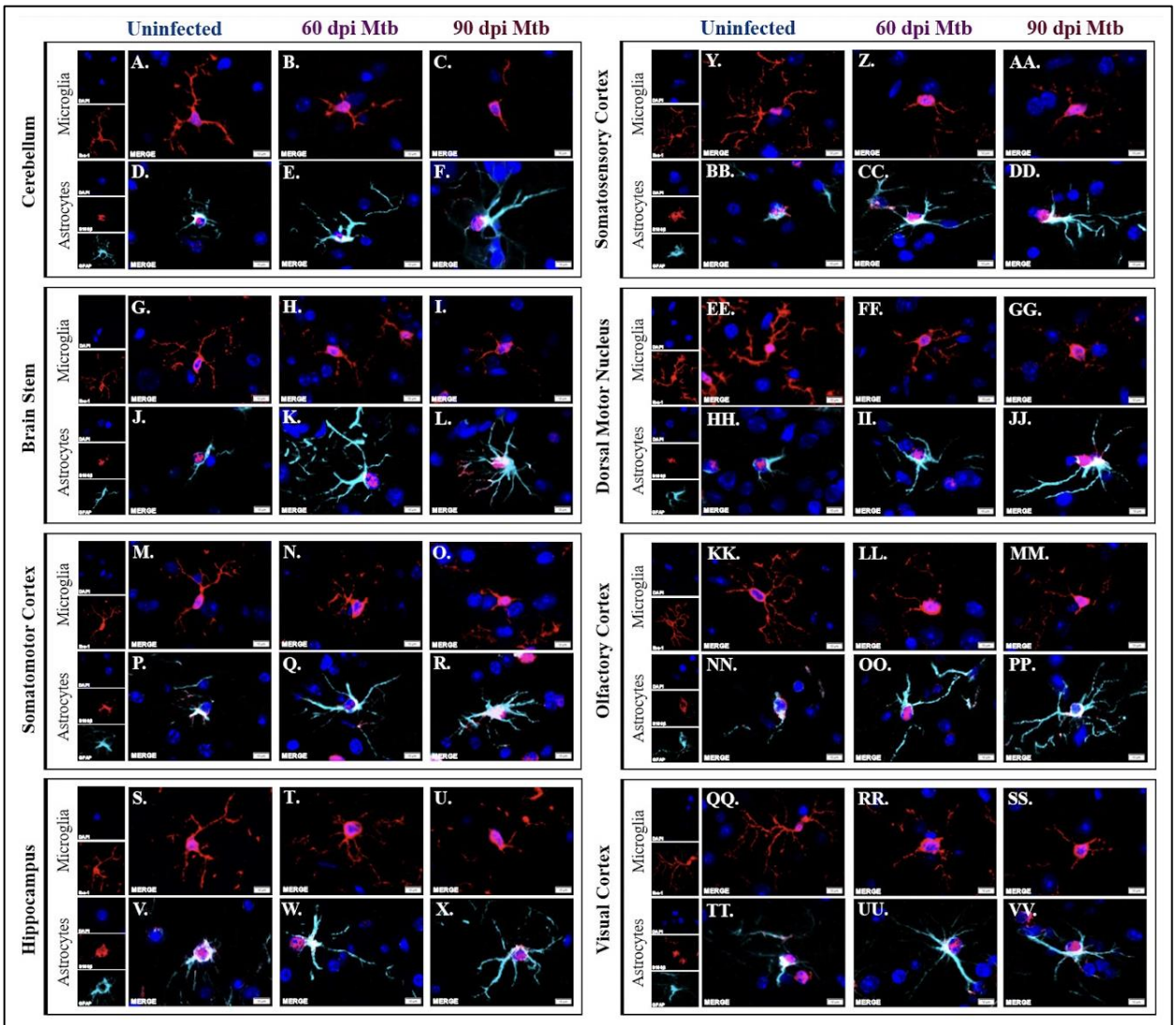

Figure 10. Activated glial morphology sustained throughout disease. Immunofluorescent staining of brain tissue was performed for identification of microglia, using an anti-Iba-1 antibody, and astrocytes, using anti-S100β and anti-GFAP antibodies. Representative images of cells in uninfected animals show phenotypically inactive microglia with increased branch density in the cerebellum (A), brain stem (G), somatomotor cortex (M), hippocampus (S), somatosensory cortex (Y), dorsal motor nucleus (EE) olfactory cortex (KK), and visual cortex (QQ). Microglia in those same brain regions show ameboid-like, reactive microglial phenotypes 60 (B,H,N,T,Z,FF,LL,RR) and 90 days post-infection (dpi) (C,I,O,U,A,GG,MM,SS). Similarly, astrocytes in uninfected animals in those brain regions have an anti-inflammatory phenotype (D,J,P,V,BB,HH,NN,TT) whereas the cells 60 (E,K,Q,W,CC,II,OO,UU) and 90 days post-infection (F,L,R,X,DD,JJ,PP,VV) have reactive phenotypes. Scale Bar = 10 μm.

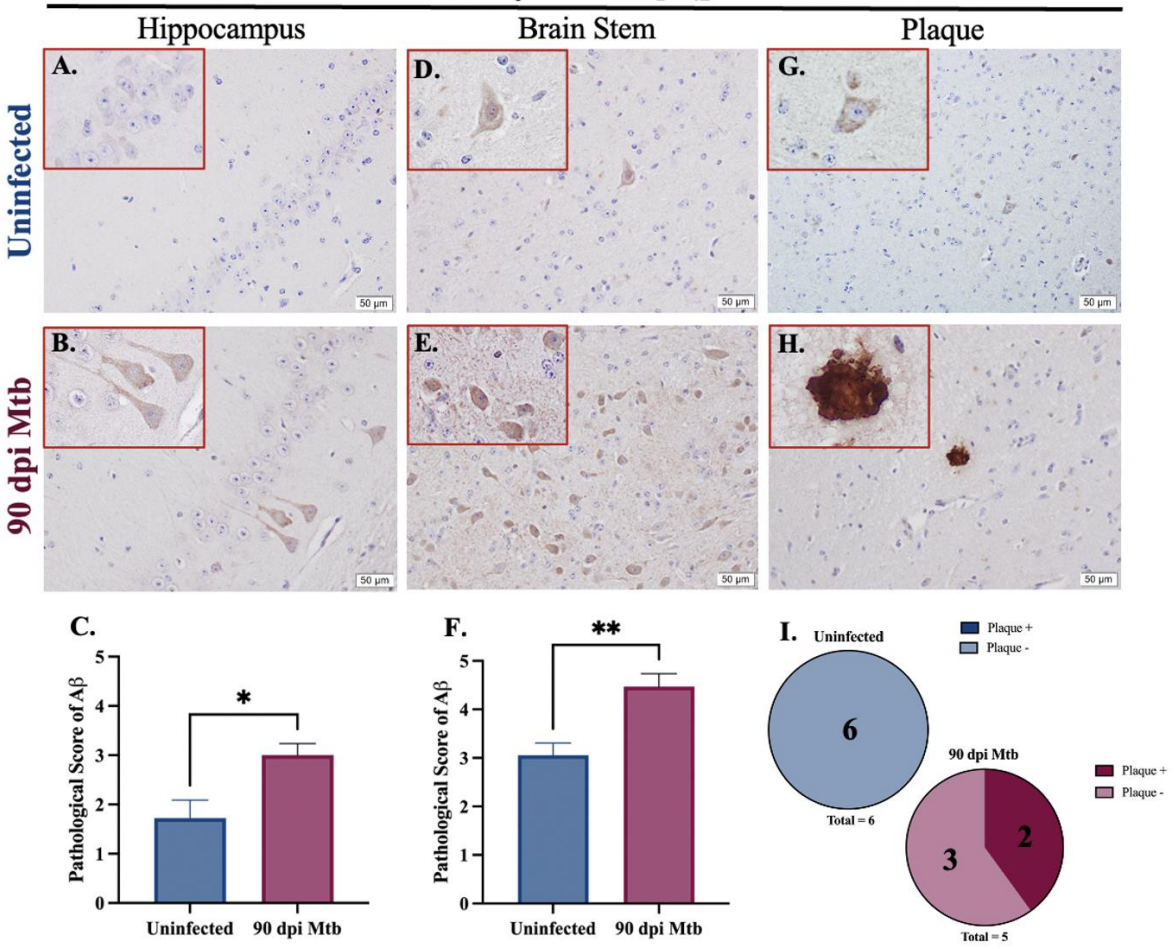

Figure 11. Amyloidosis in guinea pigs at 90 days post-infection with Mtb. Immunohistochemical staining of brain tissue was performed for identification of neurotoxic amyloid β_{1-42}. Positive staining was scored, as determined by number of amyloid β^{+} cells and degree of staining intensity, on a scale of 1–5. Increased intracellular amyloid β_{1-42} is seen in the hippocampus (B) and brain stem (E) of guinea pigs 90 dpi with Mtb compared to uninfected controls in those same brain regions (A,D). Scoring of brain pathology shows a significant increase in misfolded protein accumulation in the hippocampus (C) and brain stem (F). Extracellular plaques of amyloid beta are found in the brain stem of infected animals (H,I) but are absent in uninfected animals (G,I). Each bar represents the mean ± SEM (N = 5–6/group). Unpaired T-test analysis performed; *$p < 0.05$, **$p < 0.01$. Scale Bar = 50 µm.

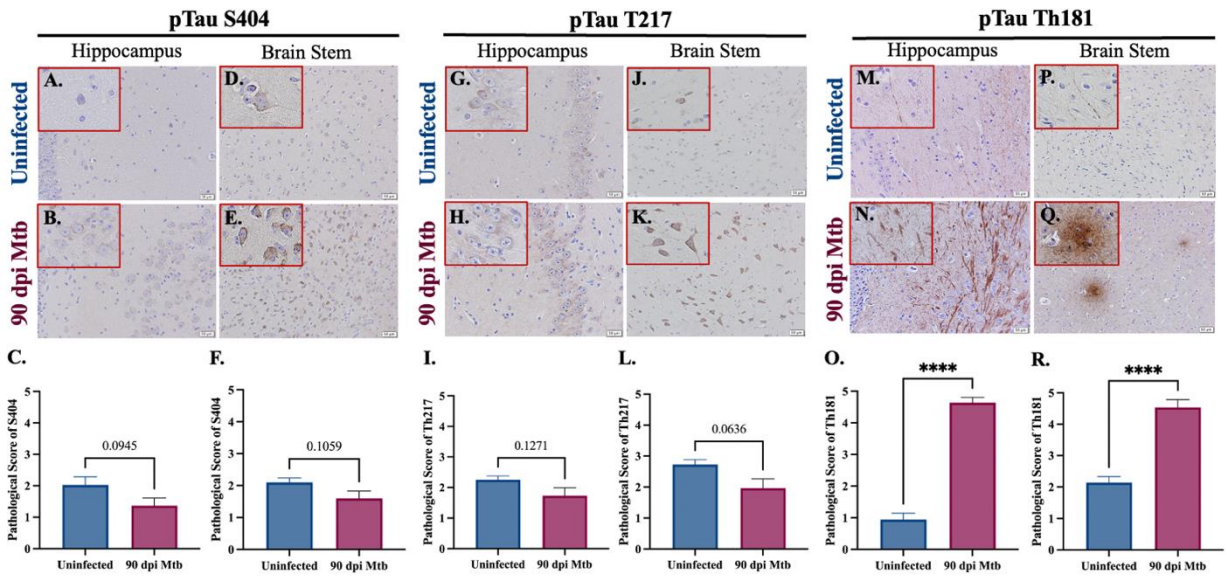

Figure 12. Hyperphosphorylated Tau and Tangles in Guinea Pigs at 90 days post-infection with Mtb. Immunohistochemical staining of brain tissue was performed for identification of tau phosphorylated at different amino acids. Positive staining was scored, as determined by number of tau+ cells and degree of intensity, on a scale of 1–5. No significant difference of tau phosphorylated at serine 404 was detected in the hippocampus (B,C) or brain stem (E,F) of guinea pigs at 90 dpi compared to uninfected controls in those same brain regions (A,C,D,F). Similarly, tau phosphorylated at threonine 217 is identified in the hippocampus and brain stem (G,H,J,K), although there is no significant change in pathological score in uninfected and infected animals (I,L). An increase in fibrils of tau phosphorylated at threonine 181 is found in the hippocampus of guinea pigs 90 dpi (N) compared to uninfected controls (M), as well as the formation of hyperphosphorylated tau tangles in the brain stem (Q) that are absent in uninfected animals (P). Scoring of brain pathology shows a significant increase in misfolded protein accumulation in the hippocampus (O) and brain stem (R). Each bar represents the mean ± SEM (N = 5–6/group). Unpaired t-test analysis performed; ns, not significant, ****$p \leq 0.0001$. Scale Bar = 50 μm.

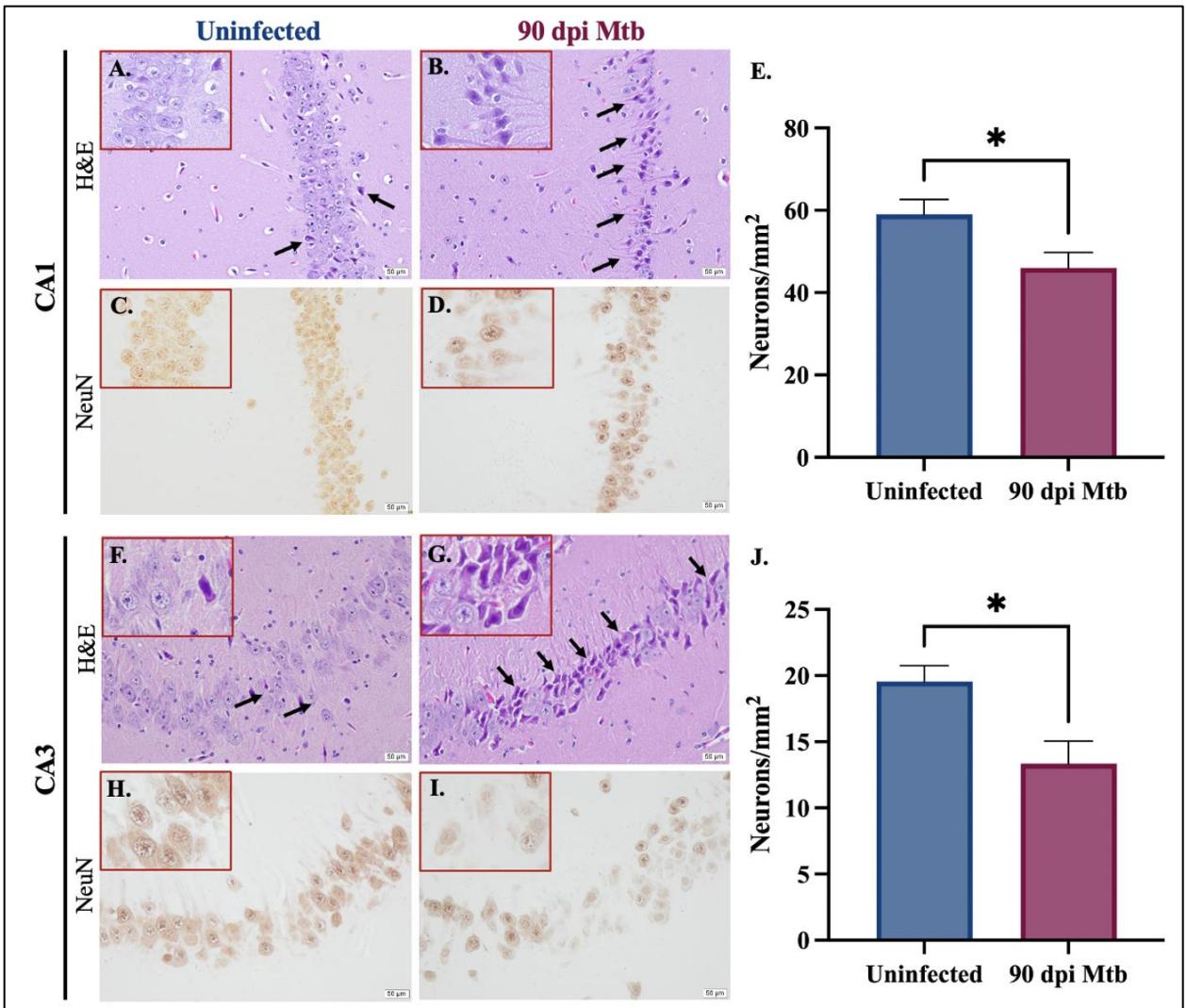

Figure 13. Neuronal loss and degradation in guinea pigs at 90 Days post-infection. H&E staining of the CA1 and CA3 anatomical regions of the hippocampus show an increase in pyknotic neurons (black arrows) in animals infected with Mtb for 90 dpi (B,G) compared to uninfected controls (A,F). Quantification of immunohistochemical staining for neuronal marker NeuN shows a significant decrease in neurons in the CA1 (C–E) and CA3 (H–J) in animals infected for 90 days compared to uninfected animals. Each bar represents the mean ± SEM (N = 5–6/group). Unpaired t-test analysis performed; *p ≤ 0.05. Scale bar = 50 µm.

CHAPTER 3

IMMUNE CELL INFILTRATION AND MODULATION OF THE BLOOD-BRAIN BARRIER IN A GUINEA PIG MODEL OF TUBERCULOSIS WITHOUT EVIDENCE OF BACTERIAL DISSEMINATION TO THE BRAIN

3.1 INTRODUCTION

Tuberculosis (TB) is catastrophic disease, caused by infection with *Mycobacterium tuberculosis* (Mtb), that affects approximately 1.7 billion people across the globe [428]. An estimated 10 million new cases of active disease occur each year worldwide, which is only worsening despite global strategies for disease elimination [330, 331]. Thus, it is crucial that research be performed to not only interfere with the progression of disease, but to better understand the long-term consequences of infection. Although much is known about the immune response to Mtb in peripheral tissues, little information exists describing the neurological effects of TB, despite published epidemiological data detailing long-term cognitive changes associated with the disease. These studies show that diagnosed TB is correlated with neurological deficits, including memory loss and decreased cognitive functioning [397]. TB also predisposes individuals to neurodegenerative disease, including Parkinson's Disease [183] and dementia [161, 357, 429]. Interestingly, these documented findings present in human patients who are not diagnosed with central nervous system (CNS) infection or tuberculosis meningitis (TBM), emphasizing the connection between pulmonary infection and the brain. Unfortunately, while it is established that TB can increase risk for disease, the complete neurological consequences, and pathological mechanisms driving them, remain unclear. Our previous findings help to characterize the neuropathologies that occur during the progression of disease in an established *in vivo* model of TB. In our model of peripheral disease without evidence of CNS infection, we correlated behavior changes to the presence of neuropathologies identified in

neurological disorders, including glial inflammation, the accumulation of misfolded and aggregated proteins, and neuronal loss in the hippocampus [430].

Glial inflammation is considered one of the earliest detectable abnormalities in neurological disease. Glia, astrocytes and microglia, can polarize from neuroprotective phenotypes into pro-inflammatory, neurotoxic ones. Although this response acutely helps to restore the microenvironment in response to stress, prolonged cellular activation compromises the brain over time. Microglia, which function as the resident immune cell of the brain, utilize their phagocytic capacity to eliminate pathogens, protein aggregates, and apoptotic cellular debris. Altogether, these actions aid in maintaining neuronal synapses. Microglial activation occurs following the recognition of antigens or cytokines and chemokines. These include tumor necrosis factor (TNF), interleukin-6 (IL-6), and interleukin-1β (IL-1β) [197]. Once in a reactive state, these cells actively secrete pro-inflammatory mediators that stimulate nearby cells; they are the primary producers of complement component 1, subcomponent q (C1q), interleukin 1α (Il-1α), and TNF. This molecular combination is one well-established method of astrocyte activation [381]. Once stimulated, neurotoxic astrocytes no longer perform supportive functions, including regulating neurogenesis and maintaining neurotransmitter levels. Similar to microglia, they contribute to pro-inflammation and produce complement proteins involved in opsonization and immune cell recruitment. Subsequently, colocalization of complement 3 (C3) in astrocytic cell bodies is an indication of cellular reactivity, along with others, such as increased expression of glial fibrillary acidic protein (GFAP) and S100 calcium-binding protein β (S100β) [382, 431]. Furthermore, astrocytes, through their terminal processes or “endfeet”, play an essential role in blood-brain barrier (BBB) function.

In addition to glial inflammation, reduced integrity of the BBB is found in numerous neurological disorders, including stroke, CNS infections, Alzheimer’s Disease (AD), and PD, among others [432, 433]. The brain is a highly controlled microenvironment composed of multiple protective mechanisms that separate the CNS from the peripheral circulation. The BBB uses both physical and metabolic methods to maintain the physiological environment of the brain. This barrier consists of molecular components, including the glycocalyx and basement membrane, as well as various cellular players. The cellular

components, endothelial cells (ECs), pericytes (PCs), and astrocyte endfeet, interact with one another to form the "neurovascular unit" that limits permeation of molecules and cellular traffic to and from the brain [434]. Although located throughout the body, the ECs forming vessels within the CNS are unique; they lack fenestrations and form extensive tight junctions (TJs) between cells [435]. The main functional elements of TJs are transmembrane claudin proteins, which tighten the paracellular cleft, form pores, and contribute to the maturation of this barrier. One claudin protein, in particular, claudin V, is the most highly expressed protein of this type in the brain. It is a critical constituent that acts as a "sealing" protein to maintain the tightness of TJs, preventing small molecules (< 800 Da) from entering the brain [436-438]. Altogether, TJs form a physical barrier that inhibits cells and other biomolecules from entering the brain parenchyma. Compromising components of these TJs, as documented during injury and disease, leads to increased paracellular solute leak [439].

On the parenchymal side of the BBB sits a basement membrane, an extracellular matrix primarily composed of collagen, laminin, nidogen, and perlecan. Collagen IV is the most abundant protein in the basement membrane and is critical for maintaining the integrity and function of the BBB [440]. Expression of collagen in microvessels is unique in that both downregulation and upregulation of this protein is implicated in disease. In murine models, mutations in alpha chains of collagen IV or complete loss of the protein results in pathology similar to porencephaly and small vessel disease, leading to brain hemorrhage [441, 442]. In models of bacterial meningitis and herpes-simplex virus encephalitis, the extent of BBB breakdown and subsequent cortical injury is directly correlated with the degree of collagen IV degradation by matrix metalloproteinases (MMPs) [443, 444]. Alternatively, collagen accumulation is associated with BBB leak and cognitive impairment in models of hypertension and ischemia [445]. Increased collagen IV content is also seen in the brains of human patients diagnosed with AD [446]. This variability in disease-associated collagen expression showcases the complexity of this protein's function in the BBB.

Critically, the BBB maintains the chemical composition of the brain, which is necessary for proper neuronal function. Such maintenance is performed, in part, by astrocytes. Astrocytic endfeet

physically contact the endothelial cells and pericytes that form the vasculature, and express proteins like aquaporin 4 (AQP4), a water transport protein. These proteins allow glial cells to regulate ion concentrations within the brain. Astrocytes also modulate neuronal activity and cerebral blood flow by controlling intracellular calcium levels in their endfeet, resulting in vasodilation and vasoconstriction [447]. The physical connection between astrocytic endfeet and vessels is highly implicated in neuroinflammation. Disruption of astrocytic endfeet and their proteins, in addition to other components of the BBB, results in neuroinflammation and cellular infiltration. Separating endfeet from the vasculature disrupts tight junction proteins, including claudins, and leads to biomolecular leak into the brain [448]. Loss of AQP4 in astrocytic endfeet is seen in experimental autoimmune encephalomyelitis and neuromyelitis optica, correlating to reduced BBB function. Overall, decline in astrocyte endfeet and their transporters disrupts ion equilibrium within the brain. This alters synaptic transmission and neuronal excitability which, ultimately, results in the loss of neuronal viability. Reactive astrocytes also secrete inflammatory mediators and reactive species, instead of supportive factors, that further reduce the integrity of the BBB and damage the cells native to the CNS.

Astrocytes develop and maintain the BBB through the release of growth factors like glial cell line-derived neurotrophic factor (GDNF) [449, 450]. In response to inflammation, astrocytes stimulate the formation of tight junctions, through other secreted factors including angiopoietin-1 (ANG1) and sonic hedgehog (SHH), to limit permeation of immune cells into the brain [450-453]. Despite evidence that astrocytes produce BBB stimulating molecules, the exact role of these cells in maintaining barrier integrity is contradictory. Several studies conclude that astrocyte ablation does not alter BBB structure or result in microvascular leak [223, 454]. Others suggest that loss of astrocytes compromises tight junctions, allowing molecules of various sizes to extravasate into the brain [455]. *In vitro* models of the BBB support this, as co-cultures of astrocytes and endothelial cells increase the formation of tight junctions compared to endothelial monocultures alone [456].

Due to the importance of various structural proteins in BBB function, their reduced expression is often used as a determination of barrier integrity, as seen in previous studies. This loss can occur through

multiple pathophysiological mechanisms, including oxidative stress and activation of cytokine-mediated intracellular signaling. Overall, these mechanisms disrupt tight junctions and alter molecular transport, leading to increased leakage of biomolecules and infiltration of immune cells from the periphery. This allows an influx of neurotoxins, microbial components, inflammatory mediators, or activated cells into the brain, promoting an inflammatory brain phenotype that is chronically damaging [457]. Subsequently, BBB dysfunction is considered an early and significant event in the pathogenesis of neurological disease. The integrity of the BBB during CNS infection has historically been of interest, as bacteria and viruses can alter the BBB to facilitate entry into the brain [209]. In an *in vitro* co-culture model of the BBB, Mtb exposure increases permeability by stimulating MMP-dependent breakdown of tight junction proteins [458]. In patients with TBM, the most common form of CNS Mtb infection, BBB permeability is significantly higher [459].

More recently, BBB damage has been implicated as a critical pathology in AD and PD. In AD, vascular permeability, which has been identified in human patients, is correlated with disease onset and severity [460]. Similarly, BBB damage and leaking has been identified in human PD patient brains [461]. Not only is barrier dysfunction implicated in CNS disease, but peripheral inflammation can also mediate BBB changes. Murine models of AD increase leakage from vessels into perivascular spaces following acute and chronic intraperitoneal treatment with lipopolysaccharide [462]. Sepsis, and the pro-inflammatory cytokines associated with it such as TNF, is known to change BBB integrity and result in vascular leak. Peripheral inflammation increases permeability of cells and molecules, as well as alters tight junctions [463-466]. In a study by Tsao et al., the pro-inflammatory molecule TNF results in BBB dysfunction, and it is well established that TNF is not only higher in TB patients, but correlates to disease severity [466, 467].

Although our previous findings describe the neuropathology associated with peripheral Mtb infection, there is a gap in knowledge on the mechanism of neurotoxicity. We hypothesize that the robust peripheral inflammatory response generated against pulmonary Mtb infection modulates the BBB. This allows for the infiltration of immune cells from the periphery into the brain parenchyma, as well as pro-

inflammatory mediators that activate and recruit native glia. Ultimately, this BBB degradation may be a critical initial mechanism that results in the long-term neuropathology associated with the disease. In this study using a relevant guinea pig model of TB, analysis of the major protein constituents of the BBB demonstrated altered expression within vessels. Modulation of BBB proteins resulted in gliosis and the infiltration of immune cells in Mtb-infected animals, localized in the frontal cortex, thalamus, brain stem, and cerebral nuclei. Due to the neuronal loss previously established in this model and its relevancy to neurodegenerative disease, the hippocampus was also evaluated in this study [430]. Through these data, we reveal a possible mechanism early in the progression of disease which may lead to neurodegeneration and permanent neurological injury.

3.2 METHODS

3.2.1 Animals and Sample Collection

Three-month-old, female, outbred Dunkin–Hartley guinea pigs (Elm Hill, USA) were used in this study. They were housed in a biosafety level 3 laboratory at the Colorado State University Laboratory Animal Resources facility accredited by the American Association for Accreditation of Laboratory Animal Care (AAALAC). Animals were pair housed under constant temperature and humidity conditions (21° ± 2 °C temperature and 30 ± 5 % humidity). A 12-hour light/12-hour dark cycle was used, and animals had *ad libitum* access to standard pelleted food and water. Animals were monitored using a clinical scoring system for signs of morbidity and weighed weekly by laboratory staff for the entirety of the experiment. Experiments were performed in accordance with the National Research Council's Guide for the Care and Use of Laboratory Animals and were approved by the Institutional Animal Care and Usage Committee (IACUC) at Colorado State University. At the time of euthanasia, guinea pigs were administered 50 mg/kg of ketamine and 5 mg/kg of xylazine via intramuscular injection for anesthetic induction. Under terminal anesthesia, guinea pigs were euthanized by intraperitoneal overdose of pentobarbital. Tissues were collected for histopathology by fixing in 10% buffered formalin or stored at -80°C for subsequent homogenization and quantification of Mtb colony forming units.

3.2.2 Mtb Aerosol Exposure

This study utilized two strains of Mtb: the laboratory strain Mtb H37Rv, which is considered less virulent, and the clinical strain Mtb HN878, a hypervirulent strain. Culture stocks of *Mycobacterium tuberculosis* (Mtb) strain H37Rv (TMC #102, Trudeau Institute) and HN878 (Clinical Isolate W210, CSU, Fort Collins, CO) were collected at an OD600 nm between 0.8 and 1.0 and frozen at -80°C in Proskauer-Beck liquid medium containing 0.05% Tween-80. Titer was determined and bacteria were diluted in sterile water to 2×10^6 colony forming units (CFU)/mL. Animals were exposed to an aerosolized dose of Mtb for twelve minutes, calibrated to deliver 50 – 100 bacilli per animal. The Glas-Col Airborne whole-body exposure apparatus was used to infect the animals in one run per strain, and approximately 80 CFU of Mtb were delivered by aerosol to each animal. Four animals were infected with Mtb H37Rv, and six animals were infected with HN878. Each run contained a single guinea pig for euthanasia and necropsy 24 hours after exposure to confirm Mtb delivery to the lungs. Animals were exposed to Mtb for a total of 15 days post-infection (dpi). Four uninfected animals were exposed to sterile water using the same procedure in the Glas-Col device.

3.2.3 Bacterial Burden/CFU Counts

For confirmation of bacterial enumeration at 24 hours, the lung was homogenized in 30 mL of PBS and plated on 150 x 50mm petri dishes containing 7H11 with 10% OADC, 10 µg/mL cycloheximide, and 50 µg/mL of carbenicillin. For quantification of bacterial dissemination at the end of the study period, lung, spleen, and brain were collected, weighed, and homogenized in PBS. The entirety of the brain homogenate for each animal was diluted 1:10 followed by serial dilutions of tissue homogenate in PBS. Dilutions were plated as stated above and all agar plates were incubated at 37 °C + 5% CO_2. Following 6 – 8 weeks of incubation, CFU's were counted, and CFU's per gram of tissue were calculated.

3.2.4 Tissue Processing, Embedding, and Histological Staining

Brains and visceral organs were fixed in 10% neutral buffered formalin at room temperature for at least 48 hours. Tissues were processed using a Leica TP1020 Automatic Benchtop Tissue Processor and embedded in paraffin wax (Cancer Diagnostics, Cat #: EEPAR56). Tissues were sectioned on a Thermo Scientific HM 325-2 Manual Microtome at 5μm thickness and mounted on positively charged glass slides (Superfrost Plus, Cancer 232 Diagnostics, Cat #: 4951) for staining and analysis. One section per animal was deparaffinized and stained with hematoxylin (Cancer Diagnostics, Cat#: #HTV-4) and eosin (Cancer Diagnostics, Cat#: #ETV) (H&E) for determination of histopathological changes. Brain sections were sent to the Colorado State University's Veterinary Diagnostic Laboratory for acid-fast staining to determine if bacterial dissemination to the brain occurred. An Mtb-positive lung tissue slide was also acid-fast stained to confirm the validity of the staining procedure.

3.2.5 Immunohistochemical Staining

Immunohistochemical stains were performed on whole brain sagittal sections. To deparaffinize the tissue sections, slides were heated for 20 minutes at 60°C followed by a series of incubations in xylene and graded ethanol (xylene, 1 part xylene to 1 part 100% EtOH, 100% EtOH, 95% EtOH, 70% EtOH, 1.0 M TBS) for 5 minutes each. Heat- and chemical-induced antigen retrieval was performed on the tissue by incubating in 0.01 M sodium citrate (pH = 6.0) for 20 minutes at 95°C. Removal of endoperoxides was performed through incubation in 0.3% hydrogen peroxide for 30 minutes at room temperature. Wash steps and tissue permeabilization was performed using 2% bovine serum albumin [468] and 2% Triton-X in 1.0 M TBS. Tissue was blocked in 10% goat or donkey serum diluted in 1.0 M TBS for 1 hour at room temperature. After being diluted to their optimized concentrations, primary antibodies were incubated on the tissue at 4°C overnight.

Astrocytes were identified using a rabbit anti-S100 calcium-binding protein β (S100β) antibody at a 1:750 concentration (Abcam, Cat #: ab41548). Microglia were identified using a goat anti-ionized calcium binding adaptor molecule 1 (Iba-1) antibody at a 1:400 concentration (Abcam, Cat #: ab5076). Washing was performed using 2% BSA in 1.0 M TBS before incubation with the secondary antibody at a

1:250 concentration for 1 hour at room temperature. The following secondary antibodies were used for the astrocyte and microglial stains, respectively: goat anti-rabbit secondary antibody (Vector Labs, Cat #: BA-1000) and donkey anti-goat secondary antibody (Jackson ImmunoResearch, Cat #: 705-065-147). Following secondary incubation, tissue was incubated an additional hour in ABC mix from an ABC HRP peroxidase detection kit (Vector Laboratories, Cat #: PK-4000). An ImmPACT DAB Substrate, Peroxidase (HRP) Kit (Vector Laboratories, Cat #: sk-4105) was used as chromogen, with a fixed chemical reaction period for each antigen of interest. Slides were counterstained with hematoxylin (Thermo Fisher Scientific, Cat #: 7231) and bluing reagent (Cancer Diagnostics, Cat #: FX2107). Stained tissue was preserved under a glass coverslip with mounting medium (Richard-Allen Scientific, Cat #: 4112) and stored at room temperature. Whole tissue images were taken for analysis using an Olympus BX53 microscope with an Olympus DP70 camera using an Olympus UPlanSApo 20x objective (N.A. = 0.75). Representative images were taken using an Olympus BX53 microscope with an Olympus DP70 camera using an Olympus UPlanSApo 20x objective (N.A. = 0.75) and Olympus UPlanFL N 40x objective (N.A. = 0.75).

Table 1. Immunohistochemistry Antibodies.

Primary Antibody and Concentration Used	**Primary Antibody Catalog Number**	**Secondary Antibody and Concentration Used**	**Secondary Antibody Catalog Number**
Rabbit anti-S100β 1:750	Abcam Cat #: ab41548	Goat anti-rabbit IgG (H+L) 1:250	Vector Labs Cat #: BA-1000
Goat anti-Iba-1 1:400	Abcam Cat #: ab5076	Donkey anti-goat IgG (H+L) 1:250	Jackson ImmunoResearch Cat #: 705-065-147

3.2.6 Immunofluorescent Staining

Whole brain sagittal sections were deparaffinized by heating slides for 20 minutes at 60°C followed by incubation in xylenes and graded ethanol (xylene, 1 part xylene to 1 part 100% EtOH, 100%

EtOH, 95% EtOH, 70% EtOH, 1.0 M TBS) for 5 minutes each. Heat- and chemical-induced antigen retrieval was performed by incubating tissue in 1X EDTA buffer (1mM EDTA disodium salt dihydrate, 0.05% Tween; pH 8.0) for 20 minutes at 95°C. Tissue was washed with 0.05 M TBS and blocked using 2% donkey and/or goat serum in TrisA (0.2% Triton-X in 1.0 M TBS) for 1 hour at room temperature. After being diluted to their optimized concentrations, primary antibodies were incubated on the tissue at 4°C overnight.

Blood-brain barrier integrity was analyzed by detecting collagen IV, claudin V, and aquaporin-4 (AQP4). Collagen IV was identified using an anti-Collagen IV antibody at a 1:100 concentration (NOVUS, Cat #: NB120-6586SS) and a donkey anti-rabbit Alexa Fluor 647 secondary antibody (Invitrogen, Cat #: A31573). Claudin V was identified using an anti-Claudin 5 polyclonal antibody at a 1:500 concentration (Invitrogen, Cat #: 34-1600) and a donkey anti-rabbit Alexa Fluor 647 secondary antibody (see above). AQP4 was identified using an anti-Aquaporin-4 monoclonal antibody at a 1:100 concentration (ABclonal, Cat #: A11210) and a donkey anti-rabbit Alexa Fluor 647 secondary antibody (see above). For visualizing astrocytes, three antibodies were used: a chicken anti-Glial fibrillary acidic protein (GFAP) antibody at a 1:200 concentration (Aves Labs, Cat #: GFAP), a rabbit anti-Complement 3 (C3) antibody at a 1:100 concentration (Abcam, Cat #: ab181147), and a mouse anti-S100 calcium-binding protein β (S100β) antibody at a 1:500 concentration (Abcam, Cat #: ab212816). The astrocyte stain used the following secondary antibodies: goat anti-chicken Alexa Fluor 488 (Invitrogen, Cat #: A11039), donkey anti-rabbit Alexa Fluor 647 (Invitrogen, Cat #: A31573), and donkey anti-mouse Alexa Fluor 555 (Invitrogen, Cat #: A31570). Infiltrating immune cells were identified by co-staining for CD45, Iba-1, and S100β. To do this, CD45 was identified using an anti-CD45 (IH-1) monoclonal antibody at a 1:100 concentration (NOVUS Biologicals, Cat #: NB100-65362) and donkey anti-mouse Alexa Fluor 555 secondary antibody at a 1:500 concentration (Invitrogen, Cat #: A31570). Microglia were identified using a goat anti-ionized calcium binding adaptor molecule 1 (Iba-1) antibody at a 1:50 concentration (Abcam, Cat #: ab5076) and Donkey anti-goat Alexa Fluor 647 secondary antibody at a 1:500 concentration (Invitrogen, Cat #: A21447). S100β was identified using an anti-S100β antibody at a 1:500 concentration

(Abcam, Cat #: ab212816) and Donkey anti-rabbit Alexa Fluor 488 secondary antibody at a 1:500 concentration (Southern Biotech, Cat #: 6441-30). A detailed table outlining the antibodies and concentrations used is included below.

Four 10-minute wash steps (1.0 M TBS) were followed by incubation with the secondary antibodies at 1:500 concentrations for at least 1 hour at room temperature in the dark. Tissue was washed three times for five minutes each (1.0 M TBS), and stained with Hoechst (Thermo Scientific, Cat #: 62249) diluted 1:2000 in PBS for three minutes followed by three additional washes (1.0 M TBS). Slides were coverslipped with Prolong Gold Anti-fade mounting medium (Cell Signaling Technology, Cat #: 9071), allowed to harden for 24 to 48 hours at room temperature, and then stored at 4°C in the dark. Whole-slide images were acquired using an Olympus BX63 fluorescence microscope equipped with a motorized stage and Hamamatsu ORCA-flash 4.0 LT CCD camera using a 20x Olympus X Apochromat air objective air objective (N.A. = 0.80). All slides, irrespective of experimental group, were imaged on the same day with the same exposure time per channel. Representative images were captured using an Olympus BX63 fluorescence microscope equipped with a motorized stage and Hamamatsu ORCA-flash 4.0 LT CCD camera using a 40x Olympus X278 Apochromat air objective air objective (N.A. = 0.80). Red blood cells were removed from representative images.

Table 2. Immunofluorescent Antibodies.

Protein of Interest:	**Primary Antibody and Concentration Used**	**Primary Antibody Catalog Number**	**Secondary Antibody and Concentration Used**	**Secondary Antibody Catalog Number**
Collagen IV	Rabbit anti-Collagen IV 1:100	NOVUS Cat #: NB120-6586SS	Donkey anti-rabbit Alexa Fluor 647 1:500	Invitrogen Cat #: A31573
Claudin V	Rabbit anti-Claudin V 1:500	Invitrogen Cat #: 34-1600	Donkey anti-rabbit Alexa Fluor 647 1:500	Invitrogen Cat #: A31573

AQP4	Rabbit anti-Aquaporin-4 1:100	ABclonal Cat #: A11210	Donkey anti-rabbit Alexa Fluor 647 1:500	Invitrogen Cat #: A31573
GFAP	Chicken anti-Glial fibrillary acidic protein (GFAP) 1:200	Aves Labs Cat #: GFAP	Goat anti-chicken Alexa Fluor 488 1:500	Invitrogen Cat #: A11039
C3	Rabbit anti-Complement 3 antibody 1:100	Abcam Cat #: ab181147	Donkey anti-rabbit Alexa Fluor 647 1:500	Invitrogen Cat #: A31573
S100β	Mouse anti-S100 calcium-binding protein β (S100β) 1:500	Abcam Cat #: ab212816	Donkey anti-mouse Alexa Fluor 555 1:500	Invitrogen Cat #: A31570
S100β	Rabbit anti-S100 calcium-binding protein β (S100β) 1:500	Abcam Cat #: ab41548	Donkey anti-rabbit Alexa Fluor 488 1:500	Southern Biotech Cat #: 6441-30
CD45	Mouse anti-CD45 (IH-1) antibody 1:100	NOVUS Biologicals Cat #: NB100-65362	Donkey anti-mouse Alexa Fluor 555 1:500	Invitrogen Cat #: A31570
Iba-1	Goat anti-Iba-1 1:50	Abcam Cat #: ab5076	Donkey anti-goat Alexa Fluor 647 1:500	Invitrogen Cat #: A21447

3.2.7 Immunofluorescent Analysis

Whole slide images of Collagen IV, Claudin V, and AQP4 stained by immunofluorescence were analyzed. For each slide, regions of interest (ROIs) were drawn around individual blood vessels of various sizes and orientations within the tissue. ROIs were evenly distributed across the following five brain regions: frontal cortex, hippocampus, thalamus, cerebral nuclei, and brainstem. At least twenty vessels per brain region were analyzed, and care was taken to exclude red blood cells and other abnormalities or artifacts from the analysis. Mean gray intensity of the proteins within each vessel were quantified using manual thresholding on the Count and Measure function of Olympus CellSens software (v1.18). Reactive astrocytes were quantified by analyzing complement 3 expression within $S100\beta^+$

astrocytes. This was performed by using manual thresholding on the Count and Measure function of Olympus CellSens software (v1.18) to identify S100β$^+$DAPI$^+$ cells, which were then converted into individual ROIs. Manual thresholding was then used to quantify the fluorescence intensity of C3 within each S100β$^+$ cell ROI. Adaptive thresholding on the Count and Measure function of CellSens was used to select for GFAP$^+$ area for each brain region. Percent relative expression was calculated for each protein of interest by determining the minimum (min) and maximum (max) quantifications for the data set. Each raw quantification (raw) for that brain region received the following calculation: [(raw – min)/(max – min)*100].

3.2.8 Statistical Analysis

All data is presented as mean +/- SEM unless otherwise specified. A ROUT (Q = 1%) outlier test was performed on all data to identify potential outliers, which were removed from the data set. Differences between experimental groups were analyzed using a nonparametric one-way ANOVA with Dunn's multiple comparisons test. Statistical analysis was completed using GraphPad Prism. Significance is denoted throughout the manuscript as * = $p \leq .05$, ** = $p \leq 0.01$, *** = $p \leq 0.001$, and **** = $p \leq 0.0001$.

3.3 RESULTS

3.3.1 Aerosolized Mtb H37Rv and HN878 Did Not Disseminate to the Brains of Guinea pigs.

Histopathology and organ bacterial burden were used to measure disease severity and bacterial dissemination. Hematoxylin and eosin (H&E) staining of uninfected lung tissue showed normal lung pulmonary structure (**Figure 14A**). The lungs of animals infected by aerosol with both the laboratory strain Mtb H37Rv (**Figure 14B**) and clinical strain HN878 (**Figure 14C**) presented with granulomatous lesions (in brackets). CFU assays confirmed the presence of bacteria in lung homogenate of Mtb H37Rv and HN878 infected animals (**Figure 14G**). Dissemination of bacteria to the spleen occurred in 50% of animals infected with Mtb H37Rv and in 33% of animals infected with Mtb HN878 (**Figure 14G**).

In contrast, CFU assays of brain homogenate from infected animals did not contain culturable Mtb bacteria (**Figure 14G**). Acid-fast staining of whole-brain sagittal tissue sections were negative for the presence of Mtb in infected animals, similar to the uninfected group; representative images of the hippocampus are shown (**Figure 14D – F**). From these data, we conclude that infection with aerosolized Mtb H37Rv and HN878 disseminated to the lungs and peripheral organs, but did not reach the brain.

3.3.2 Regionally Specific Cytosis Identified in Two Animals Infected with Both a Laboratory and Clinical Mtb Strain.

Brain tissue from guinea pigs infected with Mtb H37Rv and HN878 was stained with H&E for examination of histopathological changes. Cytosis was identified in one animal infected with Mtb H37Rv, in the brainstem and thalamus, and one animal infected with Mtb HN878, in the frontal cortex and cerebral nuclei (**Supplementary Table 1**). Due to the responses identified in two of the Mtb-infected animals in these regions, and the importance of the hippocampus in neurodegeneration, the frontal cortex, cerebral nuclei, thalamus, brain stem, and hippocampus were selected for further examination. Representative images of the frontal cortex (**Figure 15A – D**), cerebral nuclei (**Figure 15E – H**), brain stem (**Figure 15I – L**), thalamus (**Figure 15M – P**) and hippocampus (**Figure 15Q – S**) are shown. The cellular response identified in the frontal cortex of the Mtb HN878 infected guinea pig showed a high density of cellular nuclei, indicative of cellular infiltration into that brain region (**Figure 2D**, red arrows). The response identified in the cerebral nuclei of the Mtb HN878 infected guinea pig had a similarly high density of cellular nuclei (**Figure 15H**, red arrows). In the brainstem of the Mtb H37Rv infected guinea pig, a high density of cellular nuclei surrounding and within an enlarged blood vessel was identified (**Figure 15L**, red arrows), similar to the response identified in the thalamus of the Mtb H37Rv infected guinea pig (**Figure 15P**, red arrows). Within these regions of the neuroparenchyma are multifocal aggregates of moderate numbers of epithelioid macrophages, lymphocytes, and plasma cells. For each of the described brain regions, cytosis to this extent was not seen in the remaining eight Mtb-infected animals tested, nor in the uninfected animals.

3.3.3 Substantial Iba-1$^+$ Cellular Response in Animals Infected with Both a Laboratory and Clinical Mtb Strain.

Glial reactivity in response to pulmonary infection was evaluated using immunohistochemical staining. Representative images of Iba-1$^+$ microglial cells in the frontal cortex (**Figure 16A – D**), cerebral nuclei (**Figure 16E – H**), brain stem (**Figure 16I – L**), thalamus (**Figure 16M – P**) and hippocampus (**Figure 16Q – S**) are shown. Iba-1$^+$ microglial cells were seen in the frontal cortex (**Figure 16A**), cerebral nuclei (**Figure 16E**), brain stem (**Figure 16I**), thalamus (**Figure 16M**), and hippocampus (**Figure 16Q**) of uninfected animals. Animals infected with both the less virulent H37Rv and hypervirulent HN878 strains of Mtb show increased numbers of Iba-1$^+$ cells in those same brain regions (**Figure 16B, C, F, G, J, K, N, O, R,** and **S**). An exacerbated Iba-1$^+$ cellular response, with increased cell number and somal hypertrophy, is seen in the animals with regional cytosis in the frontal cortex (**Figure 16D**), cerebral nuclei (**Figure 16H**), brainstem (**Figure 16L**), and thalamus (**Figure 16P**); dense clustering of Iba-1$^+$ cells prevented quantitative analysis within these areas. A cellular response to this extent was not identified in the hippocampus, although an increase in Iba-1$^+$ cells was still observed following infection. These results establish a progressive Iba-1$^+$ cellular response to infection that is intensified in two of the Mtb-infected animals.

3.3.4 Reactive Astrogliosis in Animals Infected with Both a Laboratory and Clinical Strain of Mtb.

In addition to microglia, the astrocytic response was investigated using immunohistochemical and immunofluorescent staining. Representative images of S100β$^+$ astrocytes in the frontal cortex (**Figure 17A – D**), cerebral nuclei (**Figure 17E – H**), brain stem (**Figure 17I – L**), thalamus (**Figure 17M – P**), and hippocampus (**Figure 17Q – S**) are shown. S100β$^+$ astrocytes are seen in the frontal cortex (**Figure 17A**), cerebral nuclei (**Figure 17E**), brain stem (**Figure 17I**), thalamus (**Figure 17M**), and hippocampus (**Figure 17Q**) of uninfected animals. No change in the number of S100β$^+$ cells is seen in animals infected with both the less virulent and hypervirulent strains of Mtb in those same brain regions (**Figure 17B, C,**

F, G, J, K, N, O, R, and **S**). Similarly, animals with regions of cytosis do not show an increase in S100β$^+$ cells in the frontal cortex (**Figure 17D**), cerebral nuclei (**Figure 17H**), brainstem (**Figure 17L**), and thalamus (**Figure 17P**). Animals with cytosis show altered morphology of the S100β$^+$ cells, displaying cellular projections with upregulated S100β that are not apparent in uninfected animals (**Figure 17D, H, L,** and **P**).

Although Mtb-infected animals do not show substantial proliferation of S100β$^+$ cells compared to uninfected animals, the cells present have increased production of C3, which is characterized as an astrocyte with a reactive phenotype. Expression of C3 was quantitatively analyzed within each individual S100β$^+$ cell soma. Representative images of immunostaining for C3 in S100β$^+$ astrocyte cell bodies in control, Mtb-infected guinea pigs, and the two animals with regional cytosis are depicted in the frontal cortex (**Figure 18A – D**), cerebral nuclei (**Figure 18F – I**), brain stem (**Figure 18K – N**), thalamus (**Figure 18P – S**), and hippocampus (**Figure 18U – X**). Expression of C3 within each S100β$^+$ cell soma was significantly increased in animals infected with Mtb H37Rv in the frontal cortex ($p = <0.0001$) (**Figure 18B** and **E**), cerebral nuclei ($p = <0.0001$) (**Figure 18G** and **J**), brain stem ($p = <0.0001$) (**Figure 18L** and **O**), thalamus ($p = <0.0001$) (**Figure 18Q** and **T**), and hippocampus ($p = <0.0001$) (**Figure 18V** and **Y**) compared to uninfected controls in those same brain regions (**Figure 18A, E, F, J, K, O, P, T, U,** and **Y**). Animals infected with Mtb HN878 demonstrate a dramatic increase in C3 expression in the frontal cortex ($p = <0.0001$) (**Figure 18C** and **I**), cerebral nuclei ($p = <0.0001$) (**Figure 18H** and **J**), brain stem ($p = <0.0001$) (**Figure 18M** and **O**), thalamus ($p = <0.0001$) (**Figure 18P** and **T**), and hippocampus ($p = <0.0001$) (**Figure 18W** and **Y**) compared to uninfected animals. This change in C3 expression in Mtb HN878 infected animals was more significant than in Mtb H37Rv infected animals in the frontal cortex ($p = <0.0001$) (**Figure 18B, C,** and **E**), cerebral nuclei ($p = <0.0001$) (**Figure 18G, H,** and **J**), brainstem ($p = <0.0001$) (**Figure 18L, M,** and **O**), thalamus ($p = <0.0001$) (**Figure 18R** and **T**), and hippocampus ($p = <0.0001$) (**Figure 18V, W,** and **Y**). Animals with identified cytosis have increased somal C3 in the frontal cortex (**Figure 18D** and **I**), cerebral nuclei (**Figure 18I** and **J**), brain stem (**Figure 18N** and **O**), and

thalamus (**Figure 18S** and **T**) compared to uninfected controls in those same brain regions (**Figure 18A, E, F, J, K, O, P, T, U,** and **Y**). Less of a difference is seen between animals with cytosis and those not infected with Mtb in the hippocampus, which is not a region where cytosis was identified (**Figure 18U, X,** and **Y**). In all four brain regions, expression was decreased in cytosis$^+$ animals (**Figure 18D, E, I, J, N, O, S, T, X,** and **Y**) compared to those infected with Mtb H37Rv (**Figure 18B, E, G, J, L, O, Q, T, V,** and **Y**) and Mtb HN878 (**Figure 18C, E, H, J, M, O, R, T, W,** and **Y**). Overall, these data establish the presence of reactive astrocytes, but not cellular proliferation, in Mtb-infected animals with or without cytosis.

3.3.5 Mtb Infection Alters Aquaporin-4 Expression and Contact of Astrocytic Endfeet with Vessels.

Astrocytes, identified as GFAP$^+$ cells, and the water channel protein AQP4, which is found on astrocytic endfeet, were identified using immunofluorescence microscopy; protein expression of AQP4 in association with vessels was quantitatively analyzed. Representative images of vessels with AQP4 and GFAP$^+$ astrocyte processes in uninfected controls, Mtb-infected guinea pigs, and the two animals with regional cytosis are depicted in the frontal cortex (**Figure 19A – D**), cerebral nuclei (**Figure 19G – J**), brain stem (**Figure 19M – R**), thalamus (**Figure 19S – V**) and hippocampus (**Figure 19Y – BB**). Expression of AQP4 within vessels was significantly increased in animals infected with Mtb H37Rv compared to controls in the frontal cortex ($p = <0.0001$) (**Figure 19A, B,** and **E**), cerebral nuclei ($p = <0.0001$) (**Figure 19G, H,** and **K**), brainstem ($p = <0.0001$) (**Figure 19M, N,** and **Q**), thalamus ($p = <0.0001$) (**Figure 19S, T,** and **W**), and hippocampus ($p = <0.0001$) (**Figure 19Y, Z,** and **CC**). Similarly, animals infected with Mtb HN878 demonstrated significantly increased AQP4 expression compared to uninfected animals in the frontal cortex ($p = <0.0001$) (**Figure 19A, C,** and **E**), cerebral nuclei ($p = <0.0001$) (**Figure 19G, I,** and **K**), brainstem ($p = <0.0001$) (**Figure 19M, O,** and **Q**), thalamus ($p = <0.0001$) (**Figure 19S, U,** and **W**), and hippocampus ($p = <0.0001$) (**Figure 19Y, AA,** and **CC**). There was no strain-dependent difference in expression in all regions, including the frontal cortex ($p = 0.4937$) (**Figure 19B, C,** and **E**), cerebral nuclei ($p = >0.9999$) (**Figure 19H, I,** and **K**), brainstem ($p = >0.9999$)

(**Figure 19N, O,** and **Q**), thalamus (p = >0.9137) (**Figure 19T, U,** and **W**), and hippocampus (p = >0.9999) (**Figure 19Z, AA,** and **CC**). Expression of AQP4 in cytosis$^+$ animals decreased compared to not only Mtb H37Rv-infected and Mtb HN878-infected animals, but also uninfected controls in the frontal cortex (**Figure 19A – E**), cerebral nuclei (**Figure 19G – K**), and hippocampus (**Figure 19Y – CC**). A similar trend is seen between cytosis$^+$ animals and animals infected with both strains in the brain stem (**Figure 19N – Q**) and thalamus (**Figure 19T – W**), but no change was seen when compared to uninfected controls in these two brain regions.

Concurrently, GFAP$^+$ astrocyte processes appear to increase contact in animals infected with Mtb H37Rv (**Figure 19B, H, N, T,** and **Z**) and HN878 (**Figure 19C, I, O, U,** and **AA**) compared to uninfected controls (**Figure 19A, G, M, S,** and **Y**). Retraction of processes from vessels is observed in cytosis$^+$ animals (**Figure 19D, J, P, V,** and **BB**). These changes in contact of the astrocytic endfeet with vessels is supported by greater GFAP$^+$ area in the brain regions of Mtb-infected animals, which is indicative of cellular hypertrophy and increased process volume. An insignificant, but trending, increase in GFAP$^+$ area is found in animals infected with Mtb H37Rv compared to uninfected controls in the frontal cortex (p = >0.9999) (**Figure 19F**), cerebral nuclei (p = 0.4648) (**Figure 19L**), brain stem (p = 0.6783) (**Figure 19R**), thalamus (p = 0.2377) (**Figure 19X**), and hippocampus (p = 0.4390) (**Figure 19DD**). Animals infected with Mtb HN878 show a significant increase in GFAP$^+$ area compared to uninfected animals in the cerebral nuclei (p = 0.0179) (**Figure 19L**), brain stem (p = 0.0244) (**Figure 19R**), thalamus (p = 0.0168) (**Figure 19X**), and hippocampus (0.0393) (**Figure 19DD**), although no significant difference occurs in the frontal cortex (p = 0.0553) (**Figure 19F**). Cytosis$^+$ animals have a GFAP$^+$ area similar to controls, as no difference is identified in the frontal cortex (**Figure 19F**), cerebral nuclei (**Figure 19L**), brain stem (**Figure 19R**), thalamus (**Figure 19X**), and hippocampus (**Figure 19DD**). Overall, Mtb infection increases GFAP$^+$ area, astrocyte process contact with vessels, and AQP4 expression compared to controls, but this response is decreased in cytosis$^+$ animals.

3.3.6 Modulation of the Blood-Brain Barrier Following Infection with Mtb.

Immunofluorescence microscopy was utilized to evaluate the expression of BBB-associated proteins within blood vessels; this included matrix collagen IV and the tight junction protein claudin V. Representative images of immunostaining for collagen IV in control, Mtb-infected guinea pigs, and the two animals with regional cytosis are depicted for the frontal cortex (**Figure 20A – D**), cerebral nuclei (**Figure 20F – I**), brain stem (**Figure 20K – N**), thalamus (**Figure 20P – S**), and hippocampus (**Figure 20U – X**). In the frontal cortex, expression of collagen IV within blood vessels was significantly decreased in animals infected with Mtb H37Rv compared to controls ($p = <0.0001$) (**Figure 20A, B,** and **E**), and in animals infected with Mtb HN878 ($p = <0.0001$) (**Figure 20A, C,** and **E**). Expression was further decreased in Mtb HN878 infected animals compared to H37Rv ($p = 0.0010$). Animals with identified cytosis demonstrate decreased expression of collagen IV compared to uninfected animals in this brain region (**Figure 20A, D,** and **E**). Vessel collagen IV expression in the cerebral nuclei was significantly decreased in Mtb H37Rv-infected animals compared to uninfected controls ($p = <0.0001$) but not HN878-infected ($p = 0.3031$) (**Figure 20F, G, H,** and **J**); H37Rv-infected animals had significantly lower expression than HN878 ($p = 0.0186$). No change was identified between animals with cytosis and those uninfected (**Figure 20F, I,** and **J**). In the brain stem, a decrease in expression of collagen IV occurred in animals infected with Mtb H37Rv compared to uninfected animals ($p = <0.0001$) (**Figure 20K, L,** and **O**), although no significant difference was detected in animals infected with Mtb HN878 compared to controls ($p = 0.2927$) (**Figure 20K, M,** and **O**). No change was detected in animals with regional cytosis compared to uninfected controls (**Figure 20K, N,** and **O**). Similar to the frontal cortex, the thalamus showed decreased collagen IV in infected animals of both strains compared to uninfected controls ($p = <0.0001$ for both strains) (**Figure 20P, Q, R,** and **T**); animals exposed to Mtb H37Rv had statistically lower expression than Mtb HN878 ($p = 0.0357$). No change occurred between animals with cytosis and uninfected animals (**Figure 20P, S,** and **T**). This trend in expression was seen in the hippocampus as well, although animals with cytosis had a decreased expression of collagen IV

compared to uninfected animals (**Figure 20U, X,** and **Y**), but not as low as the other animals infected with Mtb H37Rv ($p = <0.0001$) (**Figure 20V, X,** and **Y**) nor HN878 ($p = <0.0001$) (**Figure 20W – Y**).

Expression of claudin V, a component of tight junctions, within vessels was also evaluated. Representative images of immunostaining for claudin V in control, Mtb-infected guinea pigs, and the two animals with regional cytosis are depicted for the frontal cortex (**Figure 21A – D**), cerebral nuclei (**Figure 21F – I**), brain stem (**Figure 21K – N**), thalamus (**Figure 21P – S**), and hippocampus (**Figure 21U – X**). In the frontal cortex, animals infected with Mtb H37Rv (**Figure 21B** and **E**) and Mtb HN878 (**Figure 21C** and **E**) showed decreased expression of claudin V compared to uninfected controls ($p = <0.0001$ for both) (**Figure 21A** and **E**). No strain difference was observed ($p = 0.2688$). Decreased expression in Mtb-infected animals compared to uninfected animals was also seen in the cerebral nuclei ($p = <0.0001$ for both), although expression in animals infected with Mtb HN878 was not as low as H37Rv and a strain-specific difference is observed ($p = 0.0264$) (**Figure 21F, G, H,** and **J**). The same trend in expression was seen in the brain stem (**Figure 21K – O**) and thalamus (**Figure 21P – T**). In these two regions, and in the hippocampus, Mtb-infected animals had significantly lower expression than uninfected controls ($p = <0.0001$ for all). Strain-specific differences were observed in the brain stem ($p = 0.0047$) (**Figure 21O**) and thalamus ($p = 0.0266$) (**Figure 21T**). In the hippocampus, claudin V expression was not significantly different between strains (**Figure 21U – Y**) ($p = 0.1361$). In all five brain regions, a decrease in claudin V expression is observed in the cytosis$^+$ animals compared to uninfected controls (**Figure 21E, J, O, T,** and **Y**). Analysis of these proteins demonstrate that Mtb infection modulates collagen IV expression in a strain-dependent manner. Expression of claudin V was decreased, regardless of strain, in Mtb-infected and cytosis$^+$ animals.

3.3.7 Infiltration of Peripheral Immune Cells into the Brain of Two Mtb-Infected Animals.

Immunofluorescence microscopy was used to phenotypically profile cells within each brain region to determine if immune cells from the periphery were infiltrating into the brain. Although glia can express lymphocyte common antigen cluster of differentiation 45 (CD45), a protein tyrosine phosphatase

that is expressed on all nucleated hematopoietic cells, it is expressed at low to intermediate levels. Therefore, peripheral immune cells were identified in this study as CD45 high expressing, Iba-1 low expressing, and S100β low expressing cells ($CD45^{hi}Iba\text{-}1^{low}S100\beta^{low}$). An increase of phenotypically $CD45^{hi}Iba\text{-}1^{low}S100\beta^{low}$ cells are detected in the brains of animals with cytosis (**Figure 22D** and **E**) but not in the other animals infected with Mtb (**Figure 22B** and **C**) nor in uninfected controls (**Figure 22A**).

3.4 DISCUSSION

The neurological effects of TB have only recently been described, clinically and in laboratory models. Our current knowledge includes the progressive activation of glia that culminates in behavior changes, aggregated misfolded proteins, and hippocampal neuronal loss in response to peripheral Mtb infection in a guinea pig model [430]. Although the neuropathologies that may contribute to TB-associated cognitive dysfunction have been described, the mechanism of neurotoxicity has not yet been elucidated. Our previous findings demonstrate that neuroinflammation and pathological changes occur without detectible bacteria in the brains of Mtb-infected animals, highlighting mechanisms of cellular stress in response to chronic systemic inflammation during Mtb infection [430]. Meningococcal diseases, including those caused by Mtb, demonstrate that bacterial and host-mediated BBB permeability occurs [469]. Previous work from Brilha et al. has shown that Mtb decreases expression of BBB proteins *in vitro* [458]. Other studies have also revealed that systemic inflammation results in BBB dysfunction which exacerbates neuroinflammation. We, therefore, hypothesized that pulmonary Mtb infection without dissemination to the brain modulates the BBB, allowing for the infiltration of peripheral immune cells and, potentially, neurotoxic molecules into the brain that initiate neuroinflammatory responses. In our current study, a guinea pig model, with the intention of reducing bacterial dissemination to the brain, was used. A short study duration of 15 days post-infection was chosen in order to evaluate the neurological changes that occur early in the progression of disease, prior to the glial and neuronal changes identified in our previously published findings [430]. We demonstrate for the first time, to our knowledge, that peripheral infection with both a laboratory and a clinical strain of Mtb, without evidence of CNS

infection, alters the expression of proteins critical to the integrity and function of the BBB *in vivo* in combination with cellular reactivity.

Bacterial diversity contributes to the variable outcomes of clinical TB cases. Although host factors play a role in the progression of pulmonary infection into clinical disease, it has become increasingly apparent that the bacteria is genetically diverse [470]. Even bacterial stocks of the same strain between laboratories have genetic variability [471]. Studies utilizing Mtb sometimes disregard strain differences, often due to experimental constraints, which limits the translational capacity of the findings. For this reason, our relevant guinea pig model of TB disease consisted of aerosolized infection with approximately 80 CFU of two different bacterial strains, Mtb H37Rv and HN878. As the first Mtb isolate to be genomically characterized, Mtb H37Rv is one of the most widely used strains in laboratory research [472, 473]. Experimentation using another strain, the virulent clinical isolate W-Beijing HN878, is becoming more common. Although HN878 has a similar doubling time as H37Rv during the first 14 days of infection, it is considered a hypervirulent bacterial strain due to decreased animal survival compared to other laboratory strains, likely because of reduced T-helper 1 (TH1) cell responses [474]. While strains like H37Rv do not cause granulomatous lesions in inherently Mtb-resistant murine models, Mtb HN878 induces granulomas in the lung with a pathology found in humans, including a core of macrophages surrounded by lymphocytes, as well as B-cell lymphoid follicles and germinal centers [475]. Some clinical strains have also proven to disseminate more readily to the CNS than laboratory strains like Mtb H37Rv, making it imperative that additional strains be utilized when studying the BBB during infection [476]. Examining the neurological effects of infection with two strains, both a laboratory and a clinical strain, helps account for the innate variability between strains in our study.

This study consisted of three-week-old, outbred Dunkin Hartley guinea pigs. Our use of a guinea pig *in vivo* model, whose pathology and cellular response to Mtb closely mimics that of humans, is the best current laboratory model of neuropathology caused by peripheral Mtb infection and enhances the translational potential of our findings [398-400]. Young animals were chosen for this study, as it is well-established that natural aging results in BBB dysfunction, neuroinflammation, and the accumulation of

neurotoxic proteins [209, 457, 477]. The Dunkin Hartley guinea pig is known to exhibit aged-related pathology as early as five months old, in both the brain and systemic tissues [478-480]. By using young animals, we eliminate possible age-related impact, although our findings of neuropathology caused by pulmonary Mtb infection may exacerbate underlying neurological changes in aged models.

In our model, granulomatous lesions were identified in the lungs of animals 15 days post-infection (dpi) (**Figure 14**), without signs of morbidity or mortality, or significant weight loss, irrespective of infectious strain (data not shown). Although cytosis was identified in some of these Mtb-infected animals, no granulomatous lesions were found in the brain as commonly seen with TBM. The gold standard bacterial colony forming unit (CFU) assay did not detect bacteria in the brain tissue of any animals despite CFUs present in lung and bacterial dissemination to the spleen in half of the animals infected with Mtb H37Rv and one third of the animals infected with Mtb HN878. This data was supported by acid-fast staining of brain tissue, which did not identify any bacilli in Mtb-infected animals (**Figure 14**). The combination of these three findings, determined utilizing well-established experimental methods, indicate that neurological changes are likely not induced by live bacteria infiltrating the CNS, despite evidence that bacterial dissemination occurred to extrapulmonary organs. Although we provide evidence that detectable bacterial dissemination to the brain did not occur through multiple methods, we acknowledge the limitations of these experiments. It is understood within the field that these methods lack sensitivity and may not detect small quantities of disseminated bacteria. While whole bacteria, both culturable and non-culturable, are not identified in the brain, our methods also do not account for bacterial components that maintain a high degree of immunogenicity.

Despite the lack of lesions in the brain, one animal from each experimental group, infected with Mtb H37Rv or HN878, showed areas with an abnormal cellular response, or cytosis. Brain regions included the frontal cortex, thalamus, brain stem, and cerebral nuclei (**Supplementary Table 1**). Histopathological staining identified the presence of increased numbers of immune cells, including lymphocytes and macrophages (**Figure 15**). Identification of these areas of cytosis determined the brain

regions studied for the remainder of the manuscript. The hippocampus was also selected, as it is an area susceptible to neurodegenerative effects and previously implicated in TB neuropathology [430]. Crosstalk between microglia and astrocytes is a known modulator of neuroinflammation. Typically considered the first cell to respond in the brain, microglia readily migrate and activate in response to stress, like trauma or contact with pathogens, sometimes as quickly as a couple of hours [481]. Under pathological conditions, microglial activation has been implicated in BBB dysfunction [314, 482]. Because of these roles, microgliosis was assessed by immunohistochemistry for the detection of Iba-1. Increased Iba-1$^+$ cells are seen in guinea pigs infected with both Mtb H37Rv and HN878, and a substantial microglial response is demonstrated in cytosis$^+$ animals (**Figure 16**). The visual appearance of the microglia in Mtb-infected animals suggests an activated phenotype, with shorter processes, cell hypertrophy, and an ameboid-like morphology; microglia with longer processes are identified in control animals [483-485]. These observations suggest that pulmonary Mtb infection promotes the polarization of microglia into a reactive morphology. Notably, activated microglia are known to secrete Il-1α, TNF, and C1q, which are sufficient in inducing a reactive astrocytic phenotype [381]. Microglia also upregulate the production of reactive oxygen species (ROS) and pro-inflammatory molecules like IL-1β when activated [486]. Unfortunately, Iba-1 is not solely a microglial marker but is also expressed at low levels on peripheral macrophages [487]. Activated microglia and peripheral macrophages also share an ameboid-like morphology, making it increasingly challenging to differentiate between these cell types. It must be considered that the cellular response, especially in cytosis$^+$ animals, may also consist of peripheral macrophages.

Despite a substantial microglial response, proliferation or the recruitment of S100β$^+$ astrocytes in any brain region of animals infected with Mtb, with or without identified cytosis, was lacking (**Figure 17**); however, this does not consider the phenotype of the cells present. The exact function of astrocytic C3 is context-dependent, but it has been shown that reactive astrocytes upregulate C3 in neuroinflammatory and neurodegenerative diseases, demonstrating C3 as a marker of astrogliosis [381, 488-490]. Upon further investigation, C3 expression within S100β$^+$ cell soma was increased in all brain

regions of Mtb-infected animals compared to uninfected controls, and this response was amplified in Mtb HN878-infected guinea pigs (**Figure 18**). Such data indicates that the astrocytes in these regions display a more reactive phenotype. This change in reactivity, but not cell number, makes sense in the context of cellular activation versus proliferation. While astrocytes respond to stimuli, such as mediators produced by nearby microglia, within hours, it can take days for these cells to expand their populations properly [491]. Temporal limitations in the study and no evidence of culturable bacteria in the brain may not have allowed sufficient time for astrocyte proliferation.

Limited changes in C3 expression were seen in the hippocampus of cytosis$^+$ animals compared to controls, although it should be noted that cytosis was not identified in any animals within this region. Alternatively, increased C3 was seen in cytosis$^+$ animals compared to uninfected controls in the other four brain regions (**Figure 18**), suggesting that the extent of astrogliosis may play a role in BBB integrity and, subsequently, the recruitment of immune cells. Polarized microglia, as seen in Mtb-infected animals, can secrete IL-1β which stimulates the release of the pro-inflammatory molecules C-C motif chemokine ligand 2 (CCL2), C-C motif chemokine ligand 20 (CCL20), and C-X-C motif chemokine ligand 2 (CXCL2) by activated astrocytes. These three mediators are known to encourage the migration of immune cells into the brain [492]. Additionally, microglial IL-1β represses the production of sonic hedgehog (SHH) by astrocytes, which results in reduced BBB integrity and decreased tight junction proteins [492]. The identification of reactive astrocytes that upregulate C3 in Mtb-infected animals and in animals with cytosis unveils a potential mechanism for the modulation of the BBB seen in these animals. Interestingly, although no change in astrocyte cell number is seen qualitatively, more GFAP$^+$ processes are present in Mtb-infected animals, along with an increase in total GFAP area (**Figure 19**). In cases of neuroinflammation, reactive astrocytes, characterized as having longer, branched processes, increase contact with the vasculature, which results in increases in total cell area [383]. The C3-secreting, phenotypically reactive astrocytes identified in Mtb-infected animals are increasing contact with the vasculature, which is supported by our data showing more GFAP$^+$ processes in association with blood

vessels (**Figure 6**). This further establishes the formation of a reactive population of astrocytes in response to pulmonary Mtb infection.

Increased expression of AQP4 was found in animals infected with Mtb H37Rv and HN878 (**Figure 19**). Expression of AQP4 was located within the endfeet of astrocytes with a reactive phenotype, as is common in neuroinflammatory states [493]. The exact function of AQP4 is disputed. Some studies exert that AQP4 expression leads to BBB changes, and is itself pro-inflammatory [494]. In a study by Zhou et al., AQP4 knockout mice opened tight junctions, downregulated GFAP expression, and increased vascular permeability [495]. In contradiction, others state that while AQP4 is involved in brain maintenance, alterations in this protein alone do not result in BBB leakage, immunoreactivity, or modified structure of microvessels [496]. Thus, we must consider the impact of altered AQP4 expression within the context of the complex BBB. A decrease in AQP4 expression is found in cytosis$^+$ animals compared to controls (**Figure 19**). This is likely due to the retraction of astrocytic endfeet, as glia can withdraw their endfeet during neuroinflammatory states [497]. Retracted endfeet may play a role in reducing barrier tightness and allowing for immune cell infiltration in areas with cytosis, as *in vivo* and *in vitro* studies show that astrocytes can reduce leukocyte traffic through the formation of TJs by upregulating claudins and junctional adhesion molecules [453]. It is possible that process retraction reduced stimulation of TJs by astrocytes in these cytosis$^+$ brain regions.

Glia are linked to the BBB in other ways, and that is through enzymatic regulation of proteins. Collagen levels are controlled by MMPs, which are endopeptidases that degrade the extracellular matrix [498]. Collagen IV, in particular, is regulated by matrix metalloproteinase-2 (MMP-2) and matrix metalloproteinase-9 (MMP-9) in the brain. These enzymes are tightly controlled, at both the level of transcription and post-translation, to prevent unnecessary damage. MMPs are often upregulated with age or in diseases, like AD, and it is proposed that these changes are due to a pro-inflammatory brain phenotype. MMPs are also highly implicated in BBB dysfunction [498]. Reactive astrocytes and microglia upregulate transcription of MMP-2 and MMP-9, and the pro-inflammatory mediators they secrete, like TNF, can enhance MMP transcription [499-502]. Activated glia also produce ROS, resulting

in proteolytic cleavage or disruption of thiol interactions that activate MMPs [502, 503]. By morphology and secretory phenotype, it has been established that reactive glia are present in Mtb-infected animals; these cells are likely upregulating MMPs and secreting mediators that indirectly modulate enzymatic activity. Together, MMPs can degrade collagen IV in the vasculature, resulting in decreased expression, as seen in our study (**Figure 20**).

Similarly, MMPs are involved in the loss of TJ proteins, like the primary constituent claudin V, which significantly decreases following Mtb exposure (**Figure 21**). Like collagen IV, claudin V is also degraded by MMP-9. Studies show that activation of MMPs during pathological events degrades tight junction proteins like claudin V, resulting in increased BBB permeability [504, 505]. This is demonstrated in other infection models; the bacteria involved in numerous meningococcal diseases, such as *Neisseria meningitidis,* can induce BBB changes through MMP-mediated proteolytic cleavage of the tight junction proteins [469, 506]. MMP-9 has also been directly implicated in peripheral immune cell infiltration into the brain [501]. Glial activation may be leading to increased activity of MMPs that are degrading matrix and TJ proteins. This mechanism seems likely given that *in vitro* studies have shown that Mtb modulates MMP activity [458].

The brain is considered an immunologically privileged organ. Peripheral immune cells, like T cells and macrophages, are found near the healthy brain in meningeal and perivascular spaces, but their existence in the parenchyma is limited [507]. Evidence shows that peripheral immune cells are more common in the resting brain than previously described, especially dendritic and memory T cells. However, the presence of infiltrating immune cells is still considered an event of the compromised brain [507-509]. Differential expression of surface proteins is a common method to differentiate immune cell populations. While glia express cluster of differentiation 45 (CD45), it is in low to intermediate levels compared to peripheral immune cells. This makes CD45 expression, in combination with other markers, a common technique used to identify neurological versus peripheral immune cells [510-512]. This study identified peripheral immune cells as S100β^{low}Iba-1^{low}CD45^{hi}; S100β^{hi}CD45^{low} astrocytes and Iba-1^{hi}CD45^{low} microglia were excluded. Based on these parameters, we detected the presence of a peripheral

immune cell population that is not evident in uninfected animals nor those infected with Mtb without cytosis (**Figure 22**). This is indicative of immune cell infiltration from the peripheral circulation. Increased BBB permeability has been correlated with the invasion of immune cells into the brain. It is partially why this event is documented in the aged brain and cases of neurodegenerative disease, including AD and PD. The function of peripherally invading immune cells has not been completely defined, and some evidence of neuroprotective roles exists, but they are primarily described as having neurotoxic functions. Invading cells activate glia and sustain neuroinflammation, leading to the degeneration of neurons and decline of cognitive function [507, 513, 514]. Although we distinguish the presence of peripheral immune cells based on surface expression, phenotyping centered on cell surface markers is incredibly complex. Cells demonstrate standard expression profiles but can upregulate or downregulate surface proteins, especially during inflammation and disease; even CD45 is modulated in inflammatory environments [515, 516]. Surface expression and morphology indicate that the cells we have identified are of peripheral origin, but we also acknowledge that an Iba-1^{+}CD45^{low} microglial population has been recently described. Cells of this phenotype exist in small populations, and are, to our current knowledge, associated with the diseased brain. This suggests that if such a microglial population exists in our TB model, they may still contribute to the pathogenesis attributed to pulmonary infection and should be further evaluated [517]. Glial markers in combination with CD45 expression alone do not allow us to properly categorize what types of cells we identify in the brains of cytosis^{+} animals. While we detect the infiltration of immune cells into the brain, further experimentation is necessary to classify these cells properly.

Despite demonstrating that pulmonary Mtb infection modulates BBB proteins, and we expect this will lead to vascular leak, experimentation is needed to establish the extent of barrier permeability fully. Future studies employing optimized permeability assays are necessary to definitively determine if vascular leakage into the brain is occurring and, if so, what size biomolecules can penetrate. That being said, even established protocols utilizing BBB tracers as a measure of permeability cannot account for small molecules and ions [518]. This is pertinent given the small size of neurotoxic microbial

components, like cell wall proteins and bacterial DNA, that may be penetrating the brain from the peripheral circulation. Permeability assays are, therefore, only sometimes a reliable way of examining barrier integrity, although they may be beneficial for future studies [518].

These results describe changes to major BBB constituents that we correlate to gliosis and peripheral immune cell infiltration without evidence of bacterial dissemination to the brain. In response to Mtb exposure, microglia and astrocyte reactivity is demonstrated in multiple brain regions. We correlate these phenotypic changes to increased AQP4 expression and astrocyte process contact with the vasculature. Additionally, we identify decreased expression of TJ proteins and altered collagen levels that can be attributed to Mtb infection. Ultimately, infiltration of peripheral immune cells is identified in animals with progressive neuropathology. Due to the limited sample size, additional experimentation is necessary to fully characterize the pathological changes occurring in the Mtb-infected animals that demonstrate cellular infiltration. Our data characterizes modifications to the BBB shown, by others in other pathological states, to contribute to barrier dysfunction, providing valuable information on the mechanism of TB-associated neurotoxicity. These findings, which have never been identified in the context of peripheral TB disease, unveil mechanisms of cellular stress that may provide future therapeutic targets.

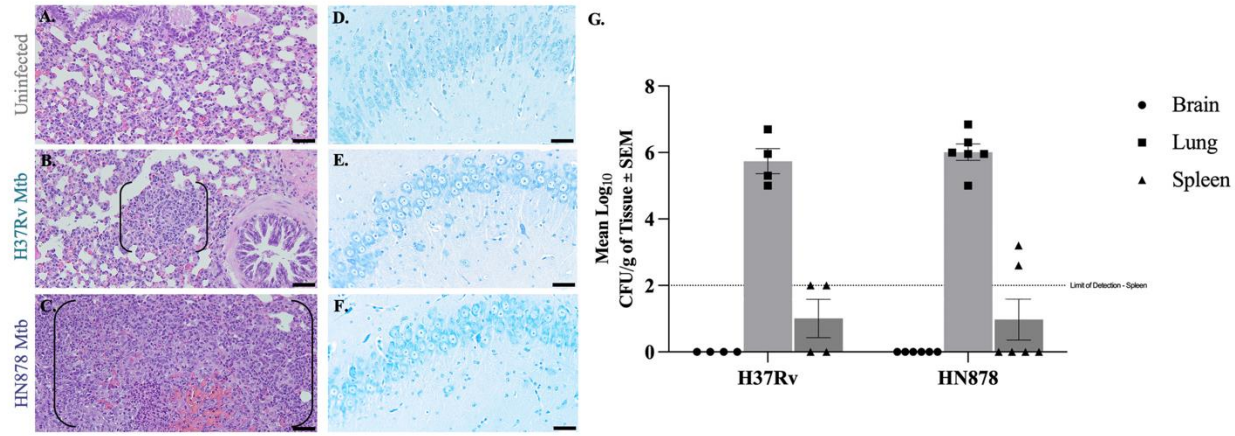

Figure 14: Bacterial dissemination to the brain is not detected despite infection of peripheral tissues. Lesions and bacteria are absent in the brains of guinea pigs infected with Mtb H37Rv and HN878 15 days post-infection. Lung histology shows granulomas (black brackets) in animals infected with Mtb H37Rv (B) and Mtb HN878 (C) but no granuloma formation is seen in uninfected animals (A). Acid-fast staining of brain tissue does not show the presence of bacteria in any brain region; representative images of the hippocampus are given for an uninfected control (D) and an animal infected with Mtb H37Rv (E) and Mtb HN878 (F). Colony-forming unit (CFU) assays indicate bacterial colonies in lung and spleen homogenates, but no bacterial colonies were detected in brain for either Mtb strain. The limit of detection for spleen is 2 log CFU (G). Each bar represents the mean ± SEM. ($N = 4 – 6$ animals/Mtb infection group). Scale Bar = 100 μm.

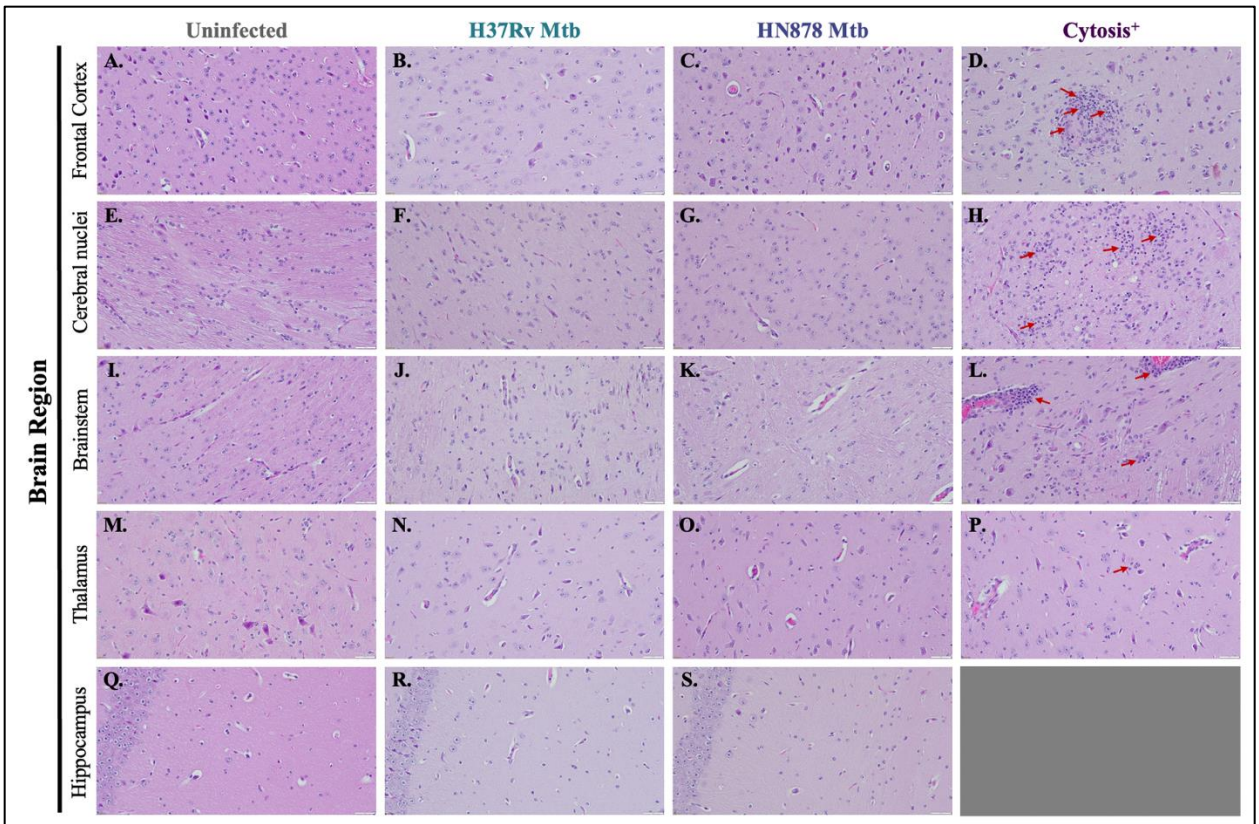

Figure 15: Increased cellular nuclei and changes in tissue morphology in cytosis^{+} animals. Cytosis was identified in the brains of only two Mtb-infected animals by H&E staining. Representative images from the two animals 15 days post-infection in the frontal cortex (A – D), cerebral nuclei (E – H), brain stem (I – L), thalamus (M – P), and hippocampus (Q – S) are shown. No evidence of an abnormal cellular response is seen in any brain region in uninfected controls (A, E, I, M, and Q) nor in the other animals infected with H37Rv (B, F, J, N, and R) and HN878 (C, G, K, O, and S). An intense cellular response, with increased cellular nuclei, is identified in one HN878-infected animal in the frontal cortex (D) and cerebral nuclei (H), and in one Mtb H37Rv-infected animal in the brain stem (L) and thalamus (P). ($N = 4 – 6$ animals/Mtb infection group; 2 animals in the cytosis^{+} group). Scale Bar = 50 μm.

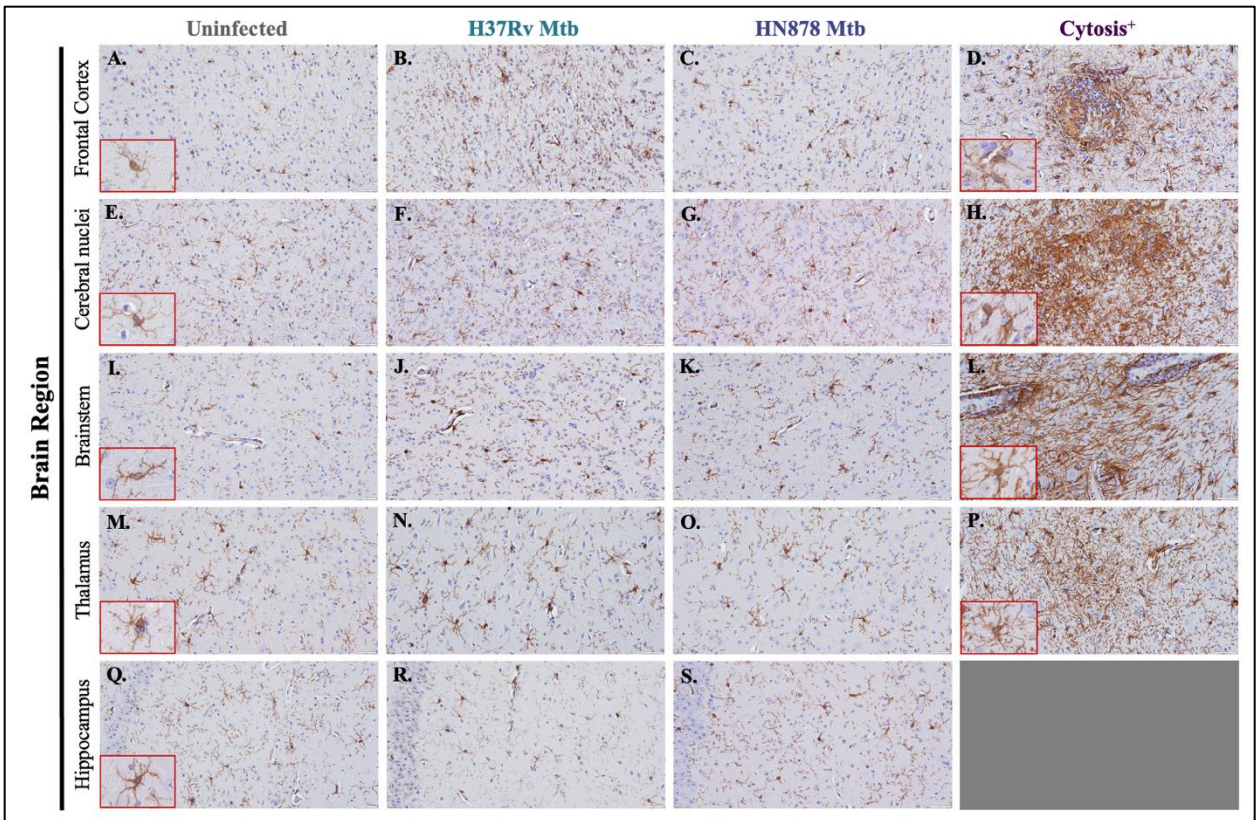

Figure 16: Increased microglial response following Mtb infection that is exacerbated in cytosis^{+} animals. Microgliosis was determined using immunohistochemical staining of guinea pig brain tissue for the microglial cell marker Iba-1. Representative images of Iba-1^{+} microglia 15 days post-infection in the frontal cortex (A – D), cerebral nuclei (E – H), brain stem (I – L), thalamus (M – P), and hippocampus (Q – S) are shown. Inlets were provided to allow for higher magnification to view the glial staining and morphological changes. The number of Iba-1^{+} cells increase in all brain regions in animals infected with Mtb H37Rv (B, F, J, N, and R) and Mtb HN878 (C, G, K, O, and S) compared to uninfected controls (A, E, I, M, and Q). An intense microglial response is identified in one HN878-infected animal in the frontal cortex (D) and cerebral nuclei (H), and in one Mtb H37Rv-infected animal in the brain stem (L) and thalamus (P). ($N = 4 – 6$ animals/Mtb infection group; 2 animals in the cytosis^{+} group). Scale Bar = 50 µm.

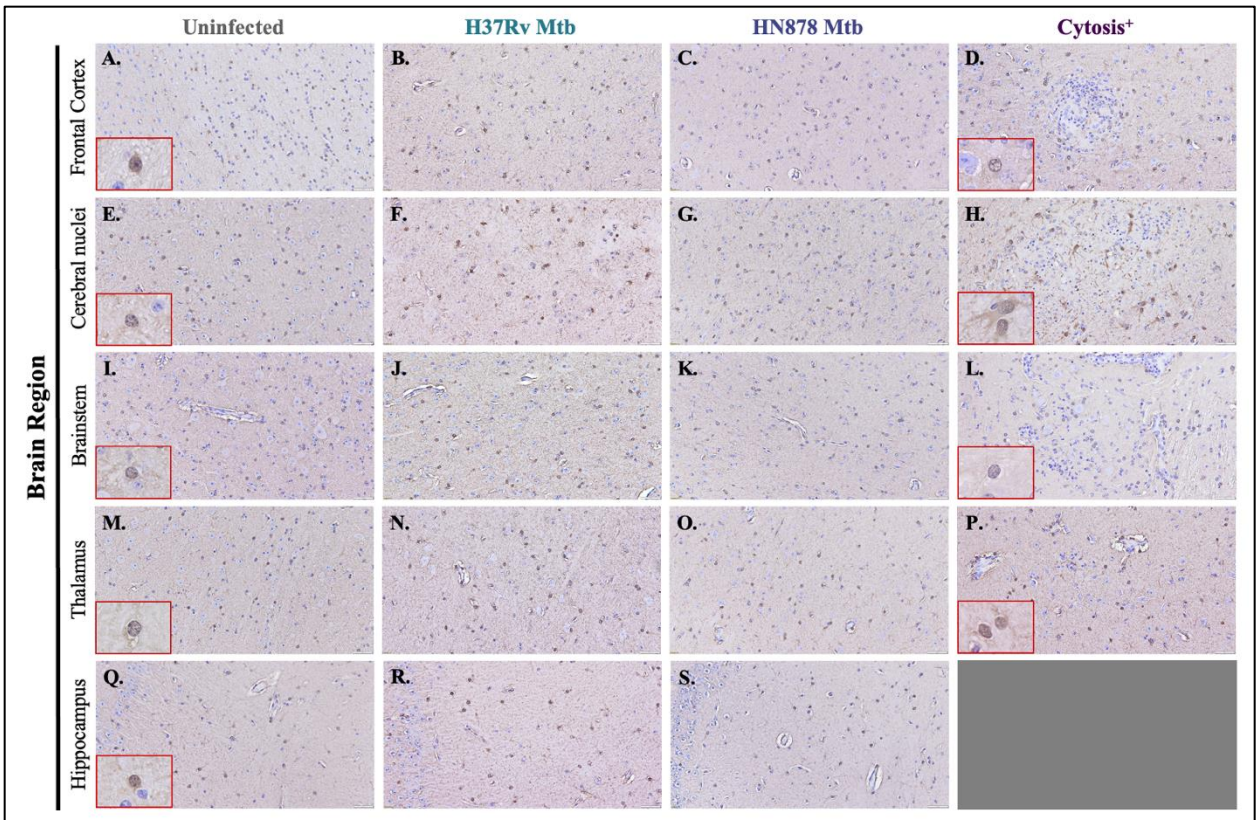

Figure 17: Limited astrocyte proliferation demonstrated following Mtb infection. Immunohistochemical staining of guinea pig brain tissue for the astrocyte marker S100β was performed to determine if proliferation of astrocytes occurred following infection with Mtb. Representative images of S100β^{+} astrocytes 15 days post-infection in the frontal cortex (A – D), cerebral nuclei (E – H), brain stem (I – L), thalamus (M – P), and hippocampus (Q – S) are shown. Inlets were provided to allow for higher magnification to view the glial staining. S100β^{+} cells do not appear to increase in any of the brain regions in animals infected with Mtb H37Rv (B, F, J, N, and R) and Mtb HN878 (C, G, K, O, and S) compared to uninfected controls (A, E, I, M, and Q). Although limited changes in cell number are apparent, cells upregulate S100β in one HN878-infected animal in the frontal cortex (D) and cerebral nuclei (H), and in one Mtb H37Rv-infected animal in the brain stem (L) and thalamus (P). ($N = 4 – 6$ animals/Mtb infection group; 2 animals in the cytosis^{+} group). Scale Bar = 50 μm.

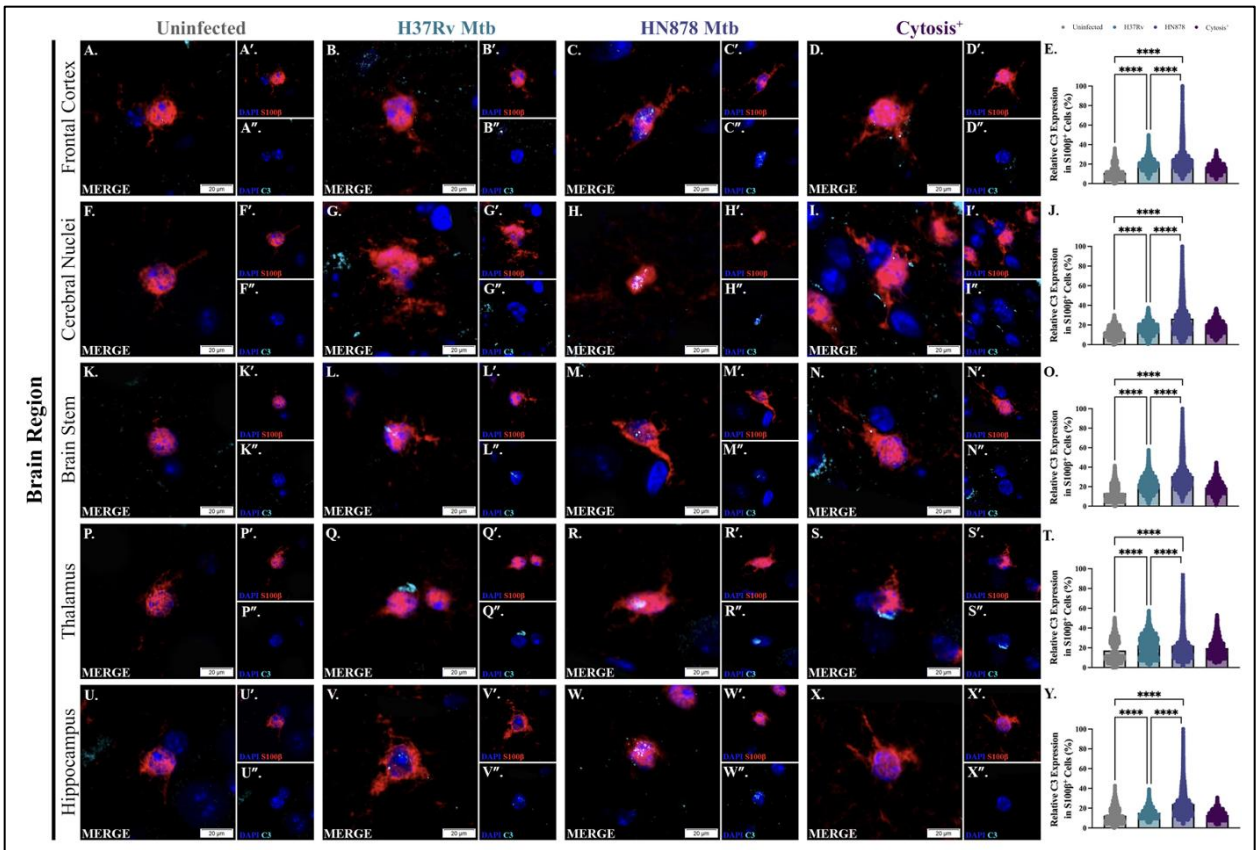

Figure 18: Astrocytes increase production of complement 3 following Mtb-infection. Astrocyte reactivity was analyzed following Mtb exposure for 15 days, as determined by co-localization of DAPI (blue), S100β (red), and C3 (cyan). C3 expression was analyzed in every $S100\beta^{+}DAPI^{+}$ cell present in each brain region for one tissue section per animal. Representative images of the frontal cortex (A – D), cerebral nuclei (F – I), brain stem (K – N), thalamus (P – S), and hippocampus (U – X) 15 days post-infection are shown. Exposure to Mtb H37Rv increased C3 expression, compared to uninfected controls, in the frontal cortex (E), cerebral nuclei (J), brain stem (O), thalamus (T), and hippocampus (Y). Expression is increased in Mtb HN878-infected animals in the frontal cortex (E), cerebral nuclei (J), brain stem (O), thalamus (T), and hippocampus (Y) compared to both H37Rv-infected and uninfected animals. Similarly, C3 is upregulated in astrocytes of $cytosis^{+}$ animals in all brain regions but the hippocampus (E, J, O, T, and Y). Each bar represents the mean ± SEM. (N = 4 – 6 animals/Mtb infection group; 2 animals in the $cytosis^{+}$ group). Nonparametric one-way ANOVA analysis performed; ****$p \leq 0.0001$. Scale Bar = 20 μm.

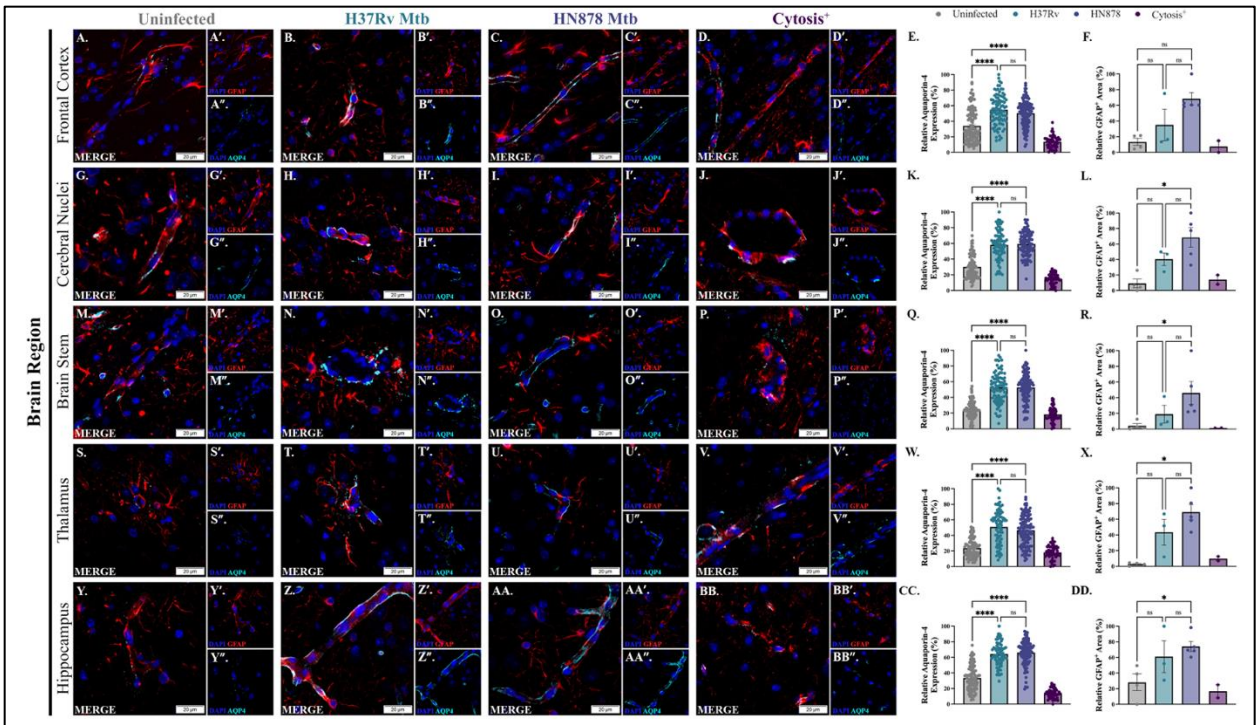

Figure 19: Astrocytes increase contact with vessels and expression of AQP4 following Mtb infection, which is decreased in cytosis$^+$ animals. Immunofluorescent staining of guinea pig brain tissue for the astrocytic marker GFAP (red), endfoot protein AQP4 (cyan), and DAPI (blue) in vessels was performed. Representative images of the frontal cortex (A – D), cerebral nuclei (G – J), brain stem (M – P), thalamus (S – V), and hippocampus (Y – BB) 15 days post-infection are shown. Exposure to Mtb H37Rv increased AQP4 expression and endfoot contact, compared to uninfected controls, in the frontal cortex (A, B, and E), cerebral nuclei (G, H, and K), brain stem (M, N, and Q), thalamus (S, T, and W), and hippocampus (Y, Z, and CC). AQP4 expression and contact is increased in Mtb HN878-infected animals in the frontal cortex (A, C, and E), cerebral nuclei (G, I, and K), brain stem (M, O, and Q), thalamus (S, U, and W), and hippocampus (Y, AA, and CC) compared to uninfected animals. Decreased expression of AQP4, and endfoot contact, is found in cytosis$^+$ animals in the frontal cortex (D and E), cerebral nuclei (J and K), brain stem (P and Q), thalamus (V and W) and hippocampus (BB and CC). Increased GFAP$^+$ area is demonstrated in animals infected with both Mtb H37Rv and HN878, but not cytosis$^+$ animals, in the frontal cortex (F), cerebral nuclei (L), brain stem (R), thalamus (X), and hippocampus (DD). Each bar represents the mean ± SEM. (N = 4 – 6 animals/Mtb infection group; 2 animals in the cytosis$^+$ group). Nonparametric one-way ANOVA analysis performed; * = $p \leq 0.05$, **** = $p \leq 0.0001$. Scale Bar = 20 µm.

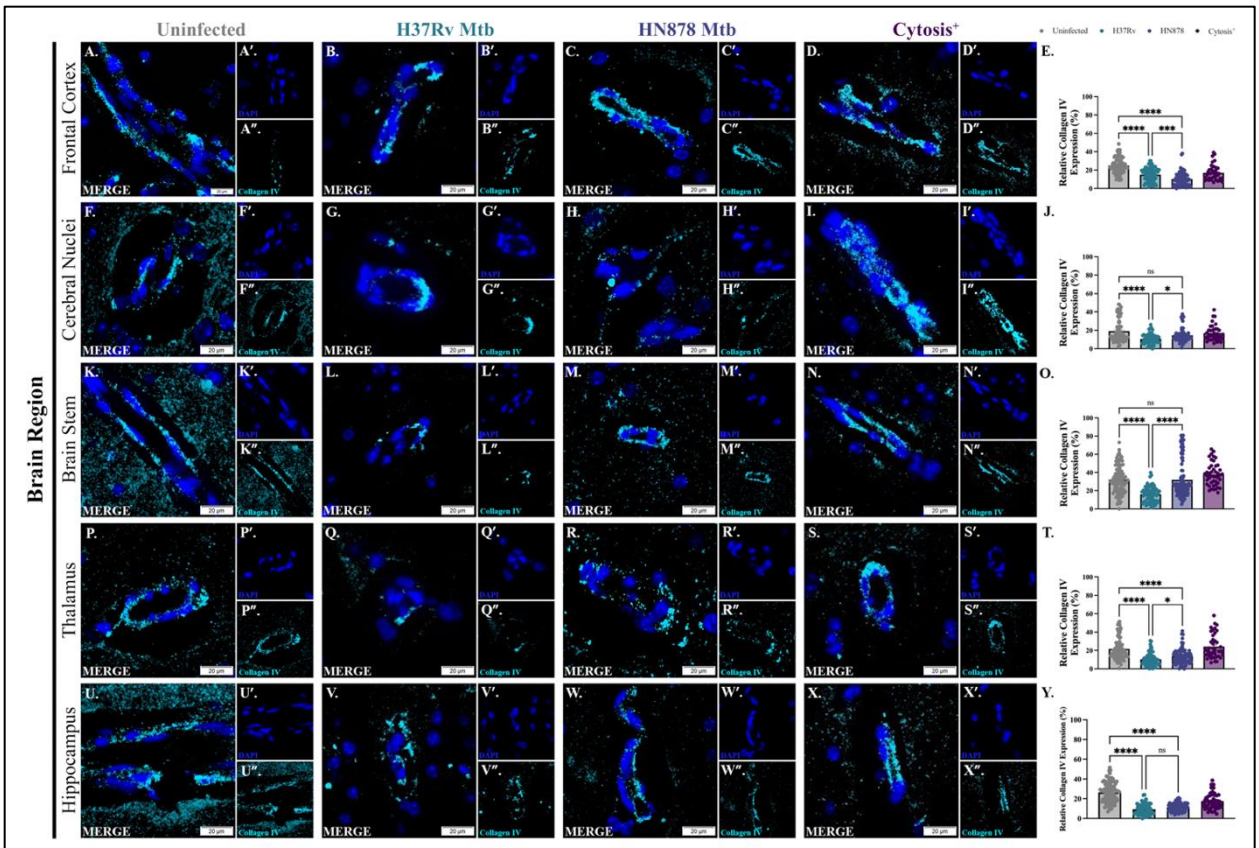

Figure 20: Collagen IV is modulated following infection with Mtb. Immunofluorescent staining of guinea pig brain tissue for DAPI (blue) and collagen IV (cyan) in vessels was performed. Representative images of the frontal cortex (A – D), cerebral nuclei (F – I), brain stem (K – N), thalamus (P – S), and hippocampus (U – X) 15 days post-infection are shown. Exposure to Mtb H37Rv and HN878 decreased collagen IV expression compared to uninfected controls in the frontal cortex (E), cerebral nuclei (J), brain stem (O), thalamus (T), and hippocampus (Y). Decreased expression of collagen IV in cytosis^{+} animals is found in the frontal cortex (E) and hippocampus (Y), but not the cerebral nuclei (J), brain stem (O), and thalamus (T). Each bar represents the mean ± SEM. ($N = 4 – 6$ animals/Mtb infection group; 2 animals in the cytosis^{+} group). Nonparametric one-way ANOVA analysis performed; *$p \leq 0.05$, ***$p \leq 0.001$, and ****$p \leq 0.0001$. Scale Bar = 20 μm.

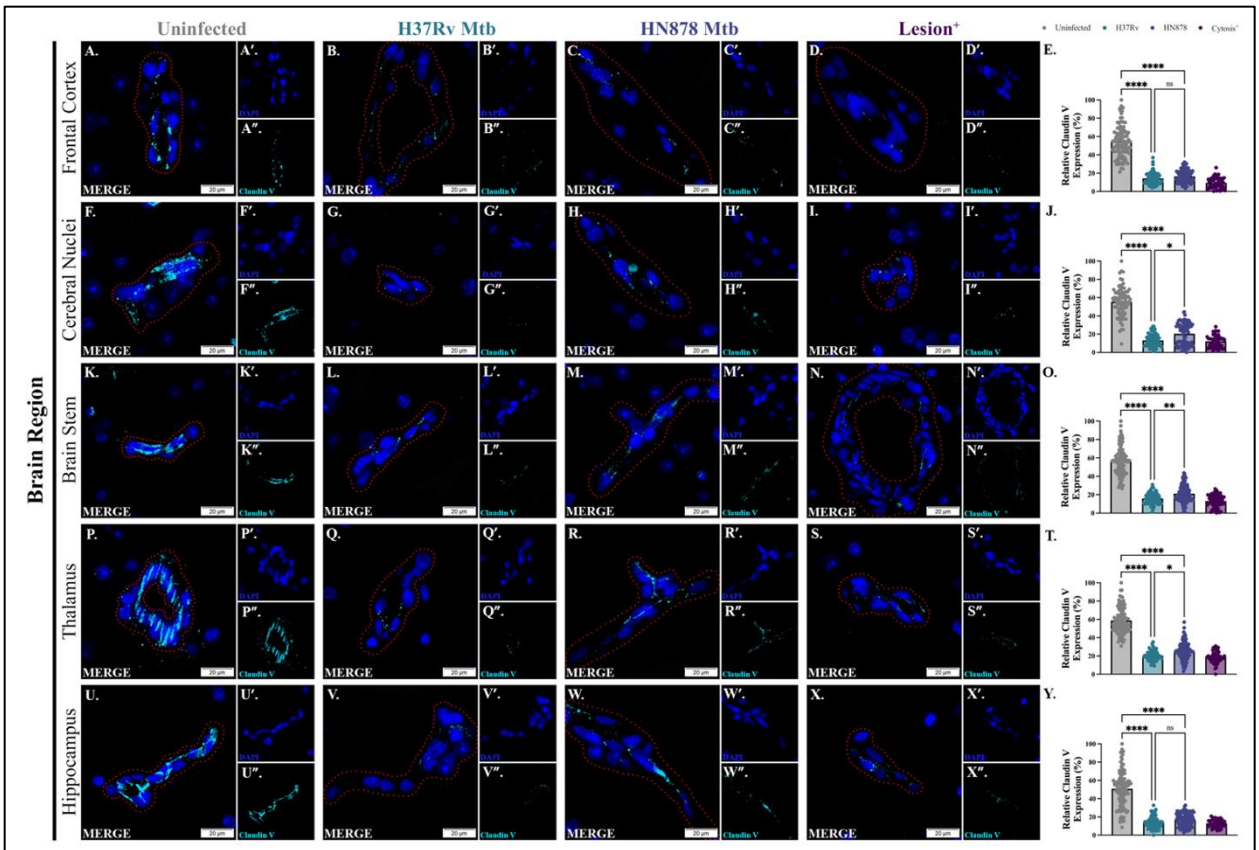

Figure 21: Claudin V is decreased following infection with Mtb. Immunofluorescent staining of guinea pig brain tissue for DAPI (blue) and claudin V (cyan) in vessels was performed. Representative images of the frontal cortex (A – D), cerebral nuclei (F – I), brain stem (K – N), thalamus (P – S), and hippocampus (U – X) 15 days post-infection are shown. Exposure to Mtb H37Rv and HN878 decreased claudin V expression compared to uninfected controls in the frontal cortex (E), cerebral nuclei (J), brain stem (O), thalamus (T), and hippocampus (Y). Decreased expression of claudin V in cytosis^{+} animals is found in the frontal cortex (E), cerebral nuclei (J), brain stem (O), thalamus (T), and hippocampus (Y) as well. Each bar represents the mean ± SEM. ($N = 4 – 6$ animals/ Mtb infection group; 2 animals in the cytosis^{+} group). Nonparametric one-way ANOVA analysis performed; *$p \leq 0.05$, **$p \leq 0.01$, and ****$p \leq 0.0001$. Scale Bar = 20 μm.

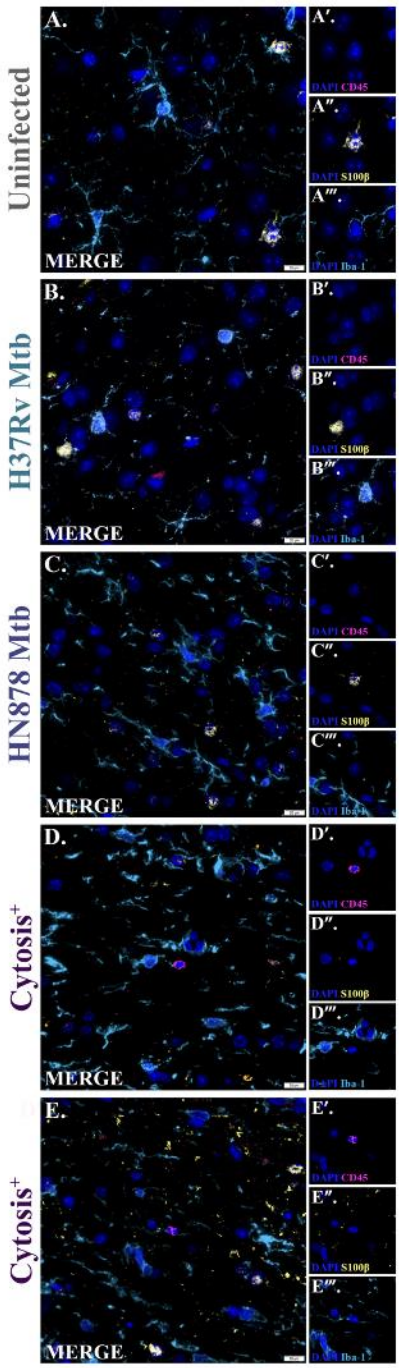

Figure 22: Peripheral immune cells identified in cytosis^{+} animals. Immunofluorescent staining of guinea pig brain tissue for CD45 (pink), S100β (yellow), Iba-1 (cyan), and DAPI (blue) for identification of peripheral immune cells. Representative images 15 days post-infection are shown. Exposure to Mtb H37Rv (B) and HN878 (C) did not show an abnormal population of cells, similar to uninfected animals (A). Alternatively, CD45^{high}S100β^{low}Iba-1^{low} peripheral immune cells are identified in cytosis^{+} animals (D and E). ($N = 4 – 6$ animals/Mtb infection group; 2 animals in the cytosis^{+} group). Scale Bar = 20 μm.

CHAPTER 4

EVALUATING THE OUTBRED, DUNKIN HARTLEY GUINEA PIG AS A LABORATORY MODEL OF NATURALLY ACQUIRED AGING NEUROPATHOLOGY

4.1 INTRODUCTION

Aging is defined as the time-dependent physical deterioration of an organism, which reduces functional capacity and increases the likelihood of acquiring diseases [519]. An important change that occurs naturally during aging is the loss of irreplaceable cells, most notably neurons in the brain. Consequently, aging is the primary risk factor for neurodegenerative diseases, which include dementia, Alzheimer's Disease (AD), and Alzheimer's Disease Related Dementias (ADRDs). The risk for amyloid β-positive AD dementia in women, in which diagnoses predominate, is approximately 1.6% in populations aged between 65 and 90, and dramatically increases to an estimated 25.4% of those aged 90 years and above [520]. Importantly, the population of individuals aged ≥ 65 years is estimated to increase from 53 million in 2018 to 88 million in the United States by 2050, making it imperative that research be performed to investigate mechanisms of dysfunction attributable to age. One contributing factor to the challenges of researching and curing age-related disease is the inadequacy of current laboratory models. Appropriate *in vivo* models must address the following requirements: neuropathologies that closely resemble human disease, short life spans, and accessibility. Other factors, such as spontaneity of neuropathology and the presence of comorbidities commonly associated with age, strengthen the translational capacity of the model. We hypothesized that the non-transgenic, outbred Dunkin Hartley (DH) strain of guinea pig is a promising model of naturally acquired neuropathologies that are characteristic of human aging and neurodegenerative disease.

Age associated neuropathologies include cellular senescence, neurotoxic protein accumulation, neuronal dysfunction, and gross changes to anatomical structures and cognition. Perhaps one of the most

prominent neuropathologies identified in the aged brain is cellular senescence, a conserved mechanism of tissue aging characterized by cell-cycle arrest in the G1 or possibly G2 phase that prevents the proliferation of damaged cells. Senescence is induced by chronic inflammation and stress, including DNA damage, telomere shortening or dysfunction, oncogene activation or loss of tumour suppressor functions, epigenetic changes, activation of anti-apoptotic pathways, and organelle damage [521]. Notably, glial cells, which perform critical homeostatic functions in the brain, can acquire a senescence-associated secretory phenotype (SASP). Such a phenotype is characterized by the production of pro-inflammatory cytokines, resembling activated cellular states, which directly contribute to a neuroinflammatory brain phenotype, as well as attract peripheral immune cells to the brain [521-524]. This results in chronic, low-grade neuroinflammation, sometimes referred to as "sterile" inflammation, that damages the brain over time [209]. Glial cells are also often seen in increased quantity in the brain and display activated morphologies [209]. In addition to the increase in inflammatory mechanisms, senescent glia likely become incompetent in their ability to degrade neurotoxic proteins, which enhances their accumulation [525]. Overall, these responses decrease neurogenesis and drive synaptic loss, contributing to cognitive impairment [525, 526].

Although typically associated with neurodegenerative disease, neurotoxic misfolded proteins are also increased during brain aging. These proteins include amyloid β (Aβ) and tau, both of which comprise the plaque and tangle pathologies identified in AD. Extracellular amyloid plaques are composed of elongated peptides of Aβ, specifically the 42 amino acid form ($A\beta_{1\text{-}42}$), and tangles of hyperphosphorylated tau. Postmortem studies discovered that most aged individuals without clinical symptoms of dementia or diagnosed neurodegenerative disease have amyloid plaques, which have been identified in 32% to 82% of study participants, and tau tangles, in 30% to 100% of people [527, 528]. This suggests that these proteinopathies may not be selective for the diseased brain but are instead driven by age but may be exacerbated in select individuals.

Neuroinflammation and protein aggregates contribute to neuronal dysfunction through the production of reactive oxygen species (ROS). Reactive species can also be generated by mitochondrial

dysfunction, as neurons are increasingly vulnerable due to their elevated energy demand and high dependency on mitochondrial oxidative phosphorylation [529]. This results in increased nuclear and mitochondrial DNA damage, which persists as a consequence of inefficient repair mechanisms associated with age [530]. Overall, this results in the loss of synaptic density and shrinkage of dendrites, and subsequently a reduction in proper neuronal function. Neuronal structural and functional changes cause cognition deficits and brain atrophy; approximately 0.5% of grey matter, especially in the frontal cortex, is lost between the ages of 20 and 80 years, and white matter degeneration is also evident [530].

It is increasingly difficult to differentiate between the effects of brain aging and neurodegenerative disease, as they share clinical symptomology and pathology. Both aged individuals and those diagnosed with a neurodegenerative disease display cognition and memory deficits, although it is considered that those diagnosed with disease have exacerbated decline. A diagnosis of AD or ADRD is characterized by the presence of extracellular plaques of amyloid β and tangles of hyperphosphorylated tau. Yet, these protein pathologies are also identified in post-mortem aged brains without official diagnoses of neurodegenerative disease. Consequently, recent studies have demonstrated that the sensitivity of current clinical and neuropathologic criteria ranges from 70.9% to 87.3%, and specificity ranges from 44.3% to 70.8% [531]. Similarly, it is expected that between 12% and 23% of patients diagnosed with AD do not have sufficient AD pathology at autopsy to account for the presence of dementia, and that as many as half of patients without a clinical diagnosis of AD have pathologic diagnoses of AD post-mortem [532, 533]. These data suggest that using *in vivo* models that demonstrate exacerbated aging neuropathology is a promising avenue for evaluating not only progressive pathological changes in the brain, but also mechanisms of neurodegenerative disease.

Although numerous *in vivo* models of brain aging and neurodegeneration exist, including rodents, non-human primates, and companion animals (felines and canines), no animal model fully recapitulates human disease while also maintaining accessibility for research purposes. For decades, murine models have been the most common laboratory model. While useful, because of the ease in which their DNA can be manipulated, mice do not have naturally occurring amyloid plaques and tau tangles, suggesting they

may be absent altogether, and they do not exhibit dramatic gross brain changes [534, 535]. Numerous transgenic murine models have been created to induce such neuropathologies but, despite progressing our understanding of the aged brain, they do not recapitulate disease in most human cases; the majority of AD cases are sporadic without a known genetic origin [536]. These differences are likely the reason studies conducted in murine models have had poor predictive power for drug efficacy in humans.

Larger animals show promise, due to their long lifespans and physiological similarity to humans. Non-human primates (NHP) demonstrate remarkable similarity to humans in their physiology, neuroanatomy (including their morphology and composition of key anatomical areas), and cognition, making them a relevant *in vivo* model to study neuropathology [537]. Notably, aged chimpanzees and rhesus monkeys naturally develop tau and amyloid pathology, synaptic loss, and cognitive deficits [538, 539]. Companion animals, including canines and felines that are maintained as household pets, also demonstrate aging pathology and disease (canine cognitive dysfunction (CCD) and feline cognitive dysfunction (FCD)), with additional translational value [540, 541]. They are often exposed to similar environmental conditions as humans, which can aid in the identification of potential factors that contribute to sporadic disease [535]. That being said, the use of larger mammal models such as primates and domesticated animals is not practical in a laboratory setting; there are ethical considerations, study limitations, additional regulations, and high associated costs compared to rodents that makes their use extremely limited in most research institutions.

Another rodent model, the guinea pig (*Cavia porcellus*), has been utilized in studies of asthma, allergies, and infectious diseases like tuberculosis (TB). Their docile nature, small size, and biological similarities to humans make them an appropriate research model, and one outbred strain, the Dunkin Hartley (DH), is commercially available from several laboratory breeders. More recent data demonstrates that the DH guinea pig has multiple morbidities characteristic of human aging, including musculoskeletal decline, vascular disease, and obesity [542, 543]. It has been previously shown that DH guinea pigs display an age-related decline in peripheral skeletal muscle density and mitochondrial respiration. This strain, as early as 4 months of age, also develops progressive osteoarthritis (OA), which is accompanied

by local and systemic inflammation [480, 544]. These data suggest that the DH guinea pig may be an suitable model of progressive neuropathology, as evidence indicates that musculoskeletal decline is often correlated with cognitive impairment.

Expanding upon this, the aged DH guinea pig demonstrates decreased mitochondrial respiration and efficiency in the hippocampus with age (Walsh et al., 2024, *Submitted).* Additionally, DH guinea pigs, by 15 months old, show increased circulating neurofilament light chain, gliosis, and proteinopathy. Altogether, these data suggest that the DH guinea pig may be a valuable *in vivo* model of naturally acquired neuropathology. Additionally, we hypothesized that this particular strain, the DH, demonstrates exacerbated neuropathology compared to other strains, the PigmEnTed (PET) guinea pig, at the same age. In this study, we showcase that DH guinea pigs, by as early as 12 months of age, display characteristics similar to those identified in the aged and AD brain, including glial reactivity, misfolded protein accumulation, and neuronal loss.

4.2 METHODS

4.2.1 Animals and Sample Collection

Male, outbred Dunkin Hartley (DH) and PigmEnTed (PET) guinea pigs (Elm Hill, USA; Chelmsford, MA, USA) were used in this study. Animals were ordered at 4 and 11 months old and housed for one month (N =8/group; total N = 32); final ages were 5 months old and 12 months old. Animals were housed at the Colorado State University Laboratory Animal Resources facility accredited by the American Association for Accreditation of Laboratory Animal Care (AAALAC). Guinea pigs were individually housed under constant temperature and humidity conditions (21° ± 2 °C temperature and 30 ± 5 % humidity). A 12-hour light/12-hour dark cycle was used, and animals had *ad libitum* access to standard pelleted food and water. Experiments were performed in accordance with the National Research Council's Guide for the Care and Use of Laboratory Animals and were approved by the Institutional Animal Care and Usage Committee (IACUC) at Colorado State University. At the time of euthanasia, guinea pigs were placed under isoflurane-induced anesthesia and euthanized by direct cardiac puncture.

One 12 month old PET animal died prior to euthanasia, with no gross pathology evident upon necropsy. Tissues were collected for histopathology by fixing in 10% neutral buffered formalin (NBF).

4.2.2 Tissue Processing and Embedding

Brains were fixed in 10% NBF at room temperature for at least 48 hours. Tissues were processed using a Leica TP1020 Automatic Benchtop Tissue Processor and embedded in paraffin wax (Cancer Diagnostics, Cat #: EEPAR56). Tissues were sectioned on a Thermo Scientific HM 325-2 Manual Microtome at 5µm thickness and mounted on positively charged glass slides (Superfrost Plus, Cancer 232 Diagnostics, Cat #: 4951) for staining and analysis.

4.2.3 Immunohistochemical Staining

Immunohistochemical stains were performed on whole brain sagittal sections. To deparaffinize the tissue sections, slides were heated for 20 minutes at 60°C followed by a series of incubations in xylene and graded ethanol (xylene, 1 part xylene to 1 part 100% EtOH, 100% EtOH, 95% EtOH, 70% EtOH, 1.0 M TBS) for 5 minutes each. Heat- and chemical-induced antigen retrieval was performed on the tissue by incubating in 1X EDTA buffer (1mM EDTA disodium salt dihydrate, 0.05% Tween; pH 8.0) for 20 minutes at 95°C. Removal of endoperoxides was performed through incubation in 0.3% hydrogen peroxide for 30 minutes at room temperature. Wash steps and tissue permeabilization was performed using 2% bovine serum albumin (BSA) and 2% Triton-X in 1.0 M TBS. Tissue was blocked in 10% goat or donkey serum diluted in 1.0 M TBS for 1 hour at room temperature. After being diluted to their optimized concentrations, primary antibodies were incubated on the tissue at 4°C overnight.

Misfolded proteins were identified using a mouse anti-phospho-Tau (Thr181) (1:800; Invitrogen, Cat #: MN1050) antibody. Washing was performed using 2% BSA and 2% Triton-X in 1M TBS, 3 times for 3 minutes each, before incubation with the secondary antibody at a 1:250 concentration for 1 hour at room temperature. Wash steps were performed using 2% BSA and 2% Triton-X in 1M TBS, 3 times for 3 minutes each. An ABC HRP peroxidase detection kit (Vector Laboratories, Cat #: pk-4,000) and

ImmPACT DAB Substrate, Peroxidase (HRP) Kit (Vector Laboratories, Cat #: sk-4,105) were used as chromogen and slides were counterstained with hematoxylin (Thermo Fisher Scientific, Cat #: 7231) and bluing solution (Cancer Diagnostics, Cat #: FX2107). All slides for each antigen of interest received the same immunoreaction period, which were visualized by a single pathologist in a blinded fashion. Slides were secured with a coverslip in mounting medium and stored at room temperature until imaging. Whole tissue images were taken using an Olympus BX53 microscope with an Olympus DP70 camera using an Olympus UPlanSApo 20x objective (N.A. = 0.75). Representative images were taken using an Olympus BX53 microscope with an Olympus DP70 camera using an Olympus UPlanFL N 40x objective (N.A. = 0.75).

4.2.4 Immunofluorescent Staining

Whole brain sagittal sections were deparaffinized by heating slides for 20 minutes at 60°C followed by incubation in xylenes and graded ethanol (xylene, 1 part xylene to 1 part 100% EtOH, 100% EtOH, 95% EtOH, 70% EtOH, 1.0 M TBS) for 5 minutes each. Heat- and chemical-induced antigen retrieval was performed by incubating tissue in 1X EDTA buffer (1mM EDTA disodium salt dihydrate, 0.05% Tween; pH 8.0) for 20 minutes at 95°C. Tissue was washed with 0.05 M TBS and blocked using 2% donkey and/or goat serum in TrisA (0.2% Triton-X in 1.0 M TBS) for 1 hour at room temperature. After being diluted to their optimized concentrations, primary antibodies were incubated on the tissue at 4°C overnight.

Astrocytes were identified using a rabbit anti-S100 calcium-binding protein β (S100β) antibody at a 1:750 concentration (Abcam, Cat #: ab41548). Microglia were identified using a goat anti-ionized calcium binding adaptor molecule 1 (Iba-1) antibody at a 1:400 concentration (Abcam, Cat #: ab5076). Washing was performed using 2% BSA in 1.0 M TBS before incubation with the secondary antibody at a 1:500 concentration for 1 hour at room temperature. The following secondary antibodies were used for the astrocyte and microglial stains, respectively: goat anti-rabbit secondary antibody at a 1:500 concentration (Vector Labs, Cat #: BA-1000) and donkey anti-goat secondary antibody at a 1:500

concentration (Jackson ImmunoResearch, Cat #: 705-065-147). Blood-brain barrier integrity was analyzed by detecting claudin V and aquaporin-4 (AQP4). Claudin V was identified using an anti-Claudin 5 polyclonal antibody at a 1:500 concentration (Invitrogen, Cat #: 34-1600) and a donkey anti-rabbit Alexa Fluor 647 secondary antibody at a 1:500 concentration (Invitrogen, Cat #: A31573). AQP4 was identified using an anti-Aquaporin-4 monoclonal antibody at a 1:200 concentration (ABclonal, Cat #: A11210) and a donkey anti-rabbit Alexa Fluor 647 secondary antibody at a 1:500 concentration (Invitrogen, Cat #: A31573).

Four 10-minute wash steps (1.0 M TBS) were followed by incubation with the secondary antibodies at 1:500 concentrations for at least 1 hour at room temperature in the dark. Tissue was washed three times for five minutes each (1.0 M TBS), and stained with Hoechst (Thermo Scientific, Cat #: 62249) diluted 1:2000 in PBS for three minutes followed by three additional washes (1.0 M TBS). Slides were coverslipped with Prolong Gold Anti-fade mounting medium (Cell Signaling Technology, Cat #: 9071), allowed to harden for 24 to 48 hours at room temperature, and then stored at 4°C in the dark. Whole-slide images were acquired using an Olympus BX63 fluorescence microscope equipped with a motorized stage and Hamamatsu ORCA-flash 4.0 LT CCD camera using a 20x Olympus X Apochromat air objective air objective (N.A. = 0.80). All slides, irrespective of experimental group, were imaged on the same day with the same exposure time per channel. Representative images were captured using an Olympus BX63 fluorescence microscope equipped with a motorized stage and Hamamatsu ORCA-flash 4.0 LT CCD camera using a 40x Olympus X278 Apochromat air objective air objective (N.A. = 0.80).

4.2.5 Immunofluorescent Analysis

Whole slide images of Claudin V and AQP4 stained by immunofluorescence were analyzed. For each slide, regions of interest (ROIs) were drawn around individual blood vessels of various sizes and orientations within the tissue. ROIs were evenly distributed across the following three brain regions: frontal cortex, hippocampus, and brainstem. At least twenty vessels per brain region were analyzed, and care was taken to exclude red blood cells and other abnormalities or artifacts from the analysis. Mean

gray intensity of the proteins within each vessel were quantified using manual thresholding on the Count and Measure function of Olympus CellSens software (v1.18). Percent relative expression was calculated for each protein of interest by determining the minimum (min) and maximum (max) quantifications for the data set. Each raw quantification (raw) for that brain region received the following calculation: [(raw – min)/(max – min)*100]. Iba-1$^+$ microglia and S100β$^+$ astrocytes were quantified by using manual thresholding on the Count and Measure function of Olympus CellSens software (v1.18) to identify S100β$^+$DAPI$^+$ cells or Iba-1$^+$DAPI$^+$ cells. Object filtering in the Olympus CellSens software was used to remove noncellular objects.

4.2.6 Statistical Analysis

All data is presented as mean +/- SEM unless otherwise specified. A ROUT (Q = 1%) outlier test was performed on all data to identify potential outliers, which were removed from the data set. Differences between experimental groups were analyzed using an ordinary two-way ANOVA with uncorrected Fisher's LSD and a single pooled variance analysis. Statistical analysis was completed using GraphPad Prism. Significance is denoted throughout the manuscript as * = $p \leq .05$, ** = $p \leq 0.01$, *** = $p \leq 0.001$, and **** = $p \leq 0.0001$.

4.3 RESULTS

4.3.1 Gliosis in Multiple Anatomical Regions is Exacerbated with Age in DH Animals Compared to PETs.

Brains from DH and PET guinea pigs aged 5 and 12 months were analyzed for glial migration and proliferation. Iba-1$^+$ microglia and S100β$^+$ astrocytes were detected in brain regions implicated in neurodegeneration. This included the following anatomical areas: regions of the hippocampus (CA1, CA2, CA3, and DG), brain stem, frontal cortex, thalamus, and hypothalamus. Representative images of Iba-1$^+$ cells in the frontal cortex of young (5 months old) and aged (12 months old) DH and PET guinea pigs are shown (**Figure 23A, B, E,** and **F**). Microglial quantifications in the aforementioned regions, except for the CA3 of the hippocampus and hypothalamus, show a significant increase in Iba-1$^+$ cells with

age in DH guinea pigs (**Figure 23C, D, G, I, J,** and **K).** An insignificant increase in cell quantity is observed in the CA3 and hypothalamus. While an increase in Iba-1$^+$ cells occurs in aged PETs, it is not significant in any brain region. Young (5 months old) PET animals demonstrate significantly more Iba-1$^+$ cells than DH animals in the DG, CA2, and CA3 of the hippocampus as well as the frontal cortex (**Figure 23C, G, H,** and **J**).

Astrocytes in those same brain regions were also quantified. Representative images of S100β$^+$ cells in the frontal cortex of young (5 months old) and aged (12 months old) DH and PET guinea pigs are shown (**Figure 24A, B, E,** and **F**). In DH animals, S100β$^+$ cells significantly increase with age in the brain stem, frontal cortex, and hypothalamus (**Figure 24I, J,** and **L**). Alternatively, aged PET animals show a significant increase in cell quantity in the DG and CA3 (**Figure 24C** and **H**).

4.3.2 Modulation of Tight Junction Proteins in Aged Guinea pigs.

Immunofluorescence microscopy was utilized to evaluate the expression of the BBB-associated, tight junction protein claudin V within blood vessels. The expression of claudin V in association with vessels was quantitatively analyzed in three regions highly implicated in aging and neurodegeneration: the frontal cortex, hippocampus, and brain stem. Representative images of immunostaining for claudin V in young and aged DH and PET guinea pigs are depicted for the frontal cortex (**Figure 25A – D**), hippocampus (**Figure 25F – I**), and brain stem (**Figure 25K – N**). In all three brain regions, no significant difference between young and aged DH animals is observed (**Figure 25E, J,** and **O**). Claudin V expression in young PET animals is significantly increased compared to aged PETs in the frontal cortex and brain stem (**Figure 25E** and **O**), but not the hippocampus, although a decrease is still observed (**Figure 25J**). Analysis of these proteins demonstrate that age modulates claudin V expression in PET animals, but not in DH, which have reduced tight junction proteins compared to PETs by as early as 5 months old.

4.3.3 Age Alters Aquaporin-4 Expression and Contact of Astrocytic Endfeet with Vessels.

Astrocytes, identified as $GFAP^+$ cells, and the protein AQP4, a water channel that is localized primarily to astrocytic endfeet, were identified using immunofluorescence microscopy. The expression of AQP4 in association with vessels was quantitatively analyzed in three regions highly implicated in aging and neurodegeneration: the frontal cortex, hippocampus, and brain stem. In the brain stem, a significant decrease in AQP4 expression occurs in aged DH animals (**Figure 26C**); no significant difference is observed in the other two brain regions for this strain (**Figure 26A** and **B**). In the hippocampus, a significant decrease in AQP4 expression occurs in PET animals, and young PET controls express higher AQP4 than young DH guinea pigs (**Figure 26B**). Concurrently, $GFAP^+$ astrocyte processes appear to increase contact in young PET guinea pigs compared to young DH animals (not shown). In the brain stem, an insignificant decrease in expression occurs with age in the PET strain (**Figure 26C**).

4.3.4 Intracellular Accumulation of Hyperphosphorylated Tau in Aged Guinea pigs.

The presence of the neurodegenerative biomarker hyperphosphorylated tau was evaluated in aged DH and PET guinea pigs through immunohistochemistry. The quantity of neurons positive for tau phosphorylated at threonine 181 (pTau T181) was evaluated in the frontal cortex and brain stem. Representative images of the frontal cortex in young and aged animals are shown (**Figure 27A – D**). Quantification of neurons positive for pTau T181 demonstrate a significant increase with age, regardless of strain (**Figure 27E**). An insignificant increase occurs in the brain stem of both aged DH and PET animals (**Figure 27F**).

4.3.5 Neuronal Loss with Age in the Hippocampus of DH and PET Animals.

Immunofluorescent staining for the neuronal nuclei marker NeuN was performed to determine if neuronal loss occurred in three relevant anatomical regions of the hippocampus. Representative images are shown for the Cornu Ammonis 1 (CA1) (**Figure 28A – D**), Cornu Ammonis 2 (CA2) (**Figure 28F – I**), and Cornu Ammonis 3 (CA3) (**Figure 28K – N**). Quantifications demonstrate a significant decrease in

the quantity of $NeuN^+$ neurons in the CA2 of aged PET animals (**Figure 28J**). An insignificant decrease in the quantity of $NeuN^+$ neurons occurs in aged PET animals in the CA1 (**Figure 28E**) and CA3 (**Figure 28O**) regions of the hippocampus compared to young controls. An insignificant decrease is also seen in the CA3 of aged DH animals (**Figure 28O**). Although insignificant, young DH animals demonstrate reduced quantities of neurons in all three anatomical regions compared to PET animals at the same age (**Figure 28E, J,** and **O**).

4.4 DISCUSSION

Age-related neurodegenerative disease cases are expected to double over the next twenty years, making it imperative that scientific advancements be made to better understand the progression of neuropathology and possible therapeutic interventions. One major hurdle to research is the lack of available laboratory models that are both widely accessible and naturally acquire age-related pathologies. Previously published data demonstrates that the Dunkin Hartley (DH) guinea pig shows glial changes and misfolded protein aggregates by as early as 15 months old [478]. Expanding upon this, our data characterizes age-related neuropathologies in the outbred, DH guinea pig, a laboratory strain that also shows co-morbidities such as osteoarthritis and skeletal muscle decline with age [542, 543]. Although the DH guinea pig has been implicated as a potential model of aging neuropathology and AD, in-depth characterization of the glial, neuronal, and misfolded protein changes in critical brain regions is lacking. We hypothesized that the DH guinea pig, by 12 months old, demonstrates advanced neuropathology compared to other laboratory strains, such as the PigMenTed (PET) guinea pig. Multiple anatomical brain regions were investigated in order to determine not only the involvement of regions heavily implicated in disease, but also if cellular changes occur throughout other regions of the brain. Areas included the frontal cortex, brain stem, thalamus, and hypothalamus, as well as multiple anatomical regions of the hippocampus. Through these data, we demonstrate that the DH guinea pig recapitulates the following age-related and neurodegenerative pathologies: gliosis, alterations to the BBB, and misfolded protein aggregation.

Aging neuropathology and neurodegenerative disease are closely associated, as they share characteristic neuropathological changes. In fact, in is estimated that almost all aged brains show neuropathologies typically indicative of disease. Over the course of numerous studies, it was shown that in aged individuals without diagnosed neurodegenerative disease nor dementia, 80 – 82% had amyloid plaques, 36 – 40% had inclusions of TDP-43, 8% to 31% had α-synuclein pathology, and as much as 98 – 100% had aggregations of hyperphosphorylated tau [527, 528, 545, 546]. The observation that almost all aged brains show these characteristic changes in correlation with the fact that age is the primary risk factor for disease indicates that age-related pathology is likely an initial driver of disease. Therefore, studying age-related pathologies, which requires an appropriate laboratory model that recapitulates natural brain aging, may provide valuable insight into mechanisms of disease.

Neuroinflammation mediated by glia has been heavily implicated in both brain aging and neurodegenerative disease. Microglia, which are the resident macrophages of the central nervous system (CNS), perform immunological surveillance. In response to pathogens or stress, microglia readily activate, increasing their capacity for phagocytosis of misfolded proteins, pathogens, and cellular debris. In both age and neurodegeneration, microglia proliferate and maintain pro-inflammatory secretory profiles and morphologies that may damage neurons over time [209]. Thus, Iba-1$^+$ microglia were quantified in the hippocampus, frontal cortex, brain stem, thalamus, and hypothalamus of young (5 month-old) and aged (12 month-old) animals of both strains (**Figure 23**). In DH guinea pigs, a significant increase in the quantity of Iba-1$^+$ cells is observed in every anatomical region evaluated except for the CA3 and hypothalamus; although insignificant, increased Iba-1$^+$ cell numbers were also identified in aged DH animals in those two brain regions. Alternatively, PET guinea pigs, which are expected to demonstrate delayed neuropathology, do not exhibit a significant difference between ages in any brain region. The increase in Iba-1$^+$ cell quantity may contribute to neurodegeneration through complement-dependent synaptic engulfment and secretion of pro-inflammatory mediators, as is often observed in aged glia, that that can directly injure neurons [547]. Additionally, although activated microglia typically eliminate proteins and debris, naturally aged microglia downregulate phagocytic receptors and

demonstrate an overall reduced phagocytic capacity, which exacerbates aggregation of misfolded proteins that may contribute to progression of pathology [548].

Astrocytes are specialized glial cells that provide structural support for neurons, as well as stimulate the BBB, synaptogenesis, and regulate neurotransmitters. Similar to microglia, astrocytes have been heavily implicated in the progression of neuropathology [209]. Upon activation, astrocytes activate into pro-inflammatory phenotypes, of which at least nine morphological subtypes have been described [549]. In aged DH animals, a significant increase in S100β$^+$ cells occurred in the brain stem, frontal cortex, and hypothalamus (**Figure 24**). A significant increase in the number of S100β$^+$ cells was observed in the dentate gyrus and CA3 of the hippocampus in aged PET animal compared to young controls (**Figure 24**). Dramatic changes in the quantity of S100β$^+$ astrocytes did not occur in all brain regions, notably the other anatomical regions of the hippocampus, but the astrocytes in the adult brain have moderate proliferative capacity [547]. Although changes in astrocytic volume or branching occurs with age, substantial increases in the quantity of astrocytes are not expected. These data are in line with the findings of others, which demonstrate that there is little, if any, increase in astrocyte quantity in the neocortex and hippocampus in both postmortem human neocortical tissue, non-human primates, and murine models [550-553]. Despite little change in the quantity of astrocytes present in these regions of the aged brain, the cells present may have a more reactive or pro-inflammatory phenotype, which can contribute to neuronal damage [209, 549]. In summary, from these experiments we can conclude that brain aging is accompanied by glial changes that are in line with human cases and established models.

One hypothesis for the stimulation of glia into reactive phenotypes is degradation of the BBB. The BBB, which uses metabolic and physical barriers to protect the brain, can be altered in response to physiological stimuli, which would result in leakiness that allows immunogenic antigens and immune cells from the circulation to enter the brain. In addition to their role as neuronal support cells, astrocytes are also implicated in BBB function. The endfeet of astrocytes form a fine lamellae on the outer surface of the endothelial cell layer comprising brain vessels [554]. This close proximity between astrocytic

endfeet and vessels allows astrocytes to maintain the BBB by up-regulating tight junction proteins, thereby stimulating BBB tightness [555]. The increase in astrocyte process contact, and subsequently the augmented expression of AQP4, with vessels identified in young PET guinea pigs may be neuroprotective by upregulating tight junction proteins, like claudin V (**Figure 25 and 26**). Alternatively, DH guinea pigs have lower AQP4 expression within vessels, especially in the hippocampus, which may contribute to an early neurodegenerative phenotype in this strain and reduced claudin V expression by as early as 5 months (**Figure 25** and **26**). While astrocytes are critical mediators of the BBB, evidence from models of neurological disease show that activated astrocytes in the parenchyma can secrete pro-inflammatory factors that disrupt the integrity of the BBB by decreasing tight junction proteins, including claudin V, which makes the barrier more permeable. As the guinea pigs age, a strain independent reduction in AQP4 associated with vessels occurs, which suggests that processes are retracted from vessels and likely reduce protective BBB stimulation (**Figure 26**).

Although gliosis, BBB modulation, and misfolded protein accumulation likely result in deficits in memory and cognition, evaluating the quantity of neurons in the hippocampus determines the extent of neurological changes. Interestingly, only aged PET animals demonstrate a significant decrease in neurons in the CA2 of the hippocampus (**Figure 28**). No significant difference is observed between 5 month and 12 month-old DH animals, but young DH animals have fewer neurons than young PETs (**Figure 28**). This suggests that neurodegeneration may occur as early as 5 months in the DH guinea pig model, and that in comparison PET animals show delayed neurodegenerative pathology. Although insignificant decreases were observed, it is important to note that actual neuronal loss in the hippocampus is thought to be minimal in clinical cases, but still results in cognition decline in human patients. In line with this current understanding, insignificant neuronal changes observed in DH and PET animals may still result in cognition deficits, and, similar to humans, we do not expected a dramatic decrease in neuronal quantity in the hippocampus by 12 months old.

In conclusion, pathological changes within the brains of guinea pigs establish the efficacy of the DH guinea pig as a laboratory model of brain aging and disease. The DH guinea pig exhibits exacerbated

neuropathology compared to the PET strain, including reductions in tight junction proteins, increased microglial and astrocyte quantities throughout the brain, and tau pathology by 12 months old, as well as reduced neuron quantity by 5 months old (**Figure 29**). Although these data play a key role in elucidating the neuropathology associated with the disease, further research is necessary to fully phenotype the cells present, to determine if pro-inflammatory or reactive glia exist in this model as is expected and if these changes confer functional deficits in neurons. It must also be considered that dementia and AD are more common in women, and these data were evaluated in male guinea pigs [556]. Due to this experimental limitation, the neuropathological conclusions made may actually be exacerbated in a female guinea pig model; sex differences should be evaluated further in future studies. Overall, these data effectively demonstrate that the DH guinea pig presents with neuropathology that closely mimics clinical disease in human patients, and, therefore, it is reasonable to infer that this strain may be a more effective laboratory model to study drivers of neuropathology and disease.

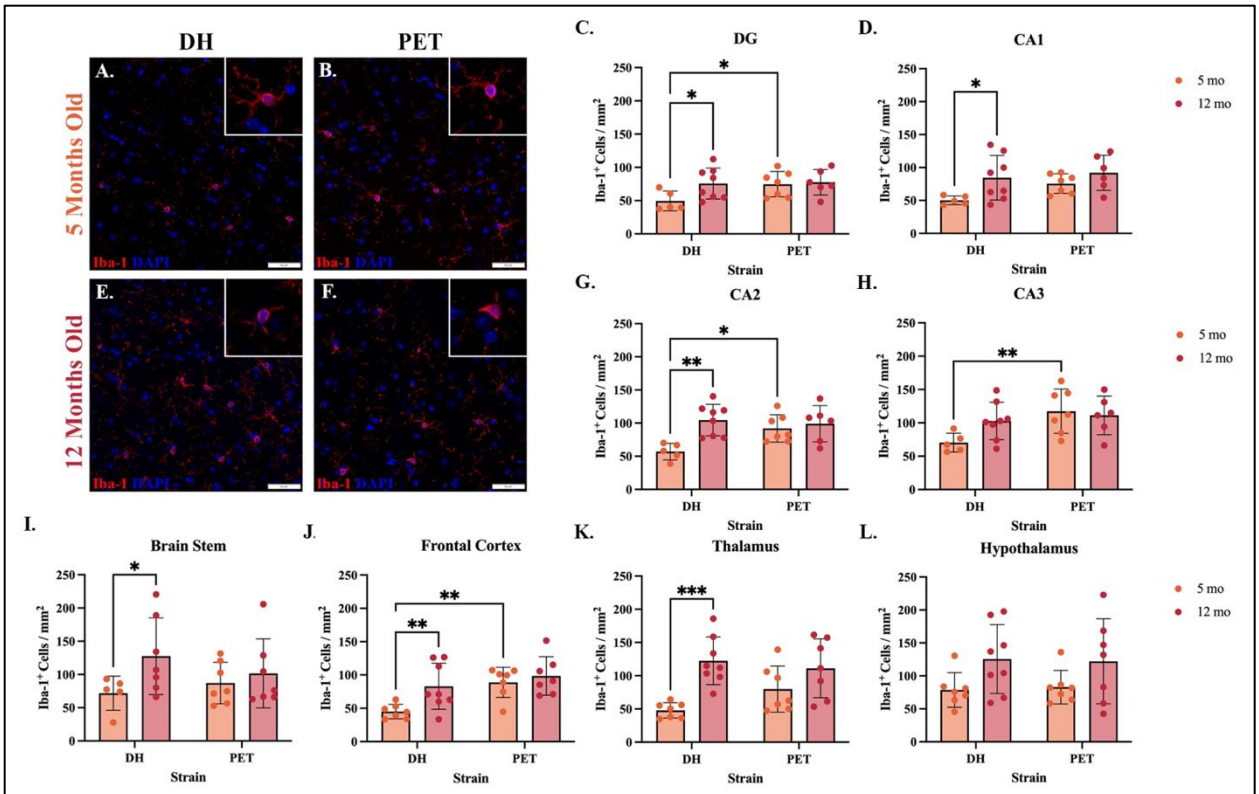

Figure 23. Microgliosis identified in aged DH, but not PET, animals in multiple brain regions.
Immunofluorescent labeling of microglia (Iba-1, red) was performed; representative high-magnification images are shown for the frontal cortex of 5 month-old DH (A), 12 month-old DH (E), 5 month-old PET (B), and 12 month-old PET (F). Cellular quantifications were performed in the DG (C), CA1 (D), CA2 (G), CA3 (H), Brain stem (I), frontal cortex (J), thalamus (K), and hypothalamus (L). Ordinary two-way ANOVA with uncorrected Fisher's LSD and a single pooled variance analysis performed. ($N = 5 – 8$/group). *p < .05; **p < .01; ***p < .001.

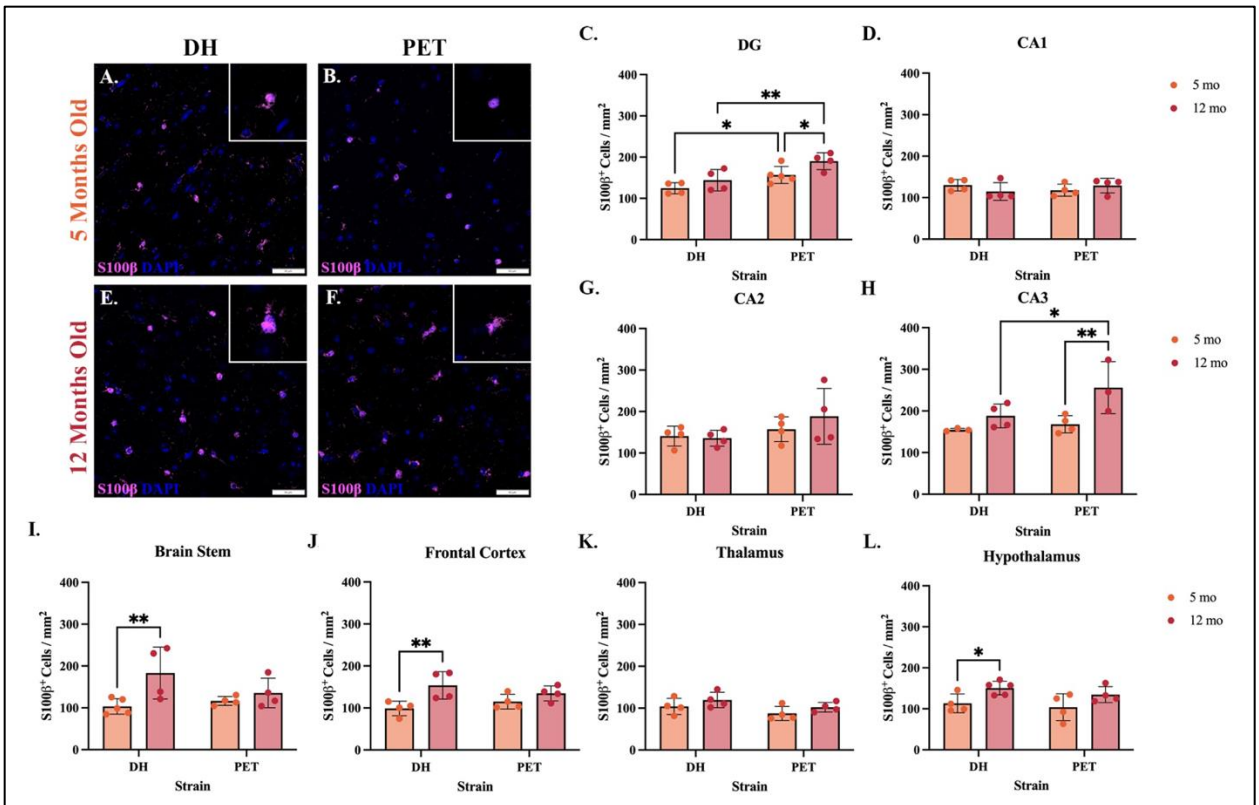

Figure 24. Astrocytosis identified in aged DH, but not PET, animals in brain regions implicated in neurodegenerative disease. Immunofluorescent labeling of astrocytes (S100β, purple) was performed; representative high-magnification images are shown for the frontal cortex of 5 month-old DH (A), 12 month-old DH (E), 5 month-old PET (B), and 12 month-old PET (F). Cellular quantifications were performed in the DG (C), CA1 (D), CA2 (G), CA3 (H), brain stem (I), frontal cortex (J), thalamus (K), and hypothalamus (L). Ordinary two-way ANOVA with uncorrected Fisher's LSD and a single pooled variance analysis performed. ($N = 4 – 5$/group). *$p < .05$; **$p < .01$.

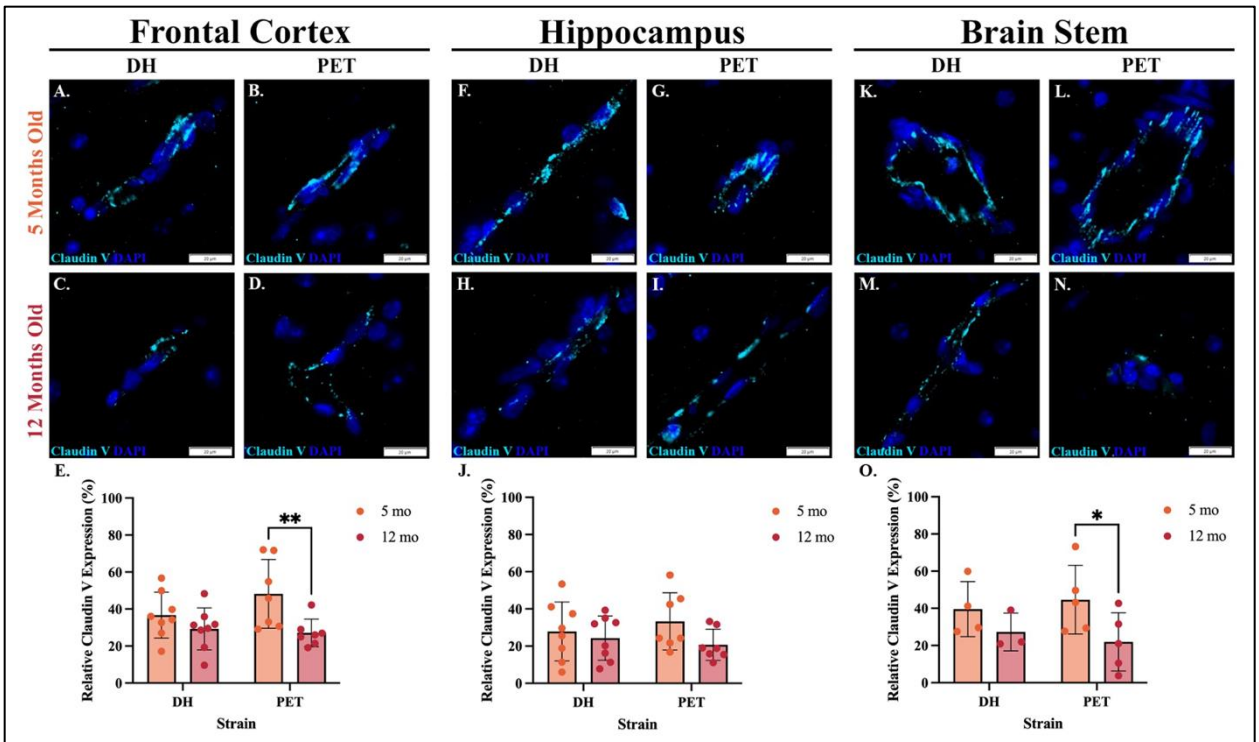

Figure 25. Tight junction proteins are modulated in PET guinea pigs. Immunofluorescent labeling of a tight junction protein (claudin V, cyan) was performed; representative high-magnification images are shown for the frontal cortex (A – D), hippocampus (F – I) and brain stem (K – N) of 5 month-old DH, 12 month-old DH, 5 month-old PET, and 12 month-old PET animals. Cellular quantification of protein expression within vessels was performed in the frontal cortex (E), hippocampus (J), and brain stem (O). Twenty individual vessels were analyzed, and the average expression per animal is shown. Ordinary two-way ANOVA with uncorrected Fisher's LSD and a single pooled variance analysis performed. (N = 4 – 8/group). *p < .05; **p < .01. Scale bar = 20 μm.

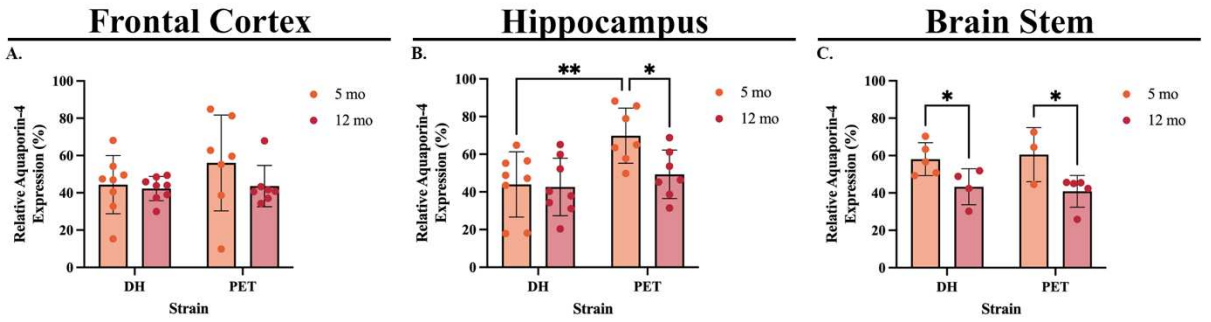

Figure 26. Aquaporin-4 proteins and astrocytic endfeet are modulated in PET guinea pigs. Immunofluorescent labeling of GFAP$^+$ astrocytes and the endfoot protein aquaporin-4 (AQP4) was performed. Quantification of protein expression within vessels was performed in the frontal cortex (A), hippocampus (B), and brain stem (C). Twenty individual vessels were analyzed, and the average expression per animal is shown. Ordinary two-way ANOVA with uncorrected Fisher's LSD and a single pooled variance analysis performed. ($N = 4 – 8$/group). *$p < .05$; **$p < .01$.

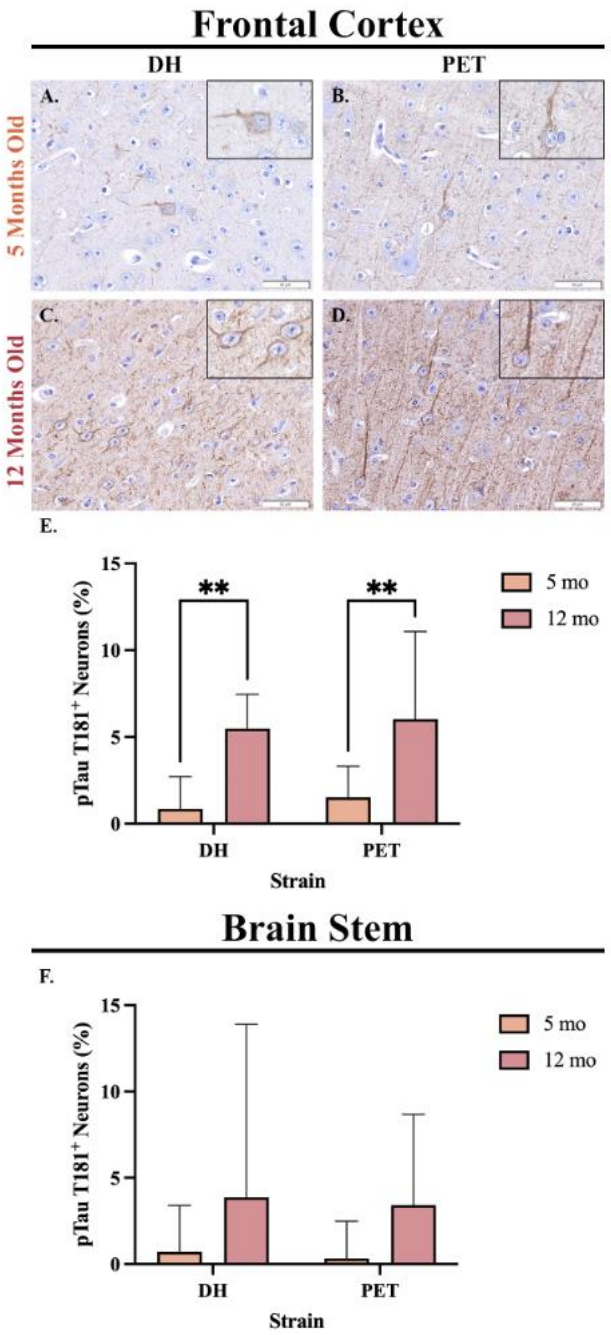

Figure 27: Increased neurons positive for hyperphosphorylated tau in aged DH and PET guinea pigs. Immunohistochemical staining of guinea pig brain tissue for tau phosphorylated at threonine 181 (pTau T181) was performed; representative high-magnification images are shown for the frontal cortex (A – D) of 5 month-old DH, 12 month-old DH, 5 month-old PET, and 12 month-old PET animals. Quantification of the percent of pTau T181 positive neurons in the frontal cortex (E) and brain stem (F) was performed. Ordinary two-way ANOVA with uncorrected Fisher's LSD and a single pooled variance analysis performed. ($N = 7 – 8$/group). *$p < .05$; **$p < .01$. Scale bar = 50 μm.

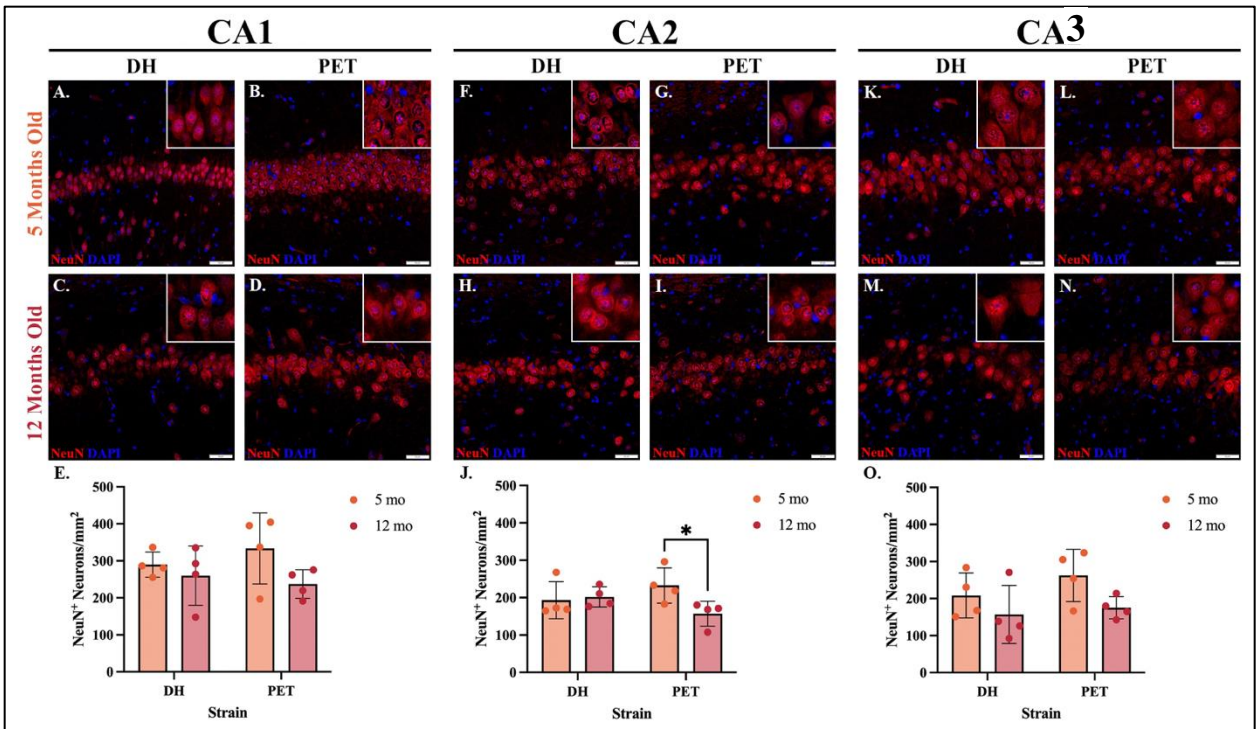

Figure 28. Neuronal loss in anatomical regions of the hippocampus in aged DH and PET guinea pigs. Immunofluorescent labeling of neurons (NeuN, red) was performed; representative high-magnification images are shown for the CA1 (A – D), CA2 (F – I), and CA3 (K – N) of 5 month-old DH, 12 month-old DH, 5 month-old PET, and 12 month-old PET animals. Cellular quantifications were performed in the CA1 (E), CA2 (J), and CA3 (O). Ordinary two-way ANOVA with uncorrected Fisher's LSD and a single pooled variance analysis performed. ($N = 4$/group). *$p < .05$. Scale bar = 50 μm.

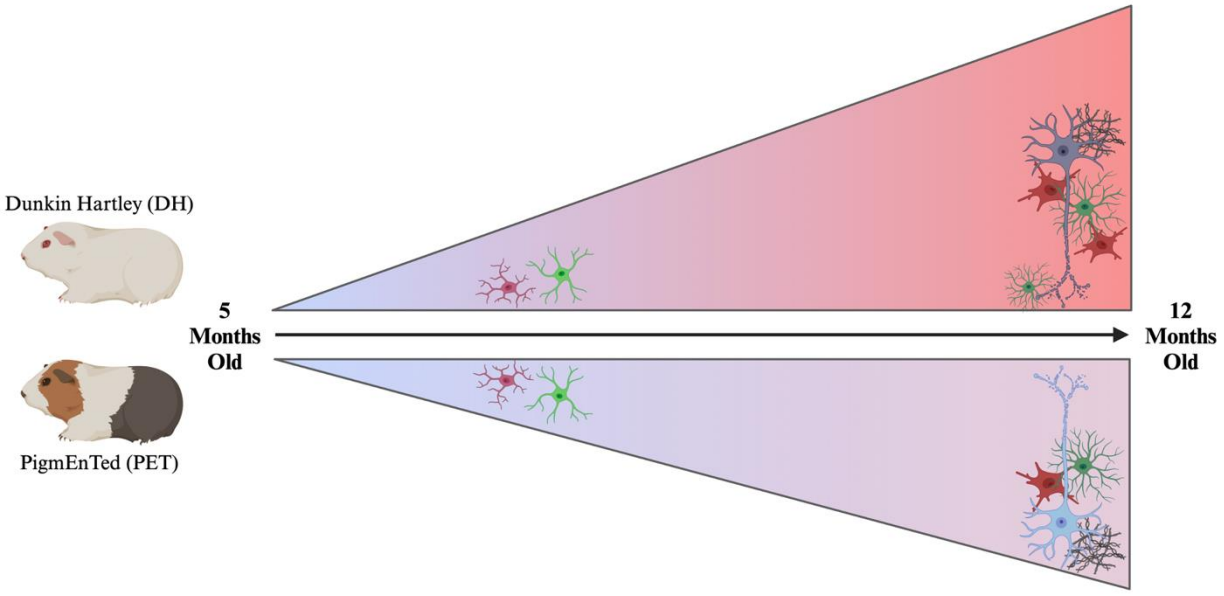

Figure 29. Dunkin Hartley guinea pigs demonstrate neuropathology, including gliosis and misfolded protein aggregation, by 12 months-old. Pigmented guinea pigs do not show as advanced glial responses, although misfolded protein accumulation is still evident, by this same timepoint.

CHAPTER 5

NEUROPROTECTIVE EFFICACY OF THE GLUCOCORTICOID RECEPTOR MODULATOR PT150 IN A ROTENONE MODEL OF PARKINSON'S DISEASE

5.1 INTRODUCTION

Parkinson's Disease (PD) is the second most common neurodegenerative disorder, with an estimated six million individuals that are directly affected worldwide [557, 558]. The impact of PD may be underestimated due to challenges in accurate diagnostic modalities of the disease, making the current and projected disease burden higher than previously reported [559]. PD is characterized clinically by motor symptoms, including resting tremor, rigidity, bradykinesia, and postural instability, in addition to non-motor features [560]. Non-motor symptoms occur early in prodromal disease, preceding motor symptoms by as much as decades. These non-motor disturbances include anxiety, depression, and gastrointestinal dysfunction [560]. The etiology of PD remains largely unknown, and it is primarily considered an age-related disorder, but epidemiological and experimental evidence suggests that risk factors include genetic mutations and exposure to environmental contaminants. Pesticides, such as rotenone, have been associated with increased risk of developing PD [561]. Rotenone is a mitochondrial complex I inhibitor that results in high levels of reactive oxygen species, culminating in oxidative stress and disrupted cellular signaling [562]. Ultimately, exposure to rotenone causes selective loss of dopaminergic neurons (DAn) in the substantia nigra pars compacta (SNpc) and retraction of terminal axonal projections within the striatum (ST). This, along with chronic neuroinflammation and the hyperphosphorylation and subsequent aggregation of α-synuclein (α-syn) into intra-neuronal Lewy bodies, comprise the primary neuropathological features of PD. We previously demonstrated that in mice exposed to rotenone for 14 days by intraperitoneal injection, neuroinflammatory activation of glia and widespread aggregation of α-

synuclein occurred prior to loss of DAn in the SNpc, indicating that these pathologic changes were key drivers of neuronal injury [563].

During neuroinflammation, microglia and astrocytes polarize from resting states to neurotoxic or pro-inflammatory phenotypes in response to environmental, pathogenic, or genetic stressors. These activated states aid in restoring brain homeostasis during stress by recruiting immune cells, removing pathogens and misfolded proteins through phagocytosis, and by secreting neurotrophic factors [564]. Despite these beneficial activities associated with adaptive glial reactivity, prolonged glial activation creates a pro-inflammatory environment that chronically damages the brain [565]. The dysregulation of neurotransmitters and the production of reactive oxygen species resulting from glial activation promotes neuronal dysfunction and neurodegeneration. In addition, neuroinflammation is hypothesized to contribute to the propagation of neurotoxic α-syn, as these pathologies are dynamically interconnected, which exacerbates the formation of Lewy bodies and worsens neuropathology [566]. Therefore, modulation of glial activation and subsequent neuroinflammation remains a promising target for therapeutic intervention.

Notable inflammatory signaling pathways mediated by glia that have been identified in PD include the nuclear factor-kappa B (NF-κB) and nucleotide-binding oligomerization domain, leucine-rich repeat-containing protein 3 (NLRP3). Activation of these pathways increases production of pro-inflammatory cytokines [567]. One potential avenue for controlling this pathological response is through the glucocorticoid receptor (GR), which is found ubiquitously in all parenchymal cells of the brain, particularly in astrocytes and microglia. GR has the capacity to regulate inflammatory signaling, dependent on the brain region, cell type, and the physiological context involved. Upon activation of the cytosolic GR by glucocorticoid (GC) hormones, it releases from chaperone proteins and translocates to the nucleus. There, it binds glucocorticoid response elements (GREs), thereby altering the transcription of inflammatory genes. The GR-GC complex can also interact with cytosolic proteins for post-translational regulation of inflammation. High quantities of GRs on both DAn and glia in the midbrain have been identified in rodent models, which have the capacity to trigger functional changes in the dopamine system [568]. GCs also have an expansive history of clinical use as anti-inflammatories for numerous chronic inflammatory diseases,

such as multiple sclerosis and rheumatoid arthritis [569]. Altogether, this suggests that targeting the GR is a potential therapeutic avenue for treating the neuroinflammation associated with PD.

In addition to its anti-inflammatory potential, GR has been directly linked to the neuropathology associated with both the aged brain and neurodegenerative diseases, including PD. GR and the GC hormone, cortisol in humans or corticosterone in rodents, are altered during aging and disease. Not only is GR function selectively reduced with age, murine models of PD exhibit fewer GRs in the SN [570, 571]. Similarly, analysis of post-mortem PD midbrain tissue demonstrates a significant decrease in the number of astrocytes expressing nuclear GR, which prohibits the capacity for anti-inflammatory mechanisms [572]. Moreover, an imbalance of the hypothalamic-pituitary-adrenal axis described in PD patients, and in rodent models, results in chronically increased cortisol/corticosterone levels [294, 573, 574]. High cortisol is linked to cognition decline and risk for neurodegenerative disease, as well as neuroinflammatory effects. It is unclear whether this is simply correlation or a causal effect, although studies show that stress, which induces the metabolism of cortisol, can worsen the motor symptoms associated with PD [575]. GRs can become inactivated or desensitized in the presence of chronically increased cortisol/corticosteroid, therefore disrupting the GRs ability to regulate inflammation [17, 18].

The function of GR in the central nervous system (CNS) is complex, as its actions cannot be uniformly classified as anti-inflammatory, but targeting GR has shown neuroprotective effects. PD models show that inactivating astrocytic GRs exacerbate DAn loss in the substantia nigra (SN) compared to controls, and increases glial reactivity and levels of pro-inflammatory mediators [571,576]. In experimental models of PD, activating microglial GRs impedes neurotoxic glial activation, reducing DAn degeneration [574]. Limiting neuroinflammation in microglia-specific NF-κB knockout mice reduced reactive gliosis and preserved the number of DA neurons in the SNpc [577]. However, complete inhibition of glial activation can exacerbate damage in response to stress by preventing secretion of trophic factors, limiting repair mechanisms, and preventing removal of misfolded proteins, which are necessary homeostatic responses to injury [578]. Therefore, therapeutics that modulate the neuroinflammatory signaling from glia, but do not completely attenuate their activity, may be more protective.

In this study, we examined the therapeutic efficacy of the GR modulator, (11b,17b)-11-(1,3-benzodioxol-5-yl)-17-hydroxy-17-(1-propynyl)-estra-4,9-dien-3-one (PT150), in preventing neuropathology associated with rotenone neurotoxicity [579]. We previously reported the anti-viral activity and anti-inflammatory effects of PT150, as well as its capacity to modulate GR-dependent gene expression [580]. Based on these data, we hypothesized that PT150 would effectively decrease glial inflammation, prohibit the aggregation of α-syn, and reduce the degeneration of DAn in the SNpc. Herein, mice exposed daily to rotenone (2.5mg/kg/day for 14 days), followed by daily oral administration of PT150 for the duration of the 14 day lesioning period revealed that PT150 treatment altered glial reactivity, ultimately decreasing intra-neuronal α-syn and retaining DAn cell bodies in the SNpc, although no protective effects were seen in axonal projections in the ST. These data suggest that modulation of GR is neuroprotective in the rotenone model of PD by altering pro-inflammatory glial responses.

5.2 METHODS

5.2.1 Animal Procedures and Sample Collection

Experiments consisted of male and female C57Bl/6J mice three months of age (N = 8/group) randomly assigned to experimental groups. Animals were housed at the Colorado State University Laboratory Animal Resources facility accredited by the American Association for Accreditation of Laboratory Animal Care (AAALAC). All animal experiments were performed in accordance with the National Research Council's Guide for the Care and Use of Laboratory Animals and were approved by the Institutional Animal Care and Usage Committee (IACUC) at Colorado State University. Experimental animals were housed under constant temperature and humidity conditions (21° ± 2 °C temperature and 30 ± 5 % humidity) and a 12-hour light/12-hour dark cycle was used. Mice had *ad libitum* access to standard pelleted food and water and were monitored using a clinical scoring system for signs of morbidity.

Rotenone was diluted to a final working solution daily in medium chain-triglyceride, miglyol + 2% dimethyl sulfoxide (DMSO)[581]; a 50X stock solution was prepared in 100% DMSO every 48 hours and

stored at −20°C. The head space of the vial was purged with nitrogen to prevent oxidation of the compound. Working concentrations were prepared by diluting 50X stock solutions in Miglyol 812 as previously described [563, 577]. Rotenone was delivered by intraperitoneal (i.p.) injection (2.5 mg/kg/day), as previously determined [563]. Vehicle groups received an equivalent volume of 100% miglyol by i.p. injection. Mice were weighed daily and a dosage of 2 µL/g body weight rotenone or vehicle was measured using a 50 µL Hamilton syringe, which was then transferred to an insulin syringe for i.p. injection once daily for 14 days. Hamilton syringes were cleaned daily in 10% bleach for 10 minutes, followed by 70% ethanol, then sterile water to prevent precipitate buildup within the needle.

Animals were randomly assigned to the following experimental groupings ($N = 8$ animals/group): vehicle (Miglyol), 2.5 mg/kg rotenone + vehicle (Miglyol), 2.5 mg/kg rotenone + 30 mg/kg PT150, and 2.5 mg/kg rotenone + 100 mg/kg PT150. Treatment dosage of the experimental drug, PT150, was calculated using dosing schemes and toxicity data from human clinical trials, which treated with 500 mg of PT150, or approximately 7 mg/kg. Calculations normalizing to body surface area determined that a dose of approximately 86 mg/kg in mice equates to a Human Equivalent Dose (HED) of 7 mg/kg [579, 582]. Thus, two doses of PT150 were evaluated for the duration of the study, a low dose of 30 mg/kg and high dose of 100 mg/kg. PT150 was dissolved in miglyol and delivered by oral gavage at 8µL/g body weight once daily for 14 days after the conclusion of rotenone dosing. Vehicle groups received 100% miglyol by oral gavage. At the conclusion of the study, animals were euthanized by decapitation under isoflurane anesthesia and tissues were collected for histopathology by fixation in 10% neutral buffered formalin.

5.2.2 Histopathological Processing and Immunofluorescent Staining

Brains isolated from mice were fixed for 72 hours in 10% neutral buffered formalin before being transferred to Colorado State University's Veterinary Diagnostic Laboratory for tissue sectioning. Paraffin-embedded brain tissue was sectioned at 5µm thickness and mounted onto charged slides. Brain sections were deparaffinized and stained for immunofluorescence detection using the Leica Bond RX_m automated

robotic staining system (Leica Biosystems, Nussloch GmbH). Antigen retrieval was performed using Bond Epitope Retrieval Solution 1 for 20 minutes at 60°C. Sections were permeabilized (0.1% Triton X in 1X tris-buffered saline/TBS) and blocked in 1% donkey serum or 1% donkey + goat serum in 1X TBS. Primary antibodies were diluted in 1X TBS and incubated for 1 hour per antibody. The following antibodies were used: rabbit anti-tyrosine hydroxylase (TH) (1:500; Millipore, cat #: AB152), mouse anti-neuronal nuclei [78] (1:200; Abcam, Cat #: ab279296), mouse anti-glial fibrillary acidic protein (GFAP) (1:1000; Abcam, Cat #: ab4648), rabbit anti-S100 Calcium Binding Protein B (S100β) (1:750; Abcam, Cat #: ab41548), rat anti-complement component 3 (C3) (1:250; Abcam, Cat #: ab11862), goat anti-ionized calcium binding adaptor molecule 1 (Iba-1) (1:50; Abcam, Cat #: ab5076), mouse anti-α-syn phosphorylation at serine position 129 (p129) (1:100; FUJIFILM Wako Chemicals, Cat #: 015-25191), and rabbit anti-α-syn (1:100; Abclonal, Cat #: A7215). Sections were stained with Hoescht 33342 (DAPI) (diluted 1:5000 in PBS; Invitrogen, Cat #: H3570) and mounted on glass coverslips in ProLong Gold Antifade hard set mounting medium (Fisher Scientific, Cat #: P36930). Slides were kept at room temperature for 24 – 48 hours to allow mounting medium to harden, and then stored at 4°C prior to imaging.

5.2.3 Immunofluorescence Imaging and Protein Quantification

Whole-tissue immunofluorescence montage images were captured using an Olympus VS200 slide scanning fluorescent microscope equipped with a Hamamatsu ORCA-fusion CMOS digital camera and collected using Olympus CellSens software. Full slide images were acquired using an Olympus X-line Apochromat 20X air objective (0.8 N.A.). All images were obtained using the same exposure time, light source intensity, camera gain, and filter application per channel. Brain regions were identified anatomically and regions of interest (ROIs) were manually drawn using Olympus CellSens software. The manual or adaptive thresholding features of the Count and Measure function of Olympus CellSens software were used to quantify immunofluorescence images for $S100\beta^+$ cell number and $GFAP^+$ area. Object filtering was used to remove non-cellular objects from the analysis. Intracellular protein expression was analyzed by using manual thresholding on the Count and Measure function of Olympus CellSens software to identify cells

(S100β$^+$ or GFAP$^{+)}$, creating an ROI from each detected object, and then analyzing the fluorescence intensity of each individual cellular ROI.

5.2.4 Stereological and Immunofluorescent Quantification of Dopaminergic Neurons in the SN and ST

Quantification of DAn was conducted using unbiased stereological methods adapted from our previous reports [150, 563, 577, 583]. Six sections per animal spanning the entire substantia nigra (SN) were analyzed blindly by a single investigator. Regions of interest (ROIs) were drawn manually using TH$^+$ immunolabelling in combination with the Allen Brain Atlas (Allen Institute for Brain Science, Seattle, WA, USA) to identify the SN and surrounding anatomical landmarks. TH$^+$ and NeuN$^+$ cells were quantified by using adaptive thresholding in the Count and Measure feature on the Olympus CellSens software, followed by object filtering. Quantitative stereological analysis using the motorized stage method was performed as previously described [227]. Striatal sections were immunostained for TH and fluorescence intensity was analyzed by manually drawing an ROI and using manual thresholding on the Count and Measure function of Olympus CellSens software as previously reported [563].

5.2.5 Morphological Characterization of Glia

Morphometric analysis was performed using Imaris image analysis software (version 9.8.2, Bitplane Imaris, South Windsor, CT, USA). Four randomized 400 × magnification images spanning the entirety of the substantia nigra were taken using an Olympus X-line Apochromat 40X air objective (0.95 N.A.). The Filament Tracing module was used to identify GFAP$^+$ astroglial and Iba-1$^+$ microglial processes. A total sum of processes per cell (filament length [sum]), branch number per cell (filament number of dendrite terminal points), and overall volume of processes per cell (filament volume [sum]), were utilized to determine morphometric changes present within each animal. Skeletonized renderings of glial cells were performed by using Imaris software (version 9.8.2, Bitplane Imaris, South Windsor, CT, USA) using high-magnification images.

5.2.6 Statistical Analysis

All data is shown as mean +/- SEM, unless otherwise noted. Experimental values were analyzed using a ROUT (α=0.05) test, and significant outliers there removed from the data set. Differences between each experimental group were analyzed using a one-way ANOVA with Tukey's post hoc test. All statistical analysis was conducted using Prism. Significance is denoted as * $p < 0.05$, ** $p < 0.01$, *** $p < 0.001$, **** $p < 0.0001$.

5.3 RESULTS

5.3.1 Treatment with 30 mg/kg PT150 did not result in unexpected mortality.

Two doses of PT150 were evaluated for the duration of the study, 30 mg/kg and 100 mg/kg. Adult male and female C57Bl/6 mice were exposed to a daily intraperitoneal (i.p.) dose of 2.5 mg/kg rotenone or vehicle for 14 days, followed by daily treatment with PT150 or vehicle for 14 days by oral gavage (**Figure 30A**). Signs of morbidity or mortality were monitored daily for each animal. Upon conclusion of the study, animals that received rotenone in combination with 100 mg/kg PT150 had a 50% mortality (**Figure 30B**). There was no difference in mortality between the rotenone-exposed animals that received 30 mg/kg PT150 or vehicle by the conclusion of the study (**Figure 30B**). Due to adverse health effects associated with rotenone + 100 mg/kg PT150 treatment, only the rotenone + 30 mg/kg PT150 treated group was analyzed for the remainder of the study.

5.3.2 PT150 treatment reduces the loss of dopaminergic neurons in the substantia nigra caused by rotenone neurotoxicity.

To determine the efficacy of PT150 in treating PD, the extent of neurodegeneration in the SNpc and ST were evaluated. The number of DAn in the SNpc were determined by quantitative stereology of whole-brain tissue sections stained for tyrosine hydroxylase (TH) and neuronal nuclei [78] as previously described [583]. Representative images of DAn in the SNpc of control, rotenone-exposed, and 30 mg/kg PT150 treated animals are shown (**Figure 31**). Compared to vehicle controls, animals exposed to rotenone

showed a significant decrease, an approximate 50% loss, of TH^+NeuN^+ DAn cell bodies in the SNpc by 4 weeks post exposure (**Figure 31F**). Animals exposed to rotenone followed by treatment with 30 mg/kg PT150 had more TH^+NeuN^+ cell bodies, which were not statistically different than controls (**Figure 31F**). These data are supported by hemotoxylin and eosin staining of brain tissue, which allows for morphological characterization of DAn in the SNpc. In correlation with reduced TH^+NeuN^+ cell number, rotenone-exposed animals show cells with pyknotic nuclei (**Figure 31I**, red arrows), whereas PT150 treated animals (**Figure 31N**) appear to have healthy nuclei similar to those observed in the control group (**Figure 31C**, white arrows).

The integrity of DAn axons projecting to the ST was determined by analyzing the fluorescence intensity of TH in this region. Representative images of control, rotenone-exposed, and 30 mg/kg PT150 treated groups are depicted for the ST (**Figure 31**). Striatal DAn terminal integrity was reduced 4 weeks post exposure to rotenone, as demonstrated by loss of TH^+ immunostaining compared to vehicle controls (**Figure 31Q**). Protection by PT150 did not appear to occur in the ST, as TH^+ immunostaining in this group was also significantly reduced in the ST compared to controls, and no difference was observed when compared to the rotenone-exposed group (**Figure 31Q**).

5.3.3 Rotenone-induced microgliosis is reduced in the substantia nigra following PT150 treatment.

Microglial reactivity was assessed through quantification of Iba-1^+ cells in combination with analysis of cellular morphology using immunofluorescence microscopy in the SN and ST of control, rotenone-exposed, and rotenone + 30 mg/kg PT150-treated animals (**Figure 32**). Representative images of Iba-1^+ immunostaining in the SN (**Figure 32A**, **F**, and **K**) and ST (**Figure 32B**, **G**, and **L**) are shown. An increase in the number of Iba-1^+ cells occurred in the SNpc in response to rotenone exposure, which was significantly reduced by oral treatment with PT150 (**Figure 32C**). Interestingly, no significant difference in the quantity of Iba-1^+ cells occurred in the SNpr or ST, regardless of experimental group (**Figure 32D** and **E**, respectively).

Imaris software was used to skeletonize microglial cells in the SN and ST to determine if there were morphological changes between control, rotenone-exposed, and 30 mg/kg PT150-treated groups. Skeletonized representations of cells for the SN (**Figure 32A**, **F**, and **K**) and ST (**Figure 32B**, **G**, and **L**) are shown for each brain region. Alterations in cellular process length and the number of process branches were quantified as a morphological indication of microglial reactivity. Cellular complexity was reduced in rotenone-exposed animals compared to vehicle controls in the SNpc (**Figure 32H** and **M**), SNpr (**Figure 32I** and **N**), and ST (**Figure 32J** and **O**). Treatment with PT150 significantly increased both length and branching of microglial processes in all three anatomical regions. These data show that treatment with PT150 decreased reactive morphological changes in microglia, but not the overall cell number.

5.3.4 PT150 treatment modulates rotenone-induced astrogliosis in the substantia nigra and the striatum.

Reactive astrogliosis was assessed by quantifying the number of astrocytes as well as their secretory and morphometric phenotype. Whole-brain scanning microscopy was used to quantify the number of S100β$^+$ cells and GFAP$^+$ area, as reactive astrocytes are proliferative and upregulate GFAP; representative images of control, rotenone-exposed, and rotenone-exposed animals treated with 30 mg/kg PT150 are shown for the SN (**Figure 33A**, **C**, and **E**) and ST (**Figure 33B**, **D**, and **F**). Interestingly, no significant difference in the number of S100β$^+$ cells is observed following rotenone exposure in any brain region (**Figure 33G**, **H**, and **I**). A trending decrease in the number of S100β$^+$ cells occurs in the SNpc and ST following treatment with PT150; no difference in S100β$^+$ cell number occurs in the SNpr. Similarly, there is no difference in GFAP$^+$ area observed between groups in the SNpc and ST, although PT150 treatment slightly increased GFAP$^+$ area compared to controls in the SNpr (**Figure 33J**, **K**, and **L**).

High-resolution fluorescence microscopy was also used to evaluate the phenotype of astrocytes by examining the cellular distribution of C3 in S100β$^+$ cell soma and GFAP$^+$ processes as an indication of inflammatory activation. The co-expression of C3 and either GFAP or S100β was quantitively analyzed in the SNpc, SNpr, and ST (**Figure 33**). Representative images of control, rotenone-exposed, and rotenone-exposed animals treated with 30 mg/kg PT150 are shown for the SN (**Figure 33A**, **C**, and **E**) and ST (**Figure**

33B, **D**, and **F**). Somal C3 in the SNpc was significantly increased in astrocytes following rotenone exposure, but decreased with PT150 treatment, whereas no significant difference between control and PT150-treated animals was observed (**Figure 33M**). C3 in astrocyte processes in PT150 treated animals was significantly increased compared to both control and rotenone-exposed animals in this same brain region (**Figure 33P**). In the SNpr, somal expression of C3 was significantly increased in PT150 treated animals compared to controls, but is not as high as the rotenone-exposed group (**Figure 33N**). Process C3 expression is upregulated following both rotenone exposure and PT150 treatment in this anatomical region (**Figure 33Q**). Interestingly, C3 expression in both the soma and processes is significantly higher in PT150 treated animals compared to the other groups in the ST (**Figure 33O** and **R**).

Morphological changes of the astrocytes, including process length, area, and branching, were analyzed using Imaris software; representative images of control (**Figure 34A** and **B**), rotenone-exposed (**Figure 34C** and **D**), and rotenone-exposed animals treated with 30 mg/kg PT150 (**Figure 34E** and **F**) are shown for the SN and ST, respectively. In the SNpc, no statistically significant difference in cell body size, determined by S100β$^+$ cell area, was observed between groups (**Figure 34G**). Exposure to rotenone resulted in astrocytes with decreased process branching (**Figure 34P**) and length (**Figure 34M**), but no change in process area (**Figure 34J**), compared to controls in this same brain region. PT150 treatment further decreased process branching (**Figure 34P**) and length (**Figure 34M**), but increased process area (**Figure 34J**) compared to vehicle controls in the SNpc. In the SNpr, significant cell body hypertrophy is demonstrated in animals exposed to rotenone. This morphologic response was increased in animals treated with PT150 compared to controls but was not different from rotenone-treated animals (**Figure 34H**). Rotenone-exposed animals contain astrocytes with morphology similar to controls, with no significant difference in process area (**Figure 34K**) or length (**Figure 34N**), but an increase in branching (**Figure 34Q**). PT150 treatment significantly increased process branching (**Figure 34Q**) and area (**Figure 34K**), but not length (**Figure 34N**). In the ST, no evidence of hypertrophic cell body changes were observed (**Figure 34I**), although both rotenone exposure and PT150 treatment resulted in process elongation (**Figure 34O**) and increased branching (**Figure 34R**) compared to controls. Altogether, these data establish that PT150

treatment modulated astrocyte reactivity towards a more activated morphological phenotype in a brain region-dependent manner.

5.3.5 PT150 treatment reduces accumulation of α-synuclein in neurons and alters glial trafficking of phosphorylated α-synuclein.

Accumulation of α-synuclein was determined by immunofluorescence staining for the aggregation-prone phospho-serine 129 form of the protein (p129 α-syn) in the SN (**Figure 35**). The extent of accumulation of misfolded protein in neurons was determined by analyzing the intensity of p129 α-syn in TH^+ neurons in the SNpc. Representative images of control, rotenone-exposed, and rotenone + 30 mg/kg PT150 treated animals are shown (**Figure 35**). Rotenone-exposed animals had an increase in intra-neuronal p129 α-syn compared to control animals (**Figure 35J**). Notably, p129 α-syn expression was reduced in DAn in the PT150 treated animals (**Figure 35J**).

To determine the role glia may play in removing or trafficking misfolded α-synuclein in the SN, p129 α-syn accumulation was also analyzed within $GFAP^+$ astrocytes and $Iba\text{-}1^+$ microglia. There is a significant increase in p129 α-syn within Iba-1 cells following rotenone exposure (**Figure 35K**). Animals treated with PT150 show more p129 α-syn within microglia compared to controls, but significantly less than the untreated, rotenone-exposed group (**Figure 35K**). While less p129 α-syn was detected in $GFAP^+$ cells in both the rotenone-exposed and PT150 treated groups (Supplemental Figure 2), ratiometric analysis of p129 α-syn expression to total synuclein shows that PT150 treatment drives removal of p129 α-syn in the SN compared to astrocytes in the rotenone-exposed group (**Figure 35L Supplemental Figure 4**).

5.4 DISCUSSION

With cases of PD projected to double over the next twenty years, it is imperative that therapeutic options be developed to improve the quality of life for those who are affected [584]. Current dopamine mimetics treat the motor symptoms of PD but are ineffective at slowing the progression of disease. Here, we report that post-lesioning treatment with the GR modulator, PT150, reduced loss of DAn in the SNpc

of C57Bl/6 mice in the rotenone model of PD. Compared to other models of PD, the rotenone model accurately recapitulates many of the key pathological hallmarks of PD, including inhibition of mitochondrial complex I [562]. In parallel to the neuropathological progression of clinical disease, rotenone neurotoxicity in murine models results in glial reactivity peaking at 2 weeks post exposure, followed by synucleinopathy and DAn loss in the nigrostriatal pathway by 4 weeks post exposure [563].

PT150 has been described as an allosteric modulator of GR, therefore, we postulated that therapeutic modulation of this receptor would be neuroprotective by reducing pro-inflammatory activity amongst microglia and astrocytes, as well as preventing the propagation of misfolded α-syn in neurons. In the present study, mice were exposed to daily intraperitoneal administration of rotenone or vehicle for 14 days, followed by treatment with vehicle, 30 mg/kg, or 100 mg/kg PT150 by oral gavage for 14 days (**Figure 30**). Mortality occurred in approximately 50% of the animals exposed to 100 mg/kg PT150, whereas 30 mg/kg was well-tolerated, as demonstrated by a mortality rate similar to the rotenone-exposed group (**Figure 30**). Oral treatment with PT150 immediately following daily rotenone exposure preserved the number of TH^+ neuronal cell bodies in the SN, although no protection of striatal axons was seen (**Figure 31**). Treatment with PT150 also decreased cytoplasmic inclusions of phosphorylated α-syn in DAn, likely caused by altered microglial and astrocytic responses in the nigrostriatal pathway. Although incompletely understood, it is likely that axonal degeneration occurs prior to complete loss of DAn cell bodies, and is the primary determinant of clinical disease [585, 586]. Therefore, because PT150 treatments began after treatment with rotenone, it is likely that the majority of degeneration of DAn axons had already occurred. Although decreased expression of TH is often correlated to neurodegeneration, transmitter-associated enzyme expression may be independent of neuronal survival following stress or neurotoxic injury [587]. Acute damage mediated by rotenone may result in fluctuations in enzymatic expression in terminals, and subsequently synaptic dysfunction, but TH immunostaining does not definitively indicate complete neuronal degeneration in the ST [588]. Although loss of cell bodies is irreversible, neurons within the CNS have, to a certain extent, the capacity to induce regrowth of axons and rescue function following injury.

Ultimately, PT150 treatment was neuroprotective, as it was effective at preventing the irreversible loss of DAn cell bodies in the SNpc following rotenone neurotoxicity.

Neuroinflammation is an early critical feature of PD, and DAn are especially vulnerable to the toxic effects of pro-inflammatory mediators. Therefore, inhibiting neuroinflammatory signaling has therapeutic potential [589, 590]. The ability of the GR to modulate key inflammatory pathways identified in PD, as well as the high quantities of the receptor identified on both DAn and glia in rodent models, suggests that targeting the GR is a promising avenue for treating PD. While largely anti-inflammatory effects of GR modulation have been described, it must be noted that GCs do not have solely immunosuppressive actions. GR agonism can sometimes increase pro-inflammatory responses in the brain, though these inflammatory actions have, thus far, been described primarily in the hippocampus [591]. The ubiquitous expression of GRs on parenchymal cells of the CNS also means there is the potential for undesired effects in some cell populations, such that therapeutics that solely act as GR agonists or antagonists may prove ineffective. This is demonstrated by other models of PD, such as 1-methyl-4-phenyl-1,2,3,6-tetrahydropyridine (MPTP) neurotoxicity, where inactivating astrocytic GRs exacerbated DAn loss [576, 591]. Because PT150 is thought to allosterically modulate GR by binding to the co-activator domain of the receptor and thereby inhibit transcription, it may function as a better inhibitor of neuroinflammation that compounds targeting the ligand binding pocket [580]. In support of this mechanism, we observed decreased number of reactive microglia in the SNpc in PT150-treated animals (**Figure 32**). A reduction in microgliosis was not observed in the ST of animals treated with PT150, as no change in cell quantity was observed, although the cells in this region had an anti-inflammatory or inactivated morphology (**Figure 32**). Reactive, or disease-associated, microglia (DAM's) are described as having an ameboid-like morphology, with decreased branch length and volume, as well as increased cell body size [592-594]. They readily produce reactive species and pro-inflammatory mediators, which, when prolonged, contributes to the progression of neuronal injury and the misfolding of native proteins into neurotoxic forms [486, 595]. Dystrophic microglia have been implicated in both clinical and laboratory models of disease, and sustained microgliosis has been identified in human PD patients [563, 596]. In the present study, the observed reduction in both the number

and reactivity of microglia in the SNpc in these studies indicates that PT150 treatment reduces pro-inflammatory microglial responses, but this occurs in a brain region-dependent manner. The suppressed microglial response following PT150 treatment in the SN may be beneficial, as experimental evidence from others demonstrates that reducing microgliosis can protect DAn [577].

Although glial reactivity is identified in numerous neurodegenerative diseases, the function of activated astrocytes cannot be grouped simply as neurotoxic or neuroprotective, but instead resides within a spectrum of molecular and cellular changes that dictate their function [597, 598]. Chronic or severe neuroinflammatory activation of astrocytes contributes to neuronal injury, but complete inhibition of glial activation can lead to pathogenic protein accumulation and the loss of critical homeostatic functions, like neurotransmitter regulation and cellular repair mechanisms. The extent of astrogliosis was evaluated through analysis of the quantity, morphology, and secretory phenotype of the astrocytes present in the SN and ST, including $C3^+$ immunolabeling in the cell body (S100β) and processes (GFAP) to identify reactive astrocytes. Morphological measures included cell body area, the number of branches per process, process length, and process area. Upon activation, astrocytes increase process complexity and volume, as well as elongate them, which allows these cells to facilitate cellular communication [599]. Activated cells upregulate production of complement in an effort to opsonize pathogens and recruit immune cells, but overactivation of the complement pathway can contribute to neuronal damage and overpruning of synapses [600]. In the present study, rotenone exposure induced activated morphology and robust production of C3 by astrocytes in the SN and ST (**Figure 33** and **34**). Unexpectedly, these cellular responses were augmented following PT150 treatment. An increase in C3 is identified in the cell bodies and processes of astrocytes in both the SN and ST following PT150 exposure (**Figure 33**). The astrocytes in these regions also increase process length and branching, and demonstrate cell body hypertrophy in a brain-region dependent manner (**Figure 34**).

This apparent increase in glial reactivity may have neuroprotective functions. More complex and longer processes on activated astrocytes allows for increased contact with nearby cells and vasculature, which permits them to stimulate cell-to-cell communication and blood-brain barrier tightness [599]. During

disease states, activated astrocytes secrete pro-inflammatory cytokines and other factors, such as glial derived neurotrophic factor (GDNF) and Gata3, that stimulate neurogenesis [601-605]. Some evidence postulates that astrocytes can also facilitate neuronal regeneration through their collagen-rich processes, which form scaffolds for the formation of neurites [606]. Furthermore, while neurotoxic effects of C3 have been described, it's role in disease is context-dependent, and therefore may be neuroprotective in some situations [488]. Complement is involved in cellular activation and recruitment, thereby increasing microglial responses like phagocytosis, which removes debris and prohibits the formation of misfolded protein aggregates [607]. Activated astrocytes have also been implicated in the removal of cellular debris in the ST, which can decrease microglia-mediated degeneration of DAn in the SN [608]. Models of Alzheimer's Disease show that C3 deficiency can increase amyloid burden and decrease neuronal viability, highlighting the neuroprotective function of this protein in the brain [609, 610]. It is possible that the astroglial reactivity documented in response to PT150 treatment stimulates neuroprotective mechanisms, enhancing the capacity of these cells to mitigate damage caused by microglial populations and produce factors that stimulate neuronal regeneration.

Another key pathological feature of PD is the aggregation of hyperphosphorylated α-syn in DAn cell bodies of the SNpc. This neurotoxic form of synuclein mediates synaptic disturbances, mitochondrial and lysosomal dysfunction, and persistent neuroinflammatory signaling; ultimately, this results in progressive neuronal death [611]. Neurons secrete soluble forms of α-syn, in an effort to reduce toxicity, that is then endocytosed by nearby cells. This process allows for cell-to-cell spread of the protein in a prion-like manner that results in insoluble aggregates throughout the brain [612-614]. Glia surrounding DAn phagocytose and degrade secreted α-syn, thereby clearing neurotoxic proteins from the brain. Following PT150 treatment, a reduction in the accumulation of phosphorylated α-syn is observed in DAn in the SN compared to rotenone-exposed, untreated animals (**Figure 35**). A decrease in α-syn within Iba-1$^+$ cells also occurs following treatment, suggesting that the microglia in the SN, which have an anti-inflammatory morphology, may reduce phagocytosis of α-syn (**Figure 35**). Interestingly, when evaluating the ratio of phosphorylated α-syn to total synuclein within astrocytes, an increase in observed (**Figure 35**,

Supplemental Figure 4). This suggests that the astrocytes in the SN, which show markers of having an activated phenotype, may be upregulating their capacity to phagocytose. Although the state of activation in which astrocytes enhance their phagocytic capacity is sometimes contradictory, such a mechanism has been established in reactive astrocytes identified in other laboratory models [228, 381]. This function allows astrocytes to efficiently remove fibrillar α-syn through lysosomal degradation, decreasing the accumulation of α-syn in neurons [615]. Although reducing glial responses may be neuroprotective, it can also perpetuate synucleinopathy. It is possible that through modulation of glia by PT150, astrocytes in the SN increase their capacity for neurotoxic α-syn removal, which promotes DAn survival in the SN.

The computational-based molecular docking studies indicated that PT150 prefers to bind to and interact with the co-activator site of the ligand binding domain of the glucocorticoid receptor rather than the steroid binding site (**Figure 36**). PT150 interacts favorably with the co-activator site, suggesting this as a site of allosteric modulation that could inhibit transcriptional activity without directly competing for binding with endogenous corticosteroid ligands. These molecular docking studies support that PT150 may well function as an allosteric modulator of these receptors, resulting in a mechanism of transcriptional control. From our modeling we demonstrate that PT150 has the potential to bind the co-activator peptide site, it is logical to assume that this site would be more accessible over the steroid binding site and that PT150 may have a higher binding affinity for this site due to a lower steric and conformationally restricted penalty for binding. Therefore, it is highly conceivable that PT150 can modulate both AR and GR signaling as an allosteric inhibitor by inducing a conformational change in the receptor upon binding the co-activator domain, leading to mediation of transcriptional activity.

Collectively, this study highlights the potential role of GR modulation as a method of interfering with the progression of PD neuropathology. We demonstrate that treatment with 30 mg/kg of the novel therapeutic PT150 following exposure to rotenone reduced microglial reactivity, modulated the astrocytic response, and interfered with the accumulation of hyperphosphorylated a-syn in DAn. Overall, PT150 reduced the loss of DAn cell bodies in the SN, although was not completely protective, as demonstrated by

evidence of axonal dysfunction in the ST. Altogether, these findings effectively illuminate neuroprotective mechanisms of targeting the GR to impede PD neuropathology.

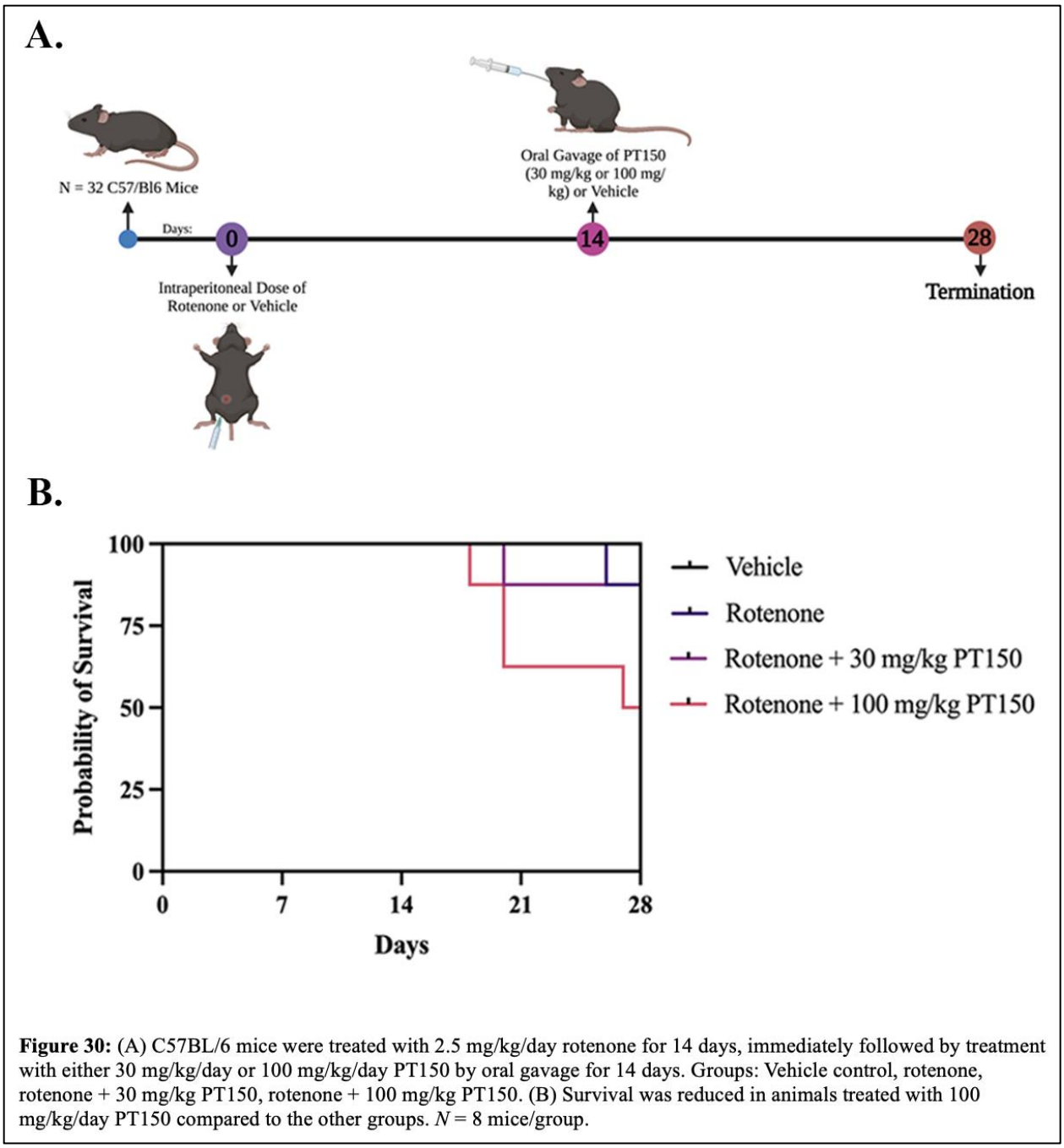

Figure 30: (A) C57BL/6 mice were treated with 2.5 mg/kg/day rotenone for 14 days, immediately followed by treatment with either 30 mg/kg/day or 100 mg/kg/day PT150 by oral gavage for 14 days. Groups: Vehicle control, rotenone, rotenone + 30 mg/kg PT150, rotenone + 100 mg/kg PT150. (B) Survival was reduced in animals treated with 100 mg/kg/day PT150 compared to the other groups. *N* = 8 mice/group.

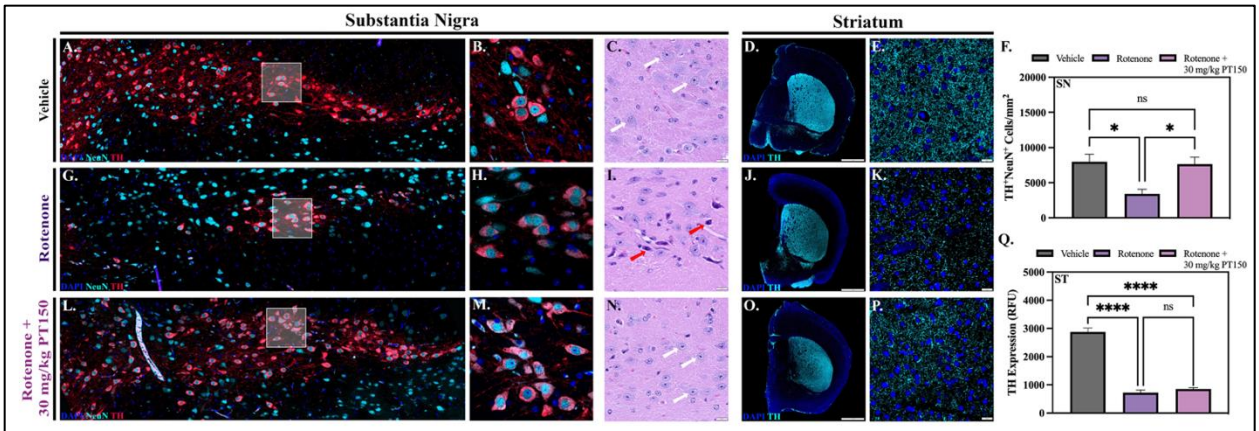

Figure 31: PT150 treatment reduces the loss of dopaminergic neurons in the SNpc. Representative images are shown for the substantia nigra (SN) and striatum (ST), with immunostaining for dopaminergic neurons (DAn) (TH, red) and total neurons (NeuN, cyan). (F) Dopaminergic neuron cell bodies were decreased in rotenone-exposed animals, which increased following PT150 treatment. (Q) Intensity measurements for TH^+ projecting fibers in the ST showed decreases in TH intensity in both rotenone-exposed and rotenone + 30 mg/kg PT150 groups. Parametric one-way ANOVA analysis performed. $N = 3 – 5$/group. *p < .05; ****p < .0001. Scale bar = 1 mm (montage) and 20 µm.

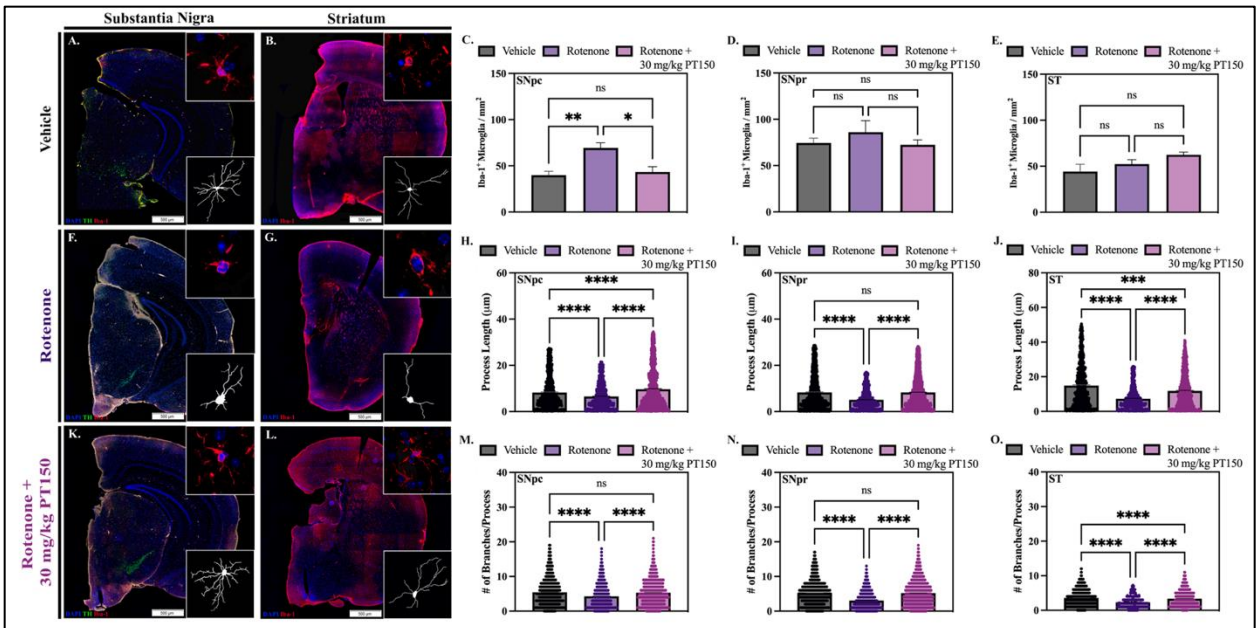

Figure 32: PT150 treatment reduced microgliosis in the SN and ST. Immunofluorescent labeling of microglia (Iba-1, red) and dopaminergic neurons (TH, green) was performed; representative montage and high-magnification images are shown for the SN (A, F, and K) and ST (B, G, and L). Cellular quantifications were performed in the SNpc (C), SNpr (D), and ST (E). Morphological analysis was performed using Imaris software for quantifications of process length (H – J) and the number of process branches (M – O); skeletonized renderings are shown for the SN (A, F, and K) and the ST (B, G, and L). Nonparametric one-way ANOVA with Dunn's correction analysis performed. (N = 3 – 5/group). ns = not significant; *p < .05; **p < .01; ***p < .001; ****p < .0001. Scale bar = 500 µm.

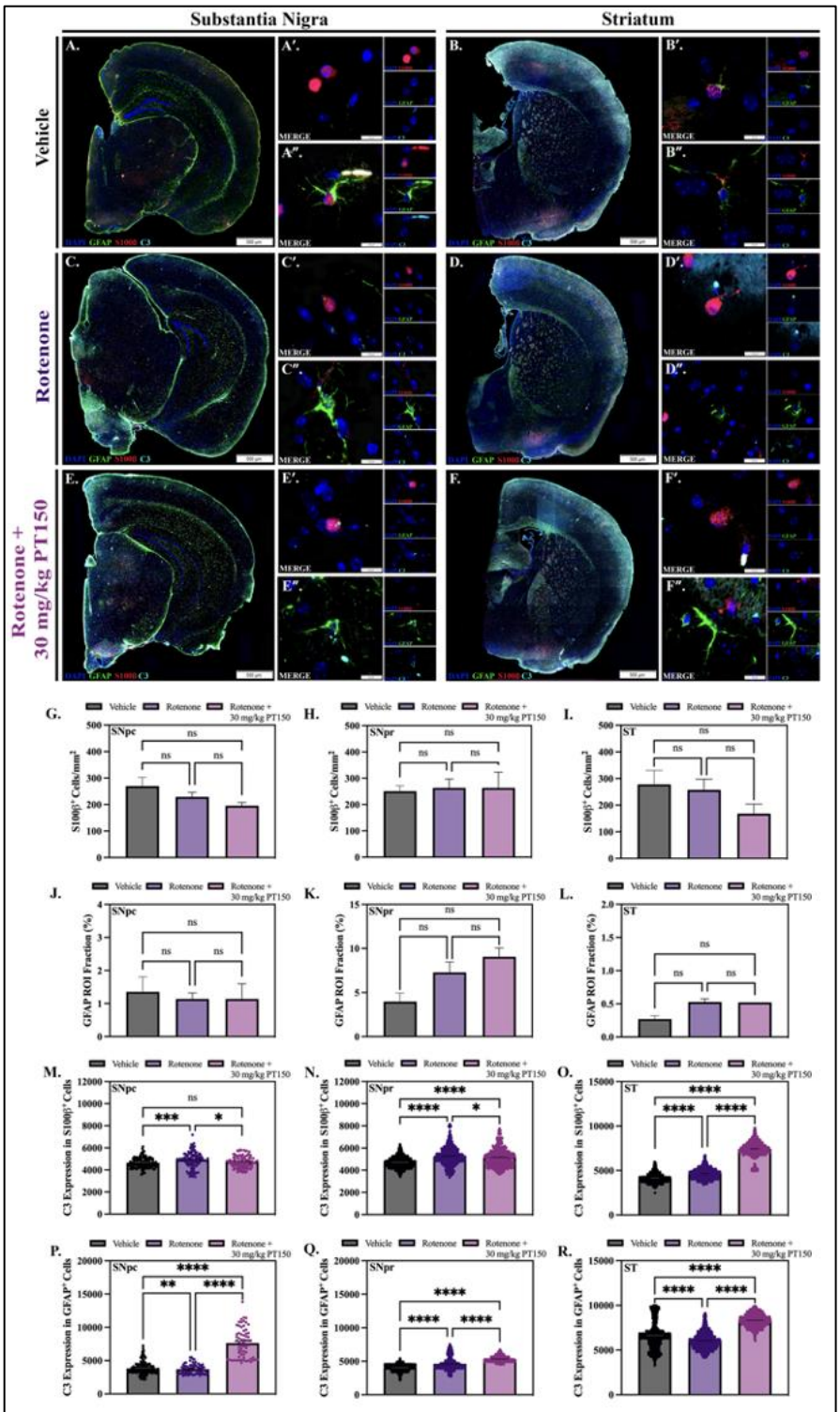

Figure 33: Astrocyte populations were modulated following PT150 treatment. Immunofluorescent labeling of astrocytes (GFAP, green; S100β, red; C3, cyan) was performed; representative montage and high-magnification images are shown for the SN (A, C, and E) and ST (B, D, and F). The quantity of S100β$^+$ cells is shown for the SNpc (G), SNpr (H), and ST (I). Immunostaining was quantified for the maximum expression of GFAP (% per regional area) in the SNpc (J), SNpr (K), and ST (L). Maximal C3 expression in S100β$^+$ soma and GFAP$^+$ processes was determined within the SNpc (M, P), SNpr (N, Q), and ST (O, R), respectively. Nonparametric one-way ANOVA with Dunn's correction analysis performed. ($N = 3 – 5$/group). ns = not significant; *p < .05; **p < .01; ***p < .001; ****p < .0001. Scale bar = 500 μm (montage) and 20 μm.

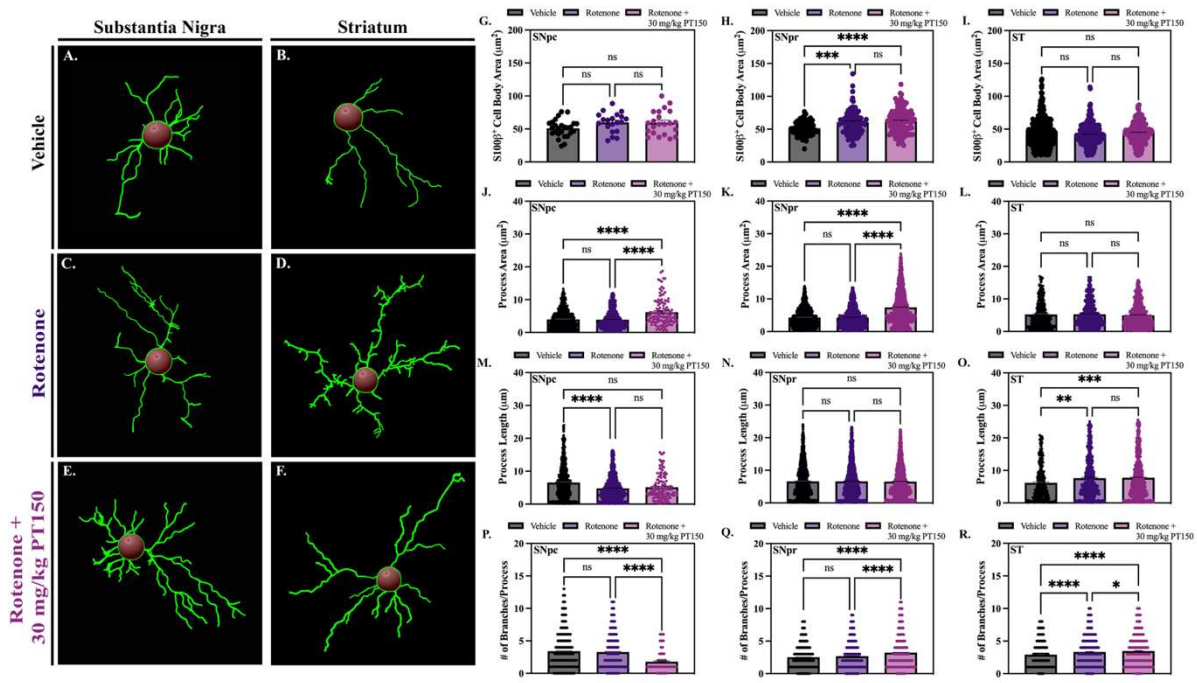

Figure 34: Astrocyte morphology was modulated following PT150 treatment. Morphological analysis was performed using CellSens for quantification of cell body area (G – I) and Imaris software for quantifications of process area (J – L), process length (M – O) and the number of process branches (P – R); skeletonized renderings are shown for the SN (A, C, and E) and the ST (B, D, and F). Nonparametric one-way ANOVA with Dunn's correction analysis performed. ($N = 3 – 5$/group). ns = not significant; *p < .05; **p < .01; ***p < .001; ****p < .0001.

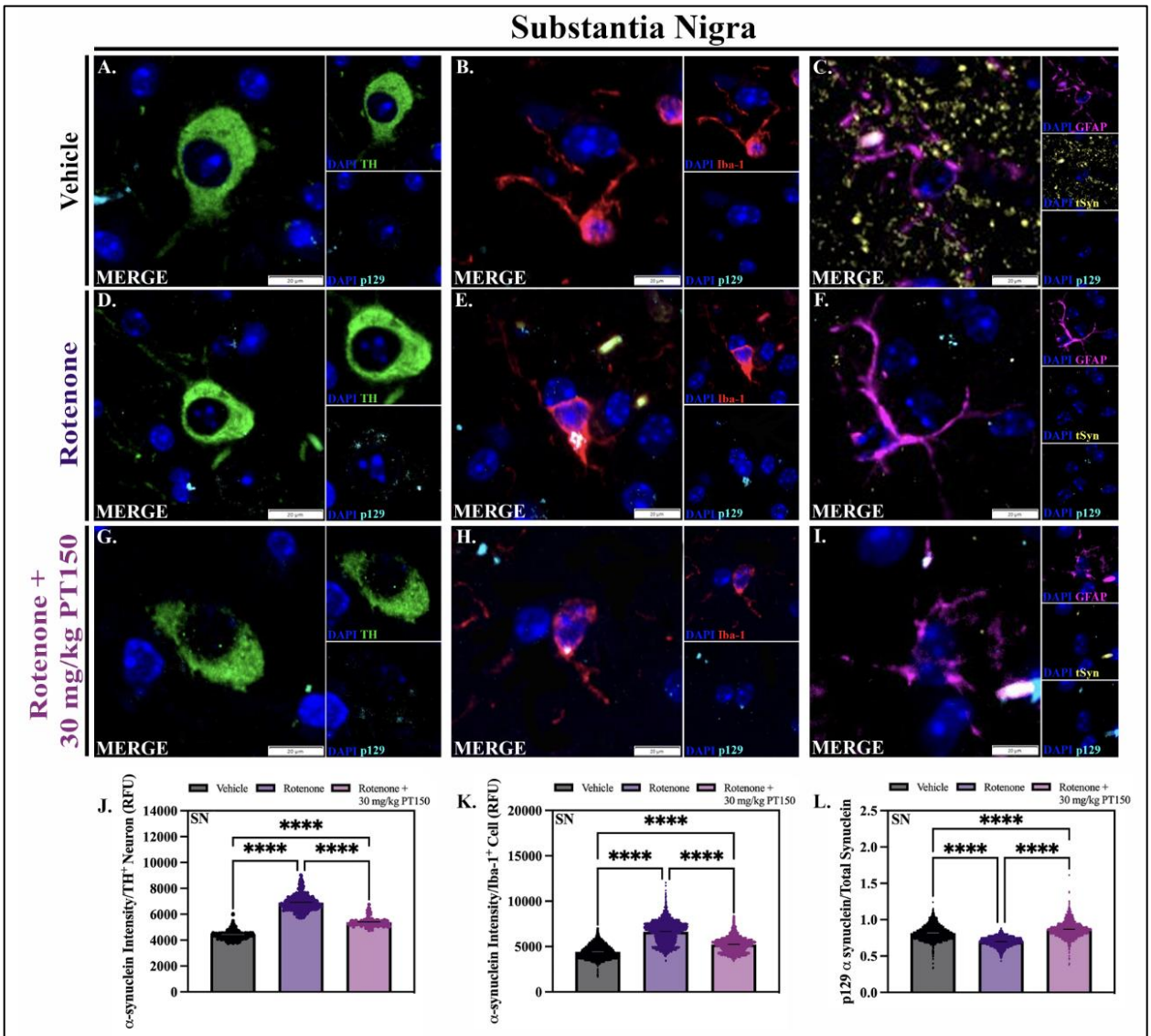

Figure 35: PT150 treatment reduced α-synuclein accumulation in dopaminergic neurons, but increased glial trafficking. Immunofluorescent labeling of α-synuclein phosphorylated at serine 129 (p129, cyan), dopaminergic neurons (TH, green), microglia (Iba-1, red), and astrocytes (GFAP, yellow) was performed; representative high-magnification images are shown for the SN. Maximal p129 expression within dopaminergic neurons (D), microglia (H), and astrocytes (L) was determined. Nonparametric one-way ANOVA with Dunn's correction analysis performed. ($N = 3 – 5$/group). ****$p < .0001$. Scale bar = 20 μm.

CHAPTER 6 – CONCLUSION

Neurodegenerative diseases affect millions of individuals worldwide and, despite over a century of research, our complete understanding of the mechanisms that contribute to disease and potential therapeutic interventions is lacking. Our knowledge of the genetic, age-related, and environmental factors that contribute to disease is limited, as the etiology of PD and AD is largely unknown. This is complicated by the fact that not every individual exposed to a neurotoxicant or experiencing normal aging is diagnosed with clinical disease, which indicates that disease is likely the result of the compounding effect of multiple factors in tandem with aging neuropathology. Additionally, numerous individuals without a known exposure to a neurotoxicant progress into disease, which suggests that other factors that are not yet identified contribute to susceptibility. The unknown interplay between peripheral infections and the brain, lack of a laboratory model to appropriately study aging neuropathology, and our incomplete understanding of how glial mechanisms drive disease are all research hurdles.

Although *Mycobacterium tuberculosis* (Mtb) has been associated with increased susceptibility to neurodegenerative disease, the cellular changes that facilitate clinical symptomology is incompletely understood. The data herein describes cognition deficits, glial changes, modulation of the blood-brain barrier (BBB), accumulation of misfolded proteins, and neuronal loss that altogether reveal a potential driver of neurodegenerative disease in human patients. Not only do these data highlight the neurological effects of a disease that affects millions globally every year, and disproportionately influences vulnerable populations, but it also highlights the impact peripheral infections may have on the brain, even without dissemination of infectious agents to the central nervous system.

The lack of evidence that Mtb has penetrated the brain suggests that neurotoxicity is not in direct response to the bacteria itself; subsequently, future studies should be performed to explore the neurotoxic mechanism(s). Hypotheses include the generation of microbial antigens, such as cell wall constituents or bacterial DNA, that are known to enter the circulation and may penetrate the brain as well as stimulation of peripheral nerves innervating the lung, both of which could elicit pro-inflammatory glial responses.

Furthermore, while the data herein feature neurological changes that occur in response to Mtb infection of peripheral tissues, it is unknown if these changes are augmented by persistent infection, nor if they can be reversed by standard antibiotic treatment. Along these lines, further study should be performed to determine if latent or subclinical TB disease, which is the primary clinical presentation of Mtb infection worldwide, elicit the same neurological changes.

Additionally, the lack of current laboratory models that accurately recapitulate aging neuropathology prevents successful scientific and clinical progress. Natural aging and neurodegenerative diseases substantially overlap in their neuropathological presentation, which implies that a better understanding of brain aging may also uncover important mechanisms that drive disease. Although numerous models of aging and neurodegeneration exist, they are typically transgenic murine models, which are not an accurate representation of neuropathological progression in most people who are diagnosed with disease or suffering from age-related deficiencies. Larger *in vivo* models, including companion animals and non-human primates, have been implicated as ideal models of disease, but are impractical in a laboratory setting. The Dunkin Hartley guinea pig may be a promising alternative, as this strain presents with not only age-related changes in peripheral systems, but also key neuropathologies which include glial changes, modulation of the BBB, misfolded protein accumulation, and neuronal loss. While valuable, data addressing mechanistic initiators of neuropathology and a more comprehensive evaluation of both neuronal dysfunction and protein misfolding will heighten these data. This includes exploring the how senescence-associated secretory cell phenotypes may contribute to neuroinflammation and cognitive dysfunction.

Finally, though glia have been routinely implicated in disease progression, their exact role is mysterious. Production of pro-inflammatory mediators and aberrant phagocytosis contribute to the degradation of neurons, but eliminating glia altogether is not neuroprotective. Using a novel drug termed PT150, which allosterically binds to the glucocorticoid receptor, we uncover neuroprotective mechanisms mediated by glia in models of neurodegenerative disease. Modulating microglia to reduce pro-inflammatory signaling, and astrocytes to stimulate removal of neurotoxic proteins from the brain,

prevents the degradation of dopaminergic neurons in the substantia nigra in a rotenone model of PD. In addition to obtaining critical information regarding neuroprotective roles of glia in disease, these data uncover the therapeutic potential of targeting the glucocorticoid receptor. Ultimately, such results establish that further comprehensive investigation should be performed to determine what aspects of glial activation drive disease, and methods of modulating these responses to preferentially dictate their function.

Altogether, the studies described herein provide substantial contributions to the field, describing potential etiologies of disease, proposing a laboratory model of aging, and identifying neuroprotective mechanisms by glia that altogether dramatically improve our current understanding. Further efforts should be made to more thoroughly investigate how peripheral infections, like respiratory infection with *Mycobacterium tuberculosis*, results in neurological deficits. The combination of infectious disease in the Dunkin Hartley aging model may also showcase how multiple environmental or physiological factors, which more closely mimic exposure throughout a person's lifetime, alter glia and exacerbate pathology compared to a single exposure.

REFERENCES

1. Zimmerman, M.R., *Pulmonary and osseous tuberculosis in an Egyptian mummy.* Bull N Y Acad Med, 1979. **55**(6): p. 604-8.
2. Cave, A.J.E. and A. Demonstrator, *The evidence for the incidence of tuberculosis in ancient Egypt.* The British journal of tuberculosis, 1939. **33**(3): p. 142-152.
3. Barberis, I., et al., *The history of tuberculosis: from the first historical records to the isolation of Koch's bacillus.* J Prev Med Hyg, 2017. **58**(1): p. E9-e12.
4. Sabbatani, S., *[Historical insights into tuberculosis. Girolamo Fracastoro's intuition on the transmission of tuberculosis and his opponents. History of an idea].* Infez Med, 2004. **12**(4): p. 284-91.
5. Shiloh, M.U., *Mechanisms of mycobacterial transmission: how does Mycobacterium tuberculosis enter and escape from the human host.* Future Microbiol, 2016. **11**(12): p. 1503-1506.
6. Organization, W.H., *The end TB strategy.* 16 August 2015.
7. *Global, regional, and national burden of tuberculosis, 1990-2016: results from the Global Burden of Diseases, Injuries, and Risk Factors 2016 Study.* Lancet Infect Dis, 2018. **18**(12): p. 1329-1349.
8. Organization, W.H., *Global tuberculosis report 2022*, W.H. Organization, Editor. 2022.
9. Houben, R.M. and P.J. Dodd, *The Global Burden of Latent Tuberculosis Infection: A Re-estimation Using Mathematical Modelling.* PLoS Med, 2016. **13**(10): p. e1002152.
10. Fennelly, K.P., et al., *Cough-generated aerosols of Mycobacterium tuberculosis: a new method to study infectiousness.* Am J Respir Crit Care Med, 2004. **169**(5): p. 604-9.
11. Roy, C.J. and D.K. Milton, *Airborne transmission of communicable infection--the elusive pathway.* N Engl J Med, 2004. **350**(17): p. 1710-2.
12. Riley, R.L., et al., *Aerial dissemination of pulmonary tuberculosis. A two-year study of contagion in a tuberculosis ward. 1959.* Am J Epidemiol, 1995. **142**(1): p. 3-14.
13. Wells, W.F., H.L. Ratcliffe, and C. Grumb, *On the mechanics of droplet nuclei infection; quantitative experimental air-borne tuberculosis in rabbits.* Am J Hyg, 1948. **47**(1): p. 11-28.
14. Zelner, J.L., et al., *Age-specific risks of tuberculosis infection from household and community exposures and opportunities for interventions in a high-burden setting.* Am J Epidemiol, 2014. **180**(8): p. 853-61.
15. Acuña-Villaorduña, C., et al., *Host Determinants of Infectiousness in Smear-Positive Patients With Pulmonary Tuberculosis.* Open Forum Infect Dis, 2019. **6**(6): p. ofz184.
16. Fennelly, K.P., et al., *Variability of infectious aerosols produced during coughing by patients with pulmonary tuberculosis.* Am J Respir Crit Care Med, 2012. **186**(5): p. 450-7.
17. Pienaar, E., et al., *A model of tuberculosis transmission and intervention strategies in an urban residential area.* Comput Biol Chem, 2010. **34**(2): p. 86-96.
18. Mathema, B., et al., *Drivers of Tuberculosis Transmission.* The Journal of Infectious Diseases, 2017. **216**(suppl_6): p. S644-S653.
19. Singh, A.K. and U.D. Gupta, *Animal models of tuberculosis: Lesson learnt.* Indian J Med Res, 2018. **147**(5): p. 456-463.
20. Furin, J., H. Cox, and M. Pai, *Tuberculosis.* Lancet, 2019. **393**(10181): p. 1642-1656.
21. Huddart, S., E. MacLean, and M. Pai, *Location, location, location: tuberculosis services in highest burden countries.* The Lancet Global Health, 2016. **4**(12): p. e907-e908.
22. Abdulgader, S.M., et al., *Diagnosing Tuberculosis: What Do New Technologies Allow Us to (Not) Do?* Respiration, 2022. **101**(9): p. 797-813.
23. Nathavitharana, R.R., et al., *Guidance for Studies Evaluating the Accuracy of Tuberculosis Triage Tests.* The Journal of Infectious Diseases, 2019. **220**(Supplement_3): p. S116-S125.

24. Cazabon, D., et al., *Quality of tuberculosis care in high burden countries: the urgent need to address gaps in the care cascade.* Int J Infect Dis, 2017. **56**: p. 111-116.
25. Steingart, K.R., et al., *Xpert® MTB/RIF assay for pulmonary tuberculosis and rifampicin resistance in adults.* Cochrane Database Syst Rev, 2014. **2014**(1): p. Cd009593.
26. Andrews, J.R., et al., *Risk of Progression to Active Tuberculosis Following Reinfection With Mycobacterium tuberculosis.* Clinical Infectious Diseases, 2012. **54**(6): p. 784-791.
27. Drain Paul, K., et al., *Incipient and Subclinical Tuberculosis: a Clinical Review of Early Stages and Progression of Infection.* Clinical Microbiology Reviews, 2018. **31**(4): p. 10.1128/cmr.00021-18.
28. Giovanni Battista, M., et al., *The definition of tuberculosis infection based on the spectrum of tuberculosis disease.* Breathe, 2021. **17**(3): p. 210079.
29. Onozaki, I., et al., *National tuberculosis prevalence surveys in Asia, 1990-2012: an overview of results and lessons learned.* Trop Med Int Health, 2015. **20**(9): p. 1128-1145.
30. Hopewell, P.C. and R.M. Jasmer, *Overview of Clinical Tuberculosis*, in *Tuberculosis and the Tubercle Bacillus*. 2004. p. 13-31.
31. Zhai, W., et al., *The Immune Escape Mechanisms of Mycobacterium Tuberculosis.* Int J Mol Sci, 2019. **20**(2).
32. Divangahi, M., et al., *Mycobacterium tuberculosis evades macrophage defenses by inhibiting plasma membrane repair.* Nature Immunology, 2009. **10**(8): p. 899-906.
33. Srinivasan, L., S. Ahlbrand, and V. Briken, *Interaction of Mycobacterium tuberculosis with host cell death pathways.* Cold Spring Harb Perspect Med, 2014. **4**(8).
34. Zhang, Q. and I. Sugawara, *Immunology of tuberculosis.* World J Exp Med, 2012. **2**(4): p. 70-4.
35. Lavin, Y., et al., *Tissue-Resident Macrophage Enhancer Landscapes Are Shaped by the Local Microenvironment.* Cell, 2014. **159**(6): p. 1312-1326.
36. Sertl, K., et al., *Dendritic cells with antigen-presenting capability reside in airway epithelium, lung parenchyma, and visceral pleura.* J Exp Med, 1986. **163**(2): p. 436-51.
37. Martineau, A.R., et al., *Neutrophil-mediated innate immune resistance to mycobacteria.* J Clin Invest, 2007. **117**(7): p. 1988-94.
38. Borkute, R.R., et al., *Neutrophils in Tuberculosis: Cell Biology, Cellular Networking and Multitasking in Host Defense.* Int J Mol Sci, 2021. **22**(9).
39. Dallenga, T., et al., *Targeting neutrophils for host-directed therapy to treat tuberculosis.* International Journal of Medical Microbiology, 2018. **308**(1): p. 142-147.
40. Hilda, J.N., et al., *Role of neutrophils in tuberculosis: A bird's eye view.* Innate Immun, 2020. **26**(4): p. 240-247.
41. Cavalcante-Silva, L.H.A., et al., *Mycobacterium tuberculosis in a Trap: The Role of Neutrophil Extracellular Traps in Tuberculosis.* Int J Mol Sci, 2023. **24**(14).
42. Kroon, E.E., et al., *Neutrophils: Innate Effectors of TB Resistance?* Frontiers in Immunology, 2018. **9**.
43. Orme, I.M., R.T. Robinson, and A.M. Cooper, *The balance between protective and pathogenic immune responses in the TB-infected lung.* Nature Immunology, 2015. **16**(1): p. 57-63.
44. Allen, M., et al., *Mechanisms of Control of Mycobacterium tuberculosis by NK Cells: Role of Glutathione.* Front Immunol, 2015. **6**: p. 508.
45. Chen, Z.W., *Multifunctional immune responses of HMBPP-specific Vγ2Vδ2 T cells in M. tuberculosis and other infections.* Cell Mol Immunol, 2013. **10**(1): p. 58-64.
46. Robertson, K.R., et al., *Human Immunodeficiency Virus Type 1 and Tuberculosis Coinfection in Multinational, Resource-limited Settings: Increased Neurological Dysfunction.* Clinical Infectious Diseases, 2018. **68**(10): p. 1739-1746.
47. Caruso, A.M., et al., *Mice deficient in CD4 T cells have only transiently diminished levels of IFN-gamma, yet succumb to tuberculosis.* J Immunol, 1999. **162**(9): p. 5407-16.
48. Urdahl, K.B., S. Shafiani, and J.D. Ernst, *Initiation and regulation of T-cell responses in tuberculosis.* Mucosal Immunology, 2011. **4**(3): p. 288-293.

49. Chackerian, A.A., et al., *Dissemination of Mycobacterium tuberculosis Is Influenced by Host Factors and Precedes the Initiation of T-Cell Immunity.* Infection and Immunity, 2002. **70**(8): p. 4501-4509.
50. Samstein, M., et al., *Essential yet limited role for CCR2+ inflammatory monocytes during Mycobacterium tuberculosis-specific T cell priming.* eLife, 2013. **2**: p. e01086.
51. Jasenosky, L.D., et al., *T cells and adaptive immunity to Mycobacterium tuberculosis in humans.* Immunological Reviews, 2015. **264**(1): p. 74-87.
52. Flynn, J.L., et al., *An essential role for interferon gamma in resistance to Mycobacterium tuberculosis infection.* J Exp Med, 1993. **178**(6): p. 2249-54.
53. Herbst, S., U.E. Schaible, and B.E. Schneider, *Interferon Gamma Activated Macrophages Kill Mycobacteria by Nitric Oxide Induced Apoptosis.* PLOS ONE, 2011. **6**(5): p. e19105.
54. Musvosvi, M., et al., *T cell receptor repertoires associated with control and disease progression following Mycobacterium tuberculosis infection.* Nature Medicine, 2023. **29**(1): p. 258-269.
55. Liu, X., et al., *IL-2 Restores T-Cell Dysfunction Induced by Persistent Mycobacterium tuberculosis Antigen Stimulation.* Frontiers in Immunology, 2019. **10**.
56. Lin, P.L., et al., *Sterilization of granulomas is common in active and latent tuberculosis despite within-host variability in bacterial killing.* Nature Medicine, 2014. **20**(1): p. 75-79.
57. Ramakrishnan, L., *Revisiting the role of the granuloma in tuberculosis.* Nature Reviews Immunology, 2012. **12**(5): p. 352-366.
58. McCaffrey, E.F., et al., *The immunoregulatory landscape of human tuberculosis granulomas.* Nature Immunology, 2022. **23**(2): p. 318-329.
59. Silva Miranda, M., et al., *The tuberculous granuloma: an unsuccessful host defence mechanism providing a safety shelter for the bacteria?* Clin Dev Immunol, 2012. **2012**: p. 139127.
60. Helming, L. and S. Gordon, *The molecular basis of macrophage fusion.* Immunobiology, 2008. **212**(9): p. 785-793.
61. Guerrini, V., et al., *Storage lipid studies in tuberculosis reveal that foam cell biogenesis is disease-specific.* PLOS Pathogens, 2018. **14**(8): p. e1007223.
62. Cronan, Mark R., et al., *Macrophage Epithelial Reprogramming Underlies Mycobacterial Granuloma Formation and Promotes Infection.* Immunity, 2016. **45**(4): p. 861-876.
63. Millar, J.A., et al., *Spatial Organization and Recruitment of Non-Specific T Cells May Limit T Cell-Macrophage Interactions Within Mycobacterium tuberculosis Granulomas.* Frontiers in Immunology, 2021. **11**.
64. Co, D.O., et al., *T Cell Interactions in Mycobacterial Granulomas: Non-Specific T Cells Regulate Mycobacteria-Specific T Cells in Granulomatous Lesions.* Cells, 2021. **10**(12).
65. Cronan, M.R., *In the Thick of It: Formation of the Tuberculous Granuloma and Its Effects on Host and Therapeutic Responses.* Frontiers in Immunology, 2022. **13**.
66. Cadena, A.M., S.M. Fortune, and J.L. Flynn, *Heterogeneity in tuberculosis.* Nature Reviews Immunology, 2017. **17**(11): p. 691-702.
67. Volkman, H.E., et al., *Tuberculous Granuloma Induction via Interaction of a Bacterial Secreted Protein with Host Epithelium.* Science, 2010. **327**(5964): p. 466-469.
68. Volkman, H.E., et al., *Tuberculous Granuloma Formation Is Enhanced by a Mycobacterium Virulence Determinant.* PLOS Biology, 2004. **2**(11): p. e367.
69. Davis, J.M. and L. Ramakrishnan, *The Role of the Granuloma in Expansion and Dissemination of Early Tuberculous Infection.* Cell, 2009. **136**(1): p. 37-49.
70. Schreiber, H.A. and M. Sandor, *The role of dendritic cells in mycobacterium-induced granulomas.* Immunol Lett, 2010. **130**(1-2): p. 26-31.
71. Slavin, R.E., T.J. Walsh, and A.D. Pollack, *Late generalized tuberculosis: a clinical pathologic analysis and comparison of 100 cases in the preantibiotic and antibiotic eras.* Medicine (Baltimore), 1980. **59**(5): p. 352-66.
72. Rock, R.B., et al., *Central nervous system tuberculosis: pathogenesis and clinical aspects.* Clin Microbiol Rev, 2008. **21**(2): p. 243-61, table of contents.

73. Zaharie, S.-D., et al., *The immunological architecture of granulomatous inflammation in central nervous system tuberculosis.* Tuberculosis, 2020. **125**: p. 102016.
74. Saukkonen, K., et al., *The role of cytokines in the generation of inflammation and tissue damage in experimental gram-positive meningitis.* J Exp Med, 1990. **171**(2): p. 439-48.
75. *WHO Guidelines Approved by the Guidelines Review Committee*, in *Treatment of Tuberculosis: Guidelines*. 2010, World Health Organization
Copyright © 2010, World Health Organization.: Geneva.
76. *Consensus Recommendations for the Postmortem Diagnosis of Alzheimer's Disease.* Neurobiology of Aging, 1997. **18**(4, Supplement 1): p. S1-S2.
77. Nelson, P.T., et al., *Alzheimer's disease is not "brain aging": neuropathological, genetic, and epidemiological human studies.* Acta Neuropathologica, 2011. **121**(5): p. 571-587.
78. Hippius, H. and G. Neundörfer, *The discovery of Alzheimer's disease.* Dialogues in Clinical Neuroscience, 2003. **5**(1): p. 101-108.
79. Nichols, E., et al., *Estimation of the global prevalence of dementia in 2019 and forecasted prevalence in 2050: an analysis for the Global Burden of Disease Study 2019.* The Lancet Public Health, 2022. **7**(2): p. e105-e125.
80. López, O.L. and S.T. DeKosky, *Clinical symptoms in Alzheimer's disease*, in *Handbook of Clinical Neurology*. 2008, Elsevier. p. 207-216.
81. Becker, J.T., O.L. Lopez, and J. Wess, *Material-specific memory loss in probable Alzheimer's disease.* Journal of Neurology, Neurosurgery & Psychiatry, 1992. **55**(12): p. 1177.
82. Vermunt, L., et al., *Duration of preclinical, prodromal, and dementia stages of Alzheimer's disease in relation to age, sex, and APOE genotype.* Alzheimers Dement, 2019. **15**(7): p. 888-898.
83. Scharre, D.W. *Preclinical , Prodromal , and Dementia Stages of Alzheimer ' s Disease*. 2019.
84. DeTure, M.A. and D.W. Dickson, *The neuropathological diagnosis of Alzheimer's disease.* Molecular Neurodegeneration, 2019. **14**(1): p. 32.
85. Braak, H. and E. Braak, *Evolution of neuronal changes in the course of Alzheimer's disease.* J Neural Transm Suppl, 1998. **53**: p. 127-40.
86. Srivastava, S., R. Ahmad, and S.K. Khare, *Alzheimer's disease and its treatment by different approaches: A review.* European Journal of Medicinal Chemistry, 2021. **216**: p. 113320.
87. McKhann, G., et al., *Clinical diagnosis of Alzheimer's disease.* Neurology, 1984. **34**(7): p. 939-939.
88. Storandt, M., *Cognitive Deficits in the Early Stages of Alzheimer's Disease.* Current Directions in Psychological Science, 2008. **17**(3): p. 198-202.
89. Zvěřová, M., *Clinical aspects of Alzheimer's disease.* Clin Biochem, 2019. **72**: p. 3-6.
90. Bellenguez, C., et al., *New insights into the genetic etiology of Alzheimer's disease and related dementias.* Nature Genetics, 2022. **54**(4): p. 412-436.
91. Naj, A.C., G.D. Schellenberg, and C. for the Alzheimer's Disease Genetics, *Genomic variants, genes, and pathways of Alzheimer's disease: An overview.* American Journal of Medical Genetics Part B: Neuropsychiatric Genetics, 2017. **174**(1): p. 5-26.
92. Kelleher, R.J., 3rd and J. Shen, *Presenilin-1 mutations and Alzheimer's disease.* Proc Natl Acad Sci U S A, 2017. **114**(4): p. 629-631.
93. Liu, C.C., et al., *Apolipoprotein E and Alzheimer disease: risk, mechanisms and therapy.* Nat Rev Neurol, 2013. **9**(2): p. 106-18.
94. Itzhaki, R.F., et al., *Microbes and Alzheimer's Disease.* J Alzheimers Dis, 2016. **51**(4): p. 979-84.
95. Vigasova, D., et al., *Multi-pathogen infections and Alzheimer's disease.* Microbial Cell Factories, 2021. **20**(1): p. 25.
96. Jeffery-Smith, A. and A. Riddell, *Herpesviruses.* Medicine, 2021. **49**(12): p. 780-784.
97. Bradshaw, M.J. and A. Venkatesan, *Herpes Simplex Virus-1 Encephalitis in Adults: Pathophysiology, Diagnosis, and Management.* Neurotherapeutics, 2016. **13**(3): p. 493-508.

98. Wang, E., et al., *Persistent inflammation and neuronal loss in the mouse brain induced by a modified form of attenuated herpes simplex virus type I.* Virologica Sinica, 2023. **38**(1): p. 108-118.
99. Joe, E. and J.M. Ringman, *Cognitive symptoms of Alzheimer's disease: clinical management and prevention.* Bmj, 2019. **367**: p. l6217.
100. Manyam, B.V., *Paralysis agitans and levodopa in "Ayurveda": Ancient Indian medical treatise.* Movement Disorders, 1990. **5**(1): p. 47-48.
101. Zhang, Z.X., Z.H. Dong, and G.C. Román, *Early descriptions of Parkinson disease in ancient China.* Arch Neurol, 2006. **63**(5): p. 782-4.
102. Parkinson, J., *An Essay on the Shaking Palsy.* The Journal of Neuropsychiatry and Clinical Neurosciences, 2002. **14**(2): p. 223-236.
103. Li, S. and W. Le, *Milestones of Parkinson's Disease Research: 200 Years of History and Beyond.* Neuroscience Bulletin, 2017. **33**(5): p. 598-602.
104. Deng, H., P. Wang, and J. Jankovic, *The genetics of Parkinson disease.* Ageing Res Rev, 2018. **42**: p. 72-85.
105. Billingsley, K.J., et al., *Genetic risk factors in Parkinson's disease.* Cell Tissue Res, 2018. **373**(1): p. 9-20.
106. James, S.L., et al., *Global, regional, and national incidence, prevalence, and years lived with disability for 354 diseases and injuries for 195 countries and territories, 1990–2017: a systematic analysis for the Global Burden of Disease Study 2017.* The Lancet, 2018. **392**(10159): p. 1789-1858.
107. Muangpaisan, W., et al., *A systematic review of the worldwide prevalence and incidence of Parkinson's disease.* Journal of the Medical Association of Thailand, 2011. **94**(6): p. 749.
108. Dorsey, E.R., et al., *Projected number of people with Parkinson disease in the most populous nations, 2005 through 2030.* Neurology, 2007. **68**(5): p. 384-386.
109. Dexter, D.T. and P. Jenner, *Parkinson disease: from pathology to molecular disease mechanisms.* Free Radic Biol Med, 2013. **62**: p. 132-144.
110. Cerri, S., L. Mus, and F. Blandini, *Parkinson's Disease in Women and Men: What's the Difference?* J Parkinsons Dis, 2019. **9**(3): p. 501-515.
111. Tolosa, E., et al., *Challenges in the diagnosis of Parkinson's disease.* The Lancet Neurology, 2021. **20**(5): p. 385-397.
112. Mahlknecht, P., K. Seppi, and W. Poewe, *The Concept of Prodromal Parkinson's Disease.* Journal of Parkinson's Disease, 2015. **5**: p. 681-697.
113. Berg, D., et al., *Prodromal Parkinson disease subtypes — key to understanding heterogeneity.* Nature Reviews Neurology, 2021. **17**(6): p. 349-361.
114. Kouli, A., K.M. Torsney, and W.L. Kuan, *Parkinson's Disease: Etiology, Neuropathology, and Pathogenesis*, in *Parkinson's Disease: Pathogenesis and Clinical Aspects*, T.B. Stoker and J.C. Greenland, Editors. 2018, Codon Publications
Copyright: The Authors.: Brisbane (AU).
115. Roos, D.S., et al., *Prevalence of Prodromal Symptoms of Parkinson's Disease in the Late Middle-Aged Population.* J Parkinsons Dis, 2022. **12**(3): p. 967-974.
116. Postuma, R.B., et al., *MDS clinical diagnostic criteria for Parkinson's disease.* Movement Disorders, 2015. **30**(12): p. 1591-1601.
117. Jankovic, J., *Parkinson's disease: clinical features and diagnosis.* Journal of Neurology, Neurosurgery & Psychiatry, 2008. **79**(4): p. 368.
118. Miller-Patterson, C., et al., *Motor asymmetry over time in Parkinson's disease.* J Neurol Sci, 2018. **393**: p. 14-17.
119. Cheng, H.C., C.M. Ulane, and R.E. Burke, *Clinical progression in Parkinson disease and the neurobiology of axons.* Ann Neurol, 2010. **67**(6): p. 715-25.
120. Fearnley, J.M. and A.J. Lees, *AGEING AND PARKINSON'S DISEASE: SUBSTANTIA NIGRA REGIONAL SELECTIVITY.* Brain, 1991. **114**(5): p. 2283-2301.

121. Giguère, N., S. Burke Nanni, and L.-E. Trudeau, *On Cell Loss and Selective Vulnerability of Neuronal Populations in Parkinson's Disease.* Frontiers in Neurology, 2018. **9**.
122. Braak, H., et al., *Staging of brain pathology related to sporadic Parkinson's disease.* Neurobiology of Aging, 2003. **24**(2): p. 197-211.
123. Li, T. and W. Le, *Biomarkers for Parkinson's Disease: How Good Are They?* Neuroscience Bulletin, 2020. **36**(2): p. 183-194.
124. Calne, D.B., B.J. Snow, and C. Lee, *Criteria for diagnosing Parkinson's disease.* Annals of Neurology, 1992. **32**(S1): p. S125-S127.
125. Massano, J. and K.P. Bhatia, *Clinical approach to Parkinson's disease: features, diagnosis, and principles of management.* Cold Spring Harb Perspect Med, 2012. **2**(6): p. a008870.
126. Gelb, D.J., E. Oliver, and S. Gilman, *Diagnostic criteria for Parkinson disease.* Arch Neurol, 1999. **56**(1): p. 33-9.
127. Rajput, A.H. and A. Rajput, *Accuracy of Parkinson disease diagnosis unchanged in 2 decades.* Neurology, 2014. **83**(5): p. 386-7.
128. Hughes, A.J., et al., *The accuracy of diagnosis of parkinsonian syndromes in a specialist movement disorder service.* Brain, 2002. **125**(Pt 4): p. 861-70.
129. Gomperts, S.N., *Lewy Body Dementias: Dementia With Lewy Bodies and Parkinson Disease Dementia.* Continuum (Minneap Minn), 2016. **22**(2 Dementia): p. 435-63.
130. Jellinger, K.A. and A.D. Korczyn, *Are dementia with Lewy bodies and Parkinson's disease dementia the same disease?* BMC Med, 2018. **16**(1): p. 34.
131. Klein, C. and A. Westenberger, *Genetics of Parkinson's disease.* Cold Spring Harb Perspect Med, 2012. **2**(1): p. a008888.
132. Bertoncini, C.W., et al., *Familial mutants of alpha-synuclein with increased neurotoxicity have a destabilized conformation.* J Biol Chem, 2005. **280**(35): p. 30649-52.
133. Dawson, T.M. and V.L. Dawson, *The role of parkin in familial and sporadic Parkinson's disease.* Mov Disord, 2010. **25 Suppl 1**(0 1): p. S32-9.
134. Vizziello, M., et al., *Disruption of Mitochondrial Homeostasis: The Role of PINK1 in Parkinson's Disease.* Cells, 2021. **10**(11).
135. Repici, M. and F. Giorgini, *DJ-1 in Parkinson's Disease: Clinical Insights and Therapeutic Perspectives.* J Clin Med, 2019. **8**(9).
136. Yang, X. and Y. Xu, *Mutations in the ATP13A2 gene and Parkinsonism: a preliminary review.* Biomed Res Int, 2014. **2014**: p. 371256.
137. Verstraeten, A., J. Theuns, and C. Van Broeckhoven, *Progress in unraveling the genetic etiology of Parkinson disease in a genomic era.* Trends in Genetics, 2015. **31**(3): p. 140-149.
138. Brown, T.P., et al., *Pesticides and Parkinson's disease--is there a link?* Environ Health Perspect, 2006. **114**(2): p. 156-64.
139. Di Monte, D., et al., *Comparative studies on the mechanisms of paraquat and 1-methyl-4-phenylpyridine (MPP+) cytotoxicity.* Biochem Biophys Res Commun, 1986. **137**(1): p. 303-9.
140. Elbaz, A., et al., *Professional exposure to pesticides and Parkinson disease.* Annals of Neurology, 2009. **66**(4): p. 494-504.
141. Lawana, V. and J.R. Cannon, *Chapter Five - Rotenone neurotoxicity: Relevance to Parkinson's disease*, in *Advances in Neurotoxicology*, M. Aschner and L.G. Costa, Editors. 2020, Academic Press. p. 209-254.
142. Henchcliffe, C. and M.F. Beal, *Mitochondrial biology and oxidative stress in Parkinson disease pathogenesis.* Nat Clin Pract Neurol, 2008. **4**(11): p. 600-9.
143. Betarbet, R., et al., *Chronic systemic pesticide exposure reproduces features of Parkinson's disease.* Nat Neurosci, 2000. **3**(12): p. 1301-6.
144. Betarbet, R., et al., *Mechanistic Approaches to Parkinson's Disease Pathogenesis.* Brain Pathology, 2002. **12**(4): p. 499-510.

145. Meng, L., L. Shen, and H.-F. Ji, *Impact of infection on risk of Parkinson's disease: a quantitative assessment of case-control and cohort studies.* Journal of NeuroVirology, 2019. **25**(2): p. 221-228.
146. Henry, J., et al., *Parkinsonism and neurological manifestations of influenza throughout the 20th and 21st centuries.* Parkinsonism Relat Disord, 2010. **16**(9): p. 566-71.
147. Leta, V., et al., *Viruses, parkinsonism and Parkinson's disease: the past, present and future.* J Neural Transm (Vienna), 2022. **129**(9): p. 1119-1132.
148. Caggiu, E., et al., *Humoral cross reactivity between α-synuclein and herpes simplex-1 epitope in Parkinson's disease, a triggering role in the disease?* Journal of Neuroimmunology, 2016. **291**: p. 110-114.
149. Woulfe, J., et al., *Monoclonal antibodies against Epstein-Barr virus cross-react with alpha-synuclein in human brain.* Neurology, 2000. **55**(9): p. 1398-401.
150. Bantle, C.M., et al., *Infection with mosquito-borne alphavirus induces selective loss of dopaminergic neurons, neuroinflammation and widespread protein aggregation.* npj Parkinson's Disease, 2019. **5**(1): p. 20.
151. Sasco, A.J. and R.S. Paffenbarger, Jr., *Measles infection and Parkinson's disease.* Am J Epidemiol, 1985. **122**(6): p. 1017-31.
152. Hemling, N., et al., *Herpesviruses in brains in Alzheimer's and Parkinson's diseases.* Annals of Neurology, 2003. **54**(2): p. 267-271.
153. Mattson, M.P., *Infectious agents and age-related neurodegenerative disorders.* Ageing Research Reviews, 2004. **3**(1): p. 105-120.
154. Cassarino, D.S., et al., *Lyme-associated parkinsonism: a neuropathologic case study and review of the literature.* Arch Pathol Lab Med, 2003. **127**(9): p. 1204-6.
155. Forrester, J.D., et al., *No Geographic Correlation between Lyme Disease and Death Due to 4 Neurodegenerative Disorders, United States, 2001-2010.* Emerg Infect Dis, 2015. **21**(11): p. 2036-9.
156. Li, Z., et al., *Gut bacterial profiles in Parkinson's disease: A systematic review.* CNS Neurosci Ther, 2023. **29**(1): p. 140-157.
157. Bhattacharyya, D., et al., *Lipopolysaccharide from Gut Microbiota Modulates α-Synuclein Aggregation and Alters Its Biological Function.* ACS Chemical Neuroscience, 2019. **10**(5): p. 2229-2236.
158. Kim, S., et al., *Transneuronal Propagation of Pathologic α-Synuclein from the Gut to the Brain Models Parkinson's Disease.* Neuron, 2019. **103**(4): p. 627-641.e7.
159. Kang, X., et al., *Clostridium difficile infection and risk of Parkinson's disease: a Swedish population-based cohort study.* Eur J Neurol, 2020. **27**(11): p. 2134-2141.
160. Chen, C.-K., Y.-T. Wu, and Y.-C. Chang, *Periodontal inflammatory disease is associated with the risk of Parkinson's disease: a population-based retrospective matched-cohort study.* PeerJ, 2017. **5**: p. e3647.
161. Shen, C.H., et al., *Association Between Tuberculosis and Parkinson Disease: A Nationwide, Population-Based Cohort Study.* Medicine (Baltimore), 2016. **95**(8): p. e2883.
162. Lees, A.J., E. Tolosa, and C.W. Olanow, *Four pioneers of L-dopa treatment: Arvid Carlsson, Oleh Hornykiewicz, George Cotzias, and Melvin Yahr.* Movement Disorders, 2015. **30**(1): p. 19-36.
163. Salat, D. and E. Tolosa, *Levodopa in the Treatment of Parkinson's Disease: Current Status and New Developments.* Journal of Parkinson's Disease, 2013. **3**: p. 255-269.
164. Jankovic, J., *Levodopa strengths and weaknesses.* Neurology, 2002. **58**(suppl_1): p. S19-S32.
165. Chaudhuri, K.R. and A.H. Schapira, *Non-motor symptoms of Parkinson's disease: dopaminergic pathophysiology and treatment.* Lancet Neurol, 2009. **8**(5): p. 464-74.
166. Zappia, M., et al., *Sex Differences in Clinical and Genetic Determinants of Levodopa Peak-Dose Dyskinesias in Parkinson Disease: An Exploratory Study.* Archives of Neurology, 2005. **62**(4): p. 601-605.

167. Warren Olanow, C., et al., *Factors predictive of the development of Levodopa-induced dyskinesia and wearing-off in Parkinson's disease.* Mov Disord, 2013. **28**(8): p. 1064-71.
168. Hely, M.A., et al., *Sydney Multicenter Study of Parkinson's disease: non-L-dopa-responsive problems dominate at 15 years.* Mov Disord, 2005. **20**(2): p. 190-9.
169. Paolini Paoletti, F., N. Tambasco, and L. Parnetti, *Levodopa treatment in Parkinson's disease: earlier or later?* Ann Transl Med, 2019. **7**(Suppl 6): p. S189.
170. Carlson, J.D., et al., *Postoperative delirium in Parkinson's disease patients following deep brain stimulation surgery.* J Clin Neurosci, 2014. **21**(7): p. 1192-5.
171. Foley, J.A., et al., *Apathy and Reduced Speed of Processing Underlie Decline in Verbal Fluency following DBS.* Behav Neurol, 2017. **2017**: p. 7348101.
172. Højlund, A., et al., *Worsening of Verbal Fluency After Deep Brain Stimulation in Parkinson's Disease: A Focused Review.* Comput Struct Biotechnol J, 2017. **15**: p. 68-74.
173. Iarkov, A., et al., *Strategies for the Treatment of Parkinson's Disease: Beyond Dopamine.* Front Aging Neurosci, 2020. **12**: p. 4.
174. Limousin, P. and I. Martinez-Torres, *Deep brain stimulation for Parkinson's disease.* Neurotherapeutics, 2008. **5**(2): p. 309-19.
175. Benabid, A.L., *Deep brain stimulation for Parkinson's disease.* Current Opinion in Neurobiology, 2003. **13**(6): p. 696-706.
176. Azam, S., et al., *The Ageing Brain: Molecular and Cellular Basis of Neurodegeneration.* Frontiers in Cell and Developmental Biology, 2021. **9**.
177. Carmona, J.J. and S. Michan, *Biology of Healthy Aging and Longevity.* Rev Invest Clin, 2016. **68**(1): p. 7-16.
178. Organization, W.H. *Ageing and Health*. 2022 January 22, 2024].
179. Gonzales, M.M., et al., *Biological aging processes underlying cognitive decline and neurodegenerative disease.* The Journal of Clinical Investigation, 2022. **132**(10).
180. Lawson, L.J., et al., *Heterogeneity in the distribution and morphology of microglia in the normal adult mouse brain.* Neuroscience, 1990. **39**(1): p. 151-70.
181. Ginhoux, F., et al., *Fate Mapping Analysis Reveals That Adult Microglia Derive from Primitive Macrophages.* Science, 2010. **330**(6005): p. 841-845.
182. Gomez Perdiguero, E., et al., *Tissue-resident macrophages originate from yolk-sac-derived erythro-myeloid progenitors.* Nature, 2015. **518**(7540): p. 547-551.
183. Kierdorf, K., et al., *Microglia emerge from erythromyeloid precursors via Pu.1- and Irf8-dependent pathways.* Nature Neuroscience, 2013. **16**(3): p. 273-280.
184. Lenz, K.M. and L.H. Nelson, *Microglia and Beyond: Innate Immune Cells As Regulators of Brain Development and Behavioral Function.* Frontiers in Immunology, 2018. **9**.
185. Erblich, B., et al., *Absence of Colony Stimulation Factor-1 Receptor Results in Loss of Microglia, Disrupted Brain Development and Olfactory Deficits.* PLOS ONE, 2011. **6**(10): p. e26317.
186. Nikodemova, M., et al., *Microglial numbers attain adult levels after undergoing a rapid decrease in cell number in the third postnatal week.* Journal of Neuroimmunology, 2015. **278**: p. 280-288.
187. Goldmann, T., et al., *Origin, fate and dynamics of macrophages at central nervous system interfaces.* Nat Immunol, 2016. **17**(7): p. 797-805.
188. Huang, Y., et al., *Repopulated microglia are solely derived from the proliferation of residual microglia after acute depletion.* Nature Neuroscience, 2018. **21**(4): p. 530-540.
189. Réu, P., et al., *The Lifespan and Turnover of Microglia in the Human Brain.* Cell Reports, 2017. **20**(4): p. 779-784.
190. Schwarz, J.M., P.W. Sholar, and S.D. Bilbo, *Sex differences in microglial colonization of the developing rat brain.* Journal of Neurochemistry, 2012. **120**(6): p. 948-963.
191. Nelson, L.H., S. Warden, and K.M. Lenz, *Sex differences in microglial phagocytosis in the neonatal hippocampus.* Brain, Behavior, and Immunity, 2017. **64**: p. 11-22.
192. Murtaj, V., et al., *Age and Sex Influence the Neuro-inflammatory Response to a Peripheral Acute LPS Challenge.* Front Aging Neurosci, 2019. **11**: p. 299.

193. Verdonk, F., et al., *Phenotypic clustering: a novel method for microglial morphology analysis.* Journal of Neuroinflammation, 2016. **13**(1): p. 153.
194. Stowell, R.D., et al., *Cerebellar microglia are dynamically unique and survey Purkinje neurons in vivo.* Developmental Neurobiology, 2018. **78**(6): p. 627-644.
195. Frederiksen, H.R., H. Haukedal, and K. Freude, *Cell Type Specific Expression of Toll-Like Receptors in Human Brains and Implications in Alzheimer's Disease.* Biomed Res Int, 2019. **2019**: p. 7420189.
196. Hagemeyer, N., et al., *Microglia contribute to normal myelinogenesis and to oligodendrocyte progenitor maintenance during adulthood.* Acta Neuropathologica, 2017. **134**(3): p. 441-458.
197. Colonna, M. and O. Butovsky, *Microglia Function in the Central Nervous System During Health and Neurodegeneration.* Annu Rev Immunol, 2017. **35**: p. 441-468.
198. Wang, X.L. and L. Li, *Microglia Regulate Neuronal Circuits in Homeostatic and High-Fat Diet-Induced Inflammatory Conditions.* Front Cell Neurosci, 2021. **15**: p. 722028.
199. Li, Q. and B.A. Barres, *Microglia and macrophages in brain homeostasis and disease.* Nature Reviews Immunology, 2018. **18**(4): p. 225-242.
200. Fourgeaud, L., et al., *TAM receptors regulate multiple features of microglial physiology.* Nature, 2016. **532**(7598): p. 240-244.
201. Chen, Z. and B.D. Trapp, *Microglia and neuroprotection.* Journal of Neurochemistry, 2016. **136**(S1): p. 10-17.
202. Stence, N., M. Waite, and M.E. Dailey, *Dynamics of microglial activation: A confocal time-lapse analysis in hippocampal slices.* Glia, 2001. **33**(3): p. 256-266.
203. Vidal-Itriago, A., et al., *Microglia morphophysiological diversity and its implications for the CNS.* Frontiers in Immunology, 2022. **13**.
204. Doens, D. and P.L. Fernández, *Microglia receptors and their implications in the response to amyloid β for Alzheimer's disease pathogenesis.* Journal of Neuroinflammation, 2014. **11**(1): p. 48.
205. Lively, S. and L.C. Schlichter, *The microglial activation state regulates migration and roles of matrix-dissolving enzymes for invasion.* Journal of Neuroinflammation, 2013. **10**(1): p. 843.
206. Stojiljkovic, M.R., C. Schmeer, and O.W. Witte, *Pharmacological Depletion of Microglia Leads to a Dose-Dependent Reduction in Inflammation and Senescence in the Aged Murine Brain.* Neuroscience, 2022. **488**: p. 1-9.
207. Shahidehpour, R.K., et al., *Dystrophic microglia are associated with neurodegenerative disease and not healthy aging in the human brain.* Neurobiology of Aging, 2021. **99**: p. 19-27.
208. Damani, M.R., et al., *Age-related alterations in the dynamic behavior of microglia.* Aging Cell, 2011. **10**(2): p. 263-76.
209. Latham, A.S., J.A. Moreno, and C.E. Geer, *Biological agents and the aging brain: glial inflammation and neurotoxic signaling.* Frontiers in Aging, 2023. **4**.
210. Safaiyan, S., et al., *Age-related myelin degradation burdens the clearance function of microglia during aging.* Nature Neuroscience, 2016. **19**(8): p. 995-998.
211. Luan W, Q.X., Liang F, Zhang X, Jin Z, Shi L, Luo B, Dai X, *Microglia Impede Oligodendrocyte Generation in Aged Brain.* J Inflamm Res. , 2021.
212. Sierra, A., et al., *Microglia derived from aging mice exhibit an altered inflammatory profile.* Glia, 2007. **55**(4): p. 412-424.
213. Meng, J., et al., *Nucleus distribution of cathepsin B in senescent microglia promotes brain aging through degradation of sirtuins.* Neurobiology of Aging, 2020. **96**: p. 255-266.
214. Frank, M.G., et al., *Aging sensitizes rapidly isolated hippocampal microglia to LPS ex vivo.* Journal of Neuroimmunology, 2010. **226**(1): p. 181-184.
215. Bayraktar, O.A., et al., *Astrocyte development and heterogeneity.* Cold Spring Harb Perspect Biol, 2014. **7**(1): p. a020362.
216. Clavreul, S., L. Dumas, and K. Loulier, *Astrocyte development in the cerebral cortex: Complexity of their origin, genesis, and maturation.* Frontiers in Neuroscience, 2022. **16**.

217. Lee, J., S.W. Kim, and K.T. Kim, *Region-Specific Characteristics of Astrocytes and Microglia: A Possible Involvement in Aging and Diseases.* Cells, 2022. **11**(12).
218. Santos-Galindo, M., et al., *Sex differences in the inflammatory response of primary astrocytes to lipopolysaccharide.* Biology of Sex Differences, 2011. **2**(1): p. 7.
219. Pfrieger, F.W. and B.A. Barres, *Synaptic Efficacy Enhanced by Glial Cells in Vitro.* Science, 1997. **277**(5332): p. 1684-1687.
220. Mauch, D.H., et al., *CNS synaptogenesis promoted by glia-derived cholesterol.* Science, 2001. **294**(5545): p. 1354-7.
221. Christopherson, K.S., et al., *Thrombospondins Are Astrocyte-Secreted Proteins that Promote CNS Synaptogenesis.* Cell, 2005. **120**(3): p. 421-433.
222. Tani, H., et al., *A Local Glutamate-Glutamine Cycle Sustains Synaptic Excitatory Transmitter Release.* Neuron, 2014. **81**(4): p. 888-900.
223. Kubotera, H., et al., *Astrocytic endfeet re-cover blood vessels after removal by laser ablation.* Scientific Reports, 2019. **9**(1): p. 1263.
224. Guérit, S., et al., *Astrocyte-derived Wnt growth factors are required for endothelial blood-brain barrier maintenance.* Progress in Neurobiology, 2021. **199**: p. 101937.
225. Carpentier, P.A., et al., *Differential activation of astrocytes by innate and adaptive immune stimuli.* Glia, 2005. **49**(3): p. 360-374.
226. Jack, C.S., et al., *TLR Signaling Tailors Innate Immune Responses in Human Microglia and Astrocytes1.* The Journal of Immunology, 2005. **175**(7): p. 4320-4330.
227. Vardjan, N., et al., *IFN-γ-induced increase in the mobility of MHC class II compartments in astrocytes depends on intermediate filaments.* Journal of Neuroinflammation, 2012. **9**(1): p. 144.
228. Morizawa, Y.M., et al., *Reactive astrocytes function as phagocytes after brain ischemia via ABCA1-mediated pathway.* Nature Communications, 2017. **8**(1): p. 28.
229. Popov, A., et al., *Astrocyte dystrophy in ageing brain parallels impaired synaptic plasticity.* Aging Cell, 2021. **20**(3): p. e13334.
230. Wu, Y., A.-Q. Zhang, and D.T. Yew, *Age related changes of various markers of astrocytes in senescence-accelerated mice hippocampus.* Neurochemistry International, 2005. **46**(7): p. 565-574.
231. Suda, Y., et al., *Normal aging induces PD-1-enriched exhausted microglia and A1-like reactive astrocytes in the hypothalamus.* Biochemical and Biophysical Research Communications, 2021. **541**: p. 22-29.
232. Dejanovic, B., et al., *Complement C1q-dependent excitatory and inhibitory synapse elimination by astrocytes and microglia in Alzheimer's disease mouse models.* Nature Aging, 2022. **2**(9): p. 837-850.
233. Boisvert, M.M., et al., *The Aging Astrocyte Transcriptome from Multiple Regions of the Mouse Brain.* Cell Reports, 2018. **22**(1): p. 269-285.
234. Norden, D.M., et al., *Age-related impairments in the dynamic regulation of active microglia by astrocytes.* Brain, Behavior, and Immunity, 2015. **49**: p. e16-e17.
235. Norden, D.M., et al., *Insensitivity of astrocytes to interleukin 10 signaling following peripheral immune challenge results in prolonged microglial activation in the aged brain.* Neurobiology of Aging, 2016. **44**: p. 22-41.
236. Ding, F., et al., *Astrocytes exhibit diverse Ca2+ changes at subcellular domains during brain aging.* Frontiers in Aging Neuroscience, 2022. **14**.
237. Mills, W.A., et al., *Astrocyte plasticity in mice ensures continued endfoot coverage of cerebral blood vessels following injury and declines with age.* Nature Communications, 2022. **13**(1): p. 1794.
238. Pan, J., et al., *Age-associated changes in microglia and astrocytes ameliorate blood-brain barrier dysfunction.* Molecular Therapy - Nucleic Acids, 2021. **26**: p. 970-986.
239. Dill, K.A. and J.L. MacCallum, *The Protein-Folding Problem, 50 Years On.* Science, 2012. **338**(6110): p. 1042-1046.

240. Biro, J.C., *Amino acid size, charge, hydropathy indices and matrices for protein structure analysis.* Theor Biol Med Model, 2006. **3**: p. 15.
241. Pauling, L., R.B. Corey, and H.R. Branson, *The structure of proteins: Two hydrogen-bonded helical configurations of the polypeptide chain.* Proceedings of the National Academy of Sciences, 1951. **37**(4): p. 205-211.
242. Whitford, P.C. and J.N. Onuchic, *What protein folding teaches us about biological function and molecular machines.* Curr Opin Struct Biol, 2015. **30**: p. 57-62.
243. Hartl, F.U., A. Bracher, and M. Hayer-Hartl, *Molecular chaperones in protein folding and proteostasis.* Nature, 2011. **475**(7356): p. 324-332.
244. Ramazi, S. and J. Zahiri, *Posttranslational modifications in proteins: resources, tools and prediction methods.* Database (Oxford), 2021. **2021**.
245. Moreno-Gonzalez, I. and C. Soto, *Misfolded protein aggregates: mechanisms, structures and potential for disease transmission.* Semin Cell Dev Biol, 2011. **22**(5): p. 482-7.
246. Ciechanover, A. and A.L. Schwartz, *The ubiquitin-proteasome pathway: the complexity and myriad functions of proteins death.* Proc Natl Acad Sci U S A, 1998. **95**(6): p. 2727-30.
247. Jackson, M.P. and E.W. Hewitt, *Cellular proteostasis: degradation of misfolded proteins by lysosomes.* Essays Biochem, 2016. **60**(2): p. 173-180.
248. Cuervo, A.M., *Chaperone-mediated autophagy: selectivity pays off.* Trends Endocrinol Metab, 2010. **21**(3): p. 142-50.
249. MacGurn, J.A., *Garbage on, garbage off: new insights into plasma membrane protein quality control.* Curr Opin Cell Biol, 2014. **29**: p. 92-8.
250. Ciechanover, A., *Proteolysis: from the lysosome to ubiquitin and the proteasome.* Nature Reviews Molecular Cell Biology, 2005. **6**(1): p. 79-87.
251. Hur, J.-Y., *γ-Secretase in Alzheimer's disease.* Experimental & Molecular Medicine, 2022. **54**(4): p. 433-446.
252. Niikura, T., H. Tajima, and Y. Kita, *Neuronal cell death in Alzheimer's disease and a neuroprotective factor, humanin.* Curr Neuropharmacol, 2006. **4**(2): p. 139-47.
253. Volicer, L., *Physiological and Pathological Functions of Beta-Amyloid in the Brain and Alzheimer'S Disease: A Review.* Journal of Physiological Investigation, 2020. **63**(3).
254. Selkoe, D.J., *Soluble oligomers of the amyloid β-protein impair synaptic plasticity and behavior.* Behavioural Brain Research, 2008. **192**(1): p. 106-113.
255. Shankar, G.M., et al., *Amyloid-β protein dimers isolated directly from Alzheimer's brains impair synaptic plasticity and memory.* Nature Medicine, 2008. **14**(8): p. 837-842.
256. Cleary, J.P., et al., *Natural oligomers of the amyloid-β protein specifically disrupt cognitive function.* Nature Neuroscience, 2005. **8**(1): p. 79-84.
257. Palop, J.J. and L. Mucke, *Amyloid-β–induced neuronal dysfunction in Alzheimer's disease: from synapses toward neural networks.* Nature Neuroscience, 2010. **13**(7): p. 812-818.
258. Thal, D.R., et al., *The Development of Amyloid β Protein Deposits in the Aged Brain.* Science of Aging Knowledge Environment, 2006. **2006**(6): p. re1-re1.
259. Barbier, P., et al., *Role of Tau as a Microtubule-Associated Protein: Structural and Functional Aspects.* Frontiers in Aging Neuroscience, 2019. **11**.
260. Wang, Y. and E. Mandelkow, *Tau in physiology and pathology.* Nature Reviews Neuroscience, 2016. **17**(1): p. 22-35.
261. Morrison, B.M., Y. Lee, and J.D. Rothstein, *Oligodendroglia: metabolic supporters of axons.* Trends Cell Biol, 2013. **23**(12): p. 644-51.
262. Mitchison, T. and M. Kirschner, *Cytoskeletal dynamics and nerve growth.* Neuron, 1988. **1**(9): p. 761-72.
263. Qiang, L., et al., *Tau Does Not Stabilize Axonal Microtubules but Rather Enables Them to Have Long Labile Domains.* Current Biology, 2018. **28**(13): p. 2181-2189.e4.
264. Binder, L.I., A. Frankfurter, and L.I. Rebhun, *The distribution of tau in the mammalian central nervous system.* J Cell Biol, 1985. **101**(4): p. 1371-8.

265. Hill, E., et al., *Understanding the Pathophysiological Actions of Tau Oligomers: A Critical Review of Current Electrophysiological Approaches.* Frontiers in Molecular Neuroscience, 2020. **13**.
266. Biernat, J. and E.-M. Mandelkow, *The Development of Cell Processes Induced by tau Protein Requires Phosphorylation of Serine 262 and 356 in the Repeat Domain and Is Inhibited by Phosphorylation in the Proline-rich Domains.* Molecular Biology of the Cell, 1999. **10**(3): p. 727-740.
267. Biernat, J., et al., *Protein Kinase MARK/PAR-1 Is Required for Neurite Outgrowth and Establishment of Neuronal Polarity.* Molecular Biology of the Cell, 2002. **13**(11): p. 4013-4028.
268. Köpke, E., et al., *Microtubule-associated protein tau. Abnormal phosphorylation of a non-paired helical filament pool in Alzheimer disease.* J Biol Chem, 1993. **268**(32): p. 24374-84.
269. Gendron, T.F. and L. Petrucelli, *The role of tau in neurodegeneration.* Molecular Neurodegeneration, 2009. **4**(1): p. 13.
270. Lasagna-Reeves, C.A., et al., *Identification of oligomers at early stages of tau aggregation in Alzheimer's disease.* Faseb j, 2012. **26**(5): p. 1946-59.
271. Shafiei, S.S., M.J. Guerrero-Muñoz, and D.L. Castillo-Carranza, *Tau Oligomers: Cytotoxicity, Propagation, and Mitochondrial Damage.* Frontiers in Aging Neuroscience, 2017. **9**.
272. Gong, C.X. and K. Iqbal, *Hyperphosphorylation of microtubule-associated protein tau: a promising therapeutic target for Alzheimer disease.* Curr Med Chem, 2008. **15**(23): p. 2321-8.
273. Gerson, J. and R. Kayed, *Formation and Propagation of Tau Oligomeric Seeds.* Frontiers in Neurology, 2013. **4**.
274. Arriagada, P.V., et al., *Neurofibrillary tangles but not senile plaques parallel duration and severity of Alzheimer's disease.* Neurology, 1992. **42**(3 Pt 1): p. 631-9.
275. Lin, W.L., et al., *Ultrastructural neuronal pathology in transgenic mice expressing mutant (P301L) human tau.* J Neurocytol, 2003. **32**(9): p. 1091-105.
276. Brelstaff, J., et al., *Living Neurons with Tau Filaments Aberrantly Expose Phosphatidylserine and Are Phagocytosed by Microglia.* Cell Rep, 2018. **24**(8): p. 1939-1948.e4.
277. Chesser, A., S. Pritchard, and G. Johnson, *Tau Clearance Mechanisms and Their Possible Role in the Pathogenesis of Alzheimer Disease.* Frontiers in Neurology, 2013. **4**.
278. Zhang, H., et al., *Possible Mechanisms of Tau Spread and Toxicity in Alzheimer's Disease.* Front Cell Dev Biol, 2021. **9**: p. 707268.
279. Malek, N., et al., *Alpha-synuclein in peripheral tissues and body fluids as a biomarker for Parkinson's disease – a systematic review.* Acta Neurologica Scandinavica, 2014. **130**(2): p. 59-72.
280. Maroteaux, L., J.T. Campanelli, and R.H. Scheller, *Synuclein: a neuron-specific protein localized to the nucleus and presynaptic nerve terminal.* J Neurosci, 1988. **8**(8): p. 2804-15.
281. Li, W.W., et al., *Localization of alpha-synuclein to mitochondria within midbrain of mice.* Neuroreport, 2007. **18**(15): p. 1543-6.
282. Goedert, M., *Alpha-synuclein and neurodegenerative diseases.* Nat Rev Neurosci, 2001. **2**(7): p. 492-501.
283. Bernal-Conde, L.D., et al., *Alpha-Synuclein Physiology and Pathology: A Perspective on Cellular Structures and Organelles.* Front Neurosci, 2019. **13**: p. 1399.
284. Mehra, S., S. Sahay, and S.K. Maji, *α-Synuclein misfolding and aggregation: Implications in Parkinson's disease pathogenesis.* Biochim Biophys Acta Proteins Proteom, 2019. **1867**(10): p. 890-908.
285. Gibb, W.R. and A.J. Lees, *The relevance of the Lewy body to the pathogenesis of idiopathic Parkinson's disease.* J Neurol Neurosurg Psychiatry, 1988. **51**(6): p. 745-52.
286. Burré, J., *The Synaptic Function of α-Synuclein.* J Parkinsons Dis, 2015. **5**(4): p. 699-713.
287. Abeliovich, A., et al., *Mice lacking alpha-synuclein display functional deficits in the nigrostriatal dopamine system.* Neuron, 2000. **25**(1): p. 239-52.

288. Nadal, A., et al., *Plasma albumin is a potent trigger of calcium signals and DNA synthesis in astrocytes.* Proceedings of the National Academy of Sciences, 1995. **92**(5): p. 1426-1430.
289. Abbott, N.J., et al., *Structure and function of the blood–brain barrier.* Neurobiology of Disease, 2010. **37**(1): p. 13-25.
290. Kadry, H., B. Noorani, and L. Cucullo, *A blood–brain barrier overview on structure, function, impairment, and biomarkers of integrity.* Fluids and Barriers of the CNS, 2020. **17**(1): p. 69.
291. Pardridge, W.M., J. Eisenberg, and J. Yang, *Human Blood—Brain Barrier Insulin Receptor.* Journal of Neurochemistry, 1985. **44**(6): p. 1771-1778.
292. Wolburg, H. and A. Lippoldt, *Tight junctions of the blood-brain barrier: development, composition and regulation.* Vascul Pharmacol, 2002. **38**(6): p. 323-37.
293. Risau, W. and H. Wolburg, *Development of the blood-brain barrier.* Trends in Neurosciences, 1990. **13**(5): p. 174-178.
294. Atbin, D., et al., *Salivary cortisol levels in Parkinson's disease and its correlation to risk behaviour.* Journal of Neurology, Neurosurgery & Psychiatry, 2011. **82**(10): p. 1107.
295. Kubota, K., et al., *Ca(2+)-independent cell-adhesion activity of claudins, a family of integral membrane proteins localized at tight junctions.* Curr Biol, 1999. **9**(18): p. 1035-8.
296. Mitic, L.L., C.M. Van Itallie, and J.M. Anderson, *Molecular physiology and pathophysiology of tight junctions I. Tight junction structure and function: lessons from mutant animals and proteins.* Am J Physiol Gastrointest Liver Physiol, 2000. **279**(2): p. G250-4.
297. Greene, C., N. Hanley, and M. Campbell, *Claudin-5: gatekeeper of neurological function.* Fluids and Barriers of the CNS, 2019. **16**(1): p. 3.
298. Furuse, M., et al., *A single gene product, claudin-1 or -2, reconstitutes tight junction strands and recruits occludin in fibroblasts.* J Cell Biol, 1998. **143**(2): p. 391-401.
299. Günzel, D. and A.S. Yu, *Claudins and the modulation of tight junction permeability.* Physiol Rev, 2013. **93**(2): p. 525-69.
300. Nitta, T., et al., *Size-selective loosening of the blood-brain barrier in claudin-5-deficient mice.* J Cell Biol, 2003. **161**(3): p. 653-60.
301. Saitou, M., et al., *Complex phenotype of mice lacking occludin, a component of tight junction strands.* Mol Biol Cell, 2000. **11**(12): p. 4131-42.
302. Aurrand-Lions, M., et al., *Heterogeneity of endothelial junctions is reflected by differential expression and specific subcellular localization of the three JAM family members.* Blood, 2001. **98**(13): p. 3699-3707.
303. Abbott, N.J., L. Rönnbäck, and E. Hansson, *Astrocyte–endothelial interactions at the blood–brain barrier.* Nature Reviews Neuroscience, 2006. **7**(1): p. 41-53.
304. Hösli, L., et al., *Direct vascular contact is a hallmark of cerebral astrocytes.* Cell Reports, 2022. **39**(1).
305. Díaz-Castro, B., S. Robel, and A. Mishra, *Astrocyte Endfeet in Brain Function and Pathology: Open Questions.* Annual Review of Neuroscience, 2023. **46**(1): p. 101-121.
306. Wang, M.X., et al., *Varying perivascular astroglial endfoot dimensions along the vascular tree maintain perivascular-interstitial flux through the cortical mantle.* Glia, 2021. **69**(3): p. 715-728.
307. Janzer, R.C. and M.C. Raff, *Astrocytes induce blood–brain barrier properties in endothelial cells.* Nature, 1987. **325**(6101): p. 253-257.
308. Hayashi, Y., et al., *Induction of various blood-brain barrier properties in non-neural endothelial cells by close apposition to co-cultured astrocytes.* Glia, 1997. **19**(1): p. 13-26.
309. Mathiisen, T.M., et al., *The perivascular astroglial sheath provides a complete covering of the brain microvessels: An electron microscopic 3D reconstruction.* Glia, 2010. **58**(9): p. 1094-1103.
310. Winkler, E.A., R.D. Bell, and B.V. Zlokovic, *Central nervous system pericytes in health and disease.* Nature Neuroscience, 2011. **14**(11): p. 1398-1405.
311. Armulik, A., et al., *Pericytes regulate the blood–brain barrier.* Nature, 2010. **468**(7323): p. 557-561.

312. Peppiatt, C.M., et al., *Bidirectional control of CNS capillary diameter by pericytes.* Nature, 2006. **443**(7112): p. 700-704.
313. Hall, C.N., et al., *Capillary pericytes regulate cerebral blood flow in health and disease.* Nature, 2014. **508**(7494): p. 55-60.
314. Zlokovic, B.V., *The Blood-Brain Barrier in Health and Chronic Neurodegenerative Disorders.* Neuron, 2008. **57**(2): p. 178-201.
315. Zipser, B.D., et al., *Microvascular injury and blood-brain barrier leakage in Alzheimer's disease.* Neurobiol Aging, 2007. **28**(7): p. 977-86.
316. Ryu, J.K. and J.G. McLarnon, *A leaky blood–brain barrier, fibrinogen infiltration and microglial reactivity in inflamed Alzheimer's disease brain.* Journal of Cellular and Molecular Medicine, 2009. **13**(9a): p. 2911-2925.
317. Cullen, K.M., Z. Kócsi, and J. Stone, *Pericapillary Haem-Rich Deposits: Evidence for Microhaemorrhages in Aging Human Cerebral Cortex.* Journal of Cerebral Blood Flow & Metabolism, 2005. **25**(12): p. 1656-1667.
318. Goos, J.D.C., et al., *Patients With Alzheimer Disease With Multiple Microbleeds.* Stroke, 2009. **40**(11): p. 3455-3460.
319. Salloway, S., et al., *Effect of APOE genotype on microvascular basement membrane in Alzheimer's disease.* Journal of the Neurological Sciences, 2002. **203**: p. 183-187.
320. Sengillo, J.D., et al., *Deficiency in Mural Vascular Cells Coincides with Blood–Brain Barrier Disruption in Alzheimer's Disease.* Brain Pathology, 2013. **23**(3): p. 303-310.
321. Farkas, E. and P.G. Luiten, *Cerebral microvascular pathology in aging and Alzheimer's disease.* Prog Neurobiol, 2001. **64**(6): p. 575-611.
322. Bell, R.D., et al., *Pericytes Control Key Neurovascular Functions and Neuronal Phenotype in the Adult Brain and during Brain Aging.* Neuron, 2010. **68**(3): p. 409-427.
323. Sagare, A.P., et al., *Pericyte loss influences Alzheimer-like neurodegeneration in mice.* Nature Communications, 2013. **4**(1): p. 2932.
324. Wolburg, H., et al., *Localization of claudin-3 in tight junctions of the blood-brain barrier is selectively lost during experimental autoimmune encephalomyelitis and human glioblastoma multiforme.* Acta Neuropathologica, 2003. **105**(6): p. 586-592.
325. Hermans, S., C.R. Horsburgh Jr, and R. Wood, *A Century of Tuberculosis Epidemiology in the Northern and Southern Hemisphere: The Differential Impact of Control Interventions.* PLOS ONE, 2015. **10**(8): p. e0135179.
326. Appiah, M.A., et al., *Barriers to tuberculosis treatment adherence in high-burden tuberculosis settings in Ashanti region, Ghana: a qualitative study from patient's perspective.* BMC Public Health, 2023. **23**(1): p. 1317.
327. Tadesse, T., et al., *Long distance travelling and financial burdens discourage tuberculosis DOTs treatment initiation and compliance in Ethiopia: a qualitative study.* BMC Public Health, 2013. **13**(1): p. 424.
328. Hargreaves, J.R., et al., *The social determinants of tuberculosis: from evidence to action.* Am J Public Health, 2011. **101**(4): p. 654-62.
329. Xu, G.J., et al., *Comprehensive serological profiling of human populations using a synthetic human virome.* Science, 2015. **348**(6239): p. aaa0698.
330. Harding, E., *WHO global progress report on tuberculosis elimination.* The Lancet Respiratory Medicine, 2020. **8**(1): p. 19.
331. R, F., et al., *Epidemiology of Tuberculosis and Progress Toward Meeting Global Targets - Worldwide 2019.* MMWR Morb Mortal Wkly Reports, 2021(1545-861X (Electronic)).
332. Hogan, A.B., et al., *Potential impact of the COVID-19 pandemic on HIV, tuberculosis, and malaria in low-income and middle-income countries: a modelling study.* The Lancet Global Health, 2020. **8**(9): p. e1132-e1141.
333. Jain, V.K., et al., *Tuberculosis in the era of COVID-19 in India.* Diabetes & Metabolic Syndrome: Clinical Research & Reviews, 2020. **14**(5): p. 1439-1443.

334. Migliori, G.B., et al., *Worldwide Effects of Coronavirus Disease Pandemic on Tuberculosis Services, January-April 2020.* Emerg Infect Dis, 2020. **26**(11): p. 2709-2712.
335. Glaziou, P., *Predicted impact of the COVID-19 pandemic on global tuberculosis deaths in 2020.* medRxiv, 2021: p. 2020.04.28.20079582.
336. Ernst, J.D., *The immunological life cycle of tuberculosis.* Nature Reviews Immunology, 2012. **12**(8): p. 581-591.
337. O'Garra, A., et al., *The Immune Response in Tuberculosis.* Annual Review of Immunology, 2013. **31**(1): p. 475-527.
338. de Martino, M., et al., *Immune Response to Mycobacterium tuberculosis: A Narrative Review.* Front Pediatr, 2019. **7**: p. 350.
339. Curto, M., et al., *Inhibition of cytokines expression in human microglia infected by virulent and non-virulent mycobacteria.* Neurochemistry International, 2004. **44**(6): p. 381-392.
340. Rock, R.B., et al., *Mycobacterium tuberculosis–Induced Cytokine and Chemokine Expression by Human Microglia and Astrocytes: Effects of Dexamethasone.* The Journal of Infectious Diseases, 2005. **192**(12): p. 2054-2058.
341. Harris, J.E., et al., *Monocytes infected with Mycobacterium tuberculosis regulate MAP kinase-dependent astrocyte MMP-9 secretion.* Journal of Leukocyte Biology, 2007. **81**(2): p. 548-556.
342. Husain, N., et al., *Vascular endothelial growth factor as a marker of disease activity in neurotuberculosis.* Journal of Infection, 2008. **56**(2): p. 114-119.
343. Yang, C.-S., et al., *Secretory phospholipase A2 plays an essential role in microglial inflammatory responses to Mycobacterium tuberculosis.* Glia, 2009. **57**(10): p. 1091-1103.
344. Cannas, S., et al., *Interaction between Mycobacterium tuberculosis, Mycobacterium bovis, Mycobacterium avium subspecies paratuberculosis with the enteric glia and microglial cells.* Gut Pathogens, 2011. **3**(1): p. 19.
345. Green, J.A., et al., *Mycobacterium tuberculosis-infected human monocytes down-regulate microglial MMP-2 secretion in CNS tuberculosis via TNFα, NFκB, p38 and caspase 8 dependent pathways.* Journal of Neuroinflammation, 2011. **8**(1): p. 46.
346. Randall, P.J., et al., *Neurons Are Host Cells for Mycobacterium tuberculosis.* Infection and Immunity, 2014. **82**(5): p. 1880-1890.
347. Tripathi, S., et al., *Glial alterations in tuberculous and cryptococcal meningitis and their relation to HIV co-infection--a study on human brains.* J Infect Dev Ctries, 2014. **8**(11): p. 1421-43.
348. Francisco, N.M., et al., *TNF-dependent regulation and activation of innate immune cells are essential for host protection against cerebral tuberculosis.* Journal of Neuroinflammation, 2015. **12**(1): p. 125.
349. Mason, S., et al., *A hypothetical astrocyte–microglia lactate shuttle derived from a 1H NMR metabolomics analysis of cerebrospinal fluid from a cohort of South African children with tuberculous meningitis.* Metabolomics, 2015. **11**(4): p. 822-837.
350. Qin, Y., et al., *Macrophage-Microglia Networks Drive M1 Microglia Polarization After Mycobacterium Infection.* Inflammation, 2015. **38**(4): p. 1609-1616.
351. Tucker, E.W., et al., *Microglia activation in a pediatric rabbit model of tuberculous meningitis.* Disease Models & Mechanisms, 2016. **9**(12): p. 1497-1506.
352. Rohlwink, U.K., et al., *Biomarkers of Cerebral Injury and Inflammation in Pediatric Tuberculous Meningitis.* Clinical Infectious Diseases, 2017. **65**(8): p. 1298-1307.
353. Othman, F.N., et al., *Human tuberculosis brain promotes neuronal apoptosis but not in astrocytes with high expression of vascular endothelial growth factor.* Tuberculosis, 2018. **112**: p. 45-51.
354. Lara-Espinosa, J.V., et al., *Experimental Pulmonary Tuberculosis in the Absence of Detectable Brain Infection Induces Neuroinflammation and Behavioural Abnormalities in Male BALB/c Mice.* International Journal of Molecular Sciences, 2020. **21**(24): p. 9483.
355. Xie, Z., et al., *By Regulating the NLRP3 Inflammasome Can Reduce the Release of Inflammatory Factors in the Co-Culture Model of Tuberculosis H37Ra Strain and Rat Microglia.* Frontiers in Cellular and Infection Microbiology, 2021. **11**.

356. Dodd, P.J., et al., *The global burden of tuberculous meningitis in adults: A modelling study.* PLOS Global Public Health, 2021. **1**(12): p. e0000069.
357. Frecker, M.F., W.E.M. Pryse-Philli, and H.R. Strong, *Immunological Associations in Familial and Non-Familial Alzheimer Patients and Their Families.* Canadian Journal of Neurological Sciences / Journal Canadien des Sciences Neurologiques, 1994. **21**(2): p. 112-119.
358. Peng, Y.-H., et al., *Increased Risk of Dementia Among Patients With Pulmonary Tuberculosis:A Retrospective Population-Based Cohort Study.* American Journal of Alzheimer's Disease & Other Dementias®, 2015. **30**(6): p. 629-634.
359. Hestad, K.A., et al., *Cognitive Impairment in Zambians With HIV Infection and Pulmonary Tuberculosis.* J Acquir Immune Defic Syndr, 2019. **80**(1): p. 110-117.
360. Isik, A., et al., *Anxiety and depression in patients with rheumatoid arthritis.* Clinical Rheumatology, 2007. **26**(6): p. 872-878.
361. Shin, S.Y., et al., *Cognitive impairment in persons with rheumatoid arthritis.* Arthritis Care & Research, 2012. **64**(8): p. 1144-1150.
362. Wallin, K., et al., *Midlife Rheumatoid Arthritis Increases the Risk of Cognitive Impairment Two Decades Later: A Population-Based Study.* Journal of Alzheimer's Disease, 2012. **31**: p. 669-676.
363. Püntener, U., et al., *Long-term impact of systemic bacterial infection on the cerebral vasculature and microglia.* Journal of Neuroinflammation, 2012. **9**(1): p. 146.
364. Do, J. and J. Woo, *From Gut to Brain: Alteration in Inflammation Markers in the Brain of Dextran Sodium Sulfate-induced Colitis Model Mice.* Clin Psychopharmacol Neurosci, 2018. **16**(4): p. 422-433.
365. Combrinck, M.I., V.H. Perry, and C. Cunningham, *Peripheral infection evokes exaggerated sickness behaviour in pre-clinical murine prion disease.* Neuroscience, 2002. **112**(1): p. 7-11.
366. Machado, A., et al., *Peripheral Inflammation Increases the Damage in Animal Models of Nigrostriatal Dopaminergic Neurodegeneration: Possible Implication in Parkinson's Disease Incidence.* Parkinson's Disease, 2011. **2011**: p. 393769.
367. García-Domínguez, I., et al., *Peripheral Inflammation Enhances Microglia Response and Nigral Dopaminergic Cell Death in an in vivo MPTP Model of Parkinson's Disease.* Frontiers in Cellular Neuroscience, 2018. **12**.
368. Süß, P., et al., *Chronic Peripheral Inflammation Causes a Region-Specific Myeloid Response in the Central Nervous System.* Cell Reports, 2020. **30**(12): p. 4082-4095.e6.
369. Chouhan, J.K., et al., *Systemic Inflammation Accelerates Changes in Microglial and Synaptic Markers in an Experimental Model of Chronic Neurodegeneration.* Front Neurosci, 2021. **15**: p. 760721.
370. Cunningham, C., et al., *Central and Systemic Endotoxin Challenges Exacerbate the Local Inflammatory Response and Increase Neuronal Death during Chronic Neurodegeneration.* The Journal of Neuroscience, 2005. **25**(40): p. 9275.
371. Perry, V.H., C. Cunningham, and C. Holmes, *Systemic infections and inflammation affect chronic neurodegeneration.* Nature Reviews Immunology, 2007. **7**(2): p. 161-167.
372. Lopez-Rodriguez, A.B., et al., *Acute systemic inflammation exacerbates neuroinflammation in Alzheimer's disease: IL-1β drives amplified responses in primed astrocytes and neuronal network dysfunction.* Alzheimer's & Dementia, 2021. **17**(10): p. 1735-1755.
373. Kim, Y.-K., et al., *Cytokine imbalance in the pathophysiology of major depressive disorder.* Progress in Neuro-Psychopharmacology and Biological Psychiatry, 2007. **31**(5): p. 1044-1053.
374. Dowlati, Y., et al., *A meta-analysis of cytokines in major depression.* Biol Psychiatry, 2010. **67**(5): p. 446-57.
375. Skaper, S.D., et al., *An Inflammation-Centric View of Neurological Disease: Beyond the Neuron.* Frontiers in Cellular Neuroscience, 2018. **12**.
376. Allen, N.J. and D.A. Lyons, *Glia as architects of central nervous system formation and function.* Science, 2018. **362**(6411): p. 181-185.

377. Giovannoni, F. and F.J. Quintana, *The Role of Astrocytes in CNS Inflammation*. Trends Immunol, 2020. **41**(9): p. 805-819.
378. Kreutzberg, G.W., *Microglia: a sensor for pathological events in the CNS.* Trends in Neurosciences, 1996. **19**(8): p. 312-318.
379. Boche, D., V.H. Perry, and J.A.R. Nicoll, *Review: Activation patterns of microglia and their identification in the human brain.* Neuropathology and Applied Neurobiology, 2013. **39**(1): p. 3-18.
380. Streit, W.J., et al., *Microglial pathology.* Acta Neuropathologica Communications, 2014. **2**(1): p. 142.
381. Liddelow, S.A., et al., *Neurotoxic reactive astrocytes are induced by activated microglia.* Nature, 2017. **541**(7638): p. 481-487.
382. Eng, L.F. and R.S. Ghirnikar, *GFAP and Astrogliosis.* Brain Pathology, 1994. **4**(3): p. 229-237.
383. O'Callaghan, J.P. and K. Sriram, *Glial fibrillary acidic protein and related glial proteins as biomarkers of neurotoxicity.* Expert Opinion on Drug Safety, 2005. **4**(3): p. 433-442.
384. Jha, M.K., et al., *Microglia-Astrocyte Crosstalk: An Intimate Molecular Conversation.* The Neuroscientist, 2019. **25**(3): p. 227-240.
385. Sanz, P. and M.A. Garcia-Gimeno, *Reactive Glia Inflammatory Signaling Pathways and Epilepsy.* International Journal of Molecular Sciences, 2020. **21**(11): p. 4096.
386. Gómez-Nicola, D., et al., *Regulation of Microglial Proliferation during Chronic Neurodegeneration.* The Journal of Neuroscience, 2013. **33**(6): p. 2481.
387. Chéret, C., et al., *Neurotoxic Activation of Microglia Is Promoted by a Nox1-Dependent NADPH Oxidase.* The Journal of Neuroscience, 2008. **28**(46): p. 12039.
388. Sheng, W.S., et al., *Reactive oxygen species from human astrocytes induced functional impairment and oxidative damage.* Neurochem Res, 2013. **38**(10): p. 2148-59.
389. Ransohoff, R.M., *How neuroinflammation contributes to neurodegeneration.* Science, 2016. **353**(6301): p. 777-783.
390. Lu, D.C., et al., *Caspase cleavage of the amyloid precursor protein modulates amyloid β-protein toxicity.* Journal of Neurochemistry, 2003. **87**(3): p. 733-741.
391. Frost, B., R.L. Jacks, and M.I. Diamond, *Propagation of Tau Misfolding from the Outside to the Inside of a Cell*.* Journal of Biological Chemistry, 2009. **284**(19): p. 12845-12852.
392. Brunello, C.A., et al., *Mechanisms of secretion and spreading of pathological tau protein.* Cellular and Molecular Life Sciences, 2020. **77**(9): p. 1721-1744.
393. Wang, Y., et al., *The release and trans-synaptic transmission of Tau via exosomes.* Molecular Neurodegeneration, 2017. **12**(1): p. 5.
394. Ciechanover, A. and Y.T. Kwon, *Degradation of misfolded proteins in neurodegenerative diseases: therapeutic targets and strategies.* Experimental & Molecular Medicine, 2015. **47**(3): p. e147-e147.
395. Currais, A., et al., *Intraneuronal protein aggregation as a trigger for inflammation and neurodegeneration in the aging brain.* Faseb j, 2017. **31**(1): p. 5-10.
396. Rodriguez, A., Zhang, H., Klaminder, J., Brodin, T., Andersson, P. L. and Andersson, M, *ToxTrac: a fast and robust software for tracking organisms.* Methods in Ecology and Evolution, 2018. **9**(3): p. 460–464.
397. Robertson, K.R., et al., *Human Immunodeficiency Virus Type 1 and Tuberculosis Coinfection in Multinational, Resource-limited Settings: Increased Neurological Dysfunction.* Clin Infect Dis, 2019. **68**(10): p. 1739-1746.
398. Ordway, D., et al., *The Cellular Immune Response to Mycobacterium tuberculosis Infection in the Guinea Pig1.* The Journal of Immunology, 2007. **179**(4): p. 2532-2541.
399. Dharmadhikari, A.S. and E.A. Nardell, *What animal models teach humans about tuberculosis.* Am J Respir Cell Mol Biol, 2008. **39**(5): p. 503-8.
400. Padilla-Carlin, D.J., D.N. McMurray, and A.J. Hickey, *The guinea pig as a model of infectious diseases.* Comparative medicine, 2008. **58**(4): p. 324-340.

401. Hol, E.M. and M. Pekny, *Glial fibrillary acidic protein (GFAP) and the astrocyte intermediate filament system in diseases of the central nervous system.* Current Opinion in Cell Biology, 2015. **32**: p. 121-130.
402. Kamphuis, W., et al., *Differential cell proliferation in the cortex of the appsweps1de9 alzheimer's disease mouse model.* Glia, 2012. **60**(4): p. 615-629.
403. Tan, Y.L., Y. Yuan, and L. Tian, *Microglial regional heterogeneity and its role in the brain.* Mol Psychiatry, 2020. **25**(2): p. 351-367.
404. Mannix, R., et al., *Chronic gliosis and behavioral deficits in mice following repetitive mild traumatic brain injury.* J Neurosurg, 2014. **121**(6): p. 1342-50.
405. Deloulme, J.C., et al., *Nuclear expression of S100B in oligodendrocyte progenitor cells correlates with differentiation toward the oligodendroglial lineage and modulates oligodendrocytes maturation.* Mol Cell Neurosci, 2004. **27**(4): p. 453-65.
406. Hachem, S., et al., *Spatial and temporal expression of S100B in cells of oligodendrocyte lineage.* Glia, 2005. **51**(2): p. 81-97.
407. Du, J., et al., *S100B is selectively expressed by gray matter protoplasmic astrocytes and myelinating oligodendrocytes in the developing CNS.* Molecular Brain, 2021. **14**(1): p. 154.
408. Smajić, S., et al., *Single-cell sequencing of human midbrain reveals glial activation and a Parkinson-specific neuronal state.* Brain, 2021. **145**(3): p. 964-978.
409. Perry, V.H. and C. Holmes, *Microglial priming in neurodegenerative disease.* Nat Rev Neurol, 2014. **10**(4): p. 217-24.
410. Li, J.W., et al., *Microglial priming in Alzheimer's disease.* Ann Transl Med, 2018. **6**(10): p. 176.
411. Noble, W., et al., *The importance of tau phosphorylation for neurodegenerative diseases.* Front Neurol, 2013. **4**: p. 83.
412. Evans, D.B., et al., *Tau phosphorylation at serine 396 and serine 404 by human recombinant tau protein kinase II inhibits tau's ability to promote microtubule assembly.* J Biol Chem, 2000. **275**(32): p. 24977-83.
413. Rajbanshi, B., et al., *Localization, induction, and cellular effects of tau phosphorylated at threonine 217.* Alzheimers Dement, 2023.
414. Musi, N., et al., *Tau protein aggregation is associated with cellular senescence in the brain.* Aging Cell, 2018. **17**(6): p. e12840.
415. Wesseling, H., et al., *Tau PTM Profiles Identify Patient Heterogeneity and Stages of Alzheimer's Disease.* Cell, 2020. **183**(6): p. 1699-1713.e13.
416. Thijssen, E.H., et al., *Plasma phosphorylated tau 217 and phosphorylated tau 181 as biomarkers in Alzheimer's disease and frontotemporal lobar degeneration: a retrospective diagnostic performance study.* The Lancet Neurology, 2021. **20**(9): p. 739-752.
417. Arimoto, T. and G. Bing, *Up-regulation of inducible nitric oxide synthase in the substantia nigra by lipopolysaccharide causes microglial activation and neurodegeneration.* Neurobiology of Disease, 2003. **12**(1): p. 35-45.
418. Xie, Z., C.J. Smith, and L.J. Van Eldik, *Activated glia induce neuron death via MAP kinase signaling pathways involving JNK and p38.* Glia, 2004. **45**(2): p. 170-179.
419. Lee, I. and R.P. Kesner, *Differential contributions of dorsal hippocampal subregions to memory acquisition and retrieval in contextual fear-conditioning.* Hippocampus, 2004. **14**(3): p. 301-310.
420. WEST, M.J., et al., *The CA1 Region of the Human Hippocampus Is a Hot Spot in Alzheimer's Disease.* Annals of the New York Academy of Sciences, 2000. **908**(1): p. 255-259.
421. Padurariu, M., et al., *Hippocampal neuronal loss in the CA1 and CA3 areas of Alzheimer's disease patients.* Psychiatria Danubina, 2012. **24**(2.): p. 152-158.
422. Ugolini, F., et al., *Different Patterns of Neurodegeneration and Glia Activation in CA1 and CA3 Hippocampal Regions of TgCRND8 Mice.* Frontiers in Aging Neuroscience, 2018. **10**.
423. Gusel'nikova, V.V. and D.E. Korzhevskiy, *NeuN As a Neuronal Nuclear Antigen and Neuron Differentiation Marker.* Acta Naturae, 2015. **7**(2): p. 42-7.

424. Steinberg, B.E., et al., *Cytokine-specific Neurograms in the Sensory Vagus Nerve.* Bioelectronic Medicine, 2016. **3**(1): p. 7-17.
425. Yang, J., et al., *Laparotomy-Induced Peripheral Inflammation Activates NR2B Receptors on the Brain Mast Cells and Results in Neuroinflammation in a Vagus Nerve-Dependent Manner.* Frontiers in Cellular Neuroscience, 2022. **16**.
426. Hickey, W.F., B.L. Hsu, and H. Kimura, *T-lymphocyte entry into the central nervous system.* Journal of Neuroscience Research, 1991. **28**(2): p. 254-260.
427. McManus, R.M., et al., *Respiratory infection promotes T cell infiltration and amyloid-β deposition in APP/PS1 mice.* Neurobiology of Aging, 2014. **35**(1): p. 109-121.
428. Organization, W.H., *Global tuberculosis report 2021.*, W.H. Organization, Editor. 2021.
429. Peng, Y.H., et al., *Increased risk of dementia among patients with pulmonary tuberculosis: a retrospective population-based cohort study.* Am J Alzheimers Dis Other Demen, 2015. **30**(6): p. 629-34.
430. Latham, A.S., et al., *Gliosis, misfolded protein aggregation, and neuronal loss in a guinea pig model of pulmonary tuberculosis.* Frontiers in Neuroscience, 2023. **17**.
431. Clementi, M.E., et al., *S100B Expression Plays a Crucial Role in Cytotoxicity, Reactive Oxygen Species Generation and Nitric Oxide Synthase Activation Induced by Amyloid β-Protein in an Astrocytoma Cell Line.* Int J Mol Sci, 2023. **24**(6).
432. Archie, S.R., A. Al Shoyaib, and L. Cucullo, *Blood-Brain Barrier Dysfunction in CNS Disorders and Putative Therapeutic Targets: An Overview.* Pharmaceutics, 2021. **13**(11).
433. Xiao, M., et al., *Blood-Brain Barrier: More Contributor to Disruption of Central Nervous System Homeostasis Than Victim in Neurological Disorders.* Frontiers in Neuroscience, 2020. **14**.
434. Abbott, N.J., *Blood–brain barrier structure and function and the challenges for CNS drug delivery.* Journal of Inherited Metabolic Disease, 2013. **36**(3): p. 437-449.
435. Stamatovic, S.M., R.F. Keep, and A.V. Andjelkovic, *Brain endothelial cell-cell junctions: how to "open" the blood brain barrier.* Curr Neuropharmacol, 2008. **6**(3): p. 179-92.
436. Winkler, L., et al., *Tight junctions in the blood–brain barrier promote edema formation and infarct size in stroke – Ambivalent effects of sealing proteins.* Journal of Cerebral Blood Flow & Metabolism, 2021. **41**(1): p. 132-145.
437. Tsukita, S. and M. Furuse, *Occludin and claudins in tight-junction strands: leading or supporting players?* Trends Cell Biol, 1999. **9**(7): p. 268-73.
438. Ohtsuki, S., et al., *Exogenous expression of claudin-5 induces barrier properties in cultured rat brain capillary endothelial cells.* Journal of Cellular Physiology, 2007. **210**(1): p. 81-86.
439. Abdullahi, W., D. Tripathi, and P.T. Ronaldson, *Blood-brain barrier dysfunction in ischemic stroke: targeting tight junctions and transporters for vascular protection.* Am J Physiol Cell Physiol, 2018. **315**(3): p. C343-c356.
440. Pöschl, E., et al., *Collagen IV is essential for basement membrane stability but dispensable for initiation of its assembly during early development.* Development, 2004. **131**(7): p. 1619-1628.
441. Gould, D.B., et al., *Mutations in Col4a1 cause perinatal cerebral hemorrhage and porencephaly.* Science, 2005. **308**(5725): p. 1167-71.
442. Gould, D.B., et al., *Role of COL4A1 in small-vessel disease and hemorrhagic stroke.* N Engl J Med, 2006. **354**(14): p. 1489-96.
443. Sellner, J. and S.L. Leib, *In bacterial meningitis cortical brain damage is associated with changes in parenchymal MMP-9/TIMP-1 ratio and increased collagen type IV degradation.* Neurobiology of Disease, 2006. **21**(3): p. 647-656.
444. Sellner, J., et al., *Herpes-simplex virus encephalitis is characterized by an early MMP-9 increase and collagen type IV degradation.* Brain Research, 2006. **1125**(1): p. 155-162.
445. Michalski, D., et al., *Increased Immunosignals of Collagen IV and Fibronectin Indicate Ischemic Consequences for the Neurovascular Matrix Adhesion Zone in Various Animal Models and Human Stroke Tissue.* Front Physiol, 2020. **11**: p. 575598.

446. Kalaria, R.N. and A.B. Pax, *Increased collagen content of cerebral microvessels in Alzheimer's disease.* Brain Research, 1995. **705**(1): p. 349-352.
447. MacVicar, B.A. and E.A. Newman, *Astrocyte regulation of blood flow in the brain.* Cold Spring Harb Perspect Biol, 2015. **7**(5).
448. Watkins, S., et al., *Disruption of astrocyte–vascular coupling and the blood–brain barrier by invading glioma cells.* Nature Communications, 2014. **5**(1): p. 4196.
449. Alvarez, J.I., T. Katayama, and A. Prat, *Glial influence on the blood brain barrier.* Glia, 2013. **61**(12): p. 1939-58.
450. Wong, A.D., et al., *The blood-brain barrier: an engineering perspective.* Front Neuroeng, 2013. **6**: p. 7.
451. Xia, Y.-p., et al., *Recombinant Human Sonic Hedgehog Protein Regulates the Expression of ZO-1 and Occludin by Activating Angiopoietin-1 in Stroke Damage.* PLOS ONE, 2013. **8**(7): p. e68891.
452. Sirko, S., et al., *Reactive Glia in the Injured Brain Acquire Stem Cell Properties in Response to Sonic Hedgehog.* Cell Stem Cell, 2013. **12**(4): p. 426-439.
453. Horng, S., et al., *Astrocytic tight junctions control inflammatory CNS lesion pathogenesis.* J Clin Invest, 2017. **127**(8): p. 3136-3151.
454. Schreiner, B., et al., *Astrocyte Depletion Impairs Redox Homeostasis and Triggers Neuronal Loss in the Adult CNS.* Cell Reports, 2015. **12**(9): p. 1377-1384.
455. Heithoff, B.P., et al., *Astrocytes are necessary for blood–brain barrier maintenance in the adult mouse brain.* Glia, 2021. **69**(2): p. 436-472.
456. Nakagawa, S., et al., *A new blood–brain barrier model using primary rat brain endothelial cells, pericytes and astrocytes.* Neurochemistry International, 2009. **54**(3): p. 253-263.
457. Knox, E.G., et al., *The blood-brain barrier in aging and neurodegeneration.* Molecular Psychiatry, 2022. **27**(6): p. 2659-2673.
458. Brilha, S., et al., *Matrix metalloproteinase-9 activity and a downregulated Hedgehog pathway impair blood-brain barrier function in an in vitro model of CNS tuberculosis.* Scientific Reports, 2017. **7**(1): p. 16031.
459. Kumar, S., et al., *Assessment of Blood-Brain Barrier Integrity in Tuberculous Meningitis Using Dynamic Contrast-Enhanced MR Perfusion.* Indian J Radiol Imaging, 2021. **31**(1): p. 30-36.
460. Starr, J.M., et al., *Blood–brain barrier permeability in Alzheimer's disease: a case–control MRI study.* Psychiatry Research: Neuroimaging, 2009. **171**(3): p. 232-241.
461. Al-Bachari, S., et al., *Blood–Brain Barrier Leakage Is Increased in Parkinson's Disease.* Frontiers in Physiology, 2020. **11**.
462. Liu, Y., et al., *Peripheral inflammation promotes brain tau transmission via disrupting blood–brain barrier.* Bioscience Reports, 2020. **40**(2): p. BSR20193629.
463. Huber, J.D., et al., *Inflammatory pain alters blood-brain barrier permeability and tight junctional protein expression.* American Journal of Physiology-Heart and Circulatory Physiology, 2001. **280**(3): p. H1241-H1248.
464. Rabchevsky, A.G., J.-D. Degos, and P.A. Dreyfus, *Peripheral injections of Freund's adjuvant in mice provoke leakage of serum proteins through the blood–brain barrier without inducing reactive gliosis.* Brain Research, 1999. **832**(1): p. 84-96.
465. Dénes, Á., S. Ferenczi, and K.J. Kovács, *Systemic inflammatory challenges compromise survival after experimental stroke via augmenting brain inflammation, blood- brain barrier damage and brain oedema independently of infarct size.* Journal of Neuroinflammation, 2011. **8**(1): p. 164.
466. TSAO, N., et al., *Tumour necrosis factor-α causes an increase in blood-brain barrier permeability during sepsis.* Journal of Medical Microbiology, 2001. **50**(9): p. 812-821.
467. Kumar, N.P., et al., *Plasma Proinflammatory Cytokines Are Markers of Disease Severity and Bacterial Burden in Pulmonary Tuberculosis.* Open Forum Infect Dis, 2019. **6**(7): p. ofz257.
468. Kim, S., et al., *Transneuronal Propagation of Pathologic α-Synuclein from the Gut to the Brain Models Parkinson's Disease.* Neuron, 2019. **103**(4): p. 627-641.e7.

469. Yang, R., et al., *Blood–Brain Barrier Integrity Damage in Bacterial Meningitis: The Underlying Link, Mechanisms, and Therapeutic Targets.* International Journal of Molecular Sciences, 2023. **24**(3): p. 2852.
470. Borrell, S., et al., *Reference set of Mycobacterium tuberculosis clinical strains: A tool for research and product development.* PLoS One, 2019. **14**(3): p. e0214088.
471. Ioerger, T.R., et al., *Variation among Genome Sequences of H37Rv Strains of Mycobacterium tuberculosis from Multiple Laboratories.* Journal of Bacteriology, 2010. **192**(14): p. 3645-3653.
472. Cole, S.T., et al., *Deciphering the biology of Mycobacterium tuberculosis from the complete genome sequence.* Nature, 1998. **396**(6707): p. 190-190.
473. Chitale, P., et al., *A comprehensive update to the Mycobacterium tuberculosis H37Rv reference genome.* Nature Communications, 2022. **13**(1): p. 7068.
474. Manca, C., et al., *Mycobacterium tuberculosis CDC1551 Induces a More Vigorous Host Response In Vivo and In Vitro, But Is Not More Virulent Than Other Clinical Isolates1.* The Journal of Immunology, 1999. **162**(11): p. 6740-6746.
475. Choreño-Parra, J.A., et al., *Mycobacterium tuberculosis HN878 Infection Induces Human-Like B-Cell Follicles in Mice.* J Infect Dis, 2020. **221**(10): p. 1636-1646.
476. Hernandez Pando, R., et al., *Specific bacterial genotypes of Mycobacterium tuberculosis cause extensive dissemination and brain infection in an experimental model.* Tuberculosis, 2010. **90**(4): p. 268-277.
477. Cuanalo-Contreras, K., et al., *Extensive accumulation of misfolded protein aggregates during natural aging and senescence.* Front Aging Neurosci, 2022. **14**: p. 1090109.
478. Wahl, D., et al., *Nontransgenic Guinea Pig Strains Exhibit Hallmarks of Human Brain Aging and Alzheimer's Disease.* J Gerontol A Biol Sci Med Sci, 2022. **77**(9): p. 1766-1774.
479. Musci, R.V., et al., *The Dunkin Hartley Guinea Pig Is a Model of Primary Osteoarthritis That Also Exhibits Early Onset Myofiber Remodeling That Resembles Human Musculoskeletal Aging.* Front Physiol, 2020. **11**: p. 571372.
480. Radakovich, L.B., et al., *Development of a microcomputed tomography scoring system to characterize disease progression in the Hartley guinea pig model of spontaneous osteoarthritis.* Connect Tissue Res, 2018. **59**(6): p. 523-533.
481. Stoll, G., S. Jander, and M. Schroeter, *Inflammation and glial responses in ischemic brain lesions.* Progress in Neurobiology, 1998. **56**(2): p. 149-171.
482. Nishioku, T., et al., *Tumor necrosis factor-alpha mediates the blood-brain barrier dysfunction induced by activated microglia in mouse brain microvascular endothelial cells.* J Pharmacol Sci, 2010. **112**(2): p. 251-4.
483. Jurga, A.M., M. Paleczna, and K.Z. Kuter, *Overview of General and Discriminating Markers of Differential Microglia Phenotypes.* Front Cell Neurosci, 2020. **14**: p. 198.
484. Dihné, M., et al., *Time course of glial proliferation and glial apoptosis following excitotoxic CNS injury.* Brain Res, 2001. **902**(2): p. 178-89.
485. Fernández-Arjona, M.d.M., et al., *Microglial activation by microbial neuraminidase through TLR2 and TLR4 receptors.* Journal of Neuroinflammation, 2019. **16**(1): p. 245.
486. Simpson, D.S.A. and P.L. Oliver, *ROS Generation in Microglia: Understanding Oxidative Stress and Inflammation in Neurodegenerative Disease.* Antioxidants (Basel), 2020. **9**(8).
487. Imai, Y., et al., *A Novel Geneiba1in the Major Histocompatibility Complex Class III Region Encoding an EF Hand Protein Expressed in a Monocytic Lineage.* Biochemical and Biophysical Research Communications, 1996. **224**(3): p. 855-862.
488. Pekna, M. and M. Pekny, *The Complement System: A Powerful Modulator and Effector of Astrocyte Function in the Healthy and Diseased Central Nervous System.* Cells, 2021. **10**(7): p. 1812.

489. Hartmann, K., et al., *Complement 3(+)-astrocytes are highly abundant in prion diseases, but their abolishment led to an accelerated disease course and early dysregulation of microglia.* Acta Neuropathol Commun, 2019. **7**(1): p. 83.
490. Escartin, C., et al., *Reactive astrocyte nomenclature, definitions, and future directions.* Nature Neuroscience, 2021. **24**(3): p. 312-325.
491. Yang, T., et al., *Dissecting the Dual Role of the Glial Scar and Scar-Forming Astrocytes in Spinal Cord Injury.* Frontiers in Cellular Neuroscience, 2020. **14**.
492. Wang, Y., et al., *Interleukin-1β Induces Blood–Brain Barrier Disruption by Downregulating Sonic Hedgehog in Astrocytes.* PLOS ONE, 2014. **9**(10): p. e110024.
493. Vandebroek, A. and M. Yasui, *Regulation of AQP4 in the Central Nervous System.* Int J Mol Sci, 2020. **21**(5).
494. Li, L., et al., *Proinflammatory role of aquaporin-4 in autoimmune neuroinflammation.* Faseb j, 2011. **25**(5): p. 1556-66.
495. Zhou, J., et al., *Altered blood–brain barrier integrity in adult aquaporin-4 knockout mice.* NeuroReport, 2008. **19**(1): p. 1-5.
496. Saadoun, S., et al., *AQP4 gene deletion in mice does not alter blood–brain barrier integrity or brain morphology.* Neuroscience, 2009. **161**(3): p. 764-772.
497. Xingi, E., et al., *LPS-Induced Systemic Inflammation Affects the Dynamic Interactions of Astrocytes and Microglia with the Vasculature of the Mouse Brain Cortex.* Cells, 2023. **12**(10).
498. Sternlicht, M.D. and Z. Werb, *How matrix metalloproteinases regulate cell behavior.* Annu Rev Cell Dev Biol, 2001. **17**: p. 463-516.
499. Hsu, J.Y., et al., *Matrix metalloproteinase-2 facilitates wound healing events that promote functional recovery after spinal cord injury.* J Neurosci, 2006. **26**(39): p. 9841-50.
500. Noble, L.J., et al., *Matrix metalloproteinases limit functional recovery after spinal cord injury by modulation of early vascular events.* J Neurosci, 2002. **22**(17): p. 7526-35.
501. Könnecke, H. and I. Bechmann, *The role of microglia and matrix metalloproteinases involvement in neuroinflammation and gliomas.* Clin Dev Immunol, 2013. **2013**: p. 914104.
502. Nelson, K.K. and J.A. Melendez, *Mitochondrial redox control of matrix metalloproteinases.* Free Radical Biology and Medicine, 2004. **37**(6): p. 768-784.
503. Kar, S., et al., *Redox-control of matrix metalloproteinase-1: a critical link between free radicals, matrix remodeling and degenerative disease.* Respir Physiol Neurobiol, 2010. **174**(3): p. 299-306.
504. Yang, Y. and G.A. Rosenberg, *MMP-mediated disruption of claudin-5 in the blood-brain barrier of rat brain after cerebral ischemia.* Methods Mol Biol, 2011. **762**: p. 333-45.
505. Chiu, P.-S. and S.-C. Lai, *Matrix Metalloproteinase-9 Leads to Claudin-5 Degradation via the NF-κB Pathway in BALB/c Mice with Eosinophilic Meningoencephalitis Caused by Angiostrongylus cantonensis.* PLOS ONE, 2013. **8**(3): p. e53370.
506. Schubert-Unkmeir, A., et al., *Neisseria meningitidis induces brain microvascular endothelial cell detachment from the matrix and cleavage of occludin: a role for MMP-8.* PLoS Pathog, 2010. **6**(4): p. e1000874.
507. C, N.C. and M.A. Lynch, *The role of the immune system in driving neuroinflammation.* Brain Neurosci Adv, 2020. **4**: p. 2398212819901082.
508. Bulloch, K., et al., *CD11c/EYFP transgene illuminates a discrete network of dendritic cells within the embryonic, neonatal, adult, and injured mouse brain.* Journal of Comparative Neurology, 2008. **508**(5): p. 687-710.
509. Smolders, J., et al., *Tissue-resident memory T cells populate the human brain.* Nat Commun, 2018. **9**(1): p. 4593.
510. Ritzel, R.M., et al., *Functional differences between microglia and monocytes after ischemic stroke.* Journal of Neuroinflammation, 2015. **12**(1): p. 106.
511. Butovsky, O., et al., *Identification of a unique TGF-β–dependent molecular and functional signature in microglia.* Nature Neuroscience, 2014. **17**(1): p. 131-143.

512. Martin, E., et al., *Analysis of Microglia and Monocyte-derived Macrophages from the Central Nervous System by Flow Cytometry.* J Vis Exp, 2017(124).
513. Yang, Q., G. Wang, and F. Zhang, *Role of Peripheral Immune Cells-Mediated Inflammation on the Process of Neurodegenerative Diseases.* Frontiers in Immunology, 2020. **11**.
514. Zhu, H., W. Liu, and H. Fang, *Inflammation caused by peripheral immune cells across into injured mouse blood brain barrier can worsen postoperative cognitive dysfunction induced by isoflurane.* BMC Cell Biology, 2018. **19**(1): p. 23.
515. Stein, V.M., et al., *Differential expression of CD45 on canine microglial cells.* J Vet Med A Physiol Pathol Clin Med, 2007. **54**(6): p. 314-20.
516. Bennett, M.L., et al., *New tools for studying microglia in the mouse and human CNS.* Proc Natl Acad Sci U S A, 2016. **113**(12): p. E1738-46.
517. Rangaraju, S., et al., *Differential Phagocytic Properties of CD45low Microglia and CD45high Brain Mononuclear Phagocytes—Activation and Age-Related Effects.* Frontiers in Immunology, 2018. **9**.
518. Kang, E.J., et al., *Blood-brain barrier opening to large molecules does not imply blood-brain barrier opening to small ions.* Neurobiol Dis, 2013. **52**: p. 204-18.
519. Hung, C.-W., et al., *Ageing and neurodegenerative diseases.* Ageing Research Reviews, 2010. **9**: p. S36-S46.
520. Gustavsson, A., et al., *Global estimates on the number of persons across the Alzheimer's disease continuum.* Alzheimer's & Dementia, 2023. **19**(2): p. 658-670.
521. van Deursen, J.M., *The role of senescent cells in ageing.* Nature, 2014. **509**(7501): p. 439-446.
522. Ng, P.Y., T.L. McNeely, and D.J. Baker, *Untangling senescent and damage-associated microglia in the aging and diseased brain.* Febs j, 2023. **290**(5): p. 1326-1339.
523. Zhang, X., et al., *Rejuvenation of the aged brain immune cell landscape in mice through p16-positive senescent cell clearance.* Nature Communications, 2022. **13**(1): p. 5671.
524. Greenwood, E.K. and D.R. Brown, *Senescent Microglia: The Key to the Ageing Brain?* Int J Mol Sci, 2021. **22**(9).
525. Lau, V., L. Ramer, and M.-È. Tremblay, *An aging, pathology burden, and glial senescence build-up hypothesis for late onset Alzheimer's disease.* Nature Communications, 2023. **14**(1): p. 1670.
526. Shafqat, A., et al., *Cellular senescence in brain aging and cognitive decline.* Frontiers in Aging Neuroscience, 2023. **15**.
527. Boyle, P.A., et al., *Relation of neuropathology with cognitive decline among older persons without dementia.* Front Aging Neurosci, 2013. **5**: p. 50.
528. Elobeid, A., et al., *Altered Proteins in the Aging Brain.* J Neuropathol Exp Neurol, 2016. **75**(4): p. 316-25.
529. Yankner, B.A., T. Lu, and P. Loerch, *The aging brain.* Annu Rev Pathol, 2008. **3**: p. 41-66.
530. Glorioso, C. and E. Sibille, *Between destiny and disease: genetics and molecular pathways of human central nervous system aging.* Prog Neurobiol, 2011. **93**(2): p. 165-81.
531. Beach, T.G., et al., *Accuracy of the Clinical Diagnosis of Alzheimer Disease at National Institute on Aging Alzheimer Disease Centers, 2005–2010.* Journal of Neuropathology & Experimental Neurology, 2012. **71**(4): p. 266-273.
532. Pearl, G.S., *Diagnosis of Alzheimer's disease in a community hospital-based brain bank program.* South Med J, 1997. **90**(7): p. 720-2.
533. Klatka, L.A., et al., *Incorrect Diagnosis of Alzheimer's Disease: A Clinicopathologic Study.* Archives of Neurology, 1996. **53**(1): p. 35-42.
534. Fisher, E.M.C. and D.M. Bannerman, *Mouse models of neurodegeneration: Know your question, know your mouse.* Science Translational Medicine, 2019. **11**(493): p. eaaq1818.
535. de Sousa, A.A., et al., *Going beyond established model systems of Alzheimer's disease: companion animals provide novel insights into the neurobiology of aging.* Communications Biology, 2023. **6**(1): p. 655.

536. Chakrabarti, S., et al., *Metabolic Risk Factors of Sporadic Alzheimer's Disease: Implications in the Pathology, Pathogenesis and Treatment.* Aging Dis, 2015. **6**(4): p. 282-99.
537. Phillips, K.A., et al., *Why primate models matter.* American Journal of Primatology, 2014. **76**(9): p. 801-827.
538. Arnsten, A.F.T., D. Datta, and T.M. Preuss, *Studies of aging nonhuman primates illuminate the etiology of early-stage Alzheimer's-like neuropathology: An evolutionary perspective.* Am J Primatol, 2021. **83**(11): p. e23254.
539. Edler, M.K., et al., *Aged chimpanzees exhibit pathologic hallmarks of Alzheimer's disease.* Neurobiol Aging, 2017. **59**: p. 107-120.
540. Hines, A.D., et al., *Activated gliosis, accumulation of amyloid β, and hyperphosphorylation of tau in aging canines with and without cognitive decline.* Frontiers in Aging Neuroscience, 2023. **15**.
541. Bosch, M.N., et al., *Dogs with cognitive dysfunction syndrome: a natural model of Alzheimer's disease.* Curr Alzheimer Res, 2012. **9**(3): p. 298-314.
542. Radakovich, L.B., et al., *Calorie restriction with regular chow, but not a high-fat diet, delays onset of spontaneous osteoarthritis in the Hartley guinea pig model.* Arthritis Res Ther, 2019. **21**(1): p. 145.
543. Krieglstein, J., et al., *Damage of guinea pig heart and arteries by a trioleate-enriched diet and of cultured cardiomyocytes by oleic acid.* PLoS One, 2010. **5**(3): p. e9561.
544. Burton, L.H., et al., *Pharmacologic iron chelation reduces markers of chondrocyte hypertrophy and osteoarthritis-associated cartilage lesions in an animal model of idiopathic disease.* Osteoarthritis and Cartilage, 2020. **28**: p. S91.
545. Arnold, S.J., B.N. Dugger, and T.G. Beach, *TDP-43 deposition in prospectively followed, cognitively normal elderly individuals: correlation with argyrophilic grains but not other concomitant pathologies.* Acta Neuropathol, 2013. **126**(1): p. 51-7.
546. Uchino, A., et al., *Incidence and extent of TDP-43 accumulation in aging human brain.* Acta Neuropathol Commun, 2015. **3**: p. 35.
547. Salas, I.H., J. Burgado, and N.J. Allen, *Glia: victims or villains of the aging brain?* Neurobiology of Disease, 2020. **143**: p. 105008.
548. Thomas, A.L., et al., *Naturally-aged microglia exhibit phagocytic dysfunction accompanied by gene expression changes reflective of underlying neurologic disease.* Scientific Reports, 2022. **12**(1): p. 19471.
549. Monterey, M.D., et al., *The Many Faces of Astrocytes in Alzheimer's Disease.* Frontiers in Neurology, 2021. **12**.
550. Grosche, A., et al., *Versatile and Simple Approach to Determine Astrocyte Territories in Mouse Neocortex and Hippocampus.* PLOS ONE, 2013. **8**(7): p. e69143.
551. Pelvig, D.P., et al., *Neocortical glial cell numbers in human brains.* Neurobiol Aging, 2008. **29**(11): p. 1754-62.
552. Fabricius, K., J.S. Jacobsen, and B. Pakkenberg, *Effect of age on neocortical brain cells in 90+ year old human females—a cell counting study.* Neurobiology of aging, 2013. **34**(1): p. 91-99.
553. Robillard, K.N., et al., *Glial cell morphological and density changes through the lifespan of rhesus macaques.* Brain, Behavior, and Immunity, 2016. **55**: p. 60-69.
554. Kacem, K., et al., *Structural organization of the perivascular astrocyte endfeet and their relationship with the endothelial glucose transporter: a confocal microscopy study.* Glia, 1998. **23**(1): p. 1-10.
555. Abbott, N.J., *Astrocyte-endothelial interactions and blood-brain barrier permeability.* J Anat, 2002. **200**(6): p. 629-38.
556. Seshadri, S., et al., *Lifetime risk of dementia and Alzheimer's disease. The impact of mortality on risk estimates in the Framingham Study.* Neurology, 1997. **49**(6): p. 1498-504.
557. *Global, regional, and national burden of neurological disorders, 1990-2016: a systematic analysis for the Global Burden of Disease Study 2016.* Lancet Neurol, 2019. **18**(5): p. 459-480.
558. Poewe, W., et al., *Parkinson disease.* Nature Reviews Disease Primers, 2017. **3**(1): p. 17013.

559. Willis, A.W., et al., *Incidence of Parkinson disease in North America.* npj Parkinson's Disease, 2022. **8**(1): p. 170.
560. Sveinbjornsdottir, S., *The clinical symptoms of Parkinson's disease.* J Neurochem, 2016. **139 Suppl 1**: p. 318-324.
561. Tanner, C.M., et al., *Rotenone, paraquat, and Parkinson's disease.* Environ Health Perspect, 2011. **119**(6): p. 866-72.
562. Li, N., et al., *Mitochondrial complex I inhibitor rotenone induces apoptosis through enhancing mitochondrial reactive oxygen species production.* J Biol Chem, 2003. **278**(10): p. 8516-25.
563. Rocha, S.M., et al., *Rotenone induces regionally distinct α-synuclein protein aggregation and activation of glia prior to loss of dopaminergic neurons in C57Bl/6 mice.* Neurobiol Dis, 2022. **167**: p. 105685.
564. Sheeler, C., et al., *Glia in Neurodegeneration: The Housekeeper, the Defender and the Perpetrator.* Int J Mol Sci, 2020. **21**(23).
565. Kwon, H.S. and S.-H. Koh, *Neuroinflammation in neurodegenerative disorders: the roles of microglia and astrocytes.* Translational Neurodegeneration, 2020. **9**(1): p. 42.
566. Lema Tomé, C.M., et al., *Inflammation and α-synuclein's prion-like behavior in Parkinson's disease--is there a link?* Mol Neurobiol, 2013. **47**(2): p. 561-74.
567. Tansey, M.G., M.K. McCoy, and T.C. Frank-Cannon, *Neuroinflammatory mechanisms in Parkinson's disease: Potential environmental triggers, pathways, and targets for early therapeutic intervention.* Experimental Neurology, 2007. **208**(1): p. 1-25.
568. Hensleigh, E. and L.M. Pritchard, *Glucocorticoid receptor expression and sub-cellular localization in dopamine neurons of the rat midbrain.* Neurosci Lett, 2013. **556**: p. 191-5.
569. Barnes, P.J., *Anti-inflammatory actions of glucocorticoids: molecular mechanisms.* Clin Sci (Lond), 1998. **94**(6): p. 557-72.
570. Landfield, P.W., et al., *A new glucocorticoid hypothesis of brain aging: implications for Alzheimer's disease.* Curr Alzheimer Res, 2007. **4**(2): p. 205-12.
571. Ros-Bernal, F., et al., *Microglial glucocorticoid receptors play a pivotal role in regulating dopaminergic neurodegeneration in parkinsonism.* Proceedings of the National Academy of Sciences, 2011. **108**(16): p. 6632-6637.
572. Perlman, W.R., et al., *Age-related differences in glucocorticoid receptor mRNA levels in the human brain.* Neurobiology of Aging, 2007. **28**(3): p. 447-458.
573. Caudal, D., et al., *Depressive-like phenotype induced by AAV-mediated overexpression of human α-synuclein in midbrain dopaminergic neurons.* Experimental Neurology, 2015. **273**: p. 243-252.
574. Herrero, M.-T., et al., *Inflammation in Parkinson's disease: role of glucocorticoids.* Frontiers in Neuroanatomy, 2015. **9**.
575. Ouanes, S. and J. Popp, *High Cortisol and the Risk of Dementia and Alzheimer's Disease: A Review of the Literature.* Frontiers in Aging Neuroscience, 2019. **11**.
576. Maatouk, L., et al., *Glucocorticoid receptor in astrocytes regulates midbrain dopamine neurodegeneration through connexin hemichannel activity.* Cell Death & Differentiation, 2019. **26**(3): p. 580-596.
577. Rocha, S.M., et al., *Microglia-specific knock-out of NF-κB/IKK2 increases the accumulation of misfolded α-synuclein through the inhibition of p62/sequestosome-1-dependent autophagy in the rotenone model of Parkinson's disease.* Glia, 2023. **71**(9): p. 2154-2179.
578. Le, W., J. Wu, and Y. Tang, *Protective Microglia and Their Regulation in Parkinson's Disease.* Front Mol Neurosci, 2016. **9**: p. 89.
579. Morice, C., et al., *A randomized trial of safety and pharmacodynamic interactions between a selective glucocorticoid receptor antagonist, PT150, and ethanol in healthy volunteers.* Scientific Reports, 2021. **11**(1): p. 9876.
580. Rocha, S.M., et al., *A Novel Glucocorticoid and Androgen Receptor Modulator Reduces Viral Entry and Innate Immune Inflammatory Responses in the Syrian Hamster Model of SARS-CoV-2 Infection.* Frontiers in Immunology, 2022. **13**.

581. Cannon, J.R., et al., *A highly reproducible rotenone model of Parkinson's disease.* Neurobiol Dis, 2009. **34**(2): p. 279-90.
582. Reagan-Shaw, S., M. Nihal, and N. Ahmad, *Dose translation from animal to human studies revisited.* The FASEB Journal, 2008. **22**(3): p. 659-661.
583. Tapias, V. and J.T. Greenamyre, *A Rapid and Sensitive Automated Image-Based Approach for In Vitro and In Vivo Characterization of Cell Morphology and Quantification of Cell Number and Neurite Architecture.* Current Protocols in Cytometry, 2014. **68**(1): p. 12.33.1-12.33.22.
584. Dorsey, E.R., et al., *The Emerging Evidence of the Parkinson Pandemic.* J Parkinsons Dis, 2018. **8**(s1): p. S3-s8.
585. Salvadores, N., et al., *Axonal Degeneration during Aging and Its Functional Role in Neurodegenerative Disorders.* Front Neurosci, 2017. **11**: p. 451.
586. Tagliaferro, P. and R.E. Burke, *Retrograde Axonal Degeneration in Parkinson Disease.* Journal of Parkinson's Disease, 2016. **6**: p. 1-15.
587. Lams, B.E., O. Isacson, and M.V. Sofroniew, *Loss of transmitter-associated enzyme staining following axotomy does not indicate death of brainstem cholinergic neurons.* Brain Research, 1988. **475**(2): p. 401-406.
588. Salvatore, M.F., et al., *Tyrosine Hydroxylase Inhibition in Substantia Nigra Decreases Movement Frequency.* Mol Neurobiol, 2019. **56**(4): p. 2728-2740.
589. Liu, M. and G. Bing, *Lipopolysaccharide Animal Models for Parkinson's Disease.* Parkinson's Disease, 2011. **2011**: p. 327089.
590. Surmeier, D.J., *Determinants of dopaminergic neuron loss in Parkinson's disease.* Febs j, 2018. **285**(19): p. 3657-3668.
591. De Nicola, A.F., et al., *Insights into the Therapeutic Potential of Glucocorticoid Receptor Modulators for Neurodegenerative Diseases.* Int J Mol Sci, 2020. **21**(6).
592. Heindl, S., et al., *Automated Morphological Analysis of Microglia After Stroke.* Frontiers in Cellular Neuroscience, 2018. **12**.
593. Fernández-Arjona, M.d.M., et al., *Microglial Morphometric Parameters Correlate With the Expression Level of IL-1β, and Allow Identifying Different Activated Morphotypes.* Frontiers in Cellular Neuroscience, 2019. **13**.
594. Morrison, H., et al., *Quantitative microglia analyses reveal diverse morphologic responses in the rat cortex after diffuse brain injury.* Scientific Reports, 2017. **7**(1): p. 13211.
595. Smith, J.A., et al., *Role of pro-inflammatory cytokines released from microglia in neurodegenerative diseases.* Brain Res Bull, 2012. **87**(1): p. 10-20.
596. Gerhard, A., et al., *In vivo imaging of microglial activation with [11C](R)-PK11195 PET in idiopathic Parkinson's disease.* Neurobiology of Disease, 2006. **21**(2): p. 404-412.
597. Liddelow, S.A. and B.A. Barres, *Reactive Astrocytes: Production, Function, and Therapeutic Potential.* Immunity, 2017. **46**(6): p. 957-967.
598. Moulson, A.J., et al., *Diversity of Reactive Astrogliosis in CNS Pathology: Heterogeneity or Plasticity?* Frontiers in Cellular Neuroscience, 2021. **15**.
599. Schiweck, J., B.J. Eickholt, and K. Murk, *Important Shapeshifter: Mechanisms Allowing Astrocytes to Respond to the Changing Nervous System During Development, Injury and Disease.* Frontiers in Cellular Neuroscience, 2018. **12**.
600. Lian, H., et al., *NFκB-activated astroglial release of complement C3 compromises neuronal morphology and function associated with Alzheimer's disease.* Neuron, 2015. **85**(1): p. 101-115.
601. Chiareli, R.A., et al., *The Role of Astrocytes in the Neurorepair Process.* Front Cell Dev Biol, 2021. **9**: p. 665795.
602. Duarte Azevedo, M., S. Sander, and L. Tenenbaum, *GDNF, A Neuron-Derived Factor Upregulated in Glial Cells during Disease.* J Clin Med, 2020. **9**(2).
603. Celikkaya, H., et al., *GATA3 Promotes the Neural Progenitor State but Not Neurogenesis in 3D Traumatic Injury Model of Primary Human Cortical Astrocytes.* Front Cell Neurosci, 2019. **13**: p. 23.

604. Kizil, C., et al., *Regenerative Neurogenesis from Neural Progenitor Cells Requires Injury-Induced Expression of Gata3.* Developmental Cell, 2012. **23**(6): p. 1230-1237.
605. Requejo, C., et al., *Morphological Changes in a Severe Model of Parkinson's Disease and Its Suitability to Test the Therapeutic Effects of Microencapsulated Neurotrophic Factors.* Molecular Neurobiology, 2017. **54**(10): p. 7722-7735.
606. Katiyar, K.S., et al., *Mechanical elongation of astrocyte processes to create living scaffolds for nervous system regeneration.* J Tissue Eng Regen Med, 2017. **11**(10): p. 2737-2751.
607. Kanmogne, M. and R.S. Klein, *Neuroprotective versus Neuroinflammatory Roles of Complement: From Development to Disease.* Trends Neurosci, 2021. **44**(2): p. 97-109.
608. Morales, I., et al., *Astrocytes and retrograde degeneration of nigrostriatal dopaminergic neurons in Parkinson's disease: removing axonal debris.* Translational Neurodegeneration, 2021. **10**(1): p. 43.
609. Marcel, M., et al., *Complement C3 Deficiency Leads to Accelerated Amyloid β Plaque Deposition and Neurodegeneration and Modulation of the Microglia/Macrophage Phenotype in Amyloid Precursor Protein Transgenic Mice.* The Journal of Neuroscience, 2008. **28**(25): p. 6333.
610. Wyss-Coray, T., et al., *Prominent neurodegeneration and increased plaque formation in complement-inhibited Alzheimer's mice.* Proceedings of the National Academy of Sciences, 2002. **99**(16): p. 10837-10842.
611. Rocha, E.M., B. De Miranda, and L.H. Sanders, *Alpha-synuclein: Pathology, mitochondrial dysfunction and neuroinflammation in Parkinson's disease.* Neurobiology of Disease, 2018. **109**: p. 249-257.
612. Emmanouilidou, E., et al., *Assessment of α-Synuclein Secretion in Mouse and Human Brain Parenchyma.* PLOS ONE, 2011. **6**(7): p. e22225.
613. He-Jin, L., P. Smita, and L. Seung-Jae, *Intravesicular Localization and Exocytosis of α-Synuclein and its Aggregates.* The Journal of Neuroscience, 2005. **25**(25): p. 6016.
614. Chen, K., et al., *LRP1 is a neuronal receptor for α-synuclein uptake and spread.* Molecular Neurodegeneration, 2022. **17**(1): p. 57.
615. Tsunemi, T., et al., *Astrocytes Protect Human Dopaminergic Neurons from α-Synuclein Accumulation and Propagation.* J Neurosci, 2020. **40**(45): p. 8618-8628.

APPENDIX I
CHAPTER 2 SUPPLEMENTARY FIGURES

APPENDIX 1

CHAPTER 2 SUPPLEMENTARY FIGURES

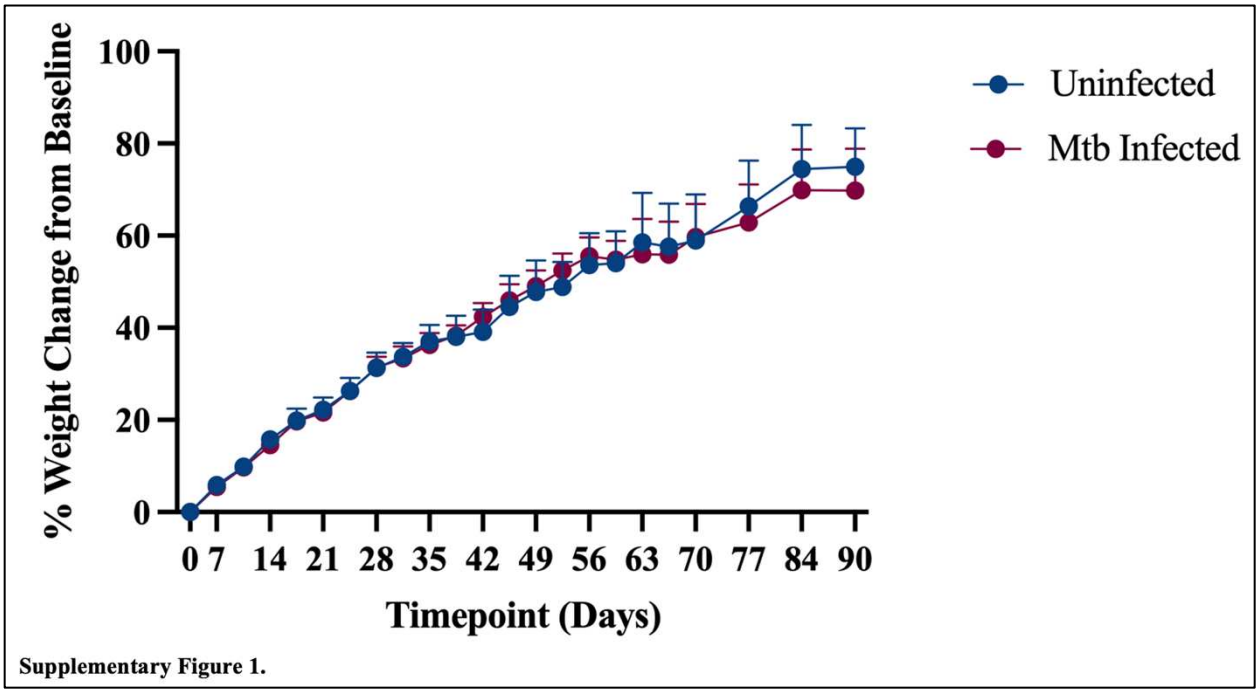

Supplementary Figure 1.

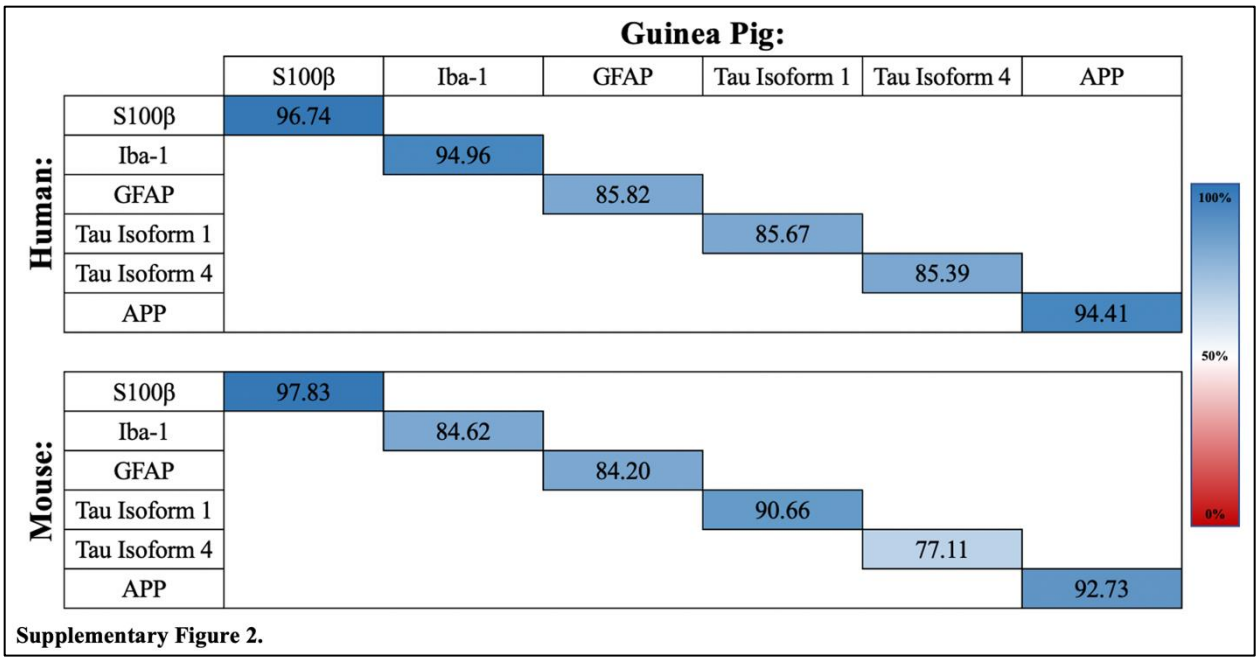

Supplementary Figure 2.

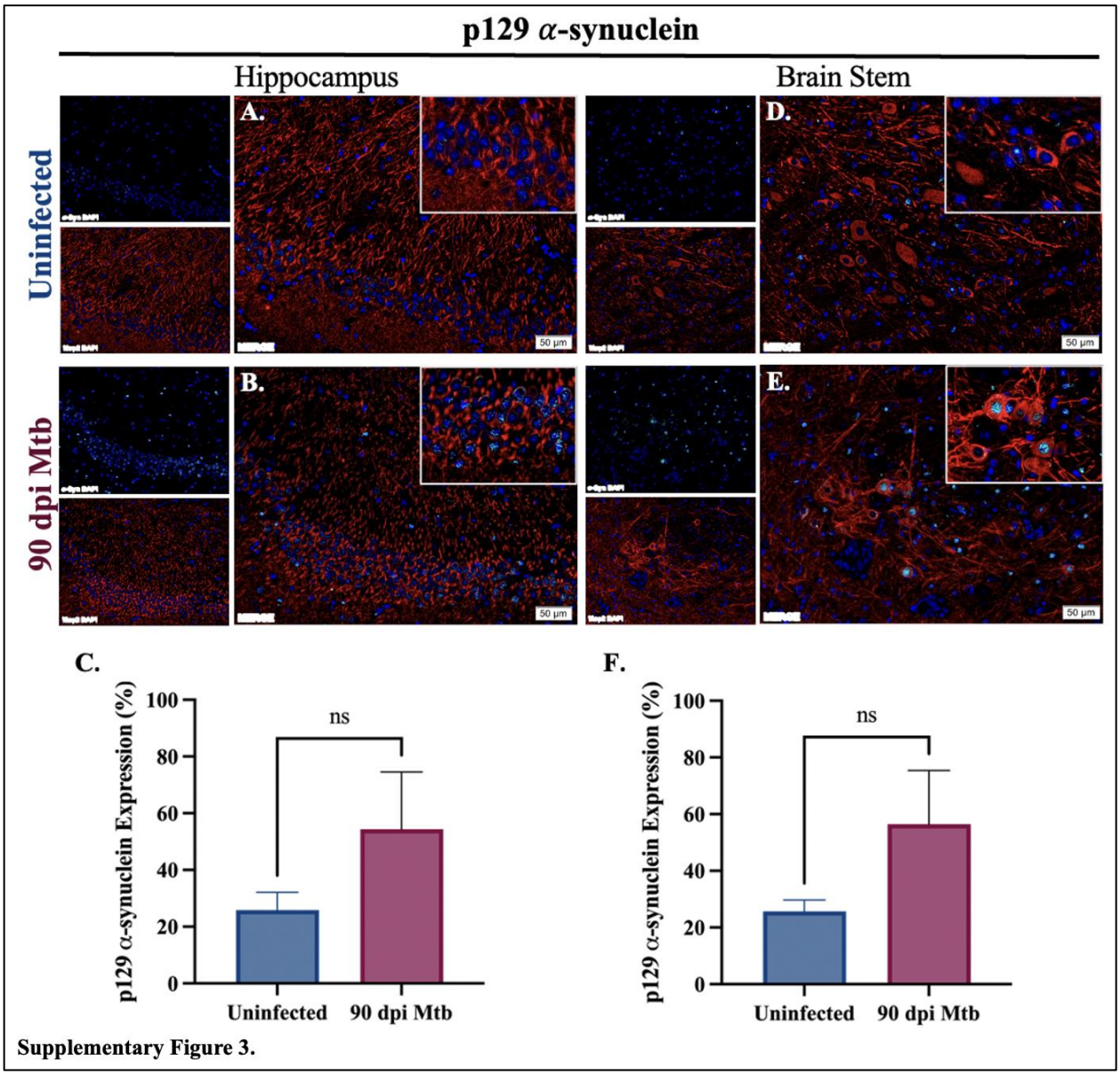

Supplementary Figure 3.

APPENDIX II
CHAPTER 5 SUPPLEMENTARY FIGURES

APPENDIX II

CHAPTER 5 SUPPLEMENTARY FIGURES

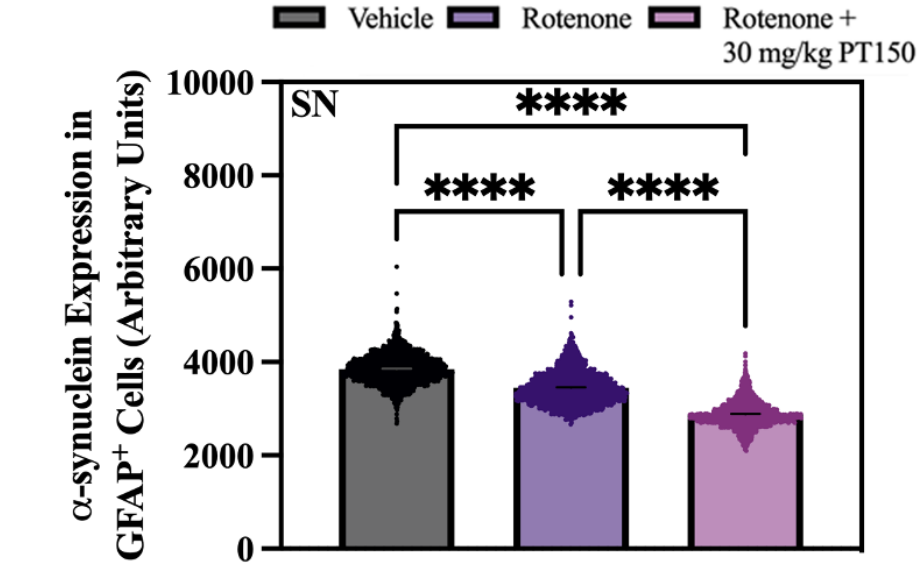

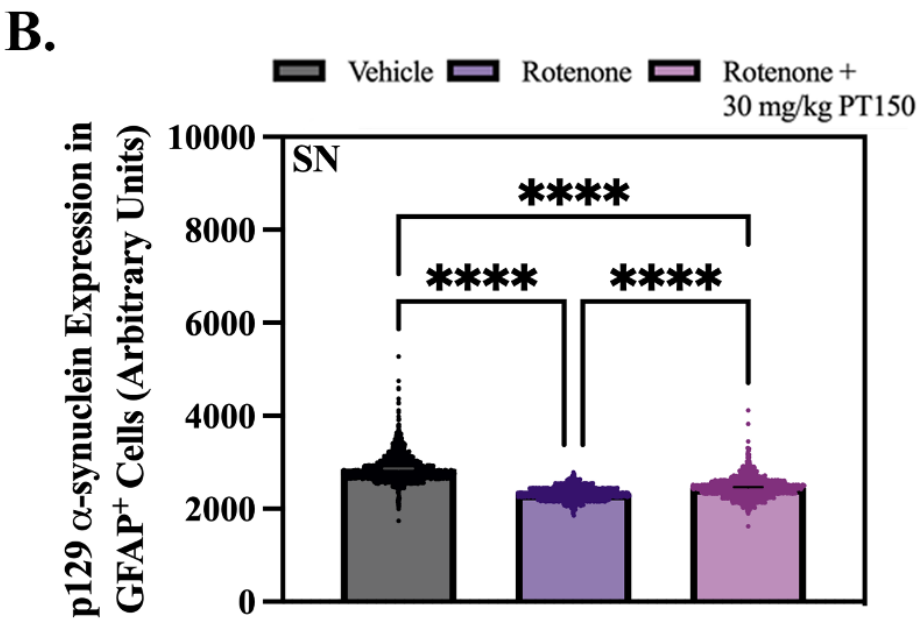

Supplemental Figure 4.